195
FERMILAB
NOV 29 1999
LIBRARY
JAERI-RESEARCH-99-055
Fermilab Library
0 1160 0071368 9

JAERI-Research
99-055

DECAY HEAT EXPERIMENT AND VALIDATION OF CALCULATION CODE SYSTEMS FOR FUSION REACTOR

October 1999

Fujio MAEKAWA, Masayuki WADA* and Yujiro IKEDA

日本原子力研究所
Japan Atomic Energy Research Institute

本レポートは，日本原子力研究所が不定期に公刊している研究報告書です。
入手の問合わせは，日本原子力研究所研究情報部研究情報課（〒319-1195　茨城県那珂郡東海村）あて，お申し越しください。なお，このほかに財団法人原子力弘済会資料センター（〒319-1195　茨城県那珂郡東海村日本原子力研究所内）で複写による実費頒布をおこなっております。

This report is issued irregularly.
Inquiries about availability of the reports should be addressed to Research Information Division, Department of Intellectual Resources, Japan Atomic Energy Research Institute, Tokai-mura, Naka-gun, Ibaraki-ken, 319-1195, Japan.

© Japan Atomic Energy Research Institute, 1999

編集兼発行　　日本原子力研究所

JAERI-Research 99-055

Decay Heat Experiment and Validation of Calculation Code Systems for Fusion Reactor

Fujio MAEKAWA, Masayuki WADA* and Yujiro IKEDA

Center for Neutron Science
Tokai Research Establishment
Japan Atomic Energy Research Institute
Tokai-mura, Naka-gun, Ibaraki-ken

(Received August 18, 1999)

Although accurate estimation of decay heat value is essential for safety analyses of fusion reactors against loss of coolant accidents and so on, no experimental work has been devoted to validating the estimation. Hence, a decay heat measurement experiment was performed as a task (T-339) of ITER/EDA.

A new detector, the Whole Energy Absorption Spectrometer (WEAS), was developed for accurate and efficient measurements of decay heat. Decay heat produced in the thirty-two sample materials which were irradiated by 14-MeV neutrons at FNS/JAERI were measured with WEAS for a wide cooling time period from 1 min to 400 days. The data presently obtained were the first experimental decay heat data in the field of fusion. Validity of decay heat calculation codes of ACT4 and CINAC-V4, activation cross section libraries of FENDL/A-2.0 and JENDL Activation File, and decay data was investigated through analyses of the experiment. As a result, several points that should be modified were found in the codes and data. After solving the problems, it was demonstrated that decay heat values calculated for most of samples were in good agreement with the experimental data. Especially for stainless steel 316 and copper, which were important materials for ITER, decay heat could be predicted with accuracy of ± 10 %.

Keywords : Decay Heat, Fusion, Safety, ITER, WEAS, 14-MeV, FNS, Experiment, Validation, JENDL Activation File, FENDL/A-2.0, ACT4, CINAC-V4

---

* Business Automation Co, Ltd.

JAERI-Research 99-055

核融合炉のための崩壊熱実験と計算コードシステムの検証

日本原子力研究所東海研究所中性子科学研究センター
前川　藤夫・和田　政行*・池田裕二郎

（1999年8月18日 受理）

核融合炉の冷却材喪失事故時等の安全性解析において、崩壊熱量の正確な評価は極めて重要であるが、その妥当性は実験的に調べられていない。そこで、ITER/EDAのタスク（T-339）として崩壊熱測定実験を行った。まず、崩壊熱を高精度かつ効率的に測定できる新たな検出器、全エネルギー吸収スペクトロメータ（WEAS）を開発した。これを用い、原研FNSの14-MeV中性子で照射した32種の試料から発生する崩壊熱を1分～400日の幅広い冷却時間範囲にわたって測定した。今回取得したデータは、核融合の分野では初の系統的な崩壊熱実験データである。実験解析により崩壊熱計算コード（ACT4、CINAC-V4）、放射化断面積ライブラリー（FENDL/A-2.0、JENDL放射化ファイル等）、及び崩壊データの妥当性を検証した結果、コードやデータに修正すべき点がいくつか見つかった。これらの問題点に対処した結果、大部分の試料に関する崩壊熱の計算値は実験値と良い一致を示した。特にITERで重要なステンレス鋼316及び銅については、崩壊熱を10%以内の精度で予測できることが分かった。

東海研究所：〒319-1195 茨城県那珂郡東海村白方白根 2-4
* ビジネスオートメーション（株）

Contents

1. Introduction ---- 1
2. Development of Whole Energy Absorption Spectrometer (WEAS) ---- 3
   2.1 Principle and Outline of WEAS ---- 3
   2.2 Components of WEAS ---- 3
   2.3 Electronics ---- 5
   2.4 Detection Efficiency ---- 6
   2.5 Background ---- 7
   2.6 Reduction of Decay Heat ---- 7
3. Decay Heat Measurement ---- 8
   3.1 Sample Preparation ---- 8
   3.2 Irradiation and Measurement with WEAS ---- 9
   3.3 Pulse Height Spectrum ---- 11
   3.4 Neutron Source Characterization ---- 12
   3.5 Determination of D-T Neutron Flux ---- 14
   3.6 Energy Calibration ---- 15
   3.7 Data Processing ---- 16
   3.8 Determination of Correction Factors ---- 18
   3.9 Fluctuation of D-T Neutron Flux During Irradiations ---- 21
   3.10 Uncertainty of Experimental Data ---- 22
   3.11 Experimental Data of Decay Heat ---- 24
   3.12 Sample and Neutron Source Specification Needed for Calculation ---- 24
   3.13 Features of Decay Heat Measurement with WEAS ---- 25
4. Decay Heat Calculation ---- 28
   4.1 Codes and Nuclear Data Bases ---- 28
   4.2 Correction of Calculation Codes ---- 29
   4.3 Production of Decay Data Library for FENDL and JENDL ---- 30
   4.4 Calculation ---- 30
   4.5 Calculation with Other Code Systems ---- 31
5. Results and Discussion ---- 32
   5.1 Graphical Presentation of Results ---- 32
   5.2 Validity of Experiment and Calculation ---- 32
   5.3 Discussion on Results of ACT4 Calculations ---- 33
   5.4 Discussion on Results of CINAC Calculations ---- 46
   5.5 Summary of the Results ---- 48
   5.6 Impact on ITER Safety Design ---- 50
6. Conclusion ---- 52
Acknowledgment ---- 53
References ---- 54

目　次

1. はじめに …… 1
2. 全エネルギー吸収スペクトロメータ（WEAS）の開発 …… 3
2.1 WEASの原理と概要 …… 3
2.2 WEASの構成 …… 3
2.3 電子回路 …… 5
2.4 検出効率 …… 6
2.5 バックグラウンド …… 7
2.6 崩壊熱の導出 …… 7
3. 崩壊熱測定 …… 8
3.1 試料の準備 …… 8
3.2 照射とWEASによる測定 …… 9
3.3 パルス波高スペクトル …… 11
3.4 中性子源特性 …… 12
3.5 D-T中性子束の決定 …… 14
3.6 エネルギー校正 …… 15
3.7 データ処理 …… 16
3.8 補正係数の決定 …… 18
3.9 照射中のD-T中性子束の揺らぎ …… 21
3.10 実験データの不確定性 …… 22
3.11 崩壊熱の実験データ …… 24
3.12 計算に必要な試料と中性子源の特性 …… 24
3.13 WEASによる崩壊熱測定の特徴 …… 25
4. 崩壊熱計算 …… 28
4.1 コード及び核データベース …… 28
4.2 計算コードの修正 …… 29
4.3 FENDLとJENDLのための崩壊データライブラリの作成 …… 30
4.4 計　算 …… 30
4.5 他のコードシステムによる計算 …… 31
5. 結果と議論 …… 32
5.1 結果の図示 …… 32
5.2 実験及び計算の妥当性 …… 32
5.3 ACT4計算結果に関する議論 …… 33
5.4 CINAC計算結果に関する議論 …… 46
5.5 結果のまとめ …… 48
5.6 ITERの安全設計に対する影響 …… 50
6. 結　論 …… 52
謝　辞 …… 53
参考文献 …… 54

1. Introduction

When a loss of coolant/flow accident (LOCA/LOFA) takes place, plasma facing components of International Thermonuclear Experimental Reactor (ITER) such as blanket modules, divertor plates and baffle plats loose their coolant. The components are heated up by decay heat accompanied by disintegrations of a large amount of radioactivity induced by heavy exposure of D-T neutrons. Since these components have little thermal contact with their supports in the current design of ITER, they are isolated in a vacuum without coolant during the accident. The components can release the heat by thermal radiation, but hardly do it than by thermal conduction. Hence, the components are very liable to be heated up by the decay of induced radioactivities. If temperature of the components exceeds the allowable temperature due to the decay heat, the accident would expand to loose the integrity of ITER. Therefore it is crucial for the safety of ITER to estimate adequately the decay heat in the plasma facing components with reliable calculation codes and their data bases.

In the recent design of ITER, the beryllium-steam chemical reaction given below is the greatest concern.[1)]

$$Be + H_2O \text{ --> } BeO + H_2 + 370 \text{ kJ/mol} \qquad (1\text{-}1)$$

Beryllium which is used for the first wall and the neutron multiplier of the breeding blanket interacts with steam to produce hydrogen gas. When the hydrogen gas is accumulated more than the flammability limits (4 % for H_2 in air at atmospheric pressure), it becomes a potential source of an explosion. The exothermic chemical reaction further enhances the hydrogen gas production. According to the literature [1)], although the coefficient depends largely on property of beryllium such as solid or porous, increase of temperature by 100 °C results roughly in increase of hydrogen production by 1 ~ 2 order(s). Moreover, estimation of the temperature is very sensitive to uncertainties associated with decay heat prediction. According to the literature [1)] again, increase of decay heat by 40 % raises the maximum temperature by 80 °C. Consequently, increase of decay heat by 40 % corresponds roughly to increase of hydrogen production by more than 1 order. Therefore, uncertainties associated with the decay heat prediction less than 15 %, hopefully less than 10 %, are strongly requested by the designers of ITER. In addition to the safety aspect of ITER, accurate decay heat prediction is required for making reasonable shutdown scenarios of ITER.

To investigate prediction uncertainty of decay heat, comparisons of calculated

decay heat values with experimental data are the most straightforward way. During the recent fifteen years, experiments on induced radioactivity produced in D-T neutron environments have been extensively carried out. Gamma-rays emitted from irradiated samples were measured by high-purity germanium (HP-Ge) detectors. Major induced radioactivity calculation codes and the associated data bases, which are used actually in the designs of ITER, have been already verified through analyses of the experiments.[2, 3] These studies are, however, not sufficient for validating decay heat calculation codes and their data bases. Decay energy released by disintegrations of induced radioactive nuclides are conveyed by gamma-rays as well as beta-rays. A certain amount of the decay energy is attributed to beta-ray energy: more than a half for a considerable number of radioactive nuclides. In the field of fusion neutronics, no experiment has been devoted to direct measurements of decay heat arisen from induced radioactive nuclides because of, probably, the difficulty of beta-ray measurement compared to the gamma-ray measurement with HP-Ge detectors. Accordingly, validity of decay heat calculation codes and the associated nuclear data bases has not been investigated experimentally at all.

To overcome the situation, this work "Decay Heat Measurement" was conducted as a task (T-339) in the field of safety and environment, nuclear analysis under the Engineering Design Activity (EDA) of ITER in the period of January 1996 ~ December 1997. The following three items are involved in the task:

(1) Development of measuring techniques for decay heat,
(2) Systematic decay heat measurement on fusion reactor relevant materials irradiated by D-T neutrons, and
(3) Validation of decay heat calculation codes and the associated nuclear data bases.

Although efforts have been devoted to developing experimental techniques of decay heat in the task, this report concentrates on the most successful technique, namely, the Whole Energy Absorption Spectrometer (WEAS), by which an experimental data base of decay heat is obtained for a variety of materials for a wide range of cooling time.

In this report, development of WEAS is described in Chapter 2. Chapter 3 deals with the decay heat measurement with WEAS. Decay heat calculations with two Japanese calculation codes are described in Chapter 4. The experimental results are compared with the calculated decay heat values in Chapter 5, and detailed discussion is given for validity of decay heat calculation systems. Finally, Chapter 6 concludes the task, "Decay Heat Measurement".

2. Development of Whole Energy Absorption Spectrometer (WEAS)

2.1 Principle and Outline of WEAS

A schematic diagram of the Whole Energy Absorption Spectrometer (WEAS) is illustrated in Fig. 2.1.1. A pair of large bismuth-germanate ($Bi_4Ge_3O_{12}$, BGO) scintillators of 120 mm in diameter and 100 mm in thickness is the essential part of WEAS. Two photomultiplier tubes (PMTs) are attached to the scintillators. The scintillators and PMTs are enclosed by radiation shields to reduce background counts. All the equipments are contained in a dark box to shut out light from outside. Figure 2.1.2 shows a picture of WEAS viewed from outside.

Decay heat arises from either beta- and gamma-ray energy emitted from radioactive nuclides in an irradiated material. The energy deposited to a surrounding material is converted to heat. For the measurement with WEAS, an irradiated sample is sandwiched tightly by the BGO scintillators to realize the 4π geometry. Beta-rays emitted from the sample deposit directly their energy to the scintillators while gamma-rays are once converted into electrons via the photoelectric effect, Compton scattering and pair creation processes, and then, the electron energy is deposited to the scintillators. Through these processes, beta- and gamma-ray energies are detected by the scintillators with ~ 100 % efficiency. The deposited energy is converted proportionally into scintillation light, and the light output is then converted into an electric signal by the PMTs. In this way, an electric pulse signal which is proportional to the total beta- and gamma-ray energy is produced for each disintegration. Decay heat can be derived by accumulating the electric signals.

2.2 Components of WEAS

The BGO scintillators are selected because of the following reasons:

(1) Detection efficiency is very high for beta-rays and even for gamma-rays due to the high Z-number of bismuth (83) and the high weight density (7.13 g/cm^3) of the crystal. The high efficiency is essential to realize the "whole energy absorption".

(2) The scintillator has no hygroscopic character. A window material between the scintillators and a sample can be eliminated to prevent beta-ray energy loss in the window material. Hygroscopic scintillators such as NaI(Tl) are not suitable for beta-ray measurement.

(3) Transparency of the crystal is high for the scintillation light itself because no activator, such as thallium in the NaI scintillator, is added in. If transparency of a large scintillation crystal is low, light output per unit energy deposition depends on a distance between a PMT and the place of energy deposition.

(4) Decay constant of the scintillation light is moderate (there are two components of 60 and 300 ns) and no after-glow exists. The moderate decay constant is needed for high counting rate measurements.

Two BGO crystals are made by Crismatec company, France, and purchased via BICRON, USA. One of plane surfaces of the scintillator is polished for connection with the PMT while the other plane surface and the side surface, except for a window for samples, are coated with scintillation light reflector paint. Dimensions of the window are 30 x 30 mm^2 to place irradiated samples of nominally 25 x 25 mm^2, and the window is left without painting. When a sample is sandwiched, the gap width between the two scintillators is ~ 1 mm.

Photomultiplier tubes used are the type R877-01 (Hamamatsu Photonics, Japan) designed for scintillation counting. The box type dynodes are adopted to achieve high energy resolution. The potassium-free window glass is used to reduce background counts due to the natural radioactive isotope of ^{40}K. The PMTs are the 127 mm (5") type (outer diameter: 133 ± 1.5 mm, minimum diameter of the photo-cathode: 111 mm).

Figure 2.2.1 shows a pulse height spectrum (PHS) for a ^{137}Cs gamma-ray source (E_γ = 662 keV) measured by one of the BGO scintillators with the PMT. When we measure gamma-rays from ^{137}Cs with ordinary scintillators, the full energy peak is always accompanied by a Compton continuum due to low detection efficiencies. In Fig. 2.2.1, however, only a full energy peak is observed indicating the high (~ 100 %) detection efficiency of the BGO scintillator even for gamma-rays. Energy resolution of 12 % is achieved for the 662 keV gamma-rays. Figure 2.2.2 shows a PHS for a ^{152}Eu gamma-ray source which emits many gamma-ray lines as indicated with vertical bars in the figure. The PHS corresponds exactly to the gamma-ray lines even the unfolding procedure is not taken. This is another evidence for the high detection efficiency.

Typical dimensions of irradiation samples are 25 x 25 x 0.01 mm^3. Thin samples are used to reduce energy loss of beta-rays in the sample itself. On the lateral side of the dark box of WEAS shown in Fig. 2.1.2, there is an opening to insert the sample to the center of the two BGO scintillators through the dark box and radiation shield. A

sample cassette shown in Fig. 2.2.3 is used to insert the thin sample. A very thin plastic film of 0.5 mg/cm^2 is spread on a metallic cassette, and the sample is mounted on the film. Figure 2.2.4 shows the inside of WEAS where the cassette is inserted between the two BGO scintillators. Figures 2.2.5 and 2.2.6 explain how the cassette is inserted in WEAS through the opening. The sample is located at the right position where the windows of the BGO scintillators locate. After the insertion, the BGO scintillators on movable racks are closed tightly each other to sandwich the sample.

The opening is shut by two rollers. When pressure is applied to the rollers by the sample cassette, the rollers slightly open by the thickness of the cassette. These rollers function as a light shield to protect PMTs from room light. Owing to these mechanics, the sample can be inserted without switching off the high voltage for PMTs. This system makes it possible to mount the sample in a short time needed for short cooling time measurements. When the irradiated sample is ready to be mounted on the sample cassette, it takes less than 10 seconds to start the measurement.

2.3 Electronics

The electronic circuit associated with WEAS is included in Fig. 2.1.1. Photo-multiplier tube bases (CANBERRA Model 2007) are attached to the PMTs in the dark box. The initial dynode series resistors of the PMT bases are 10 MΩ and the decay constant of the output signals is ~ 200 μs. The resistors are changed to 54 kΩ to shorten the decay constant into ~ 17 μs. The shorter decay constant is desired for high counting rate measurement. The energy resolution is not degraded by the change of resistors.

High voltage of 1250 V, which is the nominal value for the R877-01 PMT, is applied by a high voltage power supply (HV: ORTEC 456H). Output signals from the PMT bases are provided into pre-amplifiers (PA: ORTEC 113), and amplified by delay-line amplifiers (DLA: ORTEC 460). Pulse height spectra for the dual BGO scintillators are measured independently by a multi-channel analyzer (MCA: CANBERRA Genie System) through analog-to-digital convertors (ADC: CANBERRA 8075) with the 1024 channels conversion. Each detector in the dual system is called as "Det_A" and "Det_B" for convenience, as indicated in Fig. 2.1.1. In addition, the output signals from the two DLAs are summed by a sum-amplifier (Sum-Amp: JAERI 719-1) and its PHS, called as "Sum" spectrum, is also obtained simultaneously.

The DLAs are selected because of their excellent feature for high counting rate

operation. Piling-up of output pulses hardly occurs even though piling-up pulses from the PAs are fed into the DLAs. The moderate decay constant of the BGO scintillators, the adjustment of the dynode series resistors of the PMT bases and the use of DLAs make it possible to measure decay heat even though counting rates are very high. In the decay heat measurements which will be described later, measurement is succeeded at a counting rate of 1.54 x 10^5 cps with dead time of 34 % without significant degradation of the measured data. The capability of high counting rate measurement is very important because counting rates just after irradiations are usually very high.

2.4 Detection Efficiency

The energy absorption efficiency, defined as a ratio of absorbed energy by the BGO scintillators to total decay energy, is calculated with the Monte Carlo electron-photon transport calculation code EGS4[4]. Figure 2.4.1 shows the calculated energy absorption efficiencies for electron, positron and photon. The electron efficiencies are ~ 100 %, but slightly smaller than 100 % even in the low-energy region because a small fraction of electrons escapes through the gap between the two scintillators. The electron efficiencies decrease with increase of energy because higher energy electrons likely to produce bremsstrahlung X-rays which can escape from the scintillator conveying some portions of decay energy. The photon efficiencies are close to 100 % below 0.5 MeV, ~ 90 % at 1 MeV and ~ 80 % at 2 MeV. These values suggest that consideration of the energy absorption efficiencies are needed in the decay heat measurement. The positron efficiencies are almost equal to electron efficiencies multiplied by the photon efficiency at 0.511 MeV.

These efficiencies are considered in the data reduction of decay heat as described later. For beta-rays excluding annihilation gamma-rays associated with positive beta-rays, a constant efficiency of 98 % is assumed regardless of beta-ray energy. For photons, the calculated efficiencies are fitted by three curves as

$$\varepsilon = 98.48 + 8.6532E - 19.165E^2 + 2.8947E^3, \quad (\mathrm{E} < 1\ \mathrm{MeV}) \tag{2-1}$$

$$\varepsilon = 119.22 - 39.127E + 12.338E^2 - 1.3226E^3, \quad (1\ \mathrm{MeV} < \mathrm{E} < 4\ \mathrm{MeV}) \tag{2-2}$$

and

$$\varepsilon = 77.737 - 1.0747E + 0.27072E^2 - 0.014267E^3, \quad (4\ \mathrm{MeV} < \mathrm{E}) \tag{2-3}$$

where ε is the energy absorption efficiency and E is the photon energy. These fitted curves are shown in Fig. 2.4.1. Smooth efficiency curves were derived by fitting the calculated efficiencies at discrete energy points.

2.5 Background

Background counts are reduced by the use of the potassium-free window glass of PMTs and the radiation shield. The radiation shield consists of three layers: lead of 50 mm (and more for some regions), copper of 5 mm and acrylic-plastic of 5 mm. The combination is usually adopted for the shield of HP-Ge detectors. The lead shield mainly reduces background radiations from outside. The copper shield reduces X-rays of ~ 85 keV emitted from lead, and the acrylic-plastic shield reduces X-rays of ~ 8 keV emitted from copper. The shield materials are arranged by a decreasing order in terms of their atomic numbers.

Figure 2.5.1 shows a typical background spectra for the Det_A, Det_B and Sum. Several clear peaks are observed in the spectra. No peak of potassium-40 is found at 1460.8 keV. All of the peaks observed are due to decay of bismuth-207 ($T_{1/2}$ = 31.55 years). A simplified decay scheme of bismuth-207 is illustrated in Fig. 2.5.2. The observed peaks can be explained by gamma-rays, X-rays (~ 80 keV) and conversion electrons emitted from bismuth-207. Since the bismuth-207 nuclide are contained in the scintillators themselves, the background can not be reduced meaningfully any more by adding additional shield. The overall bismuth-207 activity is 50 [Bq] which corresponds to 0.22 [Bq/cm^3] or 0.0031 [Bq/g]. A typical background counting rate for the Sum spectrum is ~ 70 [cps].

2.6 Reduction of Decay Heat

Decay heat value is deduced from the measured Sum-PHS according to the following formula.

$$\text{Decay Heat} = e \cdot f \cdot \sum_i \left(C_i \cdot E_i\right) \Big/ T \cdot m \quad . \tag{2-4}$$

Each count of the PHS (C_i at channel i) is multiplied by the corresponding energy (E_i [eV]) of the channel, and summed to obtain total deposited energy to the BGO scintillators. The total energy in the unit of [eV] is divided by the counting time (T [s]) and the sample mass (m [g]), and multiplied by the conversion factor (e: 1.602 x 10^{-19} [J/eV]). After applying necessary correction factors (f), which will be explained later, a decay heat value averaged during the measurement period is derived in the unit of [W/g]. More details of the data reduction will be described later.

3. Decay Heat Measurement

3.1 Sample Preparation

Thirty-two fusion relevant sample materials shown in Table 3.1.1 were used for the experiment. Eighteen samples are self-sustaining foils with an area of 25 x 25 mm^2, and the other fourteen samples are powder, which are sandwiched by plastic tapes of 24 x 24 mm^2. Two sets of the samples were prepared for short (5 minutes) and long (~ 7 hours) irradiations.

All of the self-sustaining samples except for Polytetrafluoroethylene (PTFE, so-called Teflon, CF_2) are metallic foils. Tables 3.1.2 and 3.1.3 shows properties of the self-sustaining samples for the 5 minutes and 7 hours irradiations, respectively. Most of the samples are pure metallic foils of purities higher than 99.8 %. Four alloy samples are also used in the experiment. Results of chemical analyses for compositions of the alloy samples are listed in Table 3.1.4. Two types of stainless steel (SS-304 and SS-316) and Inconel-600 are selected because of their importance as fusion structural materials. Since thin chromium sample is not easy to obtain, the Nichrome sample, which is an alloy of chromium and nickel, is used. It contains a large amount of chromium of ~ 20 % without iron constituent. Weight of the self-sustaining samples ranged between 24 and 133 mg. Errors associated with the weight are 0.1 mg, and all of the errors are less than 0.4 %. Thicknesses of them are in a range of 4 ~ 21 mg/cm^2 or 5 ~ 25 μm.

Tables 3.1.5 and 3.1.6 shows properties of the powder samples used for the 5 minutes and 7 hours irradiations, respectively. The use of powder samples enable wider choice of measurable materials because thin and pure metallic foils without any supporting materials are not easy to obtain for these materials due to physical and/or chemical unstable property. Powder was spread uniformly on a plastic tape (so-called Scotch tape) of 24 x 24 mm^2, and covered with another tape to make an irradiation sample. Purities for most of powders are higher than 99.98 %. Thicknesses of the powder samples depend on their grain sizes, and are in a range of 1 ~ 33 mg/cm^2. Weights of the powder samples were measured together with the plastic tapes, and the tape weight was subtracted. The tape weight was determined as 82.62 ± 0.37 mg by averaging weights of nine blank tape samples without powder. A sum of the uncertainty of the averaged tape weight (0.37 mg) and weighing error (0.1 mg), 0.38 mg in total, was adopted for the error of the powder samples. The errors ranged between 0.2 and 6.5 %. Some of the powder samples are oxide (Si, Ca, Y, Sn), carbonate (K, Na, Sr, Ba) or compound with carbon

(B). Carbon and oxygen atoms contained in these powder samples do not cause significant decay heat except for the ^{16}N nuclei with very short half-life of 7.13 s produced by the $^{16}O(n,p)^{16}N$ reaction.

Figure 3.1.1 explains how irradiation sample packets are prepared. The self-sustaining samples were stacked triply. The central sample was the sample for which decay heat is measured after a D-T neutron irradiation. The two outer samples compensate escape loss of recoil atoms produced by nuclear reactions from the central sample, and also prevent the center sample from impingement of impurities from outside. The powder samples were used alone because the plastic tapes functioned as recoil atom stoppers.

An aluminum foil of 18 μm or 50 μm in thickness with the same area as the sample was used for determination of D-T neutron fluence during an irradiation with using the $^{27}Al(n,\alpha)^{24}Na$ reaction. The aluminum foil was wrapped by thin paper. The stack of the irradiation sample together with the aluminum monitor foil was put into a small polyethylene bag, and the bag was sealed.

To consider decay heat generated in the plastic tapes used for the powder samples, blank samples consisting of only the tapes without any powder were prepared, and irradiated in just the same way as the usual samples.

3.2 Irradiation and Measurement with WEAS

The Fusion Neutronics Source (FNS) facility[5] in Japan Atomic Energy Research Institute was used for the irradiation. Since the decay heat measurement for this task was focused on decay heat arising from pure D-T neutrons, samples were irradiated under pure D-T neutron environment produced by minimizing materials around the sample which produced scattered low energy neutrons. The FNS facility had two beam lines for 0 and 80 degrees. In this experiment, the 80 degree beam line was used. The stational tritium target for the 80 beam line which was bombarded by a deuteron beam to produce D-T neutrons was smaller considerably than the rotating tritium target for the 0 degree beam line. The experimental room of the 80 degree beam line was much larger than that of the 0 degree beam line. The smaller target and the larger experimental room were suitable to attain purer D-T neutron field. Although neutron source intensity for the 80 degree beam line of ~ 3×10^{11} n/s was one order lower than that for the 0 degree beam line of ~ 3×10^{12} n/s, the D-T neutron flux on the samples of 10^9 ~ 10^{10}

n/s/cm^2 were still intense enough for the measurements.

Two series of irradiations were conducted for each sample to measure decay heat in a wide range of cooling time.

(1) 5 minutes irradiation for cooling time of 1 and 60 minute(s)
A sample pack including an irradiation sample and an aluminum monitor foil was rounded and put into a plastic case of 15 mm in inner diameter and 36 mm in height to make a transportation packet, so-called "rabbit". During D-T neutron generation, the rabbit was sent to one of three sample positions in front of the target by a pneumatic tube as shown in Fig. 3.2.1, and irradiated for 5.0 minutes. The three positions explained in Fig. 3.2.2, namely position #1, #2 and #3, were used to adjust neutron flux strength depending on samples. The deuteron beam current was usually ~ 2 mA, and sometimes reduced to 0.5 and 1.0 mA further adjustment of the neutron flux at the sample. Fluctuation of the D-T neutron intensity was assumed to be constant for 5 minutes. After the irradiation, the rabbit was taken back. The irradiated sample was taken out from the sample pack and inserted into WEAS. It took 30 ~ 40 seconds for all the preparation. At cooling time of ~ 1 minute, a measurement of decay heat was started. The measurement automatically proceeded by a command procedure given in Fig. 3.2.3. The procedure contains a repetition of start, stop, save and erase commands for the three MCAs for Det_A, Det_B and Sum. The time schedule is as follows:

10 seconds x 3 times,	30 seconds x 3 times,	1 minute x 3 times,
2 minutes x 4 times,	4 minutes x 4 times, and	10 minutes x 3 times.

Usually, measurements for 6 samples were conducted in one day (10:00 ~ 17:00), and decay heat data for all the 32 materials were measured in 2 weeks of machine time.

(2) 7 hours irradiation for cooling time more than 0.6 days (up to 400 days so far)
Irradiations were conducted twice. A half of the 32 samples were stacked with several aluminum monitor foils distributed in it, and sealed in a plastic bag. The sample packet was attached directly on the target, namely position #7 as shown in Fig. 3.2.2, without using the pneumatic tube. Total irradiation time was 7:34:30 (0.3156 days) and 7:10:00 (0.2986 days) for the first and the second irradiations, respectively. The deuteron beam current was ~ 2 mA throughout the irradiations. Fluctuation of D-T neutron intensity during the irradiations was monitored by the associated alpha-particle counter [5], and shown in Fig. 3.2.4. After about a half of days from the end of the irradiation, the sample packet was removed from the target and the irradiated samples were taken out

from the plastic bag. Measurements with WEAS were performed at every double cooling times, i.e., 0.6, 1.3, 3, 7, 13, 24, 50, 100, 200 and 400 days. The irradiated samples were measured one by one, usually for 2 ~ 10 minutes for one sample.

3.3 Pulse Height Spectrum

In this section, four examples of the measured pulse height spectra (PHS) are given to understand clearly how decay heat is measured with WEAS.

Figure 3.3.1 shows PHS for a copper sample measured at 7 minutes cooling after 5 minutes irradiation. The dominant radioactive nuclide contributing to the spectrum is ^{62}Cu produced by the ^{63}Cu(n,2n)^{62}Cu reaction. The two singles spectra denoted as Det_A and Det_B are measured by the individual BGO scintillator. These spectra are almost identical due to the symmetric configuration of the scintillators with respect to the sample. The sum spectrum in Fig. 3.3.1 corresponds to the total decay energy distribution of ^{62}Cu except for the neutrino energy. The ^{62}Cu nuclei disintegrate with emitting a β^+-ray which maximum kinetic energy is 2.926 MeV. The β^+-ray produces two annihilation gamma-rays of 0.511 MeV going toward the opposite direction from the sample, hence, one of the scintillators usually catches only one of the annihilation gamma-rays. The sharp peaks at 0.5 MeV observed in the singles spectra correspond to the annihilation gamma-rays. The tails ranging from 0.5 MeV to 3.5 MeV in the singles spectra are produced when one of the scintillators detects a β^+-ray as well as an annihilation gamma-ray simultaneously. On the other hand, two annihilation gamma-rays and a β^+-ray are always detected by the dual scintillators. The total energy of two annihilation gamma-rays, 1.022 MeV, is always deposited to the scintillators, and the kinetic energy of β^+-ray is superposed on it. Accordingly, the sum spectrum in Fig. 3.3.1 just corresponds to the β^+-ray spectrum of ^{62}Cu shifted by 1.022 MeV. This figure obviously suggests that entire energy emitted from the copper sample is detected by WEAS. The end point of the sum spectrum is equal to the Q-value of the decay, Q_{EC}. Accordingly, Q-values of beta-decays can be determined directly from the pulse height spectra measured with WEAS. Figure 3.3.2 shows a Kurie plot for the sum spectrum in Fig. 3.3.1 for ^{62}Cu. The straight line above 1.5 MeV crosses with X-axis at 2926 keV which corresponds to the maximum beta-ray energy of ^{62}Cu.

Figure 3.3.3 shows a sum PHS for an iron sample. The manganese-56 nuclide produced by the ^{56}Fe(n,p)^{56}Mn reaction contributes predominantly to the PHS. As illustrated in Fig. 3.3.3, ^{56}Mn nuclei decay mainly into the three excited levels of ^{56}Fe,

and the measured beta-ray spectrum consists of three components. The first component starts at 0.847 MeV and ends at 3.695 MeV, i.e., the Q-value of the β^--decay, when ^{56}Mn nuclei transit into the 0.847 MeV excited level of ^{56}Fe. The second and the third components start at 2.658 MeV and 2.960 MeV, respectively, and end at 3.695 MeV. As expected from this example, the end points of all the components converge at the Q-value of the decay although the parent nuclei decay into several excited levels of the daughter nuclei. This convergence is an advantage of WEAS for measurement of a Q-value of beta-decay because the convergence makes the end point clearer.

Figures 3.3.4 and 3.3.5 show PHS for titanium and nickel samples, respectively. Scandium-48 is observed in Fig. 3.3.4. Scandium-48 nuclei disintegrate with emitting a beta-ray of maximum energy of 661 keV followed by three cascade gamma-rays of 984, 1037 and 1312 keV with almost the 100 % emission probabilities per decay for all the three. When beta-ray energy is zero, the total deposited energy is the sum of the gamma-ray energy, i.e., 3333 keV, and when a beta-ray has the maximum energy, the total deposited energy corresponds to the Q_β-value (3994 keV) of ^{48}Sc. Accordingly, in Fig. 3.3.4, the pulse height spectrum of ^{48}Sc rises from 3333 keV and ends at 3994 keV. Note that the measured PHS is broadened by the energy resolution of the spectrometer, and the broadening is being enhanced in these figures due to adoption of the logarithmic Y-axes. In Fig. 3.3.5, sharp peaks at 0.811 MeV are observed in both singles and sum PHS. These peaks attribute to the gamma-rays from ^{58g}Co, which disintegrates through the electron-capture process without emitting any other beta- and gamma-rays than the 0.811 MeV gamma-ray. Like these ways, the observed PHS in Figs. 3.3.4 and 3.3.5 can be explained by the decay scheme of radioactive nuclides produced in the samples. The following physical quantities taken from the 8th edition of Table of Isotopes [6] exactly correspond to the observed PHS.

Titanium sample		Nickel sample	
Ca-45	Q_{β^-} = 256.8 keV	Fe-59	Q_{β^-} = 1565.1 keV
Ca-47	Q_{β^-} = 1991.9 keV	Co-57	E_γ = 136.5 keV
Sc-46	Q_{β^-} = 2366.7 keV	Co-58g (EC)	E_γ = 810.8 keV
Sc-47	Q_{β^-} = 600.1 keV	Co-58g (β^+)	Q_{EC} = 2307.4 keV
Sc-48	Q_{EC} = 3994 keV	Co-60	Q_{β^-} = 2823.9 keV

3.4 Neutron Source Characterization

Precise source neutron spectra at the four irradiation positions are needed for the

determination of D-T neutron fluence on the samples, and also, for experimental analysis. If the source spectra can be measured accurately, the measured spectra should be used. The source spectra were determined with Monte Carlo calculations as described below.

The Monte Carlo transport calculation code MCNP-4A [7] with a special routine [8] to generate D-T neutrons was used for the calculations. The routine contained a probability table of D-T reaction as a function of the deuteron energy in the $TiT_{1.7}$ target layer calculated with stopping power data and the D-T reaction cross section. A deuteron energy to induce a D-T reaction was sampled from the probability table. An emission angle for the generated neutron was sampled with an empirical formula [9]. The angular distribution of the emission in the center of mass system was almost isotropic, but slightly enhanced to the forward direction with respect to the deuteron beam direction. Next, neutron energy was determined by taking account of the kinematics of the D-T reaction. A position of neutron generation was sampled on the tritium target in a disk shape of 20 mm in diameter simulating the deuteron beam profile. This calculation procedure has been adopted for many experiments at FNS, such as cross section measurement [10] and shielding benchmark experiment [8], and validity of the procedure has been confirmed in these experiments.

The real target structure, the pneumatic tube and the rabbit were modeled precisely for the calculations. Neutrons were tallied by a cell detector rounded in the rabbit for the positions #1 ~ #3 shown in Fig. 3.2.2, and by a cell detector in a square shape attached on the target. Figures 3.4.1 ~ 3.4.3 show the calculated source neutron spectra in two different vertical scales. The 14-MeV neutron peaks are very intense as shown in Fig. 3.4.1. Overall shapes of the spectra at positions #1 ~ #3 are very similar. The low energy parts of the three spectra are mainly formed by neutrons scattered with hydrogen atoms contained in the pneumatic tube and the rabbit made of plastic. Low energy neutron component of the spectrum at the position #7 is much smaller than the others because the pneumatic tube and the rabbit are not used for the position. In Figs. 3.4.2 and 3.4.3, detailed peak shape of D-T neutrons depending on the sample positions are represented.

Figure 3.4.4 shows the source neutron spectrum at the position #1 (ϕ), the $^{27}Al(n,\alpha)^{24}Na$ reaction cross section (σ) and products of them ($\phi \times \sigma$). Figure 3.4.5 is a similar one but for the $^{115}In(n,n')^{115m}In$ reaction. The former cross section represents a typical threshold reaction while the latter cross section is one of the exceptional cross sections which have very low threshold energy and relatively small cross section at

14-MeV. Figure 3.4.4 indicates that the reaction can be considered as being induced by the 14-MeV neutrons only. Actually, 96.5 % of reactions are induced by neutrons above 13.88 MeV. Even for the ^{115}In(n,n')^{115m}In reaction, most of the reactions are caused by 14-MeV neutrons as shown in Fig. 3.4.5 in which 65.7 % of reactions are induced by neutrons above 13.88 MeV. Therefore, the experimental decay heat data are useful for decay heat induced mainly by 14-MeV neutrons.

On the other hand, as far as the (n,γ) reactions are concerned, the experimental decay heat data are not useful to examine calculations due to the following two reasons: (1) since the low-energy neutron components are very small, radioactive nuclides produced by the (n,γ) reactions contribute little to the total decay heat, and (2) even though radioactive nuclides produced by the (n,γ) reactions are dominant in the measured decay heat, the low-energy components of the source neutron spectra are not characterized so accurately. Although the ^{55}Mn(n,γ)^{56}Mn reactions for steel materials and the ^{186}W(n,γ)^{187}W reactions for plasma facing components made of tungsten are very important for safety designs of ITER, this experiment does not provide necessary information for validating decay heat of these reactions. This problem can be solved by performing another type of experiment with simulating a typical neutron spectrum of ITER that has considerable fraction of low-energy neutron flux to the total.

3.5 Determination of D-T Neutron Flux

The D-T neutron flux during the irradiation for each sample was determined by using the ^{27}Al(n,α)^{24}Na reaction. After the irradiation, the Al-foil was folded twice to make a smaller sample of ~ 12 x 12 mm^2. The activity of ^{24}Na in the sample was measured with a HP-Ge detector by detecting the 1368.6 keV gamma-rays after appropriate cooling. More than 10,000 peak counts were accumulated for all the samples. Neutron fluence ϕ was then calculated by the formula:

$$\phi = \frac{C \cdot A \cdot \lambda}{\varepsilon \cdot e \cdot a \cdot N \cdot \sigma_{DT} \cdot m \cdot \left(1 - e^{-\lambda t_i}\right) \cdot e^{-\lambda t_c} \cdot \left(1 - e^{-\lambda t_m}\right)} \cdot f_{dead} \cdot f_{sput} \qquad (3\text{-}1)$$

where

C:	peak counts
A:	atomic mass of aluminum, 26.98 [g/mol]
λ:	decay constant of ^{24}Na, 1.1121 [1/day] for $T_{1/2}$ = 14.959 [hr]
ε:	detection efficiency, 0.01980
e:	gamma-ray intensity per decay, 1.0

a: abundance of ^{27}Al in natural aluminum, 1.0

N: Avogadro's number, 6.022 x 10^{23} [atoms/mol]

σ_{DT}: cross section of the ^{27}Al(n,α)^{24}Na reaction

m: mass of aluminum foil [g]

t_i, t_c, t_m: irradiation, cooling and counting time, respectively

f_{dead}: correction factor for dead time, and

f_{sput}: correction factor for sputtering loss of ^{24}Na atoms.

Throughout this experiment, "D-T neutron" is defined as neutrons which energy is higher than 10 MeV. Thus the spectrum averaged ^{27}Al(n,α)^{24}Na reaction cross section σ_{DT} was determined as follows:

$$\sigma_{DT} = \frac{\int_{10}^{\infty} \sigma(E) \cdot \phi(E) \cdot dE}{\int_{10}^{\infty} \phi(E) \cdot dE} \tag{3-2}$$

where

$\sigma(E)$: the ^{27}Al(n,α)^{24}Na reaction cross section taken from JENDL Dosimetry File[11], and

$\phi(E)$: neutron spectrum at each sample position determined by the calculation.

The σ_{DT} values are 113 [mb] for the sample positions #1 ~ #3 and 116 [mb] for the sample position #7. Since no additional foils to compensate escape of ^{24}Na atoms was used for the aluminum monitor foils, the escape loss was corrected. The correction factor f_{sput} was estimated by considering experimental sputtering yield[12] measured by Ye, et al. The correction factor is 1.020 for aluminum foils of 50 μm in thickness used for all the 5 minutes irradiations and the second 7 hours irradiation, and 1.061 for aluminum foils of 18 μm in thickness used for the first 7 hours irradiation.

For 7 hours irradiations, neutron flux at each sample is determined by interpolating neutron fluxes on aluminum monitor foils distributed in the sample stacks. The determined neutron fluxes at 2 mA deuteron beam current are approximately 1 x 10^9, 4 x 10^9, 7 x 10^9 and 2 x 10^{10} [n/cm^2/s] for the sample positions #1, #2, #3 and #7, respectively.

3.6 Energy Calibration

The BGO scintillator has a considerably high temperature coefficient of the scintillation light output, about -1 [%/K] at the room temperature. Hence, the energy scale of PHS measured with WEAS was calibrated frequently. Gamma-rays of 661.66 keV emitted from a ^{137}Cs source of ~ 4000 Bq was used for the routine calibration. Peak channel of the gamma-ray was recorded before measurements.

Linearity of the energy scale was confirmed with several gamma-ray sources. Table 3.6.1 summarizes useful gamma-ray sources for the scaling. All of them except for ^{137}Cs decay with the electron capture processes without accompanying beta-rays, therefore, sharp gamma-ray peaks are observed in the measured spectra. These gamma-ray sources can be easily produced with the reactions indicated in Table 3.6.1 by irradiating the materials with D-T neutrons, and have suitable half-lives to use. The result of calibration is shown in Fig. 3.6.1. Linearity for all the three spectra is confirmed in the energy range from 320 keV to 2734 keV. In the case of Fig. 3.6.1 when the ^{137}Cs peak is at 123 channel of the multi-channel analyzer, a relation to convert the channel of the Sum-PHS (C) into energy (E in keV) was determined as

$$E = 4.9978 \times C + 8.25. \tag{3-3}$$

The offset channel at which the calibration line for the Sum spectrum reaches to zero energy is -1.65 throughout all the measurements.

Beyond the sum energy of the two gamma-rays from ^{88}Y at 2734 keV, there is no suitable gamma-ray source for the scaling. In this high energy region, the linearity was confirmed by decay Q-values. As already described in section 3.3, decay Q-values can be determined with the measured Sum-PHS. Decay Q-values for several nuclides, such as ^{24}Na (Q_{β^-} = 5515.79 keV), ^{56}Mn (Q_{β^-} = 3695.4 keV), ^{60}Co (Q_{β^-} = 2823.9 keV) and ^{62}Cu (Q_{EC} = 3948 keV) were determined with the energy scale given in Eq. (3-3), and the Q-values were compared with those in the literature[6]. As a result, good agreements within 2 % were confirmed.

3.7 Data Processing

The procedure of data processing for a powder sample sandwiched by the plastic tapes is explained below. Total decay heat including both the sample and the tape, dh_{total} [W], is calculated from the measured Sum-PHS for the sample and the background (no sample) as

$$dh_{total} = \left(\frac{\sum_i C_i \cdot E_i}{T} - \frac{\sum_i C_i^{BG} \cdot E_i}{T^{BG}} \right) \cdot e \cdot \frac{10^{10}}{\phi} \tag{3-4}$$

where

C_i: count in channel i of the Sum spectrum for the sample,

E_i: energy at channel i [eV]

T: live counting time for the sample [s]

C_i^{BG}: count in channel i of the Sum spectrum for the background,

T^{BG}: live counting time for the background [s]

e: the conversion factor from [eV] to [J], 1.602 [J/eV], which is the same as the charge of an electron, and

ϕ: average neutron flux during the irradiation [n/s/cm^2].

All the decay heat values are normalized for a nominal D-T neutron flux condition of 10^{10} [n/s/cm^2] throughout all the samples, hence, the factor 10^{10} is applied in Eq. (3-4). Decay heat only for the blank sample, dh_{blank}, is also calculated in the same manner as Eq. (3-4). The blank sample consists of the plastic tapes without any powder to consider decay heat generated in the tapes. The decay heat for the blank sample is subtracted from the total decay heat as

$$dh_{sample} = dh_{total} - dh_{blank} \tag{3-5}$$

to obtain decay heat originating only from the sample, dh_{sample} [W].

The final decay heat value, DH, in the unit of [W/g], is derived as

$$DH = \frac{dh_{sample}}{m} \cdot f \tag{3-6}$$

where

m: sample mass [g] and

f: correction factor.

The correction factor is for the gamma-ray efficiency, beta-ray energy loss in the sample and tapes, and the energy cutoff of Sum-PHS at ~ 50 keV. Detailed explanation for the correction factor is given later.

By this procedure, decay heat values were derived for all the 32 materials with the normalization for the nominal D-T neutron flux of 10^{10} [n/s/cm^2] and for 1 [g] sample materials. The normalization is convenient for comparisons of decay heat among a variety of materials as well as for a systematic decay heat calculation.

Tables 3.7.1 and 3.7.2 summarize several important parameters which affect on the decay heat data for the 5 minutes and the 7 hours irradiations, respectively. As for the 5 minutes irradiation, the largest dead time and the highest counting rate are recorded in the measurement for chromium and tungsten, respectively. The maximum dead time and counting rate are 17.4 % 37,800, respectively.

Dead time and counting rate for the 7 hours irradiation are much higher than those for the 5 minutes irradiation. The largest dead time of 56 % is recorded at the first measurement for aluminum with a very high counting rate of 120,000. The very high dead time is one of the reason to degrade the measured decay heat data. For other materials, although dead time exceeds more than 30 % for five materials, all the dead time is less than 35 %. Under this situation, it is found that the dead time correction is adequate. After the dead time corrections, the measured decay heat follows precisely the half-lives of the dominant radioactive nuclide. If dead time is less than 35 %, a high counting rate does not cause any problem even though it exceeds 100,000 cps. Experimental errors introduced by the dead time correction will be described later.

On the other hand, when the counting rate is low, the measured decay heat may contain somewhat larger uncertainties due to the background subtraction, and the subtraction of the blank sample for the powder samples. Generally speaking, when the fraction of the background to the total (foreground + background) and the fraction of the blank sample to the total (blank + sample) are less than 30 %, the measured decay heat is stable. When these fractions exceed 50, decay curves of the measured decay heat fluctuate around the decay curves expected from the half-lives. If the fractions exceed 70 %, the measured decay heat values could contain larger uncertainties due to the subtractions.

3.8 Determination of Correction Factors

The correction factor for the gamma-ray efficiency, beta-ray energy loss in the sample and tapes, and the energy cutoff of Sum-PHS at ~ 50 keV were determined as follows.

(1) Determination of dominant radioactive nuclides

The predominantly contributing nuclides to the measured decay heat are identified from analyses of the measured PHS, and also estimated by the decay heat calculations which will be described later. The dominant nuclides are included in Tables 3.7.1 and 3.7.2.

(2) Gamma-ray efficiencies

Gamma-ray energy E_i and its intensity per decay P_i for a dominant nuclide are

inquired into Ref. 13). The subscript i distinguishes gamma-rays having different energy. Then, the gamma-ray efficiency for the nuclide, η_γ, is calculated with the following formula:

$$\eta_\gamma = \sum_i E_i \cdot P_i \cdot \varepsilon(E_i) \Big/ \sum_i E_i \cdot P_i \tag{3-7}$$

where

$\varepsilon(E_i)$: gamma-ray efficiency at energy E_i defined by Eqs. (2-1) ~ (2-3).

All the dominant nuclides and the calculated gamma-ray efficiencies are listed in Table 3.8.1. The efficiencies for all the nuclides are larger than 80 % except for several short lived nuclides of which half-lives are less than 14 s.

(3) Correction factors for beta-ray energy loss in the samples and tapes

Beta-ray energy spectrum for each dominant nuclide is calculated. Figure 3.8.1 shows a short FORTRAN program list to calculate the spectrum. The major part of the program for calculation of Γ-function, the complex function of TCGAM, is taken from FPGS90 [14], which is a computer code for calculation of radioactive nuclide generation and depletion, decay heat and gamma-ray spectrum. Figure 3.8.2 explains input cards for the short program with an example for magnesium-27. All the decay data needed for the calculations are taken from Ref. 6). Examples of the calculated beta-ray spectra for ^{27}Mg, ^{56}Mn and ^{62}Cu are given in Fig. 3.8.3.

The energy loss process of a beta-ray is simulated by electron-photon transport calculations with MCNP-4B by precisely modeling the thin sample, plastic tapes and the BGO scintillators. The calculation algorithm for electron transport is improved in MCNP-4B from the previous version of MCNP-4A. The plastic tape consists of a base film made of acetylcellulose $(C_6H_{10}O_5)_n$ and glue made of acrylic-resin $(C_5H_8O_2)_n$, and their weight ratio is 73.5 : 26.5. Hence chemical composition of the tape is assumed to be $(C_{8.752}H_{12.288}O_{3.608})_n$. The thickness of a single tape is 14.3 mg/cm^2. Kinetic energy of beta-rays is sampled based on the calculated beta-ray spectra. Source beta-rays are generated uniformly in the sample region.

The results are summarized in Table 3.8.2. In the case of ^{32}P in the sulfur sample, for example, 39 keV, 84 keV and 570 keV per decay are absorbed in the sample itself, the plastic tapes and the BGO scintillators, respectively. Thus, 82 % of decay energy is detected by BGO while 18 % of the energy is lost in the sample and the tapes. Figure 3.8.4 shows comparison of measured and calculated spectra of beta-rays emitted

from ^{32}P in the sulfur sample sandwiched by the tapes. The initial beta-ray spectrum without tapes is also shown. The measured spectrum with tapes is shifted toward lower energy due to the energy loss, and the calculation reproduces the measured spectrum fairly well. Although slight discrepancies are observed in the low-energy region, it does not affect significantly to the total decay heat value because each count has an importance that is in proportion to the corresponding energy. The good agreement gives a proof that the Monte Carlo simulation is adequate for estimating the correction factors for the beta-ray energy loss in the samples and tapes.

Conversion electrons are sometimes emitted following decays of radioactive nuclides, and their energy also induces decay heat. Correction factors of energy loss of the conversion electrons are also calculated in the same way as the beta-rays. The discrete energy spectra of the conversion electrons given in Ref. 13) are used to sample source electron energy. The results are summarized in Table 3.8.3.

(4) Correction factors for the energy cut-off

The decay heat is derived from the measured PHS which has an energy cutoff at 50 keV. Pulse counts which do not exceed the cut-off energy are lost from the PHS. Correction factors for the lost counts for beta-rays and conversion electrons are estimated for several nuclides. Contribution of beta-rays and conversion electrons on decay heat is large for the investigated nuclides, i.e., gamma-rays do not contribute to the decay heat so much. From the calculated PHS for the energy loss correction, ratios of energy due to counts below 50 keV to the total energy detected by BGO are calculated. The results are included in Tables 3.8.2 and 3.8.3. In the case of ^{32}P in the sulfur sample, for example, the energy cut-off effect is minor as 0.16 % to the total because of the high beta-ray energy. The cut-off effect is also minor as less than 8 % for most of nuclides except for ^{180g}Ta in Ta (24 %), ^{185m}W in W (16 %) and ^{185m}W in Re (27 %).

(5) Overall correction factors

Overall correction factors for the gamma-ray efficiency, the energy loss and the cut-off effect are calculated, and the results are given in Table 3.8.4. The gamma-ray efficiency given in Table 3.8.1 and the correction factors for beta-rays and conversion electrons given in Tables 3.8.2 and 3.8.3, respectively, are averaged. Decay energy is conveyed mainly by the three components, i.e., gamma-rays, beta-rays and conversion electrons. The fraction of energy for each component to the total decay energy, which is

taken from Ref. 13), is used as a weight for the averaging. The overall correction factors given in Table 3.8.4 just correspond to the overall detection efficiencies of WEAS for each nuclide. Most of them are larger than 80 %.

Finally, the correction factors are applied for the decay heat values, as explained in Tables 3.7.1 and 3.7.2. If the measured decay heat is contributed by several different dominant nuclides, the correction factors for the nuclides are averaged with considering the contribution.

3.9 Fluctuation of D-T Neutron Flux During Irradiations

During the irradiations, D-T neutron fluxes fluctuate with time, as shown in Fig. 3.2.4. The fluctuation is not meaningful for the short irradiation for 5 minutes, but it should be considered in the 7 hours irradiations. Since it is not convenient to consider precisely the fluctuation in decay heat calculations, an ideal irradiation with constant neutron flux should be assumed in the calculations. Hence, influence of the fluctuation is investigated for the 7 hours irradiations.

The influence is a function of the irradiation history and half-lives of the produced radioactive nuclides. The fluctuation ratios R, which are ratios of numbers of produced nuclides with the real irradiation conditions to those with the ideal case, are calculated for various half-lives as

$$R = \int_0^T \phi(t) \cdot \exp[-\lambda \cdot (T-t)] \cdot dt \Big/ \int_0^T \phi_{const} \cdot \exp\left[-\lambda \cdot (T-t)\right] \cdot dt \qquad (3\text{-}8)$$

where

T: irradiation time,

$\phi(t)$: real neutron flux with fluctuation,

ϕ_{const}: constant neutron flux and

λ: decay constant of the produced nuclide.

The ϕ_{const} value is determined so that total numbers of neutrons generated during the two irradiations are the same, i.e.,

$$\int_0^{T_i} \phi(t) \cdot dt = \int_0^{T_i} \phi_{const} \cdot dt = \phi_{const} \cdot T_i . \qquad (3\text{-}9)$$

The fluctuation ratios for the irradiation histories shown in Fig. 3.2.4 are summarized in Table 3.9.1. Although several drops of neutron flux are seen in the first irradiation

(Aug. 2) in Fig. 3.2.4, the irradiation is almost constant. Hence, the fluctuation factors in Table 3.9.1 for the irradiation are very close to unity. On the other hand, the neutron flux during the second irradiation (Sep. 20) gradually decrease with time. The fluctuation factors for the irradiation are smaller than unity, especially for short lived nuclides.

For both irradiations, the fluctuation effects are less than 1 % for radioactive nuclides having longer half-lives than 10 hours. Hence, the fluctuation effect is investigated for nuclides actually observed in the measurement, and also for the aluminum monitor foils, as summarized in Table 3.9.2. The effect is negligibly small for the aluminum monitors because the half-life of ^{24}Na is longer than 10 hours. The fluctuation effect is important only for the three samples, i.e., ^{18}F ($T_{1/2}$ = 109.77 m) in CF_2, ^{41}Ar ($T_{1/2}$ = 109.34 m) in K_2CO_3 and ^{87m}Sr ($T_{1/2}$ = 2.803 h) in $SrCO_3$ samples. Since the fluctuation effect is minor as a whole, the experimental data are not corrected for the fluctuation. For the three nuclides, calculated results should be decreased by ~ 4 % for more accurate comparisons with the measured data.

3.10 Uncertainty of Experimental Data

(1) Sample weight

Errors of the sample weight have been described in Section 3.1 and Tables 3.1.2 ~ 3 and 3.1.5 ~ 6. All the errors for the self-sustaining samples are less than 0.4 %. Errors for the powder samples are larger than those for the self-sustaining samples because of the subtraction of tape weight. Except for CaO, SnO_2 and $BaCO_3$, all the errors are less than 3 %.

(2) Neutron flux monitor

D-T neutron fluxes are calculated by Eq. (3-1). Dominant error sources in the estimation is the cross section of the ^{27}Al(n,α)^{24}Na reactions including the uncertainty of the source neutron spectrum (4 %), detection efficiency of the HP-Ge detector (3 %) and statistical error of the gamma-ray counts (< 1 %). As a total, a value of 5.1 % is used.

(3) Energy calibration

The peak channel of gamma-rays from the ^{137}Cs source, usually at ~ 120 channel, is determined with uncertainty of ± 1 channel. Uncertainty of 1 % is used as the error of

energy calibration.

(4) Dead time

Ten % of the dead time fraction to the total measurement time is assumed as the error associated with the dead time correction. When dead time is 30 %, the correction error is 3 %.

(5) Subtraction of the background and the tape contributions

Five % of the subtracting value is adopted by considering variations of the background and tape contributions among several measurements. When D_{total}, D_{sub} and D_{net} are the total, subtracting and net quantities, the subtraction is expressed as

$$D_{net} = D_{total} - D_{sub}. \tag{3-10}$$

In this case, a value of (0.05 x D_{sub}) is adopted for the error of D_{net}. When D_{total} and D_{sub} are 1 and 0.5, respectively, D_{net} and its absolute error are 0.5 and 0.025, respectively.

(6) Correction factor

As the error of the correction factor for gamma-ray efficiency, energy loss of beta-ray and the energy cut-off effect, 20 % of the correction is adopted. When the correction factor is 0.8, the error associated with the correction is 4 % given by the next equation.

$$(1.0-0.8) \times 20 = 4 \tag{3-11}$$

(7) Uncertainty of the low energy part of neutron spectra

The source neutron spectra previously shown in Fig. 3.4.1 are regarded as highly accurate at ~ 14-MeV, while low energy parts of the spectra below 10 MeV could contain rather large uncertainties. Since the source neutron spectra are used for decay heat calculations, the uncertainties influence on the calculated decay heat due to radioactive nuclides produced by the (n,γ) reactions. Uncertainties of 20 % are added artificially to the errors of the measured decay heat when it is dominated by nuclides produced by the (n,γ) reactions.

(8) Overall experimental uncertainty

Overall experimental uncertainties are the sum of the uncertainties (1) ~ (7), and depend on the individual experimental conditions. In general, except for some specific cases, overall experimental uncertainties are less than 10 %.

3.11 Experimental Data of Decay Heat

The final experimental decay heat data with errors for the 5 minutes and the 7 hours irradiations are shown in Table 3.11.1 and 3.11.2, respectively. As mentioned above, all the decay heat data are normalized for 1 [g] of sample material irradiated under the D-T neutron flux of 10^{10} [n/s/cm^2]. Some comments about decay heat due to impurities, decay heat due to radioactive nuclides produced by the (n,γ) reactions and low signal to noise ratios, are given in the tables. No detectable decay heat is observed for the B_4C and SiO_2 samples irradiated for 7 hours.

3.12 Sample and Neutron Source Specification Needed for Calculation

Atomic densities of the samples needed for decay heat calculations are given in Table 3.12.1. The experimental decay heat is given in the unit of [W/g] while decay heat is often calculated in the unit of [W/cm^3]. The unit of [W/g] is better than [W/cm^3] because a number of atoms contained in 1 [g] can be determined uniquely, but a number of atoms contained in 1 [cm^3] depends on its weight density. To interface the two unit systems, weight densities for all the materials are assumed to be 1.0 [g/cm^3]. Under this assumption, decay heat in the unit of [W/g] is identical with that in [W/cm^3]. The number densities given in Table 3.12.1 are calculated with the weight density of 1.0 [g/cm^3].

Some samples contain impurities which significantly contribute to the measured decay heat. The impurities are, however, not contained in Table 3.12.1 because contents of the impurities are not known precisely.

Group-wise source neutron spectra at the four sample positions with their energy group boundaries are given in the following tables:

the Vitamin-J 175-energy groups	Table 3.12.2,
the 125-energy groups	Table 3.12.3,
the GAM-II 100-energy groups	Table 3.12.4,

the 42-energy groups Table 3.12.5.
These spectra are identical to the spectra shown in Figs. 3.4.1 and 3.4.2, but in different energy boundaries. Normalization factor for each sample position is also given in the tables. These are just the normalization factors to be multiplied to the calculated decay heat with the neutron spectra. These factors do not mean the total neutron fluxes. The neutron spectra in the 100- and 42-energy groups should not be used for calculations because of the too coarse energy bin widths at ~ 14-MeV. Actually, the 14-MeV neutron peak is represented in only one energy bin, and it results in rather worse results.

3.13 Features of Decay Heat Measurement with WEAS

The WEAS developed in this work is a unique measurement system of decay heat, and quite different from existing experimental apparatus for decay heat measurement. This section summarizes features of decay heat measurement with WEAS.

It should be noted first that the most remarkable weak point of WEAS is that decay heat arising from beta- and gamma-rays can not be measured separately. The separate measurement is possible by some of existing experimental techniques by which beta- and gamma-ray spectra are measured by two different spectrometers. The separate measurement is sometimes very useful to find out reasons, when a calculation disagree with an experimental decay heat.

Nevertheless, there are many favorable features in decay heat measurement with WEAS as follows:

(1) Simplicity

The principle of the measurement is considerably simple. The configuration of the twin BGO scintillators and a sample offers the 4π geometry. Detection efficiencies for both beta- and gamma-rays are ~ 100 %. No unfolding procedure with response matrices is needed in the data processing. The simplicity makes the measured results reliable because there is little room where uncertainties are introduced in.

(2) High sensitivity

Sensitivity is very high because the detection efficiency is ~ 100 %. According to the measured data, a very little decay heat of ~ 1 pW, which almost corresponds to 2 Bq

of ^{60}Co, can be measured. The high sensitivity is needed, in particular, for measurement of decay heat arising from long-lived radioactive nuclides after long cooling time.

(3) Capability for high counting rate measurement

Owing to the intrinsic character of the BGO scintillator of the moderate decay constant and the electronic circuit endurable against pulse pile-up which is mainly due to the use of delay-line amplifiers, considerably high counting rate measurements are possible. Measurements with counting rates higher than 10^5 cps with dead time up to 35 % are succeeded without degrading the measured data. This feature is important because most of samples just after the irradiation are very active.

(4) Wide dynamic range

Owing to the features (2) and (3), dynamic range of WEAS is very wide as more than four orders of magnitude. Decay heat measurements for 1 pW ~ 2 x 10^4 pW and for cooling time from 1 minute to 400 days are actually succeeded. The wide dynamic range is crucial for decay heat measurement because activity of a sample is very large just after the irradiation, and decreases significantly with cooling time.

(5) Pulse height spectrum

Pulse height spectrum data for both the singles and the sum signals are obtained in the measurement. The spectrum is very useful for identification of radioactive nuclides and energy calibration of the detection system needed for the decay heat measurement. Moreover, the spectrum data enable the WEAS to be applied for other research purposes such as decay Q-value measurement and beta-ray spectrum measurement.

(7) Small sample size

A small amount of sample, typically 30 mg, is enough for the measurement. This feature accompanies several advantages: low cost to prepare sample materials, simultaneous irradiation of many samples and low human exposure dose for experimentalists. This feature enable us to obtain a large amount of experimental data base of decay heat in a short time.

(8) Small experimental uncertainty

Finally, experimental uncertainties of the measured decay heat are usually less than 10 %. Since good accuracy less than 15 %, hopefully less than 10 %, in predicting decay heat is required for safety designs of ITER, the experimental uncertainty less than 10 % is absolutely needed.

4. Decay Heat Calculation

4.1 Codes and Nuclear Data Bases

To investigate validity of decay heat calculation systems, the experimental analyses were performed. The decay heat calculation systems consist of calculation codes, activation cross section libraries and decay data libraries. Four combinations of codes and libraries explained in Table 4.1.1 are employed for the calculations.

Two decay heat calculation codes, ACT4 and CINAC-V4, developed in Japan are used. The ACT4 code is the main calculation module of the THIDA code system [15] developed for calculation of transmutation, activation, decay heat and dose rate. The CINAC code [16] is the same as the ACT4 code in principle, and its calculation algorithm is refined to achieve much faster computation speed.

Three activation cross section libraries are used. The FENDL/A-2.0 [17] library (hereafter, FENDL) is assigned officially as the standard activation cross section for ITER/EDA, and contains 10423 reaction cross sections. The JENDL Activation File [18] (hereafter, JENDL) is a Japanese library which contains 1246 reaction cross sections mainly for nuclides with half-lives longer than 1 day. For these two activation cross section libraries, a decay data library derived from Evaluated Nuclear Structure Data File (ENSDF) available from Brookhaven National Laboratory, USA, and the literature values [13] is used. Detail of the library is described later in the section 4.3. To compare the two calculation codes with a common nuclear data base, FENDL is used for both the ACT4 and CINAC calculations. JENDL is used only for the ACT4 calculations.

The 1990's Library (hereafter, Lib90) consists of activation cross section and decay data libraries. The activation cross sections are based mainly on JENDL-3.1 [19] and SINCROS calculations [20]. Decay data are taken mostly from the older (7th) edition of the literature [6]. It is developed for the THIDA code system, and has been used by Japanese fusion reactor designers with combination with the ACT4 and CINAC-V4 codes for a long time, still in 1997. The Lib90 is used only for the CINAC calculations in the present work. Several invalid data are found in Lib90 through decay heat calculations, however, no correction is made. The Lib90 is used as it is to grasp status of accuracy of design calculations so far performed by the designers of ITER.

4.2 Correction of Calculation Codes

In the first stage of decay heat calculation, several programming errors were found in both the ACT4 and CINAC codes. These errors were corrected before the main calculations.

The following errors were found in the ACT4 code.

(1) When a decay has plural branches, the mean beta-ray energy of the decay is not treated correctly. This error is significant for β^+-decay nuclides because zero energy of electron capture (EC) processes are adopted for the total beta-ray energy of the decay, that is, β^+-ray energy is always omitted.

(2) When a decay has plural branches, such as EC & β^+ or β^- & IT, the branching ratios are multiplied to the mean beta-ray energy for each branch in the decay data library. The branching ratios are doubly multiplied again in the code.

These errors of the ACT4 code are corrected as shown in Fig. 4.2.1.

The following errors were found in the CINAC code.

(3) There is the same error as the item (2) of the ACT4 code.

(4) Reaction identification names which contain more than 9 characters are not treated correctly. One example of the names is "SN123N2NM" for the ^{123}Sn(n,2n)^{122m}Sn reaction.

These errors in the CINAC code are corrected as shown in Fig. 4.2.2.

After the corrections, still in some cases, calculations with CINAC encounter problems as explained below. No correction is mode for these errors.

(5) Although activation chain data for ^{92}Mo are included in the decay data library, CINAC can not find the data. A reason for this has not been found.

(6) Calculations for Zr, Sn and Ta terminate abnormally. A possibility for the termination has been recognized by the developer of the code. However, adequate solution has been given so far.

4.3 Production of Decay Data Library for FENDL and JENDL

The decay data library consists of so-called "chain" and "gamma" sub-libraries. The chain sub-library contains information about decay modes, parent and daughter nuclides, branching ratios, half-lives and mean beta-ray energy. If a conversion electron is emitted, its energy is included in the beta-ray energy. The gamma sub-library contains parents nuclides, gamma-ray energy and its emission probability.

To produce decay data library which is used with the FENDL and JENDL activation cross section libraries, the ENSDF library is processed. After that, the following modifications are taken.

(1) In the processed library, all the conversion electron data are missing, and zero energy is assigned for most of gamma-rays following isomeric transition processes. These data are supplemented by referring the literature [13].

(2) Invalid data are surveyed by a checking program for the following four items, and corrected. [i] Sum of branching ratios for plural decay modes: it must be unity. [ii] Too large beta-ray energy more than 5 MeV: there is no such case except for some light nuclides. [iii] Doubly defined half-lives. [iv] Duplicate data.

(3) The ^{180g}Ta nuclide is treated as a stable isotope. It is changed to a radioactive isotope.

(4) The daughter nuclide after a decay of ^{99}Mo is changed from ^{99g}Tc to ^{99m}Tc.

4.4 Calculation

Decay heat calculations were conducted for all the measurements with the four combinations of code and data base shown in Table 4.1.1. Examples of input data for the ACT4 and CINAC codes are shown in Figs. 4.4.1 and 4.4.2, respectively. For the ACT4/FENDL, ACT4/JENDL and CINAC/FENDL calculations, the source neutron spectra in the 125 energy groups are used because the finest energy bin widths are adopted at ~ 14-MeV for the 125 energy groups. For the CINAC/Lib90 calculations, the source neutron spectra in the 42 energy groups are used because activation cross sections are given only in the 42 energy groups. Since energy bin widths of the 42 energy groups at ~ 14-MeV

are rather large, ambiguity of ~ 10 % could be involved in the calculated decay heat values for such reactions that the cross section curves at ~ 14-MeV are steep.

4.5 Calculation with Other Code Systems

There are several decay heat calculation code systems developed in other countries, such as REAC (U.S.), FISPACT (U.K.), DKR (U.S.), ANITA (Italy), and so on. Calculations with these code systems are not conducted by the authors, Japan Home Team. Each institute that has developed the calculation code system has conducted the calculation to compare with the experimental data obtained in this work. Table 4.5.1 summarizes the institutes, codes and data bases employed for the decay heat calculations. The experimental data were distributed to the institutes at the end of July, 1997, and the institutes conducted decay heat calculations with their own code systems. On October 2-3, 1997, a workshop on "Decay Heat Validation for Fusion Reactors" was held at ITER Joint Work Site at San Diego, U.S.A., and the six international organizations from four countries attended to show their results. This is the first meeting on experimental validation of decay heat calculation systems for fusion reactors. The results of the workshop is reported in a paper[21].

5. Results and Discussion

5.1 Graphical Presentation of Results

The decay heat values calculated by ACT4 with FENDL and JENDL are compared with the measured data for all the 32 materials shown in Figs. 5.1.1 ~ 5.1.32. Each figure corresponds to each material one by one. Six sub-figures are included in each figure. The left and right hand side figures correspond to the 5 minutes and 7 hours irradiations, respectively. The upper two figures compare directly the experimental and the calculated decay heat values in the unit of [μW/g]. The middle two figures indicate predominantly contributing nuclei to the decay heat based on the ACT4/FENDL calculations. The lower two figures are calculated to experimental (C/E) ratios.

The decay heat values calculated by CINAC with FENDL and Lib90 are compared with the measured data for all the 32 materials in Figs. 5.1.33 ~ 5.1.43. Each figure contains results of direct comparison between the measured and calculated decay heat values for three materials. The left and right hand side figures correspond to the 5 minutes and 7 hours irradiations, respectively. For 7 hours irradiations, decay heat values are compared up to 100 days.

5.2 Validity of Experiment and Calculation

Validity of the experimental data as well as the calculation procedure is proven in this section. Measured and calculated decay heat values which are dominated practically by a unique radioactive nuclide are compared. If the activation cross section and decay property of the nuclides are known very well, and the measured and calculated decay heat values agree each other for many nuclides, the agreements justify the experimental data as well as the calculation procedure, i.e., the basic formula of Eq. (2-4) to deduce decay heat, energy calibration, gamma-ray efficiency, correction factor of beta-ray energy loss in the sample and tapes, other corrections, determination of D-T neutron flux, calculation procedure, comparison of measured and calculated decay heat values, and so on.

Six cases shown in Table 5.2.1 are investigated. The correction factors for the gamma-ray efficiency and beta-ray energy loss in the sample and tapes adopted to deduce decay heat values are included in Table 5.2.1. Five cases, i.e., the $^{27}Al(n,\alpha)^{24}Na$, $^{27}Al(n,p)^{27}Mg$, $^{56}Fe(n,p)^{56}Mn$, $^{90}Zr(n,2n)^{89m+g}Zr$ and $^{93}Nb(n,2n)^{92m}Nb$ reactions, out of six

are selected because cross sections for these cases are measured by HP-Ge detectors at FNS in absolute values[22]. These five reactions produce gamma-ray emitters while the rest for the $^{32}S(n,p)^{32}P$ reaction produces a pure beta-ray emitter and ^{32}P is used as a standard beta-ray source. The $^{32}S(n,p)^{32}P$ reaction is measured also at FNS by the Cherenkov radiation counting method associated with the beta-rays.

Figures 5.2.1 through 5.2.6 compares the cross sections measured and taken from JENDL Activation File, and also shows the cross section ratios. The cross sections in both agree fairly good. The cross section ratios at the peak energy of the source D-T neutron spectrum for each sample position are summarized in Table 5.2.2. The ratios of calculated to experimental values (C/E values) of the decay heat by ACT4 are also shown in Table 5.2.2. One of C/E values for various cooling times are selected under the conditions that the counting rate is not very high, the remarking reaction is dominant for the decay heat, and the background contribution is small. If the cross section ratios and the C/E values in Table 5.2.2 agree each other, it means that the cross section measurements and the decay heat measurements are consistent each other and the calculation procedure is adequate.

For the $^{27}Al(n,\alpha)^{24}Na$ reaction, both ratios agree very well although the correction factor for ^{24}Na, 0.82, is one of the lowest values. This agreement is important because the reaction is used to monitor the D-T neutron flux on the samples. The ^{32}P nuclide produced by the $^{32}S(n,p)^{32}P$ reaction is a pure beta-ray emitter, and the correction factor of 0.83 is also low mainly due to the beta-ray energy loss in the sample and tapes. The difference of the two ratios is somewhat large as 8 %. It could be attributed to the larger experimental uncertainty of 6.8 % in the decay heat measurement. Nevertheless, for all the six cases, both ratios agree as a whole . From these comparisons, it is concluded that the adequacy of decay heat measurements as well as the ACT4 calculations is verified in the criterion of ~ 5 %.

5.3 Discussion on Results of ACT4 Calculations

Detailed discussion about each sample material is given in this section. Table 5.3.1 summarizes key information for the discussion: dominant nuclides with their half-lives, production cross sections and decay data. The production cross sections based on FENDL and JENDL for the ninth group (14.324 ~ 14.550 MeV) of the 125 energy bins are compared with the cross sections measured [10, 22 ~ 26] at FNS and the OKTAVIAN facility at Osaka University. Beta- and gamma-ray energy per decay used in the

calculations and taken from Ref. 13) are shown. Ratios of total decay energy due to both beta- and gamma-rays used in the calculations to those taken from Ref. 13) are also shown.

(1) Boron Carbide (B_4C) [Fig. 5.1.1]

The measurement is aimed only at the ^{11}Be production ($T_{1/2}$ = 13.81 s) by the $^{11}B(n,p)^{11}Be$ reaction. The activity is observed only in the first few minutes after the 5 minutes irradiation. Another observed radioactivity with a longer half-life of ~ 20 minutes is ^{11}C produced by the proton-incident $^{11}B(p,n)^{11}C$ reaction where protons are provided from the plastic tapes and the B(n,xp) reactions in the sample. Since the coulomb barrier for protons in boron is not so high due to the low atomic number of ^{11}B, energetic protons can induce the $^{11}B(p,n)^{11}C$ reaction. The ^{11}C nuclei can not be produced by the $^{12}C(n,2n)^{11}C$ reaction due to their too high threshold energy more than 20 MeV.

At the beginning of the measurement when a relative contribution of ^{11}C is the lowest (~ 10 %), FENDL predicts the ^{11}Be production consistently with the experiment while JENDL predicts the ^{11}Be production ~ 30 % smaller than the experiment. This result suggests the too low (~ 30 %) $^{11}B(n,p)^{11}Be$ cross section in JENDL (4.4 mb) while the cross section in FENDL (5.8 mb) is adequate.

(2) Polytetrafluoroethylene (PTFE, Teflon, CF_2) [Fig. 5.1.2]

Two radioactive nuclides are observed: ^{19}O ($T_{1/2}$ = 26.91 s) and ^{18}F (109.77 m). The C/E values for cooling time regions where ^{18}F is dominant for the 5 minutes and 7 hours irradiations are consistent with each other. The FENDL calculation agrees with the experiment for both nuclides while the JENDL calculation does not. As for the JENDL calculation, the C/E value at 1 minute cooling when ^{19}O is the major source of decay heat is 0.8, and after 5 minutes, the C/E values are ~ 1.15. The results of decay heat measurement are consistent with the cross section measurement shown in Table 5.3.1. The $^{19}F(n,p)^{19}O$ and the $^{19}F(n,2n)^{18}F$ reaction cross sections in JENDL should be increased by 20 % and decreased by 15 %, respectively.

(3) Sodium Carbonate (Na_2CO_3) [Fig. 5.1.3]

Except for the two very short-lived nuclides of ^{16}N ($T_{1/2}$ = 7.13 s) and ^{20}F (11.00 s), three radioactive nuclides are observed: ^{23}Ne (37.24 s), ^{24}Na (14.959 hr) and ^{22}Na (2.602 y). The activity of ^{24}Na produced by the $^{23}Na(n,\gamma)^{24}Na$ reactions is largely underestimated by both FENDL and JENDL calculations. However, the reason could be the unclear low-energy part of source neutron spectrum. The ^{23}Ne production is calculated with good accuracy by JENDL while FENDL predicts it ~ 20 % smaller. The ^{22}Na production

is calculated smaller by both FENDL (~ 13 %) and JENDL (~ 25 %). Most parts of these discrepancies can be explained by the too small activation cross sections for the $^{23}Na(n,p)^{23}Ne$ and $^{23}Na(n,2n)^{22}Na$ reactions in both FENDL and JENDL compared with the measured data, as shown in Table 5.3.1.

(4) Aluminum (Al) [Fig. 5.1.4]

The decay heat is dominated by the ^{27}Mg ($T_{1/2}$ = 9.458 m) and ^{24}Na (14.959 h) produced by the $^{27}Al(n,p)^{27}Mg$ and $^{27}Al(n,\alpha)^{24}Na$ reactions, respectively. Agreements between the experiment and calculations by both FENDL and JENDL are very good for the 5 minutes irradiation. For the 7 hours irradiation, C/E values are 10 ~ 20 % far from the unity up to 3 days because the counting rates for the first two measurements are extremely high, i.e., dead time of 56 and 49 %. The third measurement at 2.9 days cooling is reasonable due to the moderate dead time of 10 %, and at this moment, both calculations predict accurately the experimental decay heat. After the decay out of ^{24}Na, the C/E values decrease rapidly because of impurities in the aluminum sample. According to the manufacture's catalogue (Goodfellow, Cambridge, U.K.), typical (but not actually measured) analysis of the sample is as follows:

Si: < 5000 ppm, Mn: < 1000 ppm, Fe: < 7000 ppm,
Cu: < 1000 ppm, Zn: < 1000 ppm.

The impurities are not considered in the calculations. The ^{54}Mn nuclide produced by the $^{56}Fe(n,p)^{54}Mn$ and $^{55}Mn(n,2n)^{54}Mn$ reactions mainly contributes to the measured decay heat after 10 days.

(5) Silicon Dioxide (SiO_2) [Fig. 5.1.5]

At the beginning of the measurement for the 5 minutes irradiation, ^{28}Al ($T_{1/2}$ = 2.2414 m) produced mainly by the $^{28}Si(n,p)^{28}Al$ reaction is dominant. Both calculations give smaller decay heat values by ~ 17 % in that time region. A source of the discrepancies has not been identified. After 30 minutes cooling, the ^{29}Al (6.56 m) and ^{27}Mg (9.458 m) nuclides produced mainly by the $^{29}Si(n,p)^{29}Al$ and the $^{30}Si(n,\alpha)^{27}Mg$ reactions become the major source of decay heat. In this time region, C/E values are getting worse with increase of time. The reason could be impurities contained in the sample. In fact, for the 7 hours irradiation, no activity from silicon but some unknown activities probably from impurities are observed.

(6) Sulfur (S) [Fig. 5.1.6]

The C/E curve of FENDL has a sharp peak at the cooling time of 1.6 minutes. This implies the too large $^{32}S(n,t)^{30}P$ cross section (0.016 mb at 14.4 MeV) while JENDL

gives the adequate cross section (0.006 mb). After 10 minutes cooling for the 5 minutes irradiation, the FENDL calculation agrees with the experiment while JENDL gives smaller C/E values of ~ 0.75. The reason is attributed to the $^{34}S(n,\alpha)^{31}Si$ cross sections: 135 mb in FENDL and 48 mb in JENDL. For the 7 hours irradiation, only the ^{32}P activity is a source of decay heat, and both calculations give good results.

(7) Potassium Carbonate (K_2CO_3) [Fig. 5.1.7]

The ^{38g}K ($T_{1/2}$ = 7.636 m), ^{38g}Cl (37.24 m) and ^{41}Ar (109.34 m) nuclides produced by the $^{39}K(n,2n)$ ^{38g}K, $^{41}K(n,\alpha)^{38g}Cl$ and $^{41}K(n,p)^{41}Ar$ reactions, respectively, are the dominant radioactive nuclides. For 5 minutes irradiation, JENDL predicts adequately the decay heat from all the radioactive nuclides. Decay heat of ^{38g}K by FENDL is 20 % smaller than that of JENDL. However, there is not such a large difference in the activation cross sections of FENDL and JENDL. Although the reason is not clear, it might be in the numerical calculation, i.e., matrix operation, of ACT4. The $^{39}K(n,2n)$ cross section is given as $^{39}K(n,2n)^{38m+g}K$ in JENDL while it is given separately as $^{39}K(n,2n)^{38m}K$ and $^{39}K(n,2n)^{38g}K$ in FENDL.

For the 7 hours irradiation, comparison is not so meaningful because contribution of ^{42}K produced by the $^{41}K(n,\gamma)^{42}K$ reactions with low energy neutrons is large.

(8) Calcium Oxide (CaO) [Fig. 5.1.8]

As for the 5 minutes irradiation, decay heat values calculated by FENDL is considerably larger than the experimental data. The $^{40}Ca(n,t)^{38m+g}K$ reaction cross section in FENDL (8.0 mb) is too large. The ^{44}K ($T_{1/2}$ = 22.13 m) by the $^{44}Ca(n,p)^{44}K$ reaction is dominant for the 5 minutes irradiation. The decay heat by JENDL is ~ 30 % smaller than the measured value, although the reason has not been identified.

In the decay heat for the 7 hours irradiation up to 10 days, the ^{42}K (12.360 h) and ^{47}Ca (4.536 d) nuclides produced mainly by the $^{42}Ca(n,p)^{42}K$ and $^{48}Ca(n,2n)^{41}Ca$ reactions, respectively, are dominant. The ^{47}Sc activity (3.345 d) is gradually accumulated being provided by the β^--decay of ^{47}Ca up to ~ 8 days, and after that, it decays out. Both the calculations treat the decay chain correctly. The C/E values are smaller than unity as a whole. One of the reasons could be large uncertainty of the sample weight (6 %) given in one standard deviation. The calcium oxide powder as well as the tin dioxide powder is the finest among all the powder, hence, the sample thickness is the thinnest among all the samples. The uncertainty of the tape weight subtraction is significant in this case.

(9) Titanium (Ti) [Fig. 5.1.9]

The ^{50g}Sc ($T_{1/2}$ = 102.5 s), ^{48}Sc (43.67 h) and ^{46g}Sc (83.79 d) nuclides produced by

the ^{50}Ti(n,p)^{50g}Sc, ^{48}Ti(n,p)^{48}Sc + ^{49}Ti(n,np)^{48}Sc and ^{46}Ti(n,p)^{46g}Sc + ^{47}Ti(n,np)^{46g}Sc reactions, respectively, are the dominant radioactive nuclides. A large difference is found for the ^{50g}Sc production between FENDL and JENDL. The difference comes from the difference of cross sections as shown in Table 5.3.1. Decay heat due to ^{50g}Sc is predicted larger by 20 % and smaller by 15 % by the FENDL and JENDL calculations, respectively. Both calculations predict the ^{48}Sc production smaller by 10 % while agree with the experiment for the ^{46g}Sc production. These trends are inconsistent with the cross section data: the ^{48}Sc production cross sections are slightly (3 ~ 4 %) larger than the measured data while the ^{46g}Sc production cross sections are ~ 15 % smaller than the measured data for both FENDL and JENDL. Since decay heat by ^{48}Sc and ^{46g}Sc is induced mainly by gamma-rays and energies of all the gamma-rays emitted from both nuclides are ~ 1 MeV, the correction factors for the gamma-ray efficiency of WEAS are nearly the same as ~ 90 % for both nuclides. Hence, the reason of the inconsistency between the decay heat and the cross section measurements is not understood.

Nevertheless, the ^{50}Ti(n,p)$^{50m+g}$Sc cross section in FENDL is given larger at least 20 %. Except for this, the decay heat of titanium by both the calculations agrees within 15 % with the experimental data.

(10) Vanadium (V) [Fig. 5.1.10]

Tow nuclides, the ^{51}Ti ($T_{1/2}$ = 5.76 m) and ^{48}Sc (43.67 h) produced by the ^{51}V(n,p)^{51}Ti and ^{51}V(n,α)^{48}Sc reactions, respectively, are important for vanadium. At the beginning for the 5 minutes irradiation, both calculations predict adequately the measured decay heat. After 30 minutes, the C/E values gradually decreases. Although the reason is not clear, it might be contributions from impurities (Al, Fe, Cu, etc.) in the vanadium sample because decay heat of vanadium decrease rapidly for the 5 minutes irradiation. According to the manufacture's catalogue (Goodfellow Co.), typical (but not actually measured) analysis of the sample is as follows:

Mg: 20 ppm,	Al: 200,	Si: 300	Ca: 5	Ti: < 50,	Cr: 3,
Mn: 5,	Fe: 60,	Co: < 10,	Cu: < 40,	Nb: < 250,	Mo: < 20,
Sn: < 20,	Ta: < 250,	W: < 500,	Pb: < 20.		

For the decay heat for the 7 hours irradiation dominated by the ^{48}Sc activity, both calculations agree with the experiment. No decay heat is detected after the last measurement at 24 days due to the low activation property of vanadium as a fusion reactor material.

(11) Chromium (Cr) [Fig. 5.1.11]

The ^{52}V ($T_{1/2}$ = 3.75 m), ^{49}Cr (42.3 m) and ^{51}Cr (27.702 d) nuclides produced

mainly by the $^{52}Cr(n,p)^{52}V$, $^{50}Cr(n,2n)^{49}Cr$ and $^{52}Cr(n,2n)^{51}Cr$ reactions, respectively, are the dominant radioactive nuclides. Large differences between the calculations and the experiment are found for the 5 minutes irradiation (cooling time > 30 m) and the 7 hours irradiation (cooling time < 10 d). These are due to impurities contained in the sample, especially, aluminum and iron. According to the manufacture's catalogue (Goodfellow Co.), typical (but not actually measured) analysis of the sample is as follows:

C: < 200 ppm, S: < 200, Al: < 2000, Si: < 1000, Fe: < 6000.

Except for the impurity effect, the ^{52}V production is given slightly smaller by the FENDL calculation. It can be attributed to the activation cross section as shown in Table 5.3.1. Results by both calculations agree within 10 % with the other measured decay heat values.

(12) Manganese (Mn) [Fig. 5.1.12]

The ^{52}V ($T_{1/2}$ = 3.75 m) and ^{55}Cr (3.497 m) nuclides produced by the $^{55}Mn(n,\alpha)^{52}V$ and $^{55}Mn(n,p)^{55}Cr$ reactions, respectively, contribute significantly to the decay heat for cooling time up to 20 minutes. In this time region, both FENDL and JENDL calculations predict the decay heat larger by 20 % and 15 %, respectively, suggesting too large cross sections of the $^{55}Mn(n,\alpha)^{52}V$ and/or $^{55}Mn(n,p)^{55}Cr$ reactions. Although the last half of cooling time region is dominated by ^{56}Mn (2.5785 h) produced by the $^{55}Mn(n,\gamma)^{56}Mn$ reaction, both calculations agree with the measured data within the experimental error ranges of 20 %. If we assume that adequate cross sections for the $^{55}Mn(n,\gamma)^{56}Mn$ reaction are given in FENDL and JENDL, the good agreements indicate that the low energy part of the source neutron spectrum flux is not so far from the actual one.

The decay heat for the 7 hours irradiation is induced only by ^{54}Mn (312.12 d) produced by the $^{55}Mn(n,2n)^{54}Mn$ reaction. Both calculations agree within 10 % with the measured data.

(13) Iron (Fe) [Fig. 5.1.13]

Very good agreements between the experiment and calculations are found in the decay heat for the 5 minutes irradiation dominated by the ^{56}Mn activity ($T_{1/2}$ = 2.5785 h) produced mainly by the $^{56}Fe(n,p)^{56}Mn$ reaction.

As for the 7 hours irradiation, after decay out of the ^{56}Mn activity, the ^{54}Mn activity (312.12 d) with small amount of ^{51}Cr activity (27.702 d) produced by the $^{54}Fe(n,p)^{54}Mn$ and $^{54}Fe(n,\alpha)^{51}Cr$ reactions, respectively, contribute to the decay heat. In this time region, the C/E values are constant at ~ 0.9. The $^{54}Fe(n,p)^{54}Mn$ cross section in FENDL and JENDL are larger than the measured data at FNS, and comparable with other experimental data, therefore, the activation cross sections in FENDL and JENDL

are not the reason for the C/E values. The reason could be impurities in the iron sample. According to the manufacture's catalogue (Goodfellow Co.), typical (but not actually measured) analysis of the sample is as follows:

Mg: 8 ppm, Al: 10, Si: 8, Ca: 40, Mn: 5, Co: 400,
Ni: 400, Cu: 400, Ag: 15, In: 8.

The large contents of cobalt and nickel impurities, which can make significant decay heat at longer cooling time due to the ^{58g}Co activity, can increase the measured decay heat of iron by several percentages.

(14) Cobalt (Co) [Fig. 5.1.14]

Decay heat for the 5 minutes irradiation is dominated by the ^{56}Mn activity ($T_{1/2}$ = 2.5785 h) produced by the ^{59}Co(n,α)^{56}Mn reaction. Agreements between the calculations and the experiment are excellent for both FENDL and JENDL. At the first measurement for the 7 hours irradiation, the C/E values are high at ~ 1.3. The reason lies in the experimental data. Although ^{58m}Co (9.15 h) is produced by the ^{59}Co(n,2n)^{58m}Co reaction, decay heat due to the ^{58m}Co activity is not contained in the measured data because the decay heat due to the ^{58m}Co activity arises only from conversion electrons and X-rays of very low energy: the electron energy is 24, 17 and 6 keV and the X-ray energy is ~ 7 keV. Most of the energy is absorbed inside the sample, and no correction is made for the energy loss. When the decay energy due to ^{58m}Co is excluded in the calculated results, the C/E values at the first and the second measurements approach to 1.0. After the third measurement where the ^{58g}Co activity (70.82 d) produced by the ^{59}Co(n,2n)$^{58m+g}$Co reaction is dominant, both calculations agree within 10 % with the experimental data. The slightly smaller C/E values by FENDL are consistent with the cross section data shown in Table 5.3.1.

(15) Nickel (Ni) [Fig. 5.1.15]

Many different nuclides contribute to the decay heat for both irradiations. They are

^{62g}Co ($T_{1/2}$ = 1.50 m) produced by the ^{62}Ni(n,p)^{62g}Co reaction,
^{60m}Co ($T_{1/2}$ = 10.47 m) produced by the ^{60}Ni(n,p)^{60m}Co reaction,
^{62m}Co ($T_{1/2}$ = 13.91 m) produced by the ^{62}Ni(n,p)^{62m}Co reaction,
^{57}Ni ($T_{1/2}$ = 35.60 h) produced by the ^{58}Ni(n,2n)^{57}Ni reaction,
^{58g}Co ($T_{1/2}$ = 70.82 d) produced by the ^{58}Ni(n,p)^{58g}Co reaction,
^{57}Co ($T_{1/2}$ = 271.79 d) produced by the ^{62}Ni(n,np)^{57}Co reaction, and
^{60g}Co ($T_{1/2}$ = 5.2714 y) produced by the ^{60}Ni(n,p)^{60g}Co reaction.

As for the 5 minutes irradiation, the low C/E values by JENDL in the first several

minutes suggest the low (10 ~ 20 %) ^{62}Ni(n,p)^{62g}Co cross section in JENDL. The low C/E values in the cooling time range of 10 ~ 40 minutes are attributed to the low activation cross sections for the ^{62}Ni(n,p)^{62m}Co reaction in both FENDL and JENDL. Figure 5.3.1 shows the cross sections compared with the measured data [25]. Both the evaluated cross sections are smaller than the measured data by > 30 %. At the last moment of the measurement for the 5 minutes irradiation and the beginning of the measurement for the 7 hours irradiation, decay heat is induced by the ^{57}Ni decay. Both the calculations agree with the experimental data in these time regions. Agreements between the calculations and the experiment are also good for ^{58g}Co. However, both calculations predict the decay heat smaller at cooling times of 200 and 400 days. There are two possible reasons for the underestimation: (i) as shown in Table 5.3.1, decay energy of ^{57}Co used in the calculations is 15 % smaller than that in the Ref. 13), and (ii) the sum of the ^{58}Ni(n,np)^{57}Co and ^{58}Ni(n,d)^{57}Co cross sections is 5 % smaller than the measured data at FNS. The smaller decay energy of ^{57}Co used in the calculations is due to omission of conversion electron energy.

(16) Copper (Cu) [Fig. 5.1.16]

The ^{62}Cu ($T_{1/2}$ = 9.74 m), ^{64}Cu (12.700 h) and ^{60g}Co (5.2714 y) nuclides produced mainly by the ^{63}Cu(n,2n)^{62}Cu, ^{65}Cu(n,2n)^{64}Cu and ^{63}Cu(n,α)$^{60m+g}$Co reactions, respectively, are the dominant radioactive nuclides. Agreements between the calculations and the experimental data are excellent within 10 % for ^{62}Cu and ^{64}Cu. Both calculations give ~ 25 % smaller decay heat for cooling time more than 10 days when the ^{60g}Co is the dominant nuclide. This is simply because of the too small ^{63}Cu(n,α)$^{60m+g}$Co cross section by ~ 20 % in FENDL and JENDL, as shown in Fig. 5.3.2.

(17) Strontium Carbonate ($SrCO_3$) [Fig. 5.1.17]

There are four important nuclides: ^{88}Rb ($T_{1/2}$ = 17.78 m), ^{87m}Sr ($T_{1/2}$ = 2.803 h), ^{83g}Sr (32.41 h) and ^{85g}Sr (64.84 d) produced mainly by the ^{88}Sr(n,p)^{88}Rb, ^{88}Sr(n,2n)^{87m}Sr, ^{84}Sr(n,2n)^{83g}Sr and ^{86}Sr(n,2n)^{85g}Sr reactions, respectively. Agreements between the calculations and experiment are good for decay heat by the ^{85g}Sr. However, agreements are not good for other cases due to several reasons as follows. (i) The ^{88}Sr(n,p)^{88}Rb cross sections in both FENDL and JENDL are ~ 30 % smaller than the measurement as shown in Table 5.3.1. (ii) No activation cross section is given for the minor isotope of ^{84}Sr (abundance: 0.56 %) in JENDL. (iii) The reaction product of the ^{88}Sr(n,2n) and ^{87}Sr(n,n') reactions is assigned improperly as ^{87g}Sr instead of ^{87m}Sr in JENDL. Hence decay heat due to ^{87m}Sr is not included in the JENDL calculation. (iv) Similarly, the reaction product of the ^{86}Sr(n,2n) reaction is given improperly as ^{85g}Sr instead of ^{85m}Sr in

JENDL. Hence decay heat due to ^{85m}Sr is not included in the JENDL calculation. (v) The ^{88}Sr(n,2n)^{87m}Sr cross section in FENDL is 10 % smaller than the measured data as shown in Table 5.3.1.

(18) Yttrium Oxide (Y_2O_3) [Fig. 5.1.18]

Most of decay heat for the 7 hours irradiation is due to the ^{88}Y activity ($T_{1/2}$ = 106.65 d) produced by the ^{89}Y(n,2n)^{88}Y reaction. Both calculations agree within 10 % with the experimental data. For the 5 minutes irradiation, however, some discrepancies between the calculations and the experiment are found. The reasons are as follows. (i) The ^{89}Y(n,n')^{89m}Y (16.06 s) and ^{89}Y(n,α)^{86m}Rb (1.017 m) cross sections are not given in JENDL. (ii) The ^{89}Y(n,α)^{86m}Rb cross section given in FENDL is much smaller than the experimental data as shown in table 5.3.1. (iii) Experimental data for cooling time of 10 ~ 60 minutes are not so reliable because, as shown in Table 3.7.1, contributions of the tapes and the background are significant in the total detected energy by WEAS. Thus, larger experimental uncertainty due to the subtraction of the contributions could be considered.

(19) Zirconium (Zr) [Fig. 5.1.19]

The ^{89m}Zr ($T_{1/2}$ = 4.18 m), ^{89g}Zr (78.41 h), ^{95g}Nb (34.975 d) and ^{95}Zr (64.02 d) nuclides are dominant. The ^{89m}Zr and ^{95}Zr activity is produced mainly by the (n,2n) reactions of ^{90}Zr and ^{96}Zr, respectively. The ^{89g}Zr is produced by the ^{90}Zr(n,2n)^{89g}Zr reaction as well as the decay (isomeric transition) of ^{89m}Zr. The ^{95g}Nb is a decay product of ^{95}Zr. The FENDL calculation agrees very well with the experimental data over the whole cooling time. The agreement means accurate activation cross sections as well as the correct treatment of the decay chains from ^{89m}Zr to ^{89g}Zr and from ^{95}Zr to ^{95g}Nb. The JENDL calculation also agrees with the experimental data except for the ^{89m}Zr production. The ^{90}Zr(n,2n)^{89m}Zr cross section is missing in JENDL.

(20) Niobium (Nb) [Fig. 5.1.20]

There are three important nuclides: ^{89m}Y ($T_{1/2}$ = 16.06 s), ^{90m}Y (3.19 h) and ^{92m}Nb (10.15 d) produced by the ^{93}Nb(n,nα)^{89m}Y, ^{93}Nb(n,α)^{90m}Y and ^{93}Nb(n,2n)^{92m}Nb reactions, respectively. The JENDL calculation predicts smaller the decay heat at the beginning of the measurements for the 5 minutes irradiation because the ^{93}Nb(n,nα)^{89m}Y reaction cross section is not included in the library. After 10 minutes cooling, both calculations agree within 10 % with the experimental data.

(21) Molybdenum (Mo) [Fig. 5.1.21]

Most of decay heat for the 5 minutes irradiation is arisen from the ^{91g}Mo ($T_{1/2}$ = 15.49 m) activity produced by the ^{92}Mo(n,2n)^{91g}Mo reaction. The JENDL calculation agrees with the measurement while decay heat by the FENDL calculation is ~ 20 % larger than the measurement. The overestimation is due to the large ^{92}Mo(n,2n)^{91m}Mo and ^{92}Mo(n,2n)^{91g}Mo cross sections in FENDL compared with the measured cross sections as shown in Table 5.3.1. (Note that the ^{91m}Mo nuclei decay into ^{91g}Mo with a probability of 50.1 %) Many kinds of radioactivity contribute to the decay heat for the 7 hours irradiation. As a whole, both FENDL and JENDL predict adequately the decay heat. It should be remarked that total decay energy used in the calculation differ more than 5 % from the literature values [13] for the three nuclides, ^{91m}Mo, ^{91m}Nb and ^{99}Mo.

(22) Tin Dioxide (SnO_2) [Fig. 5.1.22]

There are many contributing nuclides for both irradiations. In general, discrepancies between the calculations and the experiment are large. In the cooling time range up to 30 days, the C/E values are smaller than unity. One of the reasons could be the large uncertainty of the sample weight (6 %) as already explained for the calcium oxide sample. Another reason for the 5 minutes irradiation is found in the nuclear data of ^{111}Sn ($T_{1/2}$ = 35.3 m) produced by the ^{112}Sn(n,2n)^{111}Sn reaction. According to Table 5.3.1, the activation cross sections in both FENDL and JENDL are ~ 20 % smaller than the measured data. The decay energy used in the calculations is also smaller than the literature value [13] by ~ 4 %. In the cooling time range of 0.6 ~ 10 days for the 7 hours irradiation, the JENDL calculation gives very small decay heat values because the ^{117m}Sn and ^{119m}Sn activity mainly by the ^{118}Sn(n,2n)^{117m}Sn and ^{120}Sn(n,2n)^{119m}Sn reactions, respectivelt, is not considered in the calculation. These reaction cross sections are given adequately in JENDL. However, the reaction products are assigned as the stable nuclides of ^{117g}Sn and ^{119g}Sn, respectively, in the decay data library.

The decay energy used in the calculations are different significantly from the literature values as shown in Table 5.3.1. The mean beta-ray energy of 1140 keV for ^{123g}Sn used in the calculations is twice as large as the literature value of 523 keV. The large mean beta-ray energy of 1140 keV seems invalid in terms of its $Q_{\beta-}$-value of 1404 keV because mean beta-ray energy is usually close to 1/3 of the $Q_{\beta-}$-value. The too large decay energy of ^{123g}Sn increases the C/E values in the cooling time range longer than 100 days.

(23) Barium Carbonate ($BaCO_3$) [Fig. 5.1.23]

It should be remarked at first that the measured decay heat for the 5 minutes irradiation is contaminated by the ^{18}F activity which is probably transferred by the PTFE sample measured just before the measurement of barium carbonate. The ^{18}F activity is identified by an pulse height spectrum analysis and its half-life. Because of the contamination, comparison of the decay heat in the cooling time region of > 10 minutes is meaningless for the 5 minutes irradiation. The contamination is effective only for the measurement of barium carbonate sample irradiated for 5 minutes among all of the measurements.

Except for the contaminated cooling time region, the FENDL calculation predicts adequately the experimental decay heat for both the 5 minutes and 7 hours irradiations. Dominant reactions are the $^{138}Ba(n,2n)^{137m}Ba$ ($T_{1/2}$ = 2.552 m), $^{136}Ba(n,2n)^{135m}Ba$ (28.7 h), $^{134}Ba(n,2n)^{133m}Ba$ (38.9 h), $^{136}Ba(n,p)^{136m+g}Cs$ (13.16 d) and $^{132}Ba(n,2n)^{131m+g}Ba$ (11.50 d). On the other hand, the JENDL calculation underestimates largely the experimental decay heat. Although the $^{138}Ba(n,2n)^{137m}Ba$ reaction cross section is given in JENDL, the cross section is missing in the activation cross section library used for the calculation. According to the description attached to the cross section of ^{136}Ba in JENDL, the $^{136}Ba(n,2n)^{135m}Ba$ cross section is given. However, the ^{135g}Ba is assigned improperly as the products of the reaction instead of ^{135m}Ba.

(24) Tantalum (Ta) [Fig. 5.1.24]

There are three important nuclides: ^{180g}Ta ($T_{1/2}$ = 8.152 h), $^{182m2}Ta$ (15.84 m) and ^{178g}Lu (28.4 m) produced by the $^{181}Ta(n,2n)^{180g}Ta$, $^{181}Ta(n,\gamma)^{182m2}Ta$ and $^{181}Ta(n,\alpha)^{178g}Lu$ reactions, respectively. Both FENDL and JENDL calculations predict the decay heat considerably smaller for the 5 minutes irradiation due to the following reasons. (i) The $^{181}Ta(n,2n)^{180g}Ta$ reaction cross section in FENDL and JENDL are 36 % larger and 11 % smaller than the experimental data, respectively, as shown in Table 5.3.1. Also, the decay energy (54 keV) used in both the calculations is about a half of the literature values (102 keV) due to omission of X-ray and gamma-ray energy associated with the decay of ^{180g}Ta. (ii) Large uncertainties are expected in the calculated decay heat by $^{182m2}Ta$ due to the uncertainty of low energy part of the source neutron flux.

As for the 7 hours irradiation, the ^{180g}Ta activity is dominant up to 3 days, and the results are similar to those for the 5 minutes irradiation. After 3 days, ^{182g}Ta (114.43 d) and ^{181}Hf (42.39 d) produced by the $^{181}Ta(n,\gamma)^{182g}Ta$ and $^{181}Ta(n,p)^{181}Hf$ reactions become the dominant nuclides. Although the ^{182g}Ta activity produced by the (n,γ) reaction is included, decay heat values by FENDL are almost in the experimental error ranges. The JENDL calculation is smaller than the FENDL calculation because the ^{182g}Ta

production is given about a half of the FENDL calculation.

(25) Tungsten (W) [Fig. 5.1.25]

The experimental data include rather large uncertainties because most part of decay heat is induced by conversion electrons and low energy gamma- and X-rays which are easily absorbed by the sample itself. Nevertheless, if we rely on the experimental data, the followings can be stated. (i) The $^{186}W(n,2n)^{185m}W$ ($T_{1/2}$ = 1.67 m) cross sections in both FENDL and JENDL are too large. (ii) The $^{186}W(n,p)^{185}Ta$ (10.5 m) cross sections in both are also too large. (iii) The decay energy of ^{185g}W used in the calculations are 25 % larger than the literature value as shown in Table 5.3.1. This could be a reason of the somewhat larger C/E values for the 7 hours irradiation.

(26) Rhenium (Re) [Fig. 5.1.26]

Important nuclides for the decay heat are ^{184g}Re ($T_{1/2}$ = 38.0 d), ^{184m}Re (169 d), ^{186g}Re (90.64 h) and ^{188g}Re (16.98 h) produced mainly by the $^{185}Re(n,2n)^{184g}Re$, $^{185}Re(n,2n)^{184m}Re$, $^{187}Re(n,2n)^{186g}Re$ and $^{187}Re(n,\gamma)^{188g}Re$ reactions, respectively. Both calculated decay heat for the 5 minutes irradiation is larger than the experimental data. One of the reasons is the 20 % larger decay energy used in the calculations compared with the literature value. Uncertainty of the ^{188g}Re production by the (n,γ) reactions is another reason. As for the 7 hours irradiation, the slightly larger C/E values by FENDL for the first four measurements could be explained by the larger decay energy of ^{186g}Re as well as the larger activation cross section compared with JENDL as shown in Table 5.3.1. The rapid increase of the C/E curve by JENDL after 50 days is due to the too large $^{185}Re(n,2n)^{184m}Re$ cross section (696 mb) compared with the experimental data (335 mb).

(27) Lead (Pb) [Fig. 5.1.27]

The FENDL calculation predicts adequately the decay heat for the 5 minutes irradiation after 10 minutes cooling when the ^{204m}Pb activity produced by the $^{204}Pb(n,n')$ reaction is dominant. The JENDL calculation underestimates largely the decay heat due to ^{204m}Pb because the activation cross section is not given. In the first several minutes, the C/E values by FENDL are slightly smaller than 1.0, and those by JENDL are ~ 0.5. These C/E values suggest too small activation cross sections for one or some of the $^{208}Pb(n,p)^{208}Tl$ (3.053 m), $^{208}Pb(n,\alpha)^{205+g}Hg$ (5.2 m), $^{206}Pb(n,p)^{206m+g}Tl$ (4.199 m) and $^{207}Pb(n,p)^{207m+g}Tl$ reactions. The decay heat for the 7 hours irradiation is dominated by the ^{203g}Pb (51.873 h) activity produced by the $^{204}Pb(n,2n)$ reaction. The C/E values for the decay heat by both the FENDL and JENDL calculations about 0.6 are rather small.

This underestimation can be explained by the too small decay energy used in the calculation as shown in Table 5.3.1. In the decay data library, only the gamma-ray energy (244 keV/decay) is considered, and the conversion electron energy (49 keV/decay) and X-ray energy (68 keV/decay) are omitted.

(28) Bismuth (Bi) [Fig. 5.1.28]

Because of very small decay in bismuth induced by D-T neutrons, experimental uncertainties are very large. Nevertheless, at the beginning of the measurement for the 5 minutes irradiation, both the FENDL and JENDL calculations predict adequately the decay heat arisen from the ^{206g}Tl activity ($T_{1/2}$ = 4.199 m) produced by the ^{209}Bi(n,α)^{206g}Tl reaction. After 10 minutes cooling, although discrepancies are in between the calculations and the experiment, no conclusion can be deduced because of the large experimental uncertainties.

(29) Inconel-600 [Fig. 5.1.29]

Inconel-600 is an alloy (Ni: 76 %, Cr: 16 %, Fe: 8 %). Although nickel is the base material, major sources of decay heat for the 5 minutes irradiation are ^{52}V and ^{56}Mn produced from chromium and iron. On the other hand, for the 7 hours irradiation, radioactive nuclides originated from nickel are the major sources of decay heat. As described that the C/E values for pure chromium, iron and nickel are close to unity or 10 ~ 20 % smaller than unity, therefore, the C/E values for Inconel-600 are also somewhat smaller than unity. The C/E values of Inconel-600 is ~ 0.8 in the cooling time period up to 30 minutes, and then gradually approach to 1.0 for the 5 minutes irradiation. For the 7 hours irradiation, calculated decay heat by both FENDL and JENDL agree within 10 % with the experimental data.

(30) Nichrome [Fig. 5.1.30]

So-called Nichrome is an alloy of nickel (80 %) and chromium (20 %) without iron constituent. Important radioactivity produced from chromium is only ^{52}V in the first 30 minutes for the 5 minutes irradiation. Trends of the C/E values are very similar to those for the Inconel-600. Except for the first 30 minutes, the calculated decay heat by both FENDL and JENDL agree within ~ 10 % with the experimental data.

(31) Type 304 Stainless Steel (SS-304) [Fig. 5.1.31]

Chemical composition of the SS-304 has been shown in Table 3.1.4. Iron, chromium and nickel are the main constituents with small amount of silicon and manganese. At the beginning of the measurement for the 5 minutes irradiation, ^{52}V as well as ^{28}Al are

important. Especially, a careful attention must be paid to the constituent of silicon because, just after the 5 minutes irradiation, 17 % of decay heat is generated by the ^{28}Al activity produced from silicon although it is contained only 0.55 wt% in the SS-304. After ^{28}Al and ^{52}V decayed out, the ^{56}Mn activity produced from iron becomes the main contributor to the decay heat. And then, several nuclides produced from nickel, i.e., ^{57}Ni, ^{58g}Co, ^{57}Co, ^{60g}Co, as well as the ^{54}Mn activity produced from manganese and iron are dominant. Except for the cooling time of 200 and 400 days, the calculations by both FENDL and JENDL agree within 10 % with the experimental data. The decrease of the C/E values at the 200 and 400 days is explained by the reasons mentioned previously for the pure nickel sample.

(32) Type 316 Stainless Steel (SS-316) [Fig. 5.1.32]

All chemical composition of the SS-316 shown in Table 3.1.4 is nearly the same as that of the SS-304, but molybdenum of 2.11 % is contained only in the SS-316. Since the silicon content is as nearly twice as SS-304, the contribution of the ^{28}Al activity is significant as 27 % just after the 5 minutes irradiation. Although molybdenum is contained in the SS-316, its contribution to the total decay heat is not so significant. The largest contribution of molybdenum is the ^{99}Mo activity for the 7 hours irradiation where ~ 10 % of decay heat is arisen from the ^{99}Mo activity for the cooling time range of 1 ~ 10 days. The ^{54}Mn activity are produced by either the ^{55}Mn(n,2n)^{54}Mn and the ^{54}Fe(n,p)^{54}Mn reactions. As far as the 14-MeV energy is concerned, the ^{54}Mn production rates by the two reactions are almost comparable. Trends of the C/E values are very similar to those for the SS-304. In the cooling time range up to 100 days, the calculated decay heat by both FENDL and JENDL agree within 10 % with the experimental data.

5.4 Discussion on Results of CINAC Calculations

(1) Results with FENDL Library

As shown in Figs. 5.1.33 ~ 5.1.43, most of the CINAC calculations with the FENDL library give identical results with the ACT4 calculations. Since the FENDL library with the associated decay data library used in the CINAC calculations are exactly the same as those used for the ACT4 calculations, the identical results confirm correct decay heat calculation algorithm for either CINAC and ACT4 codes.

As mentioned earlier in the section 4.2, however, the CINAC calculations with FENDL for zirconium, tin dioxide and tantalum samples terminate abnormally. No

results with FENDL are given for the three samples. In addition, the decay data for ^{92}Mo can not be found by the CINAC calculation although the data are given properly. Hence, the calculated results for the molybdenum sample by CINAC are smaller than those by ACT4.

(2) Results with Lib90

As a whole, the CINAC calculations with Lib90 do not agree with the experimental data as the other calculations do. The most fundamental reason of the disagreements lies in the mean beta-ray energy contained in Lib90. Table 5.4.1 summarizes the decay data in Lib90 and the processed library for FENDL used in the CINAC calculations for the sulfur, copper and SS-304 samples. As for the ratios of gamma-ray energy in Lib90 to that in the library for FENDL shown at the right end of Table 5.4.1, though they are somewhat scattered, the ratios gather around the unity. On the other hand, the ratios for mean beta-ray energy are systematically smaller than the unity, typically at 0.6 ~ 0.7, except for several cases for minor radioactive nuclides of ^{28}Mg, ^{32}Si, ^{35}P and ^{35}S for which the ratios are rather large. The mean beta-ray energy in Lib90 is smaller than the literature values [13] in most cases while the energy in the library for FENDL is almost consistent with the literature values. Therefore, it can be stated that an improper treatment of the mean beta-ray energy exists in developing Lib90.

The Lib90 was developed nearly 10 years ago while FENDL/A-2.0 and JENDL Activation File have been available recently. Hence, the activation cross sections in Lib90 are not as accurate as those in FENDL and JENDL in general. This is another reason of the inaccurate results with Lib90. Moreover, the cross sections in Lib90 are given in the 42-energy group bins, and the 14-MeV neutron peak is treated by a single energy bin. About 10 % of uncertainties at most are introduced by the treatment depending on slopes of cross section curves at ~ 14-MeV.

In Fig. 5.1.33, the CINAC calculation with Lib90 seems to predict adequately the ^{11}C production by the ^{11}B(p,n)^{11}C reaction for the boron carbide sample irradiated for 5 minutes. The prediction is, however, invalid because CINAC/Lib90 can not deal with charged particle incident reactions. The decay heat component in the cooling time range of 5 ~ 60 minutes by the CINAC/Lib90 calculation is due to invalid cross section for the ^{12}C(n,2n)^{11}C reaction. Since the threshold energy of the ^{12}C(n,2n)^{11}C reaction is higher than 20 MeV, the reaction cross section for the first energy bin of the 42-energy group structure (13.72 ~ 15.00 MeV) must be zero. In Lib90, however, a finite cross section of

6 mb is given.

Decay chain data are not given for all the elements in Lib90. Among all the sample materials employed in the measurement, decay chain data are not given for strontium and yttrium. Accordingly, decay heat of the strontium carbonate and yttrium oxide samples are calculated extremely smaller.

5.5 Summary of the Results

(1) Calculation code

Two decay heat calculation codes developed in Japan, ACT4 and CINAC-V4, are tested in this work. After the initial modifications of these codes mentioned in the section 4.2, in principle, calculation algorithms for both codes are found to be correct by the numerous decay heat calculations.

The CINAC-V4 code, however, has a problem of abnormal terminations of calculations. The possibility has been recognized by the developer of the code. The terminations happen in matrix calculations when a complicated decay chain of radioactive nuclides is treated. Elimination of the problem is strongly recommended.

(2) Activation cross section library

Three activation cross section libraries are used: FENDL/A-2.0, JENDL Activation File and the cross section library included in Lib90. Use of Lib90 should be avoided because of the problems mentioned earlier.

Although the activation cross sections in FENDL and JENDL are accurate in most cases, inaccurate activation cross sections are identified in some cases through the comparison of the measured and calculated decay heat. Table 5.5.1 summarizes recommendation for modification of the cross sections in FENDL and JENDL. The recommendation is based on considerations for the discrepancies between the measured and calculated decay heat values as well as consistency of the evaluated cross section data with the measured data [10, 22-27].

Except for the inaccurate cross sections, FENDL/A-2.0 shows a very excellent capability to be used for decay heat calculations. All the cross sections for all the stable

nuclides, and even for many unstable nuclides, needed for fusion nuclear designs are included. The total number of cross sections more than 10,000 is a proof of the completeness.

When evaluation of JENDL Activation File started, activation cross sections which produce daughter nuclides having half-lives between 1 day and 10^7 years were selected. Recently an effort has been placed for that cross sections which produce daughter nuclides having half-lives less than 1 day have been included as well. As a result, total number of reactions are 1246. Although these cross sections are enough for calculating decay heat for most of materials, important cross sections are sometimes missing. As far as the decay heat calculations are concerned, the decision of the half-lives between 1 day and 10^7 years was not acceptable. Completeness of the cross section data base is not enough. The incompleteness of the cross section is the most significant problem of JENDL in terms of decay heat calculation because designers must check whether all the important cross sections are included or not before starting design calculations.

Information of the missing cross section is included in Table 5.3.1. The missing cross sections are denoted by the "x" marks. The cross sections for isomeric state production denoted by the "+" marks seem to be given in JENDL by evaluators according to the header information of the file. The reaction products are, however, assigned as in the ground states instead of the isomeric states. As for the cross sections denoted by the "=" marks, isomeric state production cross sections are given properly in JENDL, but treated as ground state production in the processed decay data library. This suggests that there is a problem of the processing code.

(3) Decay data library

As explained previously, the decay data library used with FENDL and JENDL are based on ENSDF, and some information is supplemented from the data in Ref. 13). The decay energy contained in the library is compared with the data in Ref. 13) in Table 5.3.1. As a general trend, decay energy in the two data bases agrees within ~ 3 % for relatively light nuclides up to niobium. No problem is found in the decay data library for light nuclides. For the heavier nuclides, however, large differences of the decay energy more than 10 % are found frequently. Most of the differences can be attributed to the omission of conversion electron and X-ray energy in the library used for the calculation. According to the comparison between the measured and calculated decay heat values for heavier nuclides, the calculated decay heat values approach to the

experimental data if the decay energy data are replaced by the data in Ref. 13). Mean beta-ray energy including conversion electron energy as well as total gamma-ray energy including X-ray energy are available for all the important nuclides in Ref. 13), ENSDF and FENDL/D-1.0. Therefore, use of these integrated type of decay energy is recommended for more accurate decay heat calculation.

5.6 Impact on ITER Safety Design

Impact on ITER safety design in terms of decay heat prediction is discussed for the three most important materials, SS-316, copper and tungsten.

(1) Type 316 stainless steel (SS-316)

The SS-316 is the structural material of ITER to be used for blankets, back-plates, vacuum vessel, and so on. As shown in Figs. 5.1.32 and 5.1.43, both ACT4 and CINAC codes predict adequately the experimental decay heat of SS-316 for cooling time up to 100 days when FENDL or JENDL is used. The C/E values range between 0.9 and 1.0. Hence, as far as the 14-MeV neutron field is concerned, we can conclude that decay heat of SS-316 can be calculated with uncertainties less than 10 % with the codes, activation cross section libraries and decay data bases. The cooling time range longer than 100 days, all the calculations give the decay heat ~ 15 % smaller than the experimental data. This underestimation does not cause a meaningful problem because such a long cooling time region is out of concerns in terms of the safety aspect of ITER design.

Some of activation cross sections related to SS-316 are evaluated smaller in both FENDL and JENDL as summarized in Table 5.5.1: the ^{52}Cr(n,p)^{52}V and ^{62}Ni(n,p)^{62m}Co cross sections in FENDL and the ^{62}Ni(n,p)^{62m}Co and ^{62}Ni(n,p)^{62g}Co cross sections in JENDL. Modifications of these cross section will increase prediction accuracy for decay heat of SS-316.

The 14-MeV neutron peak is very intense in the source neutron spectrum used in the experiment. As pointed out by Cheng and Saji [28], the ^{56}Mn activity produced by the ^{55}Mn(n,γ)^{56}Mn reaction with low energy neutrons as well as the ^{56}Fe(n,p)^{56}Mn reaction is the major source of decay heat of SS-316 in the realistic ITER environment where many low energy neutrons to induce the ^{55}Mn(n,γ)^{56}Mn reaction exist. Although the ^{56}Mn production by the ^{56}Fe(n,p)^{56}Mn reaction is validated in the present work, the ^{56}Mn production by the ^{55}Mn(n,γ)^{56}Mn reaction has not been investigated because of the

considerably small fraction of the low energy neutrons. Therefore, another effort for investigation on decay heat due to the ^{56}Mn activity produced mainly by low energy neutrons is needed in the future.

(2) Copper

Copper is used as a heat sink in the first wall composite by taking advantage of its excellent thermal conductivity. As shown in Figs. 5.1.16 and 5.1.38, decay heat values calculated by the ACT4 and CINAC codes with the FENDL and JENDL libraries agree within 10 % with the experimental data as far as the cooling time period up to 3 days is concerned. In that time period, the ^{62}Cu and ^{64}Cu nuclides produced mainly by the ^{63}Cu(n,2n)^{62}Cu and ^{65}Cu(n,2n)^{64}Cu reactions contribute to the decay heat. After these nuclides decay out, the ^{60g}Co activity produced by the ^{63}Cu(n,α)$^{60m+g}$Co reaction is the major source of the decay heat. In the cooling time region longer than 5 days, the C/E values are about 0.75. Therefore, the request to achieve 10 % accuracy for decay heat calculation is not satisfied in the time region. This result does not cause a significant problem for the safety design of ITER because the decay heat due to ^{60g}Co is ~ 10 times smaller than the decay heat of SS-316. Furthermore, it is easy to solve the problem by just increasing the ^{63}Cu(n,α)$^{60m+g}$Co cross section at ~ 14-MeV by 20 % in both FENDL and JENDL, as suggested in Table 5.5.1.

(3) Tungsten

Tungsten is a high temperature resistance material to be used for baffle and divertor plates in ITER. The major interest of tungsten is the decay heat due to ^{187}W produced by the ^{186}W(n,γ)^{187}W reaction with low energy neutrons. Treatment of the self-shielding effect of neutron fluxes for the giant resonance of the ^{186}W(n,γ)^{187}W reaction cross section at 19 eV in a thick tungsten plate is the major concern. The present experiment does not provide useful information for the concern because (i) the ^{187}W activity produced in the sample does not have significant contribution to the total decay heat as shown in Fig. 5.1.25 due to the small number of low energy neutrons in the source neutron spectrum flux, (ii) the low energy part of the source neutron spectrum is not well characterized, and (iii) the self-shielding effect is almost negligible in the thin sample of 6 μm. Accordingly, a new experiment is planned with simulating the neutron field of ITER where many low energy neutrons exist, and using a thick (~ 10 mm) tungsten plate.

6. Conclusion

Accurate prediction of decay heat on plasma facing components such as the first wall, blanket module, baffle and divertor plates is important for safety designs of ITER. A slight change of the decay heat prediction makes a large difference of the maximum temperature of these plasma facing components in case of LOCA/LOFA, and the difference results in considerably large uncertainty of the hydrogen gas production by the steam-beryllium chemical reaction. Eventually, small uncertainties less than 15 %, hopefully less than 10 %, are required for the decay heat calculations in ITER nuclear designs. Accuracy of decay heat calculation systems had, however, not been investigated experimentally because there had been no available experimental data of decay heat for fusion applications. To improve the situation, this task was devoted to give experimental validation of the decay heat calculation systems.

In this task, at first, the Whole Energy Absorption Spectrometer (WEAS) was developed to measure decay heat. A systematic experiment on decay heat for fusion reactor related materials was conducted at the Fusion Neutronics Source FNS/JAERI. Experimental decay heat data for 32 materials irradiated by 14-MeV neutrons were obtained for a wide range of cooling time from 1 minute to 400 days by taking full advantages of WEAS.

The experiment was analyzed by the two calculation codes, ACT4 and CINAC-V4, developed in Japan with FENDL/A-2.0 and JENDL Activation File as the cross section libraries and the decay data library based on ENSDF. The 1990's library (Lib90), which contained both activation cross sections and decay data, developed for the THIDA code system was also used. As a result, since some of problems found in the codes, activation cross sections and decay data were corrected, the calculations by ACT4 and CINAC with FENDL and JENDL predicted adequately the experimental decay heat values in most cases. According to this work, reasonable accuracy of the decay heat calculation systems used for nuclear designs of ITER have been demonstrated experimentally for the first time. Designers can rely on the calculation systems for future safety designs of ITER.

As far as the two most important materials for ITER, i.e., type 316 stainless steel and copper, irradiated by 14-MeV neutrons are concerned, the ACT4 and CINAC calculations with FENDL/A-2.0 and JENDL Activation File agreed within ± 10 % with the experimental data for a cooling time period up to 3 days. This result demonstrated that the targeted accuracy of ± 10 % for predicting the decay heat for the two important

materials can be satisfied by those calculation systems.

Acknowledgment

The authors are grateful to Drs. H.-W. Bartels, G. Saji and N. Tailor of ITER San Diego Joint Central Team, and also, Drs. S. Matsuda, Y. Seki and T. Inabe of Japan Home Team for their promotion of this task. They deeply appreciate to Dr. E. T. Cheng of TSI Research, USA, and Dr. Y. Kasugai of Spallation Neutronics Laboratory of JAERI for their useful help and discussions for the task. They wish to express their thanks to Drs. K. Maki and K. Shibata of Hitachi, Ltd., Dr. H. Kawasaki of CRC Research, Ltd., and Dr. H. Iida of ITER Garching Joint Central Team for their suggestions for using the ACT4 and CINAC-V4 codes. They also wish to express their thanks to the operation staff of FNS, C. Kutsukake, S. Tanaka, T. Ono, Y. Abe and M. Seki, for their operation of the D-T neutron source at the FNS facility.

References

1) Bartels H.-W., Cheng E., Gaeta M., Merril B. and Petti D.: "Decay Heat Removal in the ITER Outline Design", Fusion Eng. Des., 31, pp. 203-219 (1996).

2) Ikeda Y., et al.: "Measurements and Analyses of Decay Radioactivity Induced in Simulated Deuterium-Tritium Neutron Environments for Fusion Reactor Structural Materials", Fusion Technol., 28, pp. 74-98 (1995).

3) Kumar A., et al: "Decay Radioactivity Induced in Plasma-Facing Materials by Deuterium-Tritium Neutrons", Fusion Technol., 28, pp. 99-155 (1995).

4) Nelson W. R., Hirayama H. and Rogers D. W. O.: "The EGS4 Code System", SLAC-265, Stanford Linear Accelerator Center (1985).

5) Nakamura T., Maekawa H., Ikeda Y. and Oyama Y.: "A DT Neutron Source for Fusion Neutronics Experiments at the JAERI", Proc. International. Ion Eng. Congress - ISIAT '83 & IAPT '83, Kyoto, Japan, Vol. 1, pp. 567-570 (1983).

6) Firestone R. B. and Shirley V. S. (Ed.): "Table of Isotopes, Eighth Edition", John Wiley and Sons, Inc., New York, (1996).

7) Briesmeister J. F. (Ed.): "MCNP - A General Monte Carlo N-Particle Transport Code, Version 4A", LA-12625-M, Los Alamos National Laboratory (1993).

8) Maekawa F., et al.: "Bulk Shielding Experiments on Large SS316 Assemblies Bombarded by D-T Neutrons Volume II: Analysis", JAERI-Research 94-044 (1994).

9) Benveniste J., et al: "The Problem of Measuring the Absolute Yield of 14-MeV Neutrons by Means of an Alpha Counter", Nucl. Instrum. Meth., 7, pp. 306-314 (1960).

10) Ikeda Y., et al.: "Activation Cross Section Measurements for Fusion Reactor Structural Materials at Neutron Energy from 13.3 to 15.0 MeV Using FNS Facility", JAERI 1312 (1988).

11) Nakazawa M., Kobayashi K., Iwasaki S., Iguchi T., Sakurai K., Ikeda Y. and Nakagawa T.: "JENDL Dosimetry File", JAERI 1325 (1991).

12) Ye B., Kasugai Y. and Ikeda Y.: "Systematic Study on Sputtering Yields by 14.9 MeV Neutrons", JAERI-Research 97-082 (1997).

13) Browne E. and Firestone R. B.: "Table of Radioactive Isotopes", John Wiley and Sons, Inc., New York, (1986).

14) Ihara H., Katakura J. and Nakagawa T.: "A Computer Code for Calculation of Radioactive Nuclide Generation and Depletion, Decay Heat and Gamma-Ray Spectrum - FPGS90 -", JAERI-Data/Code 95-014 (in Japanese, 1995).

15) Seki Y., et al.: "THIDA-2: An Advanced Code System for Calculation of Transmutation, Activation, Decay Heat and Dose Rate", JAERI 1301 (1986).

16) Fukumoto H.: J. Nucl. Sci. Technol., 23, pp. 97-109 (1986).

17) Pashchenko A. B.: "Summary Report for IAEA Consultants' Meeting on Selection of Evaluations for the FENDL/A-2 Activation Cross Section Library", INDC(NDS)-341, International Atomic Energy Agency (1996).

18) Nakajima Y.: "Status of the JENDL Activation File", JAERI-Conf 96-008, pp. 50-55 (1996).

19) Shibata K., et al.: "Japanese Evaluated Nuclear Data Library, Version-3 -- JENDL-3 --", JAERI 1319 (1990).

20) Yamamuro N.: "A Nuclear Cross Section Calculation System with Simplified Input Format Version II (SINCROS-II)", JAERI-M 90-006 (1990).

21) Taylor N. P., et al.: "Experimental Validation of Calculations of Decay Heat Induced by 14 MeV Neutrons Activation of ITER Materials", Fusion Eng. Des., 45, pp. 75-88 (1999).

22) Ikeda Y., Konno C., Oyama Y., Kosako K., Oishi K. and Maekawa H.: "Absolute Measurement of Activation Cross Sections of $^{27}Al(n,p)^{27}Mg$, $^{27}Al(n,\alpha)^{24}Na$, $^{56}Fe(n,p)^{56}Mn$, $^{90}Zr(n,2n)^{89m+g}Zr$ and $^{93}Nb(n,2n)^{92m}Nb$ at Energy Range of 13.3 ~ 14.9 MeV", J. Nucl. Sci. Technol., 30, pp. 26-36 (1993).

23) Verzilov Y. M., Maekawa F., Oyama Y. and Ikeda Y.: "Measurements of the $^{32}S(n,p)^{32}P$ and $^{35}Cl(n,\alpha)^{32}P$ Reaction Cross Sections in the Energy Range of 13.3-14.9 MeV and Their Integral Test below 14 MeV", Fusion Eng. Des., 37, pp. 95-105 (1997).

24) Konno C., et al.: "Activation Cross Section Measurements at Neutron Energy from 13.3 to 15.0 MeV Using the FNS Facility", JAERI 1329 (1993).

25) Kasugai Y., et al.: "Measurement of (n,p) Cross-Sections for Shortlived Products by 13.3-14.9 MeV Neutrons", Ann. Nucl. Energy, 25, pp. 23-45 (1998).

26) Kasugai Y., et al.: "Measurement of (n,α) Cross-Sections for Shortlived Products by 13.3-14.9 MeV Neutrons", Ann. Nucl. Energy, 25, pp. 1485-1502 (1998).

27) Katoh T., Kawade K. and Yamamoto H.: "Measurement of Activation Cross Sections", JAERI-M 89-083 (in Japanese, 1989).

28) E. T. Cheng and Saji G.: Fusion Technol., 30, pp. 1411-1415 (1996).

Table 3.1.1 Sample materials used in the decay heat measurement.

Self-Sustaining Sample		Powder Sample	
Al	Mo	B_4C	Y_2O_3
Ti	Ta	Na_2CO_3	SnO
V	W	SiO_2	$BaCO_3$
Fe	Pb	S	Re
Co	Inconel-600	K_2CO_3	Bi
Ni	NiChrom	CaO	
Cu	SS-304	Cr	
Zr	SS-316	Mn	
Nb	PTFE (CF_2)	$SrCO_3$	

Table 3.1.2 Properties of the self-sustaining samples used for the 5 minutes irradiation.

Material	Purity	Weight			Thickness	
	[%]	[mg]	Error [mg]	Error [%]	[mg/cm^2]	[μm]
Al	99.2	24.1	0.1	0.41	3.86	18
Ti	99.6+	37.7	0.1	0.27	6.03	12.5
V	99.8+	85.5	0.1	0.12	13.68	25
Fe	99.85	32.5	0.1	0.31	5.20	6
Co	99.9	41.3	0.1	0.24	6.61	6
Ni	99.95	31.1	0.1	0.32	4.98	6
Cu	99.9	32.7	0.1	0.31	5.23	6
Zr	99.8+	26.8	0.1	0.37	4.29	7
Nb	99.9	34.9	0.1	0.29	5.58	6
Mo	99.95	33.4	0.1	0.30	5.34	5
Ta	99.9	49.6	0.1	0.20	7.94	5
W	99.95	65.0	0.1	0.15	10.40	6
Pb	99.99+	38.8	0.1	0.26	6.21	5
Inconel-600	#	132.8	0.1	0.08	21.25	25
Nichrome	#	25.8	0.1	0.39	4.13	5
SS-304	#	37.6	0.1	0.27	6.02	8
SS-316	#	35.9	0.1	0.28	5.74	7.5
PTFE (CF_2)	--	98.2	0.1	0.10	17.05	18

See Table 3.1.4.

Table 3.1.3 Properties of the self-sustaining samples used for the 7 hours irradiation.

Material	Purity	Weight			Thickness	
	[%]	[mg]	Error [mg]	Error [%]	[mg/cm^2]	[μm]
Al	99.2	24.2	0.1	0.41	3.87	18
Ti	99.6+	37.5	0.1	0.27	6.00	12.5
V	99.8+	85.4	0.1	0.12	13.66	25
Fe	99.85	32.9	0.1	0.30	5.26	6
Co	99.9	37.7	0.1	0.27	6.03	6
Ni	99.95	31.3	0.1	0.32	5.01	6
Cu	99.9	31.3	0.1	0.32	5.01	6
Zr	99.8+	26.7	0.1	0.37	4.27	7
Nb	99.9	31.8	0.1	0.31	5.09	6
Mo	99.95	32.0	0.1	0.31	5.12	5
Ta	99.9	46.0	0.1	0.22	7.36	5
W	99.95	68.9	0.1	0.15	11.02	6
Pb	99.99+	38.6	0.1	0.26	6.18	5
Inconel-600	#	133.2	0.1	0.08	21.31	25
Nichrome	#	25.8	0.1	0.39	4.13	5
SS-304	#	38.5	0.1	0.26	6.16	8
SS-316	#	36.0	0.1	0.28	5.76	7.5
PTFE (CF_2)	--	98.1	0.1	0.10	17.03	18

See Table 3.1.4.

Table 3.1.4 Chemical compositions for alloy samples in weight percentage.

Material	Si	Cr	Mn	Fe	Ni	Mo
Inconel-600		15.97	0.39	7.82	balance	
Nichrome		19.64		0.06	balance	
SS-304	0.55	18.02	1.44	balance	8.82	
SS-316	0.96	18.28	1.57	balance	13.49	2.11

Table 3.1.5 Properties of the powder samples used for the 5 minutes irradiation.

Material [g]	Purity [%]	Sample+Tape [mg]	Weight Sample [mg]	Error [mg]	Error [%]	Thickness [mg/cm^2]
B_4C		135.9	53.3	0.38	0.72	9.25
Na_2CO_3	99.98	135.6	53.0	0.38	0.72	9.20
SiO_2		95.5	12.9	0.38	2.97	2.24
S		121.0	38.4	0.38	1.00	6.67
K_2CO_3	99.95	273.8	191.2	0.38	0.20	33.19
CaO	99.9	89.3	6.7	0.38	5.72	1.16
Cr	99.0+	152.8	70.2	0.38	0.55	12.19
Mn	99.98	114.8	32.2	0.38	1.19	5.59
$SrCO_3$	99.99	95.9	13.3	0.38	2.88	2.31
Y_2O_3	99.999	97.2	14.6	0.38	2.63	2.53
SnO_2	99.99	92.4	9.8	0.38	3.91	1.70
$BaCO_3$	99.99+	89.0	6.4	0.38	5.99	1.11
Re	99.99	140.3	57.7	0.38	0.66	10.02
Bi	99.999	150.7	68.1	0.38	0.56	11.82

Table 3.1.6 Properties of the powder samples used for the 7 hours irradiation.

Material [g]	Purity [%]	Sample+Tape [mg]	Weight Sample [mg]	Error [mg]	Error [%]	Thickness [mg/cm^2]
B_4C		134.0	51.4	0.38	0.75	8.92
Na_2CO_3	99.98	133.7	51.1	0.38	0.75	8.87
SiO_2		95.2	12.6	0.38	3.04	2.19
S		118.1	35.5	0.38	1.08	6.16
K_2CO_3	99.95	282.1	199.5	0.38	0.19	34.64
CaO	99.9	89.0	6.4	0.38	5.99	1.11
Cr	99.0+	163.4	80.8	0.38	0.47	14.03
Mn	99.98	115.2	32.6	0.38	1.18	5.66
$SrCO_3$	99.99	97.7	15.1	0.38	2.54	2.62
Y_2O_3	99.999	95.9	13.3	0.38	2.88	2.31
SnO_2	99.99	92.5	9.9	0.38	3.87	1.72
$BaCO_3$	99.99+	88.5	5.9	0.38	6.50	1.02
Re	99.99	142.6	60.0	0.38	0.64	10.42
Bi	99.999	162.4	79.8	0.38	0.48	13.85

Table 3.6.1 Gamma-ray sources useful for energy calibration of WEAS.

Nuclide	Decay Mode	Half Life	Gamma-ray Energy [keV]	Gamma-ray Intensity [%]	Production Reaction
Cr-51	EC	27.704 d	320.084	9.83	^{52}Cr(n,2n)
Mn-54	EC	312.20 d	834.826	99.975	^{55}Mn(n,2n)
Co-58g	EC, β^+	70.916 d	810.791	99.5	^{59}Co(n,2n)
Zn-65	EC, β^+	244.1 d	1115.518	50.75	^{66}Zn(n,2n)
Sr-85	EC	64.84 d	513.996	99.27	^{86}Sr(n,2n)
Y-88	EC	106.61 d	898.065	92.7	^{89}Y(n,2n)
			1836.077	99.35	
			2734.142	(Sum)	
Nb-92m	EC	10.15 d	934.53	99.0	^{93}Nb(n,2n)
Cs-137	β^-	30.0 y	661.660	85.21	#

available as a standard beta-ray source

Table 3.7.1 Important parameters affecting on the experimental data for the 5 minutes irradiation. (1/9)

Experimental Condition \ Parameters		Cooling Time [min]	Dead Time [%]	Counting Rate [cps]	BG Fraction [%]	Tape Fraction [%]	Dominant Nuclide(s)	Correction Factor
Sample	Blank Tape	1.02	0.10	216	15.39			
Date	17-Sep-96	1.28	0.20	171	24.09			
Irradiation start time	12:13:00	1.55	0.10	155	27.91			
Irradiation stop time	12:18:00	1.83	0.10	153	30.30			
Irradiation Time [min]	5.000	2.45	0.10	134	33.90			
Neutron Flux		3.07	0.10	130	36.18			
[n/sec/cm^2]	2.004E+09	3.72	0.08	124	38.20			
Cs-137 Peak Channel	115	4.78	0.08	123	40.15			
Sample Weight [g]	0.0826	5.90	0.08	119	41.65			
error [%]	0.45	7.03	0.07	110	46.49			
Back Ground	10116	9.10	0.07	103	51.28			
		11.22	0.06	99	55.33			
Position #	3	13.33	0.06	93	61.05			
		15.42	0.05	89	65.80			
		19.55	0.05	83	73.01			
		23.67	0.05	80	78.18			
		27.78	0.04	79	81.29			
		31.92	0.04	73	89.81			
		42.05	0.04	71	95.07			
		52.18	0.04	74	89.79			
Sample	B4C	1.13	1.40	2,235	1.57	9.29	Be-11	0.9279
Date	20-Sep-96	1.40	1.00	1,599	2.82	9.72	↓	0.9279
Irradiation start time	9:53:00	1.67	0.60	1,277	4.47	12.84	↓	0.9279
Irradiation stop time	9:58:00	1.95	0.50	1,090	6.42	16.76	↓	0.9279
Irradiation Time [min]	5.000	2.57	0.47	979	8.03	18.08	↓	0.9279
Neutron Flux		3.18	0.40	897	9.14	18.83	↓	0.9279
[n/sec/cm^2]	4.669E+09	3.82	0.35	832	10.20	19.51	↓	0.9279
Cs-137 Peak Channel	51	4.93	0.33	755	11.59	20.74	↓	0.9279
Sample Weight [g]	0.0533	6.05	0.32	691	13.05	22.32	↓	0.9279
error [%]	0.72	7.18	0.27	630	14.79	21.21	↓	0.9279
Back Ground	10006	9.30	0.24	559	17.22	20.98	↓	0.9279
		11.42	0.21	503	19.42	20.66	↓	0.9279
Position #	3	13.55	0.20	461	21.45	18.50	↓	0.9279
		15.68	0.17	409	24.37	17.78	↓	0.9279
		19.75	0.15	354	28.42	15.58	↓	0.9279
		23.87	0.13	310	32.48	14.25	↓	0.9279
		28.00	0.12	274	36.98	14.34	↓	0.9279
		32.08	0.10	225	45.06	9.88	↓	0.9279
		42.17	0.08	175	57.78	7.53	↓	0.9279
		52.23	0.06	140	71.51	30.31	↓	0.9279
Sample	PTFE (CF2)	1.03	3.70	7,806	0.39		O-19	0.9252
Date	20-Sep-96	1.30	2.80	5,930	0.56		↓	0.9252
Irradiation start time	12:06:30	1.57	2.20	4,647	0.77		↓	0.9252
Irradiation stop time	12:11:30	1.83	1.57	3,485	1.16		↓	0.9252
Irradiation Time [min]	5.000	2.45	1.17	2,761	1.70		↓	0.9252
Neutron Flux		3.07	1.07	2,479	2.08		O-19, F-18	0.9400
[n/sec/cm^2]	6.347E+08	3.70	0.95	2,339	2.32		F-18	0.9597
Cs-137 Peak Channel	51	4.82	0.92	2,275	2.42		↓	0.9597
Sample Weight [g]	0.0982	5.93	0.92	2,242	2.46		↓	0.9597
error [%]	0.10	7.07	0.90	2,231	2.48		↓	0.9597
Back Ground	5105	9.18	0.90	2,201	2.52		↓	0.9597
		11.30	0.87	2,170	2.55		↓	0.9597
Position #	3	13.43	0.87	2,141	2.59		↓	0.9597
		15.57	0.84	2,092	2.65		↓	0.9597
		19.63	0.83	2,043	2.71		↓	0.9597
		23.75	0.80	1,987	2.79		↓	0.9597
		27.87	0.78	1,933	2.86		↓	0.9597
		31.95	0.75	1,847	3.00		↓	0.9597
		42.03	0.70	1,733	3.20		↓	0.9597
		52.15	0.66	1,624	3.41		↓	0.9597
Sample	Na2CO3	1.12	12.20	28,021	0.10	0.91	Ne-23	0.9341
Date	20-Sep-96	1.38	8.80	19,831	0.16	0.79	↓	0.9341
Irradiation start time	13:19:00	1.65	6.50	14,428	0.22	0.92	↓	0.9341
Irradiation stop time	13:24:00	1.93	4.00	8,829	0.37	1.37	↓	0.9341
Irradiation Time [min]	5.000	2.55	2.10	4,513	0.74	2.32	↓	0.9341
Neutron Flux		3.17	1.10	2,376	1.43	4.08	↓	0.9341
[n/sec/cm^2]	3.576E+09	3.80	0.50	1,063	3.31	8.82	↓	0.9341
Cs-137 Peak Channel	51	4.92	0.23	451	8.39	21.76	↓	0.9341
Sample Weight [g]	0.0530	5.98	0.15	279	14.89	39.07	Ne-23, Na-24	0.9100
error [%]	0.72	7.12	0.09	203	22.12	52.10	↓	0.8500
Back Ground	5105	9.23	0.08	173	26.97	55.91	↓	0.8200
		11.37	0.07	162	29.15	52.94	Na-24	0.7952
Position #	3	13.47	0.07	148	32.13	48.14	↓	0.7952
		15.60	0.06	136	35.39	45.37	↓	0.7952
		19.68	0.06	124	39.01	37.68	↓	0.7952
		23.80	0.05	112	43.25	33.88	↓	0.7952
		27.87	0.05	105	46.74	32.19	↓	0.7952
		32.00	0.04	96	51.22	18.98	↓	0.7952
		42.13	0.04	88	55.38	10.25	↓	0.7952
		52.25	0.04	82	59.49	26.63	↓	0.7952

Table 3.7.1 Important parameters affecting on the experimental data for the 5 minutes irradiation. (2/9)

Experimental Condition \ Parameters		Cooling Time [min]	Dead Time [%]	Counting Rate [cps]	BG Fraction [%]	Tape Fraction [%]	Dominant Nuclide(s)	Correction Factor
Sample	Al	1.27	3.90	6,604	0.58		Mg-27	0.9446
Date	30-Jul-96	1.52	3.80	6,473	0.59		↓	0.9446
Irradiation start time	13:30:00	1.78	3.80	6,328	0.60		↓	0.9446
Irradiation stop time	13:35:00	2.07	3.57	6,128	0.62		↓	0.9446
Irradiation Time [min]	5.000	2.68	3.43	5,873	0.65		↓	0.9446
Neutron Flux		3.30	3.30	5,616	0.68		↓	0.9446
[n/sec/cm^2]	6.003E+08	3.92	3.08	5,266	0.72		↓	0.9446
Cs-137 Peak Channel	115	5.03	2.85	4,858	0.78		↓	0.9446
Sample Weight [g]	0.0241	6.15	2.65	4,475	0.85		↓	0.9446
error [%]	0.41	7.28	2.38	4,003	0.94		↓	0.9446
Back Ground	10451	9.40	2.07	3,462	1.08		↓	0.9446
		11.52	1.78	2,982	1.25		↓	0.9446
Position #	1	13.63	1.56	2,582	1.43		↓	0.9446
		15.72	1.29	2,113	1.72		Mg-27, Na-24	0.9400
		19.78	1.01	1,626	2.18		↓	0.9300
		23.90	0.79	1,258	2.73		↓	0.9200
		28.02	0.64	987	3.37		↓	0.9000
		32.10	0.46	682	4.54		↓	0.8800
		42.17	0.31	438	6.33		↓	0.8500
		52.30	0.24	318	7.83		↓	0.8200
Sample	SiO2	1.07	6.60	13,360	0.19	0.30	Al-28	0.8553
Date	20-Sep-96	1.33	6.10	12,339	0.20	0.19	↓	0.8553
Irradiation start time	11:01:30	1.60	5.60	11,354	0.22	0.17	↓	0.8553
Irradiation stop time	11:06:30	1.87	4.97	9,992	0.25	0.17	↓	0.8553
Irradiation Time [min]	5.000	2.48	4.17	8,298	0.30	0.17	↓	0.8553
Neutron Flux		3.12	3.47	6,898	0.37	0.19	↓	0.8553
[n/sec/cm^2]	6.581E+08	3.73	2.70	5,335	0.48	0.23	↓	0.8553
Cs-137 Peak Channel	51	4.85	1.98	3,853	0.67	0.29	↓	0.8553
Sample Weight [g]	0.0129	5.93	1.45	2,825	0.92	0.38	↓	0.8553
error [%]	2.97	7.07	0.93	1,803	1.45	0.50	↓	0.8553
Back Ground	5105	9.13	0.52	1,026	2.62	0.75	↓	0.8553
		11.25	0.31	603	4.63	1.15	↓	0.8553
Position #	3	13.37	0.19	374	7.89	1.60	↓	0.8553
		15.45	0.11	216	15.02	2.69	Al-28, Al-29	0.8600
		19.52	0.06	129	29.01	4.43	↓	0.8650
		23.63	0.05	96	43.72	6.36	↓	0.8700
		27.72	0.04	82	54.08	7.95	Al-29, Mg-27	0.8750
		31.85	0.03	69	67.98	7.06	↓	0.8800
		41.93	0.03	62	78.60	5.58	↓	0.8850
		52.00	0.03	59	84.07	17.61	↓	0.8900
Sample	S	1.02	0.60	759	5.45	34.92	P-34, P-30, Si-31	0.9000
Date	17-Sep-96	1.27	0.30	619	8.31	31.48	↓	0.8600
Irradiation start time	13:20:20	1.53	0.30	564	10.62	33.82	P-30, Si-31	0.8300
Irradiation stop time	13:25:20	1.82	0.30	535	11.91	34.26	↓	0.8000
Irradiation Time [min]	5.000	2.43	0.30	519	12.72	31.30	Si-31	0.7965
Neutron Flux		3.05	0.23	518	13.07	29.22	↓	0.7965
[n/sec/cm^2]	2.208E+09	3.63	0.25	505	13.72	28.35	↓	0.7965
Cs-137 Peak Channel	115	4.75	0.23	488	14.65	28.20	↓	0.7965
Sample Weight [g]	0.0384	5.87	0.23	479	15.32	27.93	↓	0.7965
error [%]	1.00	7.00	0.21	462	16.54	25.14	↓	0.7965
Back Ground	10116	9.12	0.22	453	17.33	21.94	↓	0.7965
		11.23	0.20	441	18.25	19.86	↓	0.7965
Position #	3	13.35	0.20	433	19.00	16.49	↓	0.7965
		15.43	0.18	418	20.17	14.47	↓	0.7965
		19.50	0.18	406	21.27	11.00	↓	0.7965
		23.62	0.18	395	22.17	8.76	↓	0.7965
		27.73	0.17	387	22.85	7.51	↓	0.7965
		31.83	0.17	375	23.91	3.93	↓	0.7965
		41.90	0.16	360	25.12	1.92	↓	0.7965
		52.03	0.15	355	25.13	4.21	↓	0.7965
Sample	K2CO3	1.02	8.40	14,895	0.12	1.10	K-38	0.9496
Date	20-Sep-96	1.28	7.60	13,744	0.13	0.71	↓	0.9496
Irradiation start time	14:24:00	1.55	7.40	13,296	0.14	0.61	↓	0.9496
Irradiation stop time	14:29:00	1.83	7.07	12,810	0.15	0.57	↓	0.9496
Irradiation Time [min]	5.000	2.45	6.77	12,163	0.16	0.51	↓	0.9496
Neutron Flux		3.05	6.43	11,623	0.16	0.48	↓	0.9496
[n/sec/cm^2]	3.763E+09	3.63	6.03	10,870	0.18	0.48	↓	0.9496
Cs-137 Peak Channel	51	4.75	5.55	9,961	0.19	0.48	↓	0.9496
Sample Weight [g]	0.1912	5.87	5.10	9,145	0.21	0.50	↓	0.9496
error [%]	0.20	7.00	4.52	8,101	0.24	0.47	↓	0.9496
Back Ground	5105	9.12	3.87	6,932	0.29	0.46	↓	0.9496
		11.18	3.34	5,985	0.34	0.46	↓	0.9496
Position #	3	13.32	2.86	5,157	0.40	0.43	↓	0.9496
		15.45	2.32	4,209	0.50	0.44	↓	0.9496
		19.57	1.79	3,275	0.67	0.42	K-38, Cl-38	0.9300
		23.68	1.40	2,602	0.88	0.42	↓	0.9200
		27.80	1.12	2,121	1.14	0.44	↓	0.8900
		31.95	0.82	1,604	1.63	0.32	↓	0.8600
		42.07	0.58	1,179	2.47	0.22	↓	0.8400
		52.18	0.46	950	3.31	0.65	Cl-38	0.8335

Table 3.7.1 Important parameters affecting on the experimental data for the 5 minutes irradiation. (3/9)

Experimental Condition \ Parameters		Cooling Time [min]	Dead Time [%]	Counting Rate [cps]	BG Fraction [%]	Tape Fraction [%]	Dominant Nuclide(s)	Correction Factor
Sample	CaO	1.02	0.50	548	4.88	63.83	K-47	0.8824
Date	18-Sep-96	1.28	0.30	396	7.50	57.83	↓	0.8824
Irradiation start time	14:50:30	1.55	0.30	359	8.74	55.91	↓	0.8824
Irradiation stop time	14:55:30	1.83	0.23	336	9.46	54.33	↓	0.8824
Irradiation Time [min]	5.000	2.45	0.23	316	10.28	50.54	K-47, K-44	0.8800
Neutron Flux		3.07	0.20	299	10.81	48.33	↓	0.8770
[n/sec/cm^2]	4.440E+09	3.65	0.18	284	11.50	47.54	↓	0.8740
Cs-137 Peak Channel	116	4.72	0.18	266	12.39	47.68	K-44	0.8707
Sample Weight [g]	0.0067	5.83	0.17	250	13.27	48.47	↓	0.8707
error [%]	5.72	6.97	0.15	233	14.51	44.19	↓	0.8707
Back Ground	9995	9.05	0.15	211	16.23	41.63	↓	0.8707
		11.18	0.13	197	17.84	39.63	↓	0.8707
Position #	3	13.25	0.13	180	19.79	35.60	↓	0.8707
		15.38	0.10	163	22.50	34.13	↓	0.8707
		19.45	0.09	145	25.98	29.35	↓	0.8707
		23.57	0.08	131	29.64	26.58	↓	0.8707
		27.70	0.08	120	33.29	25.98	↓	0.8707
		31.78	0.07	108	39.34	16.64	↓	0.8707
		41.90	0.06	97	47.29	10.52	↓	0.8707
		51.98	0.06	94	52.30	28.22	↓	0.8707
Sample	Ti	1.02	1.40	2,255	1.11		Sc-50	0.9106
Date	2-Aug-96	1.28	1.20	1,881	1.22		↓	0.9106
Irradiation start time	10:53:03	1.55	1.20	1,616	1.34		↓	0.9106
Irradiation stop time	10:58:03	1.83	0.97	1,397	1.53		↓	0.9106
Irradiation Time [min]	5.000	2.40	0.83	1,197	1.83		↓	0.9106
Neutron Flux		3.02	0.70	1,061	2.15		↓	0.9106
[n/sec/cm^2]	4.266E+09	3.65	0.62	940	2.63		↓	0.9106
Cs-137 Peak Channel	90	4.77	0.52	826	3.32		Sc-50, Sc-48	0.9000
Sample Weight [g]	0.0377	5.88	0.45	755	3.95		↓	0.8900
error [%]	0.27	7.02	0.39	684	4.74		Sc-48	0.8855
Back Ground	7763	9.13	0.35	638	5.51		↓	0.8855
		11.25	0.33	610	5.92		↓	0.8855
Position #	3	13.37	0.33	592	6.16		↓	0.8855
		15.50	0.31	570	6.43		↓	0.8855
		19.57	0.30	553	6.59		↓	0.8855
		23.68	0.29	537	6.74		↓	0.8855
		27.80	0.28	523	6.87		↓	0.8855
		31.93	0.27	499	7.11		↓	0.8855
		42.02	0.26	478	7.27		↓	0.8855
		52.13	0.25	455	7.50		↓	0.8855
Sample	V	1.27	3.60	7,084	0.70		Ti-51	0.9404
Date	30-Jul-96	1.53	3.60	6,870	0.73		↓	0.9404
Irradiation start time	14:39:30	1.80	3.40	6,612	0.75		↓	0.9404
Irradiation stop time	14:44:30	2.08	3.27	6,282	0.80		↓	0.9404
Irradiation Time [min]	5.000	2.70	3.03	5,857	0.86		↓	0.9404
Neutron Flux		3.32	2.83	5,415	0.93		↓	0.9404
[n/sec/cm^2]	5.338E+08	3.95	2.53	4,868	1.04		↓	0.9404
Cs-137 Peak Channel	115	5.07	2.23	4,275	1.18		↓	0.9404
Sample Weight [g]	0.0855	6.18	1.93	3,736	1.36		↓	0.9404
error [%]	0.12	7.32	1.63	3,095	1.64		↓	0.9404
Back Ground	10451	9.42	1.27	2,411	2.11		↓	0.9404
		11.55	0.99	1,889	2.70		↓	0.9404
Position #	1	13.67	0.78	1,470	3.48		↓	0.9404
		15.75	0.56	1,054	4.85		↓	0.9404
		19.87	0.37	679	7.49		↓	0.9404
		23.98	0.25	449	11.23		↓	0.9404
		28.10	0.17	310	16.09		↓	0.9404
		32.18	0.10	187	26.09		↓	0.9404
		42.25	0.07	117	40.09		Ti-51, Sc-48	0.9000
		52.38	0.06	98	47.02		Sc-48	0.8774
Sample	Cr	1.03	17.40	29,638	0.09	0.23	V-52	0.8568
Date	19-Sep-96	1.28	16.70	28,156	0.09	0.14	↓	0.8568
Irradiation start time	15:31:00	1.55	15.80	26,657	0.10	0.12	↓	0.8568
Irradiation stop time	15:36:00	1.85	14.70	24,420	0.11	0.12	↓	0.8568
Irradiation Time [min]	5.000	2.47	13.27	21,720	0.12	0.11	↓	0.8568
Neutron Flux		3.08	11.97	19,316	0.14	0.12	↓	0.8568
[n/sec/cm^2]	9.340E+08	3.72	10.30	16,413	0.16	0.13	↓	0.8568
Cs-137 Peak Channel	116	4.83	8.52	13,330	0.20	0.14	↓	0.8568
Sample Weight [g]	0.0702	5.97	7.02	10,839	0.25	0.17	↓	0.8568
error [%]	0.55	7.05	5.38	8,181	0.33	0.18	↓	0.8568
Back Ground	10006	9.17	3.75	5,620	0.49	0.22	↓	0.8568
		11.28	2.62	3,897	0.71	0.27	↓	0.8568
Position #	3	13.42	1.83	2,724	1.03	0.31	↓	0.8568
		15.55	1.11	1,656	1.73	0.43	↓	0.8568
		19.68	0.60	906	3.31	0.60	V-52, Cr-49	0.8700
		23.75	0.36	550	5.83	0.82	↓	0.8900
		27.87	0.23	373	9.32	1.12	↓	0.9100
		32.00	0.15	251	15.70	1.00	↓	0.9300
		42.13	0.11	192	22.82	0.73	Cr-49	0.9452
		52.25	0.10	172	26.84	1.98	↓	0.9452

Table 3.7.1 Important parameters affecting on the experimental data for the 5 minutes irradiation. (4/9)

Experimental Condition \ Parameters		Cooling Time [min]	Dead Time [%]	Counting Rate [cps]	BG Fraction [%]	Tape Fraction [%]	Dominant Nuclide(s)	Correction Factor
Sample	Mn	1.02	9.50	18,064	0.21	1.10	V-52, Cr-55	0.8700
Date	19-Sep-96	1.28	9.10	17,112	0.23	0.67	↓	0.8700
Irradiation start time	14:24:30	1.55	8.70	16,334	0.24	0.57	↓	0.8700
Irradiation stop time	14:29:30	1.83	8.07	15,014	0.26	0.56	↓	0.8700
Irradiation Time [min]	5.000	2.45	7.20	13,389	0.29	0.53	↓	0.8700
Neutron Flux		3.07	6.50	11,879	0.32	0.54	↓	0.8700
[n/sec/cm^2]	1.846E+09	3.72	5.52	10,069	0.38	0.58	↓	0.8700
Cs-137 Peak Channel	116	4.83	4.55	8,198	0.47	0.66	↓	0.8700
Sample Weight [g]	0.0322	5.95	3.73	6,675	0.58	0.76	↓	0.8700
error [%]	1.19	7.08	2.82	4,988	0.77	0.84	↓	0.8700
Back Ground	10006	9.18	1.94	3,402	1.13	1.02	↓	0.8700
		11.32	1.35	2,343	1.65	1.27	↓	0.8700
Position #	3	13.45	0.94	1,631	2.38	1.46	↓	0.8700
		15.58	0.59	1,006	3.90	1.98	V-52, Cr-55, Mn-56	0.8730
		19.70	0.33	576	7.02	2.62	↓	0.8760
		23.83	0.21	372	11.40	3.37	↓	0.8790
		27.90	0.16	279	16.02	4.13	↓	0.8820
		32.03	0.12	216	21.84	2.98	Mn-56	0.8837
		42.17	0.11	188	26.08	1.72	↓	0.8837
		52.28	0.10	176	28.36	4.23	↓	0.8837
Sample	Fe	1.02	3.30	5,026	0.57		Mn-57, Mn-56	0.9300
Date	31-Jul-96	1.28	3.30	4,861	0.58		↓	0.9200
Irradiation start time	13:12:00	1.55	3.10	4,772	0.59		Mn-56	0.9151
Irradiation stop time	13:17:00	1.83	3.07	4,532	0.61		↓	0.9151
Irradiation Time [min]	5.000	2.43	2.90	4,296	0.64		↓	0.9151
Neutron Flux		3.00	2.83	4,165	0.65		↓	0.9151
[n/sec/cm^2]	4.065E+09	3.63	2.73	3,997	0.67		↓	0.9151
Cs-137 Peak Channel	115	4.73	2.65	3,828	0.69		↓	0.9151
Sample Weight [g]	0.0325	5.85	2.57	3,705	0.71		↓	0.9151
error [%]	0.31	6.95	2.51	3,607	0.72		↓	0.9151
Back Ground	9920	9.07	2.43	3,491	0.74		↓	0.9151
		11.13	2.39	3,424	0.76		↓	0.9151
Position #	2	13.25	2.33	3,348	0.77		↓	0.9151
		15.33	2.28	3,273	0.79		↓	0.9151
		19.40	2.21	3,173	0.82		↓	0.9151
		23.52	2.16	3,084	0.84		↓	0.9151
		27.63	2.10	3,012	0.86		↓	0.9151
		31.77	2.03	2,899	0.90		↓	0.9151
		41.88	1.93	2,757	0.94		↓	0.9151
		52.02	1.85	2,637	0.98		↓	0.9151
Sample	Co	1.02	0.90	1,311	2.05		Mn-56	0.9128
Date	31-Jul-96	1.27	1.00	1,338	1.99		↓	0.9128
Irradiation start time	14:18:00	1.53	0.90	1,320	2.02		↓	0.9128
Irradiation stop time	14:23:00	1.82	0.93	1,321	2.02		↓	0.9128
Irradiation Time [min]	5.000	2.43	0.93	1,305	2.04		↓	0.9128
Neutron Flux		3.05	0.93	1,290	2.06		↓	0.9128
[n/sec/cm^2]	3.684E+09	3.68	0.92	1,288	2.06		↓	0.9128
Cs-137 Peak Channel	115	4.78	0.92	1,285	2.07		↓	0.9128
Sample Weight [g]	0.0413	5.90	0.90	1,270	2.09		↓	0.9128
error [%]	0.24	6.98	0.88	1,269	2.09		↓	0.9128
Back Ground	9920	9.10	0.87	1,252	2.13		↓	0.9128
		11.22	0.87	1,236	2.15		↓	0.9128
Position #	2	13.33	0.86	1,230	2.17		↓	0.9128
		15.42	0.85	1,207	2.21		↓	0.9128
		19.48	0.83	1,187	2.25		↓	0.9128
		23.62	0.81	1,164	2.30		↓	0.9128
		27.73	0.80	1,144	2.34		↓	0.9128
		31.87	0.77	1,113	2.40		↓	0.9128
		41.93	0.74	1,064	2.52		↓	0.9128
		52.00	0.71	1,025	2.63		↓	0.9128
Sample	Ni	1.02	1.40	1,638	1.31		Co-62g	0.8524
Date	1-Aug-96	1.27	1.20	1,515	1.42		↓	0.8484
Irradiation start time	10:00:00	1.53	1.20	1,364	1.60		↓	0.8441
Irradiation stop time	10:05:00	1.82	0.97	1,214	1.84		↓	0.8366
Irradiation Time [min]	5.000	2.43	0.80	1,038	2.18		↓	0.8264
Neutron Flux		3.03	0.70	913	2.55		↓	0.8166
[n/sec/cm^2]	5.957E+09	3.67	0.60	786	3.06		↓	0.8031
Cs-137 Peak Channel	116	4.78	0.50	680	3.65		↓	0.7882
Sample Weight [g]	0.0311	5.90	0.45	615	4.20		Co-62g, Co-62m, Co-60m	0.7761
error [%]	0.32	7.03	0.39	548	4.87		↓	0.7637
Back Ground	10154	9.15	0.35	501	5.53		Co-62g, Co-62m, Co-60m, Ni-57	0.7547
		11.27	0.33	467	6.13		↓	0.7512
Position #	3	13.40	0.31	437	6.64		↓	0.7511
		15.48	0.26	397	7.55		↓	0.7551
		19.55	0.24	372	8.53		Ni-57, Co-60m	0.7661
		23.65	0.23	348	9.54		↓	0.7825
		27.78	0.21	327	10.67		Ni-57	0.8031
		31.92	0.18	298	12.51		↓	0.8430
		41.98	0.16	271	14.92		↓	0.8946
		52.10	0.15	253	17.02		↓	0.9309

Table 3.7.1 Important parameters affecting on the experimental data for the 5 minutes irradiation. (5/9)

Experimental Condition \ Parameters		Cooling Time [min]	Dead Time [%]	Counting Rate [cps]	BG Fraction [%]	Tape Fraction [%]	Dominant Nuclide(s)	Correction Factor
Sample	Cu	1.02	6.20	9,069	0.29		Cu-62	0.9860
Date	30-Jul-96	1.28	6.00	8,894	0.30		↓	0.9860
Irradiation start time	12:03:58	1.55	6.00	8,706	0.31		↓	0.9860
Irradiation stop time	12:08:58	1.83	5.73	8,407	0.32		↓	0.9860
Irradiation Time [min]	5.000	2.45	5.50	8,049	0.33		↓	0.9860
Neutron Flux		3.07	5.30	7,722	0.35		↓	0.9860
[n/sec/cm^2]	2.402E+08	3.70	4.95	7,212	0.37		↓	0.9860
Cs-137 Peak Channel	115	4.77	4.60	6,693	0.40		↓	0.9860
Sample Weight [g]	0.0327	5.87	4.28	6,201	0.43		↓	0.9860
error [%]	0.31	7.00	3.83	5,532	0.49		↓	0.9860
Back Ground	10451	9.12	3.31	4,773	0.57		↓	0.9860
		11.23	2.86	4,122	0.66		↓	0.9860
Position #	1	13.35	2.48	3,560	0.76		↓	0.9860
		15.47	2.02	2,879	0.95		↓	0.9860
		19.53	1.53	2,191	1.26		↓	0.9860
		23.65	1.17	1,670	1.67		↓	0.9860
		27.77	0.88	1,274	2.23		↓	0.9860
		31.90	0.57	828	3.56		↓	0.9860
		41.97	0.31	466	6.89		↓	0.9860
		52.10	0.18	288	12.70		↓	0.9860
Sample	SrCO3	1.02	1.80	3,210	1.60	21.50	Rb-88	0.9264
Date	18-Sep-96	1.28	1.50	3,011	1.83	14.13	↓	0.9264
Irradiation start time	11:32:03	1.55	1.60	2,922	1.93	12.21	↓	0.9264
Irradiation stop time	11:37:03	1.82	1.37	2,795	2.00	11.28	↓	0.9264
Irradiation Time [min]	5.000	2.38	1.33	2,689	2.07	9.90	↓	0.9264
Neutron Flux		3.00	1.30	2,587	2.18	9.42	↓	0.9264
[n/sec/cm^2]	4.710E+09	3.58	1.22	2,494	2.27	9.03	↓	0.9264
Cs-137 Peak Channel	116	4.65	1.17	2,382	2.39	8.76	↓	0.9264
Sample Weight [g]	0.0133	5.77	1.12	2,292	2.54	8.75	↓	0.9264
error [%]	2.88	6.90	1.05	2,187	2.68	7.62	↓	0.9264
Back Ground	9995	9.03	1.00	2,084	2.92	6.87	↓	0.9264
		11.15	0.94	1,994	3.15	6.29	↓	0.9264
Position #	3	13.22	0.90	1,928	3.36	5.33	↓	0.9264
		15.35	0.84	1,834	3.70	4.78	↓	0.9264
		19.47	0.78	1,735	4.15	3.84	↓	0.9264
		23.60	0.73	1,644	4.65	3.27	Rb-88, Sr-87m	0.9300
		27.72	0.68	1,570	5.15	3.00	↓	0.9330
		31.82	0.62	1,466	6.02	1.74	↓	0.9360
		41.88	0.55	1,340	7.36	0.99	Sr-87m	0.9383
		51.97	0.50	1,248	8.65	2.58	↓	0.9383
Sample	Y2O3	1.02	6.60	14,258	0.42	7.61	Y-89m	0.9196
Date	19-Sep-96	1.28	3.60	7,504	0.81	8.44	↓	0.9196
Irradiation start time	10:01:00	1.55	2.00	4,104	1.48	12.69	↓	0.9196
Irradiation stop time	10:06:00	1.83	0.90	1,795	3.26	25.33	↓	0.9196
Irradiation Time [min]	5.000	2.45	0.40	808	6.60	45.07	Y-89m, Rb-86m, Y-88	0.9000
Neutron Flux		3.02	0.33	568	8.89	56.29	Rb-86m, Y-88	0.8800
[n/sec/cm^2]	6.428E+09	3.65	0.23	443	10.78	63.93	Y-88	0.8553
Cs-137 Peak Channel	116	4.77	0.22	370	12.46	69.35	↓	0.8553
Sample Weight [g]	0.0146	5.88	0.20	325	13.83	73.54	↓	0.8553
error [%]	2.63	7.03	0.17	279	16.04	71.95	↓	0.8553
Back Ground	10006	9.15	0.14	241	18.51	70.59	↓	0.8553
		11.27	0.12	212	21.38	71.82	↓	0.8553
Position #	3	13.33	0.12	192	24.02	65.97	↓	0.8553
		15.47	0.10	169	27.55	64.65	↓	0.8553
		19.55	0.08	147	32.50	58.22	↓	0.8553
		23.67	0.08	133	36.79	53.13	↓	0.8553
		27.78	0.07	122	40.86	52.03	↓	0.8553
		31.87	0.06	109	46.84	32.69	↓	0.8553
		42.00	0.06	100	52.20	18.51	↓	0.8553
		52.12	0.06	98	53.97	43.63	↓	0.8553
Sample	Zr	1.28	0.90	1,916	4.60		Zr-89m	0.9794
Date	30-Jul-96	1.55	0.90	1,852	4.73		↓	0.9794
Irradiation start time	10:56:08	1.80	0.80	1,771	4.99		↓	0.9794
Irradiation stop time	11:01:08	2.08	0.73	1,632	5.37		↓	0.9794
Irradiation Time [min]	5.000	2.70	0.67	1,487	5.88		↓	0.9794
Neutron Flux		3.32	0.60	1,342	6.52		↓	0.9794
[n/sec/cm^2]	2.816E+08	3.95	0.52	1,182	7.35		↓	0.9794
Cs-137 Peak Channel	115	5.07	0.45	1,002	8.55		↓	0.9794
Sample Weight [g]	0.0268	6.18	0.38	851	10.05		↓	0.9794
error [%]	0.37	7.32	0.31	680	12.37		↓	0.9794
Back Ground	10451	9.43	0.23	512	15.87		↓	0.9794
		11.50	0.18	395	20.29		↓	0.9794
Position #	1	13.57	0.16	313	24.73		↓	0.9794
		15.70	0.12	235	31.33		↓	0.9794
		19.82	0.09	176	39.70		Zr-89m, Y-94, Zr-89g	0.9760
		23.95	0.08	144	46.83		↓	0.9730
		28.07	0.07	127	52.64		Y-94, Zr-89g	0.9700
		32.20	0.06	116	57.11		↓	0.9700
		42.33	0.06	109	61.39		↓	0.9700
		52.40	0.06	107	62.50		↓	0.9700

Table 3.7.1 Important parameters affecting on the experimental data for the 5 minutes irradiation. (6/9)

Experimental Condition \ Parameters		Cooling Time [min]	Dead Time [%]	Counting Rate [cps]	BG Fraction [%]	Tape Fraction [%]	Dominant Nuclide(s)	Correction Factor
Sample	Nb	0.93	0.30	520	12.07		Y-89m	0.9196
Date	1-Aug-96	1.20	0.20	435	14.30		↓	0.9196
Irradiation start time	14:08:03	1.47	0.20	384	16.26		Y-89m, Nb-92m, Y-90m	0.9200
Irradiation stop time	14:12:40	1.75	0.20	360	17.54		Nb-92m, Y-90m	0.9300
Irradiation Time [min]	4.617	2.37	0.20	350	18.12		↓	0.9300
Neutron Flux		2.98	0.20	349	18.30		↓	0.9300
[n/sec/cm^2]	5.580E+09	3.57	0.18	348	18.49		↓	0.9300
Cs-137 Peak Channel	116	4.68	0.17	349	18.65		↓	0.9300
Sample Weight [g]	0.0349	5.80	0.17	342	19.18		↓	0.9300
error [%]	0.29	6.93	0.17	340	19.42		↓	0.9300
Back Ground	10154	9.05	0.16	333	19.94		↓	0.9300
		11.17	0.17	330	20.26		↓	0.9300
Position #	3	13.23	0.16	331	20.39		↓	0.9300
		15.37	0.16	325	20.85		↓	0.9300
		19.50	0.16	321	21.17		↓	0.9300
		23.57	0.15	316	21.63		↓	0.9300
		27.68	0.16	314	21.88		↓	0.9300
		31.82	0.15	310	22.15		↓	0.9300
		41.90	0.15	305	22.50		↓	0.9300
		52.02	0.15	301	22.83		↓	0.9300
Sample	Mo	1.02	8.80	13,434	0.20		Mo-91g	0.9876
Date	1-Aug-96	1.28	8.50	12,847	0.20		↓	0.9876
Irradiation start time	11:05:00	1.55	8.20	12,332	0.21		↓	0.9876
Irradiation stop time	11:10:00	1.83	7.73	11,550	0.22		↓	0.9876
Irradiation Time [min]	5.000	2.45	7.37	10,793	0.23		↓	0.9876
Neutron Flux		3.02	7.00	10,189	0.25		↓	0.9876
[n/sec/cm^2]	6.082E+09	3.67	6.60	9,540	0.26		↓	0.9876
Cs-137 Peak Channel	116	4.78	6.18	8,842	0.28		↓	0.9876
Sample Weight [g]	0.0334	5.85	5.85	8,320	0.29		↓	0.9876
error [%]	0.30	7.00	5.44	7,693	0.32		↓	0.9876
Back Ground	10154	9.12	4.95	6,962	0.35		↓	0.9876
		11.18	4.53	6,352	0.38		↓	0.9876
Position #	2	13.30	4.17	5,806	0.42		↓	0.9876
		15.38	3.66	5,097	0.48		↓	0.9876
		19.45	3.11	4,314	0.57		↓	0.9876
		23.58	2.63	3,658	0.68		↓	0.9876
		27.65	2.24	3,121	0.81		↓	0.9876
		31.78	1.71	2,397	1.08		↓	0.9876
		41.87	1.17	1,683	1.61		↓	0.9876
		51.98	0.83	1,220	2.35		↓	0.9876
Sample	SnO2	1.02	1.80	2,659	1.36	29.29	In-118m, Sn-123m	0.8800
Date	17-Sep-96	1.28	1.40	2,414	1.65	20.43	↓	0.8700
Irradiation start time	15:30:00	1.55	1.40	2,299	1.81	18.42	↓	0.8500
Irradiation stop time	15:35:00	1.83	1.20	2,161	2.02	18.34	↓	0.8300
Irradiation Time [min]	5.000	2.45	1.07	2,027	2.25	17.32	↓	0.8200
Neutron Flux		3.07	1.03	1,931	2.48	17.30	Sn-123m	0.8097
[n/sec/cm^2]	7.740E+09	3.72	0.95	1,838	2.71	17.40	↓	0.8097
Cs-137 Peak Channel	115	4.83	0.87	1,716	3.04	18.03	↓	0.8097
Sample Weight [g]	0.0098	5.95	0.83	1,633	3.32	18.61	↓	0.8097
error [%]	3.91	7.08	0.75	1,528	3.72	17.17	↓	0.8097
Back Ground	10116	9.22	0.68	1,401	4.28	16.41	↓	0.8097
		11.33	0.63	1,313	4.78	15.66	↓	0.8097
Position #	3	13.45	0.58	1,231	5.29	13.76	↓	0.8097
		15.58	0.53	1,140	5.96	12.73	↓	0.8097
		19.67	0.47	1,035	6.88	10.55	↓	0.8097
		23.78	0.44	949	7.74	9.04	↓	0.8097
		27.87	0.40	873	8.56	8.32	↓	0.8097
		31.95	0.35	770	9.95	4.84	↓	0.8097
		42.02	0.29	648	12.03	2.74	↓	0.8097
		52.15	0.25	555	14.17	7.26	↓	0.8097
Sample	BaCO3	1.02	10.60	26,900	0.30	3.06	Ba-137m	0.9534
Date	19-Sep-96	1.28	10.00	25,028	0.33	1.90	↓	0.9534
Irradiation start time	12:13:30	1.55	9.30	23,415	0.35	1.67	↓	0.9534
Irradiation stop time	12:18:30	1.85	8.37	20,779	0.40	1.68	↓	0.9534
Irradiation Time [min]	5.000	2.42	7.30	17,942	0.46	1.65	↓	0.9534
Neutron Flux		3.03	6.30	15,326	0.54	1.74	↓	0.9534
[n/sec/cm^2]	3.584E+09	3.68	5.07	12,136	0.68	2.02	↓	0.9534
Cs-137 Peak Channel	116	4.80	3.87	9,114	0.90	2.46	↓	0.9534
Sample Weight [g]	0.0064	5.92	2.95	6,871	1.18	3.05	↓	0.9534
error [%]	5.99	7.05	2.02	4,638	1.71	3.66	↓	0.9534
Back Ground	10006	9.18	1.25	2,814	2.73	4.86	↓	0.9534
		11.25	0.82	1,796	4.08	6.26	↓	0.9534
Position #	3	13.38	0.56	1,193	5.79	7.16	Ba-137m, Ba-139	0.9500
		15.53	0.37	762	8.36	8.65	↓	0.9400
		19.65	0.26	517	11.21	8.51	↓	0.9200
		23.72	0.22	430	12.93	7.56	↓	0.9000
		27.85	0.20	386	14.18	6.94	Ba-139	0.8906
		31.93	0.19	357	15.27	3.73	↓	0.8906
		42.03	0.17	326	16.81	1.91	↓	0.8906
		52.15	0.16	305	18.03	4.56	↓	0.8906

Table 3.7.1 Important parameters affecting on the experimental data for the 5 minutes irradiation. (7/9)

Experimental Condition \ Parameters		Cooling Time [min]	Dead Time [%]	Counting Rate [cps]	BG Fraction [%]	Tape Fraction [%]	Dominant Nuclide(s)	Correction Factor
Sample	Ta	1.00	0.90	2,342	9.81		Ta-180g	0.7448
Date	2-Aug-96	1.27	0.80	2,315	9.95		↓	0.7448
Irradiation start time	9:46:05	1.53	0.80	2,343	9.80		↓	0.7448
Irradiation stop time	9:51:05	1.82	0.80	2,330	9.95		↓	0.7448
Irradiation Time [min]	5.000	2.43	0.83	2,326	9.94		↓	0.7448
Neutron Flux		3.03	0.77	2,311	10.10		↓	0.7448
[n/sec/cm^2]	5.082E+09	3.67	0.80	2,320	10.06		↓	0.7448
Cs-137 Peak Channel	116	4.78	0.78	2,299	10.26		↓	0.7448
Sample Weight [g]	0.0496	5.90	0.77	2,288	10.36		↓	0.7448
error [%]	0.20	7.03	0.77	2,286	10.47		↓	0.7448
Back Ground	10140	9.13	0.78	2,269	10.54		↓	0.7448
		11.20	0.76	2,250	10.86		↓	0.7448
Position #	3	13.32	0.75	2,235	11.00		↓	0.7448
		15.40	0.74	2,216	11.24		↓	0.7448
		19.48	0.74	2,204	11.29		↓	0.7448
		23.60	0.73	2,182	11.51		↓	0.7448
		27.72	0.72	2,161	11.73		↓	0.7448
		31.85	0.71	2,125	12.02		↓	0.7448
		41.93	0.69	2,084	12.44		↓	0.7448
		52.05	0.68	2,049	12.77		↓	0.7448
Sample	W	1.03	10.50	37,800	1.05		W-185m	0.4118
Date	31-Jul-96	1.43	9.10	31,905	1.23		↓	0.4133
Irradiation start time	15:39:00	1.70	8.10	28,650	1.37		↓	0.4145
Irradiation stop time	15:44:00	1.98	6.93	23,912	1.62		↓	0.4166
Irradiation Time [min]	5.000	2.58	5.47	18,508	2.06		↓	0.4200
Neutron Flux		3.15	4.37	14,617	2.54		↓	0.4239
[n/sec/cm^2]	3.873E+09	3.78	3.10	10,200	3.48		↓	0.4316
Cs-137 Peak Channel	115	4.88	2.00	6,462	5.04		↓	0.4446
Sample Weight [g]	0.0650	6.00	1.30	4,089	7.07		↓	0.4628
error [%]	0.15	7.13	0.73	2,193	10.59		↓	0.5007
Back Ground	9920	9.25	0.36	1,012	15.77		W-185m, Ta-186	0.5705
		11.37	0.21	524	20.77		↓	0.6533
Position #	2	13.43	0.15	326	24.77		↓	0.7263
		15.52	0.10	216	29.14		Ta-186	0.7959
		19.57	0.09	167	33.98		↓	0.8319
		23.68	0.08	144	39.50		Ta-186, W-187, Ta-184	0.8437
		27.80	0.07	133	44.07		↓	0.8491
		31.93	0.06	123	50.07		↓	0.8560
		42.02	0.06	112	58.74		↓	0.8641
		52.08	0.06	106	64.26		↓	0.8702
Sample	Re	1.02	0.30	373	14.64	64.53	W-185m, Re-186g, Re-188g	0.6459
Date	17-Sep-96	1.28	0.20	337	21.04	57.49	↓	0.6549
Irradiation start time	14:23:00	1.55	0.20	315	23.77	55.13	↓	0.6632
Irradiation stop time	14:28:00	1.83	0.17	310	24.63	51.47	Re-186g, Re-188g	0.6759
Irradiation Time [min]	5.000	2.38	0.17	288	27.47	50.55	↓	0.6893
Neutron Flux		3.02	0.13	290	27.79	46.48	↓	0.7021
[n/sec/cm^2]	1.372E+09	3.65	0.13	286	28.41	43.95	↓	0.7158
Cs-137 Peak Channel	115	4.77	0.12	275	30.38	44.52	↓	0.7279
Sample Weight [g]	0.0577	5.90	0.13	271	30.89	42.87	↓	0.7359
error [%]	0.66	7.03	0.12	266	32.36	37.71	↓	0.7426
Back Ground	10116	9.10	0.12	261	34.09	33.64	↓	0.7467
		11.22	0.12	256	35.20	30.03	↓	0.7486
Position #	3	13.30	0.12	254	35.82	24.38	↓	0.7493
		15.43	0.11	248	37.79	21.62	↓	0.7498
		19.55	0.11	239	40.05	16.91	↓	0.7499
		23.68	0.11	236	41.04	13.30	↓	0.7500
		27.80	0.10	232	42.21	11.51	↓	0.7500
		31.90	0.10	229	42.98	5.85	↓	0.7500
		41.98	0.10	225	44.31	2.82	↓	0.7500
		52.05	0.10	226	44.18	6.16	↓	0.7499
Sample	Pb	1.02	0.60	1,080	3.57		Tl-208	0.9595
Date	1-Aug-96	1.27	0.70	1,053	3.68		↓	0.9595
Irradiation start time	15:12:30	1.55	0.60	1,001	3.94		↓	0.9595
Irradiation stop time	15:17:30	1.83	0.57	919	4.36		↓	0.9595
Irradiation Time [min]	5.000	2.45	0.50	846	4.83		↓	0.9595
Neutron Flux		3.07	0.47	776	5.39		↓	0.9595
[n/sec/cm^2]	6.384E+09	3.70	0.38	683	6.32		↓	0.9595
Cs-137 Peak Channel	116	4.77	0.35	590	7.52		↓	0.9595
Sample Weight [g]	0.0388	5.88	0.28	518	8.94		↓	0.9595
error [%]	0.26	7.02	0.24	426	11.31		Tl-208, Pb-204m	0.9500
Back Ground	10154	9.08	0.18	341	15.11		↓	0.9450
		11.20	0.16	286	18.50		↓	0.9400
Position #	3	13.32	0.13	244	22.48		Pb-204m	0.9391
		15.45	0.12	211	27.27		↓	0.9391
		19.52	0.10	179	32.71		↓	0.9391
		23.63	0.08	163	35.98		↓	0.9391
		27.77	0.08	154	38.38		↓	0.9391
		31.85	0.08	145	41.23		↓	0.9391
		41.98	0.07	138	44.59		↓	0.9391
		52.07	0.07	131	48.30		↓	0.9391

Table 3.7.1 Important parameters affecting on the experimental data for the 5 minutes irradiation. (8/9)

Experimental Condition \ Parameters		Cooling Time [min]	Dead Time [%]	Counting Rate [cps]	BG Fraction [%]	Tape Fraction [%]	Dominant Nuclide(s)	Correction Factor
Sample	Bi	1.02	0.50	660	6.03	85.35	Tl-206	0.7809
Date	18-Sep-96	1.28	0.40	540	9.39	79.01	↓	0.7809
Irradiation start time	12:40:00	1.55	0.30	496	11.07	77.76	↓	0.7809
Irradiation stop time	12:45:00	1.83	0.23	477	11.76	74.16	↓	0.7809
Irradiation Time [min]	5.000	2.45	0.27	441	12.79	69.18	↓	0.7809
Neutron Flux		3.07	0.23	408	14.00	69.48	↓	0.7809
[n/sec/cm^2]	4.749E+09	3.70	0.18	369	15.47	71.62	↓	0.7809
Cs-137 Peak Channel	116	4.82	0.18	330	17.43	76.11	↓	0.7809
Sample Weight [g]	0.0681	5.90	0.17	294	19.58	82.53	↓	0.7809
error [%]	0.56	7.03	0.13	257	22.32	80.04	↓	0.7809
Back Ground	9995	9.15	0.13	219	26.47	82.73	↓	0.7809
		11.22	0.10	188	31.14	88.29	↓	0.7809
Position #	3	13.33	0.09	166	35.19	83.81	↓	0.7809
		15.42	0.08	142	42.26	92.03	Tl-206, Pb-209	0.7000
		19.53	0.07	120	51.05	93.28	↓	0.6000
		23.67	0.06	108	58.21	94.02	↓	0.5000
		27.78	0.05	99	66.46	110.35	Pb-209	0.4699
		31.88	0.05	91	74.99	82.29	↓	0.4699
		41.97	0.04	85	82.78	60.27	↓	0.4699
		52.05	0.05	85	83.11	135.41	↓	0.4699
Sample	Inconel-600	1.02	9.80	15,085	0.17		V-52	0.8737
Date	31-Jul-96	1.27	9.40	14,220	0.18		↓	0.8737
Irradiation start time	12:04:30	1.53	8.80	13,507	0.19		↓	0.8737
Irradiation stop time	12:09:30	1.80	8.13	12,322	0.21		↓	0.8737
Irradiation Time [min]	5.000	2.42	7.23	10,867	0.24		↓	0.8737
Neutron Flux		3.03	6.43	9,660	0.27		↓	0.8737
[n/sec/cm^2]	1.134E+09	3.67	5.50	8,173	0.32		↓	0.8737
Cs-137 Peak Channel	115	4.78	4.53	6,684	0.39		↓	0.8737
Sample Weight [g]	0.1328	5.90	3.75	5,514	0.48		↓	0.8737
error [%]	0.08	7.03	2.91	4,235	0.63		↓	0.8737
Back Ground	9920	9.13	2.11	3,080	0.87		↓	0.8737
		11.27	1.58	2,300	1.18		↓	0.8737
Position #	2	13.38	1.22	1,770	1.55		V-52, Mn-56	0.8750
		15.47	0.88	1,303	2.15		↓	0.8780
		19.58	0.63	939	3.05		↓	0.8820
		23.70	0.50	754	3.90		↓	0.8850
		27.82	0.43	643	4.67		Mn-56	0.8891
		31.95	0.36	548	5.60		↓	0.8891
		42.07	0.31	479	6.57		↓	0.8891
		52.18	0.29	444	7.19		↓	0.8891
Sample	Nichrome	1.02	2.00	2,809	0.95		V-52	0.9026
Date	30-Jul-96	1.28	1.90	2,637	1.01		↓	0.9026
Irradiation start time	15:46:30	1.55	1.80	2,497	1.07		↓	0.9026
Irradiation stop time	15:51:30	1.83	1.60	2,250	1.19		↓	0.9026
Irradiation Time [min]	5.000	2.47	1.43	1,997	1.35		↓	0.9026
Neutron Flux		3.08	1.27	1,747	1.55		↓	0.9026
[n/sec/cm^2]	1.009E+09	3.72	1.07	1,494	1.82		↓	0.9026
Cs-137 Peak Channel	115	4.78	0.88	1,230	2.23		↓	0.9026
Sample Weight [g]	0.0258	5.90	0.72	1,010	2.74		↓	0.9026
error [%]	0.39	6.98	0.55	773	3.65		↓	0.9026
Back Ground	10451	9.10	0.38	554	5.24		↓	0.9026
		11.22	0.29	412	7.28		↓	0.9026
Position #	1	13.35	0.22	314	9.99		↓	0.9026
		15.48	0.15	227	14.93		↓	0.9026
		19.60	0.10	164	23.13		↓	0.9026
		23.72	0.08	133	32.05		V-52, Cr-49	0.9200
		27.83	0.08	118	39.24		↓	0.9600
		31.97	0.06	105	48.91		Cr-49, Mn-56	0.9500
		42.10	0.06	98	56.99		↓	0.9400
		52.22	0.05	95	61.36		↓	0.9300
Sample	SS-304	1.02	11.90	18,607	0.14		V-52	0.8979
Date	31-Jul-96	1.27	11.20	17,538	0.14		↓	0.8979
Irradiation start time	10:57:00	1.53	10.80	16,742	0.15		↓	0.8979
Irradiation stop time	11:02:00	1.82	9.97	15,359	0.17		↓	0.8979
Irradiation Time [min]	5.000	2.43	9.00	13,776	0.19		↓	0.8979
Neutron Flux		3.03	8.20	12,424	0.21		↓	0.8979
[n/sec/cm^2]	3.665E+09	3.62	7.23	10,844	0.24		↓	0.8979
Cs-137 Peak Channel	115	4.73	6.15	9,143	0.28		↓	0.8979
Sample Weight [g]	0.0376	5.80	5.35	7,880	0.33		↓	0.8979
error [%]	0.27	6.92	4.42	6,437	0.40		V-52, Mn-56	0.9000
Back Ground	9920	9.03	3.54	5,135	0.50		↓	0.9100
		11.15	2.97	4,272	0.60		Mn-56	0.9112
Position #	2	13.22	2.57	3,697	0.70		↓	0.9112
		15.35	2.21	3,163	0.82		↓	0.9112
		19.47	1.93	2,761	0.94		↓	0.9112
		23.58	1.78	2,538	1.02		↓	0.9112
		27.70	1.70	2,412	1.08		↓	0.9112
		31.83	1.60	2,277	1.14		↓	0.9112
		41.97	1.51	2,150	1.21		↓	0.9112
		52.10	1.44	2,047	1.27		↓	0.9112

Table 3.7.1 Important parameters affecting on the experimental data for the 5 minutes irradiation. (9/9)

Experimental Condition \ Parameters		Cooling Time [min]	Dead Time [%]	Counting Rate [cps]	BG Fraction [%]	Tape Fraction [%]	Dominant Nuclide(s)	Correction Factor
Sample	SS-316	1.05	12.90	20,342	0.12		V-52	0.8992
Date	31-Jul-96	1.32	12.30	19,245	0.13		↓	0.8992
Irradiation start time	9:49:04	1.58	11.80	18,244	0.14		↓	0.8992
Irradiation stop time	9:54:04	1.87	10.80	16,731	0.15		↓	0.8992
Irradiation Time [min]	5.000	2.50	9.77	14,918	0.17		↓	0.8992
Neutron Flux		3.12	8.80	13,337	0.19		↓	0.8992
[n/sec/cm^2]	4.013E+09	3.77	7.67	11,495	0.22		↓	0.8992
Cs-137 Peak Channel	115	4.88	6.52	9,655	0.26		↓	0.8992
Sample Weight [g]	0.0359	6.00	5.58	8,217	0.31		↓	0.8992
error [%]	0.28	7.13	4.55	6,650	0.39		V-52, Mn-56	0.9000
Back Ground	9920	9.25	3.63	5,253	0.49		↓	0.9100
		11.37	3.00	4,336	0.60		Mn-56	0.9135
Position #	2	13.43	2.60	3,729	0.69		↓	0.9135
		15.57	2.20	3,157	0.82		↓	0.9135
		19.68	1.90	2,728	0.95		↓	0.9135
		23.82	1.74	2,489	1.05		↓	0.9135
		27.93	1.65	2,344	1.11		↓	0.9135
		32.07	1.54	2,194	1.19		↓	0.9135
		42.13	1.44	2,050	1.27		↓	0.9135
		52.22	1.36	1,943	1.35		↓	0.9135

Table 3.7.2 Important parameters affecting on the experimental data for the 7 hours irradiation. (1/5)

Experimental Condition \ Parameters		Cooling Time [days]	Dead Time [%]	Counting Rate [cps]	BG Fraction [%]	Tape Fraction [%]	Dominant Nuclide(s)	Correction Factor
Sample	Blank Tape	0.63	0.12	202				
Sample Weight [g]	0.0826	1.69	0.09	151				
error [%]	0.44	3.85	0.07	128				
Neutron Flux		6.72	0.06	113				
[n/sec/cm^2]	2.168E+10	12.17	0.06	104				
		24.17	0.05	86				
		49.92	0.03	60				
		100.06	0.03	61				
		197.92	0.05	71				
		402.11	0.04	67				
Sample	PTFE (CF2)	0.66	3.09	6,035	0.81		F-18	0.9597
Sample Weight [g]	0.0981	1.72	0.04	70	96.20		↓	0.9597
error [%]	0.10							
Neutron Flux								
[n/sec/cm^2]	2.449E+10							
Sample	Na2CO3	0.67	0.41	498	4.16	9.12	Na-24	0.7952
Sample Weight [g]	0.0511	1.72	0.20	273	9.59	13.26	↓	0.9000
error [%]	0.75	3.87	0.11	181	20.95	17.87	Na-22	0.9668
Neutron Flux		6.74	0.10	165	24.67	13.37	↓	0.9668
[n/sec/cm^2]	1.278E+10	12.19	0.10	160	27.06	8.63	↓	0.9668
		24.20	0.09	148	27.00	4.84	↓	0.9668
		49.95	0.08	125	27.10	1.66	↓	0.9668
		100.08	0.08	123	29.41	0.03	↓	0.9668
		197.95	0.09	131	29.73	0.60	↓	0.9668
		402.16	0.08	119	32.89	0.21	↓	0.9668
Sample	Al	0.66	56.17	120,782	0.01		Na-24	0.8190
Sample Weight [g]	0.0242	1.34	49.57	80,805	0.02		↓	0.8190
error [%]	0.41	2.92	10.35	13,450	0.11		↓	0.8190
Neutron Flux		6.93	0.17	227	8.41		↓	0.8190
[n/sec/cm^2]	1.880E+10	12.89	0.05	83	80.90		↓	0.8190
		23.89	0.04	81	84.90		↓	0.8190
		49.74	0.04	83	79.36		↓	0.8190
Sample	S	0.68	9.77	25,256	0.34	0.75	P-32	0.8252
Sample Weight [g]	0.0355	1.74	9.11	23,348	0.37	0.48	↓	0.8252
error [%]	1.08	3.89	8.33	21,138	0.41	0.29	↓	0.8252
Neutron Flux		6.76	7.40	18,507	0.46	0.20	↓	0.8252
[n/sec/cm^2]	1.331E+10	12.20	5.82	14,293	0.63	0.15	↓	0.8252
		24.21	3.38	8,056	1.08	0.15	↓	0.8252
		49.96	0.98	2,305	3.67	0.18	↓	0.8252
		100.09	0.12	259	30.86	0.04	↓	0.8252
Sample	K2CO3	0.65	0.33	593	7.43	18.27	K-42, Ar-41	0.8100
Sample Weight [g]	0.1995	1.71	0.11	217	24.92	45.00	K-42	0.8402
error [%]	0.19							
Neutron Flux								
[n/sec/cm^2]	1.386E+10							
Sample	Ca	0.66	0.26	459	9.15	23.88	K-42, Ca-47	0.9000
Sample Weight [g]	0.0064	1.71	0.14	265	18.50	32.07	↓	0.8850
error [%]	5.99	3.87	0.10	185	33.84	38.97	Ca-47, Sc-47	0.8160
Neutron Flux		6.73	0.08	158	44.71	37.29	↓	0.8060
[n/sec/cm^2]	1.444E+10	12.18	0.06	126	62.76	44.28	↓	0.7920
		24.19	0.05	88	82.49	69.71	↓	0.7150
Sample	Ti	0.65	30.75	47,747	0.06		Sc-48	0.8855
Sample Weight [g]	0.0375	1.32	23.15	36,629	0.06		↓	0.8855
error [%]	0.27	2.90	14.37	22,025	0.10		↓	0.8855
Neutron Flux		6.87	4.31	6,673	0.43		↓	0.8855
[n/sec/cm^2]	1.882E+10	12.87	0.97	1,732	2.33		Sc-48, Sc-46	0.8900
		23.86	0.40	677	5.61		Sc-46	0.8942
		49.71	0.29	490	7.33		↓	0.8942
		99.90	0.20	327	10.25		↓	0.8942
		200.12	0.13	205	19.08		↓	0.8942
		402.96	0.07	131	59.80		↓	0.8942

Table 3.7.2 Important parameters affecting on the experimental data for the 7 hours irradiation. (2/5)

Experimental Condition \ Parameters		Cooling Time [days]	Dead Time [%]	Counting Rate [cps]	BG Fraction [%]	Tape Fraction [%]	Dominant Nuclide(s)	Correction Factor
Sample	V	0.65	21.41	29,606	0.08		Sc-48	0.8774
Sample Weight [g]	0.0854	1.32	17.40	23,137	0.08		↓	0.8774
error [%]	0.12	2.90	10.20	12,912	0.14		↓	0.8774
Neutron Flux		6.87	2.50	2,943	0.64		↓	0.8774
[n/sec/cm^2]	1.885E+10	12.86	0.30	374	5.83		↓	0.8774
		23.86	0.04	76	77.67		↓	0.8774
		49.73	0.04	74	92.07		↓	0.8774
Sample	Cr	0.69	4.58	7,714	0.43	1.46	Cr-51	0.9083
Sample Weight [g]	0.0808	1.74	2.53	5,354	1.09	2.24	↓	0.9083
error [%]	0.47	3.89	1.61	4,218	3.11	3.52	↓	0.9083
Neutron Flux		6.75	1.41	3,854	4.07	2.82	↓	0.9083
[n/sec/cm^2]	2.081E+10	12.20	1.24	3,356	5.10	2.03	↓	0.9083
		24.21	0.92	2,483	6.69	1.53	↓	0.9083
		49.96	0.48	1,316	12.77	1.06	↓	0.9083
		100.09	0.17	418	34.36	0.07	↓	0.9083
		197.96	0.05	104	81.78	10.36	↓	0.9083
Sample	Mn	0.68	1.80	3,857	1.64	5.48	Mn-54	0.9362
Sample Weight [g]	0.0326	1.73	1.66	3,621	1.88	3.75	↓	0.9362
error [%]	1.18	3.89	1.63	3,565	1.94	2.09	↓	0.9362
Neutron Flux		6.75	1.62	3,516	1.95	1.27	↓	0.9362
[n/sec/cm^2]	1.998E+10	12.20	1.59	3,442	2.10	0.78	↓	0.9362
		24.21	1.56	3,352	2.06	0.43	↓	0.9362
		49.96	1.44	3,133	2.17	0.15	↓	0.9362
		100.10	1.32	2,814	2.47	0.00	↓	0.9362
		197.97	1.10	2,298	2.94	0.07	↓	0.9362
		402.18	0.71	1,482	4.48	0.03	↓	0.9362
Sample	Fe	0.63	7.59	11,303	0.31		Mn-56	0.9151
Sample Weight [g]	0.0329	1.30	0.22	383	11.04		↓	0.9151
error [%]	0.30	2.88	0.09	200	36.75		Mn-54	0.9362
Neutron Flux		6.89	0.09	191	39.38		↓	0.9362
[n/sec/cm^2]	2.033E+10	12.88	0.09	185	39.62		↓	0.9362
		23.89	0.09	176	40.47		↓	0.9362
		49.72	0.08	166	42.07		↓	0.9362
		99.91	0.07	132	46.19		↓	0.9362
		200.13	0.07	128	49.26		↓	0.9362
		402.95	0.07	134	66.70		↓	0.9362
Sample	Co	0.63	10.56	21,488	0.29		Mn-56, Co-58g	0.9500
Sample Weight [g]	0.0377	1.31	9.02	19,577	0.29		Co-58g	0.9769
error [%]	0.27	2.89	9.08	19,955	0.28		↓	0.9769
Neutron Flux		6.86	8.81	19,221	0.30		↓	0.9769
[n/sec/cm^2]	2.046E+10	12.85	8.31	18,103	0.31		↓	0.9769
		23.84	7.55	16,219	0.34		↓	0.9769
		49.70	5.83	12,517	0.45		↓	0.9769
		99.89	3.63	7,550	0.73		↓	0.9769
		200.11	1.46	2,847	1.80		↓	0.9769
		402.95	0.24	476	15.78		↓	0.9769
Sample	Ni	0.60	12.57	23,397	0.20		Ni-57	0.9770
Sample Weight [g]	0.0313	1.31	10.20	19,118	0.20		↓	0.9770
error [%]	0.32	2.89	6.52	12,953	0.35		↓	0.9770
Neutron Flux		6.86	3.52	7,946	0.87		Co-58g	0.9773
[n/sec/cm^2]	2.185E+10	12.85	2.84	6,808	1.21		↓	0.9773
		23.85	2.60	6,275	1.36		↓	0.9773
		49.70	2.14	5,297	1.72		↓	0.9773
		99.89	1.42	3,619	2.66		↓	0.9773
		200.11	0.93	2,365	5.06		Co-58g, Co-57, Co-60g	0.9482
		402.94	0.40	1,165	20.43		↓	0.9082
Sample	Cu	0.65	28.90	90,780	0.11		Cu-64	0.9387
Sample Weight [g]	0.0313	1.32	15.16	40,806	0.20		↓	0.9387
error [%]	0.32	2.90	2.30	5,452	1.52		↓	0.9387
Neutron Flux		6.87	0.06	119	47.30		Cu-64, Co-60g	0.9000
[n/sec/cm^2]	1.888E+10	12.89	0.05	89	55.76		Co-60g	0.8757
		23.90	0.05	88	55.79		↓	0.8757
		49.72	0.06	93	54.13		↓	0.8757
		99.92	0.05	75	54.10		↓	0.8757
		200.14	0.06	90	52.41		↓	0.8757
		402.97	0.06	116	61.32		↓	0.8757

Table 3.7.2 Important parameters affecting on the experimental data for the 7 hours irradiation. (3/5)

Experimental Condition \ Parameters		Cooling Time [days]	Dead Time [%]	Counting Rate [cps]	BG Fraction [%]	Tape Fraction [%]	Dominant Nuclide(s)	Correction Factor
Sample	SrCO3	0.67	1.53	3,926	2.98	7.58	Sr-87m	0.9383
Sample Weight [g]	0.0151	1.73	0.29	629	11.26	18.66	Sr-83g, Sr-85g	0.9500
error [%]	2.54	3.88	0.22	475	16.95	16.20	Sr-85g	0.9673
Neutron Flux		6.75	0.19	410	21.19	12.91	↓	0.9673
[n/sec/cm^2]	1.504E+10	12.19	0.17	369	25.63	9.43	↓	0.9673
		24.20	0.14	313	29.09	6.32	↓	0.9673
		49.95	0.11	230	36.48	3.02	↓	0.9673
		100.08	0.07	156	52.59	0.11	↓	0.9673
		197.95	0.06	105	73.54	4.64	↓	0.9673
Sample	Y2O3	0.68	1.98	2,907	0.94	2.44	Y-88	0.8553
Sample Weight [g]	0.0133	1.73	1.92	2,792	0.96	1.49	↓	0.8553
error [%]	2.88	3.89	1.86	2,685	0.99	0.83	↓	0.8553
Neutron Flux		6.76	1.81	2,574	1.01	0.51	↓	0.8553
[n/sec/cm^2]	1.566E+10	12.20	1.74	2,438	1.11	0.32	↓	0.8553
		24.21	1.61	2,220	1.15	0.19	↓	0.8553
		49.96	1.35	1,841	1.32	0.07	↓	0.8553
		100.09	1.01	1,328	1.89	0.00	↓	0.8553
		197.96	0.57	735	3.44	0.06	↓	0.8553
		402.17	0.18	240	11.81	0.07	↓	0.8553
Sample	Zr	0.61	33.64	97,103	0.07		Zr-89g	0.9736
Sample Weight [g]	0.0267	1.33	30.30	83,705	0.06		↓	0.9736
error [%]	0.37	2.91	23.92	61,998	0.09		↓	0.9736
Neutron Flux		6.88	12.36	28,170	0.20		↓	0.9736
[n/sec/cm^2]	2.156E+10	12.88	4.04	8,540	0.69		↓	0.9736
		23.85	0.72	1,507	4.24		Zr-89g, Zr-95	0.9500
		49.71	0.33	715	10.20		Zr-95, Nb-95g	0.9220
		99.90	0.24	513	13.47		↓	0.9220
		200.12	0.14	263	24.97		↓	0.9220
		402.96	0.06	123	73.34		↓	0.9220
Sample	Nb	0.62	17.88	43,647	0.18		Nb-92m	0.9214
Sample Weight [g]	0.0318	1.32	16.96	40,810	0.14		↓	0.9214
error [%]	0.31	2.90	15.18	36,260	0.16		↓	0.9214
Neutron Flux		6.86	11.91	27,357	0.22		↓	0.9214
[n/sec/cm^2]	2.136E+10	12.86	8.17	18,146	0.33		↓	0.9214
		23.85	4.07	8,633	0.69		↓	0.9214
		49.70	0.75	1,547	3.91		↓	0.9214
		99.89	0.06	104	53.41		↓	0.9214
Sample	Mo	0.64	19.97	63,347	0.25		Mo-99	0.9379
Sample Weight [g]	0.0320	1.31	17.92	56,860	0.23		↓	0.9379
error [%]	0.31	2.90	12.79	39,296	0.36		↓	0.9379
Neutron Flux		6.86	5.39	15,346	0.96		↓	0.9379
[n/sec/cm^2]	1.891E+10	12.86	1.47	3,909	3.35		Mo-99, Nb-92m	0.9350
		23.86	0.27	642	14.15		Nb-92m, Nb-95g	0.9200
		49.71	0.11	242	34.53		Nb-95g	0.9192
		99.90	0.05	104	60.14		↓	0.9192
		200.14	0.06	94	78.28		Nb-95g, Nb-91m, Zr-95	0.8109
Sample	SnO2	0.68	1.31	3,786	5.11	14.42	Sn-117m, Sn-121g	0.6105
Sample Weight [g]	0.0099	1.73	1.11	3,213	6.30	10.73	Sn-117m	0.6401
error [%]	3.87	3.88	0.89	2,569	8.18	7.67	↓	0.6693
Neutron Flux		6.75	0.73	2,087	10.21	5.92	↓	0.6745
[n/sec/cm^2]	1.631E+10	12.20	0.54	1,548	14.55	5.05	↓	0.6691
		24.20	0.31	889	22.20	4.77	↓	0.6758
		49.95	0.12	319	43.92	4.46	Sn-117m, Sn-123g	0.7199
		100.08	0.06	122	69.20	0.23	Sn-123g	0.7891
		197.93	0.06	98	78.18	6.48	↓	0.7891
		402.13	0.05	75	92.52	6.88	↓	0.7891
Sample	BaCO3	0.67	0.99	2,840	6.94	20.82	Ba-133m, Ba-135m	0.6250
Sample Weight [g]	0.0059	1.72	0.56	1,592	12.00	22.66	↓	0.6300
error [%]	6.50	3.88	0.21	557	27.29	33.64	↓	0.6350
Neutron Flux		6.74	0.09	205	49.31	52.77	↓	0.6400
[n/sec/cm^2]	1.699E+10	12.18	0.06	110	70.83	75.05	Cs-136g, Ba-131g	0.8300
		24.18	0.05	86	82.67	83.00	↓	0.9130

Table 3.7.2 Important parameters affecting on the experimental data for the 7 hours irradiation. (4/5)

Experimental Condition \ Parameters		Cooling Time [days]	Dead Time [%]	Counting Rate [cps]	BG Fraction [%]	Tape Fraction [%]	Dominant Nuclide(s)	Correction Factor
Sample	Ta	0.60	34.17	154,166	0.24		Ta-180g	0.7448
Sample Weight [g]	0.0460	1.33	11.68	40,158	0.77		↓	0.7448
error [%]	0.22	2.91	0.60	1,714	11.74		Ta-180g, Ta-182g, Hf-181	0.8000
Neutron Flux		6.88	0.12	237	28.41		Ta-182g, Hf-181	0.8600
[n/sec/cm^2]	2.175E+10	12.88	0.11	222	29.14		↓	0.8550
		23.88	0.10	202	31.26		↓	0.8500
		49.72	0.09	175	34.87		Ta-182g	0.8448
		99.91	0.07	120	43.59		↓	0.8448
		200.13	0.07	101	56.16		↓	0.8448
		402.97	0.05	108	80.02		↓	0.8448
Sample	W	0.61	2.07	5,481	3.15		Ta-184, W-185g, W-187	0.8050
Sample Weight [g]	0.0689	1.33	1.51	4,276	4.12		↓	0.7180
error [%]	0.15	2.91	1.16	3,458	6.87		W-185g	0.5925
Neutron Flux		6.88	1.03	3,142	8.90		↓	0.5925
[n/sec/cm^2]	2.166E+10	12.87	0.96	2,936	9.58		↓	0.5925
		23.87	0.85	2,604	10.73		↓	0.5925
		49.71	0.68	2,067	13.19		↓	0.5925
		99.90	0.35	1,082	22.64		↓	0.5925
		200.12	0.27	730	31.33		↓	0.5925
		402.95	0.08	200	75.49		↓	0.5925
Sample	Re	0.69	31.25	115,433	0.10	0.31	Re-186g	0.7080
Sample Weight [g]	0.0600	1.74	27.56	97,343	0.13	0.23	↓	0.7126
error [%]	0.64	3.90	21.67	70,604	0.17	0.17	↓	0.7234
Neutron Flux		6.76	15.78	46,988	0.24	0.14	↓	0.7424
[n/sec/cm^2]	1.842E+10	12.21	9.08	23,796	0.42	0.14	Re-186g, Re-184g	0.7866
		24.22	4.48	10,063	0.70	0.13	Re-184g	0.8677
		49.97	2.55	5,472	1.16	0.08	↓	0.8939
		100.10	1.18	2,479	2.67	0.00	↓	0.8943
		197.96	0.39	814	8.65	0.19	Re-184g, Re-184m	0.8514
		402.17	0.13	277	25.55	0.22	↓	0.8289
Sample	Pb	0.61	2.32	6,326	3.39		Pb-203g	0.9548
Sample Weight [g]	0.0386	1.33	1.85	5,023	3.24		↓	0.9548
error [%]	0.26	2.91	1.13	3,046	5.31		↓	0.9548
Neutron Flux		6.88	0.34	908	16.83		↓	0.9548
[n/sec/cm^2]	2.146E+10	12.87	0.08	200	54.83		↓	0.9548
		23.88	0.04	77	92.70		↓	0.9548
		49.73	0.04	75	91.29		↓	0.9548
Sample	Bi	0.66	0.13	266	23.18	95.11	Bi-210	0.7046
Sample Weight [g]	0.0798	1.70	0.08	163	35.05	101.27	↓	0.7046
error [%]	0.48	3.85	0.07	138	49.12	97.75	↓	0.7046
Neutron Flux		6.73	0.07	120	60.98	95.78	↓	0.7046
[n/sec/cm^2]	1.919E+10	12.17	0.05	103	76.51	113.71	↓	0.7046
Sample	Nichrome	0.64	8.22	14,762	0.33		Ni-57	0.9774
Sample Weight [g]	0.0258	1.30	6.72	12,254	0.32		↓	0.9774
error [%]	0.39	2.88	4.26	8,342	0.55		↓	0.9774
Neutron Flux		6.85	2.29	5,143	1.39		Co-58g	0.9775
[n/sec/cm^2]	2.020E+10	12.85	1.83	4,399	1.94		↓	0.9775
		23.85	1.66	4,007	2.17		↓	0.9775
		49.70	1.36	3,346	2.77		↓	0.9775
		99.89	0.89	2,273	4.27		↓	0.9775
		200.12	0.57	1,473	8.12		Co-58g, Co-57, Co-60g	0.9485
		402.94	0.27	749	29.25		↓	0.9087
Sample	Inconel-600	0.62	34.61	75,923	0.06		Ni-57	0.9706
Sample Weight [g]	0.1332	1.31	26.58	58,359	0.06		↓	0.9706
error [%]	0.08	2.89	17.87	39,611	0.11		↓	0.9706
Neutron Flux		6.86	10.11	24,511	0.28		Co-58g	0.9739
[n/sec/cm^2]	2.087E+10	12.86	8.26	21,021	0.40		↓	0.9739
		23.84	7.52	19,188	0.45		↓	0.9739
		49.69	6.19	16,015	0.57		↓	0.9739
		99.88	4.08	10,677	0.90		↓	0.9739
		200.11	2.67	7,016	1.71		Co-58g, Co-57, Co-60g	0.9447
		402.94	1.13	3,332	7.70		↓	0.9037

Table 3.7.2 Important parameters affecting on the experimental data for the 7 hours irradiation. (5/5)

Experimental Condition \ Parameters		Cooling Time [days]	Dead Time [%]	Counting Rate [cps]	BG Fraction [%]	Tape Fraction [%]	Dominant Nuclide(s)	Correction Factor
Sample	SS304	0.63	8.25	12,967	0.29		Mn-56	0.9112
Sample Weight [g]	0.0385	1.30	1.60	2,948	1.51		Ni-57	0.9762
error [%]	0.26	2.88	1.02	2,081	2.67		Ni-57, Co-58g	0.9765
Neutron Flux		6.85	0.63	1,464	5.62		Co-58g	0.9768
[n/sec/cm^2]	2.060E+10	12.84	0.54	1,279	7.17		↓	0.9768
		23.84	0.48	1,132	8.04		↓	0.9768
		49.69	0.37	901	9.98		↓	0.9768
		99.88	0.25	601	14.18		↓	0.9768
		200.10	0.21	416	21.21		Mn54,Co58g,Co57,Co60g	0.9423
		402.93	0.12	274	44.80		↓	0.9262
Sample	SS316	0.62	8.68	14,711	0.29		Mn-56	0.9135
Sample Weight [g]	0.0360	1.30	2.73	5,531	0.97		Ni-57	0.9765
error [%]	0.28	2.88	1.73	3,766	1.71		Ni-57, Co-58g	0.9768
Neutron Flux		6.85	0.94	2,210	3.89		Co-58g	0.9770
[n/sec/cm^2]	2.073E+10	12.84	0.69	1,657	5.47		↓	0.9770
		23.83	0.59	1,396	6.39		↓	0.9770
		49.69	0.47	1,116	8.01		↓	0.9770
		99.88	0.31	746	11.71		↓	0.9770
		200.10	0.25	509	18.22		Mn54,Co58g,Co57,Co60g	0.9436
		402.93	0.13	313	43.13		↓	0.9232

Table 3.8.1 Nuclear data base used to determine the correction factors. (1/8)

Nuclide	Q [keV]	T-1/2	Decay Mode	Decay Mode [%]	Photon Energy [keV]	Photon Intensity [%]	Photon Energy per Deacy [keV]	Efficiency [%]	Absorbed Photon Energy [keV]	Continuous Radiation	Real Energy [keV]	Fraction [%]	Photon Effi. [%]
Be-11	11506.0	13.8 s	beta-	100.00	2124.49	35.50	754.19	79.10	596.57	beta-	4652.0	75.9	
			beta+		4666.06	1.82	84.92	77.16	65.52	beta+		0.0	
			EC		5019.08	0.47	23.44	77.35	18.13	IB	25.0	0.4	
			IT		5851.50	2.13	124.64	77.84	97.02	Atomic e		0.0	
					6789.59	4.48	304.17	78.43	238.58	Photon	1455.0	23.7	78.7
					7974.78	1.90	151.52	79.12	119.88				
N-13	2220.5	9.965 m	beta-							beta-		0.0	
			beta+	99.81						beta+	491.0	32.5	
			EC	0.20						IB	0.6	0.0	
			IT							Atomic e		0.0	
										Photon		67.5	98.5
N-16	10419.1	7.13 s	beta-	100.00	2741.10	0.89	24.40	77.43	18.89	beta-	2693.0	95.3	
			beta+		6129.22	68.80	4216.90	78.02	3289.95	beta+		0.0	
			EC		7115.20	4.70	334.41	78.63	262.96	IB	11.7	0.4	
			IT							Atomic e		0.0	
										Photon	120.0	4.2	78.1
F-18	1655.3	1.830 h	beta-							beta-		0.0	
			beta+	96.90						beta+	242.0	19.6	
			EC	3.10						IB	0.2	0.0	
			IT							Atomic e		0.0	
										Photon		80.3	98.5
O-19	4820.0	26.9 s	beta-	100.00	109.89	2.54	2.79	99.20	2.77	beta-	1742.0	64.8	
			beta+		197.14	95.90	189.06	99.46	188.04	beta+		0.0	
			EC		1356.84	50.40	683.85	85.54	584.98	IB	5.6	0.2	
			IT		1444.09	2.64	38.12	84.46	32.20	Atomic e		0.0	
					1553.97	1.39	21.60	83.25	17.98	Photon	939.0	35.0	88.3
Na-22	2842.0	2.602 y	beta-		1274.53	99.94	1273.73	86.66	1103.75	beta-		0.0	
			beta+	89.40						beta+	195.0	8.2	
			EC	10.60						IB	0.2	0.0	
			IT							Atomic e		0.0	
										Photon	1273.7	91.8	98.3
Ne-23	4375.9	37.2 s	beta-	100.00	439.85	32.90	144.71	98.82	143.01	beta-	1902.0	91.7	
			beta+		1636.50	0.99	16.20	82.43	13.36	beta+		0.0	
			EC							IB	6.3	0.3	
			IT							Atomic e		0.0	
										Photon	165.0	8.0	97.2
Na-24	5513.6	14.659 h	beta-	100.00	1368.60	100.00	1368.60	85.39	1168.65	beta-	554.0	11.8	
			beta+		2754.00	99.94	2752.45	77.42	2130.83	beta+		0.0	
			EC							IB	0.8	0.0	
			IT							Atomic e		0.0	
										Photon	4123.0	88.1	80.1
Mg-27	2610.6	9.46 m	beta-	100.00	170.68	0.79	1.35	99.41	1.34	beta-	702.0	43.4	
			beta+		843.76	73.00	615.94	93.88	578.22	beta+		0.0	
			EC		1014.43	29.10	295.20	90.84	268.17	IB	1.2	0.1	
			IT							Atomic e		0.0	
										Photon	913.0	56.5	92.9
Al-28	4641.8	2.2406 m	beta-	100.00	1778.99	100.00	1778.99	81.21	1444.79	beta-	1242.0	41.1	
			beta+							beta+		0.0	
			EC							IB	3.2	0.1	
			IT							Atomic e		0.0	
										Photon	1779.0	58.8	81.2
Al-29	3680.0	6.56 m	beta-	100.00	1152.58	1.03	11.91	88.49	10.54	beta-	977.0	41.5	
			beta+		1273.36	91.30	1162.58	86.67	1007.63	beta+		0.0	
			EC		2028.10	3.51	71.19	79.58	56.65	IB	2.1	0.1	
			IT		2425.89	5.20	126.15	78.03	98.43	Atomic e		0.0	
										Photon	1376.0	58.4	85.5
P-30	4225.8	2.498 m	beta-							beta-		0.0	
			beta+	99.86						beta+	1435.0	58.3	
			EC	0.14						IB	4.0	0.2	
			IT							Atomic e		0.0	
										Photon	1.4	41.5	98.5
Si-31	1490.5	2.622 h	beta-	100.00						beta-	595.0	99.7	
			beta+							beta+		0.0	
			EC							IB	0.9	0.2	
			IT							Atomic e		0.0	
										Photon	0.9	0.2	
P-32	1710.3	14.282 d	beta-	100.00						beta-	695.0	99.8	
			beta+							beta+		0.0	
			EC							IB	1.2	0.2	
			IT							Atomic e		0.0	
										Photon		0.0	
P-34	5374.3	12.4 s	beta-	100.00	2127.70	15.00	319.16	79.09	252.40	beta-	2306.0	87.1	
			beta+							beta+		0.0	
			EC							IB	8.6	0.3	
			IT							Atomic e		0.0	
										Photon	334.2	12.6	79.1

Table 3.8.1 Nuclear data base used to determine the correction factors. (2/8)

Nuclide	Q [keV]	T-1/2	Decay Mode	Decay Mode [%]	Photon Energy [keV]	Photon Intensity [%]	Photon Energy per Deacy [keV]	Efficiency [%]	Absorbed Photon Energy [keV]	Continuous Radiation	Real Energy [keV]	Fraction [%]	Photon Effi. [%]
Cl-38	4916.5	37.24 m	beta-	100.00	1642.69	31.00	509.23	82.38	419.49	beta-	1553.0	52.1	
			beta+		2167.68	42.00	910.43	78.91	718.40	beta+		0.0	
			EC							IB	5.2	0.2	
			IT							Atomic e		0.0	
										Photon	1421.0	47.7	80.2
K-38	5913.0	7.64 m	beta-		2167.68	99.86	2164.60	78.91	1708.04	beta-		0.0	
			beta+	99.50						beta+	1204.0	27.4	
			EC	0.50						IB	3.1	0.1	
			IT							Atomic e		0.0	
										Photon	2170.4	72.5	98.1
Ar-41	2492.3	1.83 h	beta-	100.00	1293.64	99.16	1282.77	86.39	1108.16	beta-	464.0	26.5	
			beta+							beta+		0.0	
			EC							IB	0.6	0.0	
			IT							Atomic e		0.0	
										Photon	1283.6	73.4	86.4
K-42	3525.1	12.360 h	beta-	100.00	1524.58	18.80	286.62	83.56	239.50	beta-	1425.0	82.9	
			beta+							beta+		0.0	
			EC							IB	4.1	0.2	
			IT							Atomic e		0.0	
										Photon	290.0	16.9	83.6
K-44	5660.0	22.1 m	beta-	100.00	368.22	2.25	8.28	99.21	8.22	beta-	1414.0	37.3	
			beta+		651.36	3.02	19.67	96.79	19.04	beta+		0.0	
			EC		726.49	3.77	27.39	95.76	26.23	IB	4.6	0.1	
			IT		747.64	2.09	15.63	95.45	14.91	Atomic e		0.0	
					876.55	1.73	15.16	93.29	14.15	Photon	2377.0	62.6	83.3
					1024.74	6.67	68.35	90.66	61.96				
					1126.08	7.60	85.58	88.92	76.10				
					1157.01	58.00	671.06	88.42	593.34				
					1499.46	7.87	118.01	83.83	98.93				
					1752.64	4.06	71.16	81.42	57.94				
					1777.97	2.12	37.69	81.22	30.62				
					2150.80	22.70	488.23	78.98	385.61				
					2519.00	9.69	244.09	77.81	189.92				
					3395.49	1.66	56.37	76.84	43.31				
					3661.37	6.09	222.98	76.44	170.45				
Sc-46m	142.5	18.70 s	beta-		142.53	62.00	88.37	99.33	87.78	beta-		0.0	
			beta+							beta+		0.0	
			EC							IB		0.0	
			IT	100.00						Atomic e	52.3	37.1	
										Photon	88.6	62.9	99.3
Sc-46g	2366.5	83.83 d	beta-	100.00	889.25	99.98	889.11	93.06	827.36	beta-	112.0	5.3	
			beta+		1120.51	99.99	1120.36	89.01	997.21	beta+		0.0	
			EC							IB	0.0	0.0	
			IT							Atomic e		0.0	
										Photon	2009.5	94.7	90.8
K-47	6645.0	17.5 s	beta-	100.00	564.70	14.60	82.45	97.78	80.61	beta-	1805.0	41.0	
			beta+		585.80	85.00	497.93	97.55	485.75	beta+		0.0	
			EC		2013.10	100.00	2013.10	79.66	1603.72	IB	5.8	0.1	
			IT							Atomic e		0.0	
										Photon	2596.0	58.9	83.7
Ca-47	1988.0	4.536 d	beta-	100.00	468.22	6.74	31.56	98.63	31.12	beta-	345.0	24.5	
			beta+		807.85	6.89	55.66	94.49	52.59	beta+		0.0	
			EC		1297.06	74.90	971.50	86.34	838.80	IB	0.4	0.0	
			IT							Atomic e		0.0	
										Photon	1063.0	75.5	87.1
Sc-47	600.6	3.341 d	beta-	100.00	159.38	68.00	108.38	99.38	107.71	beta-	162.0	60.0	
			beta+							beta+		0.0	
			EC							IB	0.1	0.0	
			IT							Atomic e		0.0	
										Photon	108.0	40.0	99.4
Sc-48	3994.0	1.821 d	beta-	100.00	175.36	7.47	13.10	99.42	13.02	beta-	221.0	6.2	
			beta+		983.50	100.00	983.50	91.21	897.02	beta+		0.0	
			EC		1037.50	97.50	1011.56	90.43	914.75	IB	0.2	0.0	
			IT		1212.85	2.38	28.87	87.55	25.27	Atomic e		0.0	
					1312.05	100.00	1312.05	86.14	1130.14	Photon	3349.0	93.8	89.0
Sc-49	2004.0	57.4 m	beta-	100.00						beta-	822.0	99.7	
			beta+							beta+		0.0	
			EC							IB	1.6	0.2	
			IT							Atomic e		0.0	
										Photon	1.0	0.1	
Cr-49	2627.0	42.1 m	beta-		62.29	16.70	10.40	98.95	10.29	beta-		0.0	
			beta+	93.00	90.64	54.20	49.13	99.11	48.69	beta+	595.0	35.9	
			EC	7.00	152.93	30.90	47.25	99.37	46.95	IB	1.2	0.1	
			IT							Atomic e		0.0	
										Photon	109.0	64.0	98.5
Sc-50	6888.0	1.71 m	beta-	100.00	523.81	88.70	464.62	98.17	456.12	beta-	1626.0	33.7	
			beta+		1121.14	99.50	1115.54	89.00	992.80	beta+		0.0	
			EC		1553.79	100.00	1553.79	83.25	1293.54	IB	4.9	0.1	
			IT		2205.81	1.27	28.01	78.75	22.06	Atomic e		0.0	
										Photon	3192.0	66.2	87.4

Table 3.8.1 Nuclear data base used to determine the correction factors. (3/8)

Nuclide	Q [keV]	T-1/2	Decay Mode	Decay Mode [%]	Photon Energy [keV]	Photon Intensity [%]	Photon Energy per Deacy [keV]	Efficiency [%]	Absorbed Photon Energy [keV]	Continuous Radiation	Real Energy [keV]	Fraction [%]	Photon Effi. [%]
Ti-51	2472.6	5.76 m	beta-	100.00	320.08	93.00	297.68	99.38	295.84	beta-	868.0	70.1	
			beta+		608.56	1.18	7.18	97.30	6.99	beta+		0.0	
			EC		928.64	6.90	64.08	92.31	59.15	IB	1.8	0.1	
			IT							Atomic e		0.0	
										Photon	369.0	29.8	98.1
Cr-51	751.4	27.704 d	beta-		5.00	22.00	1.10	98.52	1.08	beta-		0.0	
			beta+		320.08	9.83	31.46	99.38	31.27	beta+		0.0	
			EC	100.00						IB	0.1	0.3	
			IT							Atomic e	3.1	8.6	
										Photon	32.5	91.1	99.4
V-52	3975.7	3.75 m	beta-	100.00	1434.08	100.00	1434.08	84.58	1212.98	beta-	1068.0	42.5	
			beta+							beta+		0.0	
			EC							IB	2.5	0.1	
			IT							Atomic e		0.0	
										Photon	1445.0	57.4	84.6
V-53	3436.0	1.61 m	beta-	100.00	1006.24	90.00	905.62	90.99	824.05	beta-	1005.0	49.1	
			beta+		1289.12	10.00	128.91	86.45	111.45	beta+		0.0	
			EC							IB	2.2	0.1	
			IT							Atomic e		0.0	
										Photon	1038.0	50.8	90.4
Fe-53	3743.6	8.51 m	beta-		377.92	42.00	158.73	99.17	157.41	beta-		0.0	
			beta+	97.00						beta+	1105.0	48.4	
			EC	3.00						IB	2.9	0.1	
			IT							Atomic e		0.0	
										Photon	185.0	51.5	98.5
Mn-54	1377.1	312.2 d	beta-		5.50	25.00	1.38	98.53	1.35	beta-		0.0	
			beta+		834.83	99.98	834.62	94.03	784.80	beta+		0.0	
			EC	100.00						IB	0.0	0.0	
			IT							Atomic e	3.4	0.4	
										Photon	836.0	99.6	94.0
Cr-55	2603.2	3.497 m	beta-	100.00						beta-	1101.0	99.8	
			beta+							beta+		0.0	
			EC							IB	2.6	0.2	
			IT							Atomic e		0.0	
										Photon		0.0	
Mn-56	3695.7	2.578 h	beta-	100.00	846.81	98.90	837.50	93.82	785.76	beta-	830.0	32.9	
			beta+		1810.80	27.20	492.54	80.97	398.82	beta+		0.0	
			EC							IB		0.0	
			IT							Atomic e		0.0	
										Photon	1692.0	67.1	89.1
Mn-57	2691.0	1.45 m	beta-	100.00	6.40	26.30	1.68	98.53	1.66	beta-	1100.0	92.5	
			beta+		14.41	10.70	1.54	98.60	1.52	beta+		0.0	
			EC		122.06	10.80	13.18	99.26	13.08	IB	2.6	0.2	
			IT		136.47	1.35	1.84	99.31	1.83	Atomic e	10.8	0.9	
					352.32	1.56	5.50	99.28	5.46	Photon	75.5	6.4	97.6
					691.98	4.15	28.72	96.25	27.64				
Co-57	836.4	271.77 d	beta-		6.40	55.00	3.52	98.53	3.47	beta-		0.0	
			beta+		14.41	9.54	1.37	98.60	1.36	beta+		0.0	
			EC	100.00	122.06	85.50	104.36	99.26	103.59	IB	0.1	0.1	
			IT		136.47	10.69	14.59	99.31	14.49	Atomic e	17.6	12.3	
										Photon	125.2	87.6	99.2
Ni-57	3265.0	1.503 d	beta-		6.90	20.30	1.40	98.54	1.38	beta-		0.0	
			beta+	40.00	127.23	12.90	16.41	99.28	16.29	beta+	143.0	6.9	
			EC	60.00	1377.62	77.90	1073.17	85.28	915.15	IB	0.9	0.0	
			IT		1757.53	7.10	124.78	81.38	101.55	Atomic e	4.4	0.2	
					1919.46	14.70	282.16	80.22	226.35	Photon	1509.0	92.8	98.0
Co-58m	24.9	9.15 h	beta-		6.90	26.00	1.79	98.54	1.77	beta-		0.0	
			beta+							beta+		0.0	
			EC							IB		0.0	
			IT	100.00						Atomic e	20.8	91.9	
										Photon	1.8	8.1	98.5
Co-58g	2308.0	70.92 d	beta-		7.00	26.00	1.82	98.54	1.79	beta-		0.0	
			beta+	14.90	910.79	99.50	906.24	92.65	839.63	beta+	30.0	3.0	
			EC	85.10						IB	0.7	0.1	
			IT							Atomic e	3.6	0.4	
										Photon	824.0	96.6	98.2
Co-60g	2823.6	5.271 y	beta-	100.00	1173.24	99.90	1172.06	88.16	1033.31	beta-	96.0	3.7	
			beta+		1132.50	99.98	1132.30	88.81	1005.62	beta+		0.0	
			EC							IB	0.0	0.0	
			IT							Atomic e		0.0	
										Photon	2504.4	96.3	88.5
Co-60m	2823.6	5.271 y	beta-	0.25	58.60	2.01	1.18	98.92	1.17	beta-	1.5	2.5	
			beta+		1332.50	0.25	3.33	85.86	2.86	beta+		0.0	
			EC							IB	0.0	0.0	
			IT	99.75						Atomic e	52.1	86.6	
										Photon	6.6	11.0	89.3

Table 3.8.1 Nuclear data base used to determine the correction factors. (4/8)

Nuclide	Q [keV]	T-1/2	Decay Mode	Decay Mode [%]	Photon Energy [keV]	Photon Intensity [%]	Photon Energy per Deacy [keV]	Efficiency [%]	Absorbed Photon Energy [keV]	Continuous Radiation	Real Energy [keV]	Fraction [%]	Photon Effi. [%]
Co-62g	5315.0	1.50 m	beta-	100.00	1129.00	11.30	127.58	88.87	113.38	beta-	1639.0	50.5	
			beta+		1173.04	83.80	983.01	88.16	866.67	beta+		0.0	
			EC		1985.20	1.50	29.78	79.82	23.77	IB	5.1	0.2	
			IT		2302.01	14.70	338.40	78.40	265.29	Atomic e		0.0	
					2346.10	1.30	30.50	78.26	23.87	Photon	1599.0	49.3	85.7
Co-62m	5337.0	13.91 m	beta-	100.00	777.65	1.80	14.00	94.98	13.30	beta-	1058.0	28.2	
			beta+		874.94	1.30	11.37	93.32	10.61	beta+		0.0	
			EC		1129.00	1.32	14.90	88.87	13.24	IB	2.6	0.1	
			IT		1163.62	68.10	792.43	88.31	699.81	Atomic e		0.0	
					1173.04	97.90	1148.41	88.16	1012.49	Photon	2690.0	71.7	86.1
					1718.80	6.80	116.88	81.70	95.49				
					1753.41	0.60	10.52	81.42	8.57				
					2003.91	18.60	372.73	79.72	297.12				
					2104.75	6.50	136.81	79.19	108.34				
					2302.01	1.73	39.82	78.40	31.22				
					2882.37	1.10	31.71	77.27	24.50				
Cu-62	3949.0	9.74 m	beta-							beta-		0.0	
			beta+	97.00						beta+	1280.0	56.1	
			EC	3.00						IB	3.7	0.2	
			IT							Atomic e	0.1	0.0	
										Photon	7.1	43.7	98.5
Cu-64	1674.5	12.701 h	beta-	37.10						beta-	71.0	22.5	
			beta+	18.00						beta+	49.8	15.8	
	578.2		EC	44.90						IB	0.6	0.2	
			IT							Atomic e	1.9	0.6	
										Photon	7.7	60.9	98.5
Br-78	3574.0	6.46 m	beta-		11.20	3.44	0.39	98.57	0.38	beta-		0.0	
			beta+	92.00	613.85	13.60	83.48	97.24	81.18	beta+	1022.0	49.7	
			EC	8.00						IB	3.1	0.2	
			IT							Atomic e	0.5	0.0	
										Photon	89.2	50.1	98.5
Sr-83g	4410.0	1.350 d	beta-		381.57	11.90	45.41	99.15	45.02	beta-		0.0	
			beta+	24.00	389.71	1.55	6.04	99.11	5.99	beta+	123.0	13.1	
			EC	76.00	418.63	5.00	20.93	98.96	20.71	IB	1.1	0.1	
			IT		423.91	1.56	6.61	98.92	6.54	Atomic e	26.1	2.8	
					762.67	30.00	228.80	95.22	217.86	Photon	540.0	83.9	98.5
					778.65	1.94	15.11	94.96	14.35				
					1147.33	1.23	14.11	88.57	12.50				
					1160.22	1.53	17.75	88.37	15.69				
Sr-85m	1304.0	1.126 h	beta-		13.40	8.00	1.07	98.59	1.06	beta-		0.0	
	238.8		beta+		151.18	12.40	18.75	99.36	18.63	beta+		0.0	
			EC	13.00	231.78	84.10	194.93	99.49	193.94	IB	0.0	0.0	
			IT	87.00						Atomic e	14.0	6.1	
										Photon	216.0	93.9	99.5
Sr-85g	1065.0	64.84 d	beta-		13.40	59.00	7.91	98.59	7.79	beta-		0.0	
			beta+		514.00	99.27	510.24	98.26	501.35	beta+		0.0	
			EC							IB	0.0	0.0	
			IT	100.00						Atomic e	8.4	1.6	
										Photon	518.3	98.4	98.3
Rb-86m	556.1	1.017 m	beta-		556.07	98.19	546.01	97.86	534.34	beta-		0.0	
			beta+							beta+		0.0	
			EC							IB		0.0	
			IT	100.00						Atomic e	9.9	1.8	
										Photon	546.1	98.2	97.9
Sr-87m	388.4	2.80 h	beta-		388.40	82.30	319.65	99.12	316.84	beta-		0.0	
			beta+							beta+		0.0	
			EC	0.30						IB		0.0	
			IT	99.70						Atomic e	67.4	17.4	
										Photon	321.0	82.6	99.1
Rb-88	5316.0	17.8 m	beta-	100.00	898.07	14.10	126.63	92.89	117.63	beta-	2068.0	76.5	
			beta+		1836.08	21.40	392.92	80.79	317.43	beta+		0.0	
			EC		2677.92	1.96	52.49	77.52	40.69	IB	7.6	0.3	
			IT							Atomic e		0.0	
										Photon	629.0	23.3	83.2
Y-88	3622.6	106.61 d	beta-		14.20	60.00	8.52	98.60	8.40	beta-		0.0	
			beta+	0.22	898.07	92.70	832.51	92.89	773.32	beta+	0.8	0.0	
			EC	99.78	1836.08	99.35	1824.14	80.79	1473.67	IB	0.2	0.0	
			IT							Atomic e	5.4	0.2	
										Photon	2684.0	99.8	85.7
Y-89m	909.2	16.06 s	beta-		909.15	99.14	901.33	92.68	835.37	beta-		0.0	
			beta+							beta+		0.0	
			EC							IB		0.0	
			IT	100.00						Atomic e	7.7	0.8	
										Photon	901.4	99.2	92.7
Zr-89m	3420.7	4.18 m	beta-		15.00	5.00	0.75	98.61	0.74	beta-		0.0	
			beta+	3.02	587.70	89.50	525.99	97.53	513.02	beta+	7.1	1.0	
	587.7		EC	3.18	1507.40	6.04	91.05	83.74	76.25	IB	0.1	0.0	
			IT	93.80						Atomic e	24.7	3.6	
										Photon	618.0	95.3	98.0

Table 3.8.1 Nuclear data base used to determine the correction factors. (5/8)

Nuclide	Q [keV]	T-1/2	Decay Mode	Decay Mode [%]	Photon Energy [keV]	Photon Intensity [%]	Photon Energy per Deacy [keV]	Efficiency [%]	Absorbed Photon Energy [keV]	Continuous Radiation	Real Energy [keV]	Fraction [%]	Photon Effi. [%]
Zr-89g	2833.0	3.268 d	beta-		15.00	49.00	7.35	98.61	7.25	beta-		0.0	
			beta+	23.00	909.15	99.01	900.15	92.68	834.27	beta+	90.0	7.1	
			EC	77.00						IB	1.4	0.1	
			IT							Atomic e	11.5	0.9	
										Photon	925.7	91.9	98.3
Y-90m	682.0	3.16 h	beta-		202.47	96.60	195.59	99.47	194.55	beta-		0.0	
			beta+		479.49	91.00	436.34	98.54	429.97	beta+		0.0	
			EC							IB		0.0	
			IT	100.00						Atomic e	47.5	7.0	
										Photon	634.0	93.0	98.8
Y-91m	555.6	49.71 m	beta-		15.00	3.00	0.45	98.61	0.44	beta-		0.0	
			beta+		555.56	94.90	527.23	97.87	515.99	beta+		0.0	
			EC							IB		0.0	
			IT	100.00						Atomic e	27.9	5.0	
										Photon	527.7	95.0	97.9
Nb-91m	1357.9	60.86 d	beta-		16.50	45.00	7.43	98.62	7.32	beta-		0.0	
			beta+		18.70	7.20	1.35	98.64	1.33	beta+		0.0	
			EC	7.00	104.50	0.56	0.58	99.18	0.58	IB		0.0	
			IT	93.00	1205.00	4.00	48.20	87.67	42.26	Atomic e	90.0	63.8	
										Photon	51.0	36.2	89.5
Mo-91m	5091.0	1.09 m	beta-		17.00	5.00	0.85	98.62	0.84	beta-		0.0	
			beta+	44.00	652.98	48.20	314.74	96.76	304.55	beta+	541.0	27.8	
	653.0		EC	5.90	1207.98	18.80	227.10	87.63	199.00	IB	2.1	0.1	
			IT	50.10	1507.91	24.40	367.93	83.74	308.10	Atomic e	12.2	0.6	
										Photon	943.0	71.5	98.3
Mo-91g	4438.0	15.49 m	beta-		17.00	4.00	0.68	98.62	0.67	beta-		0.0	
			beta+	94.00						beta+	1453.0	59.6	
			EC	6.00						IB	5.5	0.2	
			IT							Atomic e	0.3	0.0	
										Photon	19.4	40.2	98.5
Nb-92m	2141.4	10.15 d	beta-		16.00	64.00	10.24	98.61	10.10	beta-		0.0	
			beta+	0.11	914.81	1.73	15.83	92.57	14.65	beta+	0.1	0.0	
			EC	99.89	934.53	99.00	925.18	92.19	852.94	IB	0.4	0.0	
			IT		1847.33	0.90	16.63	80.71	13.42	Atomic e	5.6	0.6	
										Photon	967.9	99.4	92.7
Y-94	4920.0	18.7 m	beta-	100.00	381.60	2.02	7.71	99.15	7.64	beta-	1813.0	70.0	
			beta+		550.90	4.90	26.99	97.91	26.43	beta+		0.0	
			EC		752.60	1.40	10.54	95.37	10.05	IB	6.1	0.2	
			IT		918.74	56.00	514.49	92.50	475.90	Atomic e		0.0	
					1138.90	6.00	68.33	88.71	60.62	Photon	772.0	29.8	91.8
					1671.40	2.46	41.12	82.11	33.76				
Zr-95	1124.3	64.02 d	beta-	100.00	235.68	0.29	0.69	99.49	0.69	beta-	117.0	13.7	
			beta+		724.20	44.10	319.37	95.79	305.94	beta+		0.0	
			EC		756.73	54.50	412.42	95.31	393.07	IB	0.1	0.0	
			IT							Atomic e	3.0	0.3	
										Photon	733.0	85.9	95.5
Nb-95m	1161.3	3.62 d	beta-	2.50	17.00	40.00	6.80	98.62	6.71	beta-	9.8	4.0	
			beta+		204.11	2.34	4.78	99.47	4.75	beta+		0.0	
			EC		235.68	24.90	58.68	99.49	58.39	IB	0.0	0.0	
			IT	97.50						Atomic e	161.0	66.5	
										Photon	71.2	29.4	99.4
Nb-95g	925.6	34.97 d	beta-	100.00	765.79	99.79	764.18	95.17	727.25	beta-	43.5	5.4	
			beta+							beta+		0.0	
			EC							IB	0.0	0.0	
			IT							Atomic e		0.0	
										Photon	764.3	94.6	95.2
Mo-99	1357.0	2.7477 d	beta-	100.00	18.40	11.00	2.02	98.63	2.00	beta-	390.0	57.3	
			beta+		140.47	90.70	127.41	99.33	126.55	beta+		0.0	
			EC		181.07	6.07	10.99	99.44	10.93	IB	0.5	0.1	
			IT		739.51	12.14	89.78	95.57	85.80	Atomic e	17.6	2.6	
					777.92	4.35	33.84	94.98	32.14	Photon	272.0	40.0	97.5
Tc-99m	142.7	6.006 h	beta-		18.30	8.00	1.46	98.63	1.44	beta-		0.0	
			beta+		140.47	87.20	122.49	99.33	121.67	beta+		0.0	
			EC	100.00						IB		0.0	
			IT							Atomic e	14.2	10.3	
										Photon	123.9	89.7	99.3
In-111g	864.0	2.807 d	beta-		22.98	24.10	5.54	98.67	5.47	beta-		0.0	
			beta+		23.17	45.40	10.52	98.67	10.38	beta+		0.0	
			EC	100.00	26.09	11.60	3.03	98.69	2.99	IB	0.1	0.0	
			IT		171.28	90.24	154.56	99.41	153.66	Atomic e	33.9	7.7	
					245.38	94.00	230.66	99.49	229.49	Photon	405.2	92.3	99.4
Sn-111	2451.0	35.3 m	beta-		24.00	51.00	12.24	98.68	12.08	beta-		0.0	
			beta+	31.00	762.00	1.44	10.97	95.23	10.45	beta+	195.0	27.7	
			EC	69.00	1153.20	2.70	31.14	88.48	27.55	IB	2.4	0.3	
			IT		1610.50	1.25	20.13	82.68	16.65	Atomic e	4.0	0.6	
					1915.10	1.83	35.05	80.25	28.12	Photon	186.0	71.4	98.5

Table 3.8.1 Nuclear data base used to determine the correction factors. (6/8)

Nuclide	Q [keV]	T-1/2	Decay Mode	Decay Mode [%]	Photon Energy [keV]	Photon Intensity [%]	Photon Energy per Deacy [keV]	Efficiency [%]	Absorbed Photon Energy [keV]	Continuous Radiation	Real Energy [keV]	Fraction [%]	Photon Effi. [%]
In-112m	155.5	20.9 m	beta-		24.20	58.00	14.04	98.68	13.85	beta-		0.0	
			beta+		155.50	12.80	19.90	99.37	19.78	beta+		0.0	
			EC							IB		0.0	
			IT	100.00						Atomic e	121.0	78.0	
										Photon	34.2	22.0	99.1
In-112g	2589.0	14.4 m	beta-	44.00	23.20	25.00	5.80	98.67	5.72	beta-	94.0	18.6	
			beta+	22.00	606.71	0.67	4.06	97.32	3.95	beta+	151.0	30.0	
	661.0		EC	34.00	617.48	2.80	17.29	97.20	16.80	IB	1.6	0.3	
			IT							Atomic e	1.9	0.4	
										Photon	30.9	50.7	98.5
Sn-113	1039.0	115.09 d	beta-		24.20	98.00	23.72	98.68	23.40	beta-		0.0	
			beta+		255.07	1.82	4.64	99.49	4.62	beta+		0.0	
			EC	100.00	391.69	64.00	250.68	99.10	248.43	IB	0.1	0.0	
			IT							Atomic e	139.0	33.2	
										Photon	280.0	66.8	99.1
Sn-117m	314.6	13.61 d	beta-		25.30	68.00	17.20	98.69	16.98	beta-		0.0	
			beta+		156.02	2.11	3.29	99.37	3.27	beta+		0.0	
			EC		158.56	86.40	137.00	99.38	136.15	IB		0.0	
			IT	100.00						Atomic e	161.0	50.5	
										Photon	157.9	49.5	99.3
In-118m	4260.0	4.40 m	beta-	100.00	208.74	2.30	4.80	99.48	4.78	beta-	545.0	16.7	
			beta+		445.83	5.90	26.30	98.79	25.98	beta+		0.0	
			EC		474.65	3.00	14.24	98.58	14.04	IB	0.8	0.0	
			IT		683.38	55.00	375.86	96.37	362.20	Atomic e	4.5	0.1	
					1050.75	96.90	1018.18	90.20	918.34	Photon	2718.0	83.2	89.9
					1229.69	96.00	1180.50	87.30	1030.62				
Sn-121g	388.9	1.128 d	beta-	100.00						beta-	115.0	100.0	
			beta+							beta+		0.0	
			EC							IB	0.0	0.0	
			IT							Atomic e		0.0	
										Photon		0.0	
Sn-123g	1403.0	129.2 d	beta-	100.00						beta-	523.0	98.6	
			beta+							beta+		0.0	
			EC							IB	0.8	0.1	
			IT							Atomic e		0.0	
										Photon	6.9	1.3	
Sn-123m	1427.6	40.1 m	beta-	100.00	26.36	9.05	2.39	98.69	2.35	beta-	459.0	73.9	
			beta+		29.71	1.55	0.46	98.72	0.45	beta+		0.0	
			EC		160.32	85.60	137.23	99.39	136.39	IB	0.6	0.1	
			IT							Atomic e	20.2	3.3	
										Photon	141.0	22.7	99.4
Ba-131g	2960.0	11.8 d	beta-		31.00	97.47	30.22	98.73	29.83	beta-		0.0	
			beta+	0.00	123.78	29.10	36.02	99.26	35.75	beta+	0.0	0.0	
			EC	100.00	133.58	2.19	2.93	99.30	2.90	IB	0.2	0.0	
			IT		216.05	20.00	43.21	99.48	42.99	Atomic e	44.6	8.9	
					239.61	2.41	5.77	99.49	5.75	Photon	458.0	91.1	98.5
					249.42	2.81	7.01	99.49	6.97				
					373.19	13.30	49.63	99.19	49.23				
					403.99	1.29	5.21	99.04	5.16				
					486.45	1.89	9.19	98.49	9.05				
					496.26	44.00	218.35	98.41	214.88				
					584.97	1.23	7.20	97.56	7.02				
					620.04	1.57	9.73	97.17	9.46				
					1047.58	1.00	10.48	90.25	9.45				
Ba-133m	288.4	1.621 d	beta-		32.20	53.00	17.07	98.74	16.85	beta-		0.0	
			beta+		276.09	17.50	48.32	99.47	48.06	beta+		0.0	
			EC							IB		0.0	
			IT	99.99						Atomic e	219.0	76.6	
										Photon	66.8	23.4	99.3
Ba-135m	268.3	1.20 d	beta-		32.00	57.00	18.24	98.74	18.01	beta-		0.0	
			beta+		268.27	15.60	41.85	99.48	41.63	beta+		0.0	
			EC							IB		0.0	
			IT	100.00						Atomic e	207.0	77.5	
										Photon	60.0	22.5	99.3
Cs-136g	2548.5	13.16 d	beta-	100.00	33.00	17.00	5.61	98.74	5.54	beta-	100.0	4.3	
			beta+		66.94	12.50	8.37	98.97	8.28	beta+		0.0	
			EC		86.36	6.30	5.44	99.09	5.39	IB	0.0	0.0	
			IT		153.29	7.47	11.45	99.37	11.38	Atomic e	35.4	1.5	
					163.98	4.62	7.58	99.40	7.53	Photon	2171.0	94.1	95.3
					176.64	13.60	24.02	99.43	23.89				
					273.68	12.69	34.73	99.47	34.55				
					340.62	483.60	1647.24	99.32	1636.01				
					818.56	99.76	816.60	94.31	770.13				
					1048.09	79.70	835.33	90.24	753.82				
					1235.42	19.80	244.61	87.22	213.35				
Ba-137m	661.7	2.552 m	beta-		32.00	7.40	2.37	98.74	2.34	beta-		0.0	
			beta+		661.66	90.10	596.16	96.65	576.21	beta+		0.0	
			EC							IB		0.0	
			IT	100.00						Atomic e	65.2	9.8	
										Photon	599.0	90.2	96.7

Table 3.8.1 Nuclear data base used to determine the correction factors. (7/8)

Nuclide	Q [keV]	T-1/2	Decay Mode	Decay Mode [%]	Photon Energy [keV]	Photon Intensity [%]	Photon Energy per Deacy [keV]	Efficiency [%]	Absorbed Photon Energy [keV]	Continuous Radiation	Real Energy [keV]	Fraction [%]	Photon Effi. [%]
Cs-138g	5377.0	32.2 m	beta-	100.00	408.95	4.66	19.06	99.01	18.87	beta-	1237.0	34.3	
			beta+		462.78	30.70	142.07	98.67	140.18	beta+		0.0	
			EC		546.99	10.76	58.86	97.95	57.65	IB		0.0	
			IT		871.73	5.12	44.63	93.38	41.68	Atomic e	6.4	0.2	
					1009.77	29.80	300.91	90.93	273.62	Photon	2361.0	65.5	85.5
					1435.80	76.30	1095.51	84.56	926.39				
					2217.84	15.20	337.11	78.70	265.32				
					2639.44	7.63	201.39	77.58	156.24				
Ba-139	2310.0	1.41 h	beta-	100.00	34.00	4.00	1.36	98.75	1.34	beta-	891.0	94.3	
			beta+		165.85	22.00	36.49	99.40	36.27	beta+		0.0	
			EC							IB	1.9	0.2	
			IT							Atomic e	8.1	0.9	
										Photon	43.5	4.6	99.4
Lu-178g	2112.0	28.4 m	beta-	100.00	93.16	6.80	6.33	99.12	6.28	beta-	728.0	80.3	
			beta+		1269.27	1.05	13.33	86.73	11.56	beta+		0.0	
			EC		1309.95	1.58	20.70	86.16	17.83	IB	1.4	0.2	
			IT		1340.87	5.00	67.04	85.75	57.49	Atomic e	26.0	2.9	
										Photon	151.0	16.7	86.7
Lu-178m	2412.0	23.1 m	beta-	100.00	55.79	72.00	40.17	98.90	39.73	beta-	419.0	25.8	
			beta+		88.86	62.10	55.18	99.10	54.68	beta+		0.0	
			EC		93.16	17.40	16.21	99.12	16.07	IB	0.5	0.0	
			IT		213.42	81.30	173.51	99.48	172.61	Atomic e	149.0	9.2	
					216.65	2.53	5.48	99.48	5.45	Photon	1056.0	65.0	99.2
					325.55	94.40	307.32	99.37	305.37				
					331.66	11.80	39.14	99.35	38.88				
					426.35	97.40	415.27	98.91	410.74				
Ta-180g	708.0	8.15 h	beta-	13.00	55.00	70.00	38.50	98.90	38.08	beta-	27.8	27.2	
			beta+							beta+		0.0	
	853.0		EC	87.00						IB	0.4	0.3	
			IT							Atomic e	26.0	25.5	
										Photon	48.0	47.0	98.9
Hf-181	1028.0	42.4 d	beta-	100.00	9.00	11.00	0.99	98.56	0.98	beta-	131.0	18.2	
			beta+		57.00	27.00	15.39	98.91	15.22	beta+		0.0	
			EC		132.94	35.90	47.73	99.30	47.39	IB	0.6	0.1	
			IT		136.17	5.80	7.90	99.31	7.84	Atomic e	68.2	9.5	
					345.83	15.10	52.22	99.30	51.85	Photon	518.0	72.2	98.7
					482.00	80.60	388.49	98.52	382.75				
Ta-182g	1813.6	115.0 d	beta-	100.00	10.00	13.20	1.32	98.56	1.30	beta-	126.0	8.4	
			beta+		60.00	80.00	48.00	98.93	47.49	beta+		0.0	
			EC		100.11	14.00	14.01	99.16	13.90	IB	0.1	0.0	
			IT		160.00	13.00	20.80	99.39	20.67	Atomic e	81.3	5.4	
					230.00	16.50	37.95	99.49	37.76	Photon	1301.0	86.3	89.1
					1121.30	34.70	389.09	88.99	346.27				
					1189.05	16.50	196.19	87.92	172.49				
					1221.41	27.30	333.44	87.43	291.52				
					1231.02	11.63	143.17	87.28	124.96				
					1270.00	4.00	50.80	86.72	44.05				
Hf-183	2010.0	1.07 h	beta-	100.00	70.00	64.00	44.80	98.99	44.35	beta-	423.0	35.5	
			beta+		397.86	2.90	11.54	99.07	11.43	beta+		0.0	
			EC		459.07	27.00	123.95	98.69	122.33	IB	0.5	0.0	
			IT		793.75	65.00	515.94	94.72	488.70	Atomic e	17.8	1.5	
					1470.23	2.70	39.70	84.16	33.41	Photon	751.0	63.0	95.1
Ta-184	2866.0	8.7 h	beta-	100.00	10.00	30.00	3.00	98.56	2.96	beta-	394.0	18.4	
			beta+		60.00	38.00	22.80	98.93	22.56	beta+		0.0	
			EC		111.00	27.00	29.97	99.21	29.73	IB	0.5	0.0	
			IT		215.00	25.00	53.75	99.48	53.47	Atomic e	142.0	6.6	
					252.85	52.00	131.48	99.49	130.81	Photon	1610.0	75.0	96.0
					318.01	24.00	76.32	99.39	75.86				
					414.04	98.00	405.76	98.98	401.63				
					536.68	15.00	80.50	98.05	78.93				
					792.07	15.00	118.81	94.75	112.57				
					903.28	60.00	541.97	92.79	502.91				
					1110.09	2.32	25.75	89.18	22.97				
					1173.78	5.00	58.69	88.15	51.74				
Re-184m		165 d	beta-		10.00	44.00	4.40	98.56	4.34	beta-		0.0	
			beta+		60.00	82.00	49.20	98.93	48.67	beta+		0.0	
	1680.0		EC	25.00	104.73	19.20	20.11	99.18	19.94	IB	0.1	0.0	
	188.0		IT	75.00	161.27	6.64	10.71	99.39	10.64	Atomic e	139.8	26.4	
					220.00	14.00	30.80	99.49	30.64	Photon	390.0	73.6	95.8
					252.85	10.90	27.56	99.49	27.42				
					318.01	5.87	18.67	99.39	18.55				
					384.26	3.20	12.30	99.14	12.19				
					536.68	3.37	18.09	98.05	17.73				
					792.07	3.75	29.70	94.75	28.14				
					910.00	15.00	136.50	92.67	126.49				
					1173.78	2.00	23.48	88.15	20.69				
Re-184g	1492.0	38.0 d	beta-		10.00	31.00	3.10	98.56	3.06	beta-		0.0	
			beta+		60.00	88.00	52.80	98.93	52.24	beta+		0.0	
			EC	100.00	111.21	17.10	19.02	99.21	18.87	IB	0.4	0.0	
			IT		252.85	3.02	7.64	99.49	7.60	Atomic e	54.1	5.7	
					641.91	1.94	12.45	96.90	12.07	Photon	893.0	94.3	94.1
					792.07	37.50	297.03	94.75	281.43				
					894.76	15.50	138.69	92.95	128.91				
					903.28	38.10	344.15	92.79	319.35				

Table 3.8.1 Nuclear data base used to determine the correction factors. (8/8)

Nuclide	Q [keV]	T-1/2	Decay Mode	Decay Mode [%]	Photon Energy [keV]	Photon Intensity [%]	Photon Energy per Deacy [keV]	Efficiency [%]	Absorbed Photon Energy [keV]	Continuous Radiation	Real Energy [keV]	Fraction [%]	Photon Effi. [%]
W-185g	432.8	75.1 d	beta-	100.00						beta-	127.0	99.9	
			beta+							beta+		0.0	
			EC							IB	0.1	0.0	
			IT							Atomic e	0.0	0.0	
										Photon	0.1	0.0	
W-185m	197.4	1.67 m	beta-		60.00	13.00	7.80	98.93	7.72	beta-		0.0	
			beta+		131.55	4.30	5.66	99.29	5.62	beta+		0.0	
			EC		173.68	3.29	5.71	99.42	5.68	IB		0.0	
			IT	100.00						Atomic e	165.0	85.7	
										Photon	27.5	14.3	99.2
Ta-185	1991.0	49 m	beta-	100.00	65.00	35.00	22.75	98.96	22.51	beta-	639.0	72.4	
			beta+		107.84	2.71	2.92	99.19	2.90	beta+		0.0	
			EC		173.68	22.00	38.21	99.42	37.99	IB	1.1	0.1	
			IT		177.39	25.60	45.41	99.43	45.15	Atomic e	98.0	11.1	
					243.24	3.70	9.00	99.49	8.95	Photon	144.0	16.3	99.3
Ta-186	3900.0	10.5 m	beta-	100.00	65.00	36.00	23.40	98.96	23.16	beta-	881.0	34.8	
			beta+		122.43	23.00	28.16	99.26	27.95	beta+		0.0	
			EC		198.05	62.50	123.78	99.46	123.12	IB	1.9	0.1	
			IT		215.01	49.90	107.29	99.48	106.74	Atomic e	86.0	3.4	
					290.00	23.00	66.70	99.45	66.33	Photon	1563.0	61.7	97.5
					418.03	14.80	61.87	98.96	61.22				
					460.00	4.00	18.40	98.69	18.16				
					510.68	44.00	224.70	98.29	220.85				
					615.29	8.00	49.22	97.22	47.86				
					738.00	50.00	369.00	95.59	352.73				
					800.00	11.00	88.00	94.62	83.26				
Re-186g	1074.5	3.777 d	beta-	92.20	65.00	9.00	5.85	98.96	5.79	beta-	323.0	90.6	
			beta+		137.14	9.00	12.34	99.31	12.26	beta+		0.0	
	584.2		EC	7.80						IB	0.4	0.1	
			IT							Atomic e	14.0	3.9	
										Photon	19.3	5.4	99.2
W-187	1312.4	23.9 h	beta-	100.00	65.00	33.00	21.45	98.96	21.23	beta-	274.0	37.0	
			beta+		134.23	8.56	11.49	99.30	11.41	beta+		0.0	
			EC		479.53	21.10	101.18	98.54	99.71	IB	0.3	0.0	
			IT		551.52	6.00	33.09	97.91	32.40	Atomic e	37.0	5.0	
					618.34	7.12	44.03	97.19	42.79	Photon	430.0	58.0	97.4
					685.74	26.40	181.04	96.34	174.40				
					772.89	3.98	30.76	95.06	29.24				
Re-188g	2120.2	16.98 h	beta-	100.00	155.06	14.90	23.10	99.37	22.96	beta-	765.0	91.1	
			beta+		478.01	1.04	4.97	98.55	4.90	beta+		0.0	
			EC		633.08	1.25	7.91	97.01	7.68	IB	1.5	0.2	
			IT							Atomic e	15.8	1.9	
										Photon	57.4	6.8	98.7
Pb-203g	974.0	2.169 d	beta-		13.00	33.00	4.29	98.59	4.23	beta-		0.0	
			beta+		75.00	88.00	66.00	99.02	65.35	beta+		0.0	
			EC	100.00	279.19	80.10	223.63	99.47	222.43	IB	0.6	0.2	
			IT		401.31	3.44	13.81	99.05	13.67	Atomic e	48.9	13.6	
					680.50	0.70	4.76	96.41	4.59	Photon	310.4	86.3	99.3
Pb-204m	2185.8	1.120 h	beta-		80.00	9.00	7.20	99.05	7.13	beta-		0.0	
			beta+		374.81	89.00	333.58	99.18	330.86	beta+		0.0	
			EC		899.22	99.00	890.23	92.87	826.75	IB		0.0	
			IT	100.00	911.75	94.00	857.05	92.63	793.90	Atomic e	109.0	4.9	
										Photon	2102.0	95.1	93.8
Tl-206	1531.2	4.20 m	beta-	100.00			0.00	0.00	0.00	beta-	536.0	99.7	
			beta+							beta+		0.0	
			EC							IB	0.8	0.1	
			IT							Atomic e	0.8	0.1	
										Photon	0.1	0.0	
Tl-208	4994.0	3.053 m	beta-	100.00	80.00	7.00	5.60	99.05	5.55	beta-	560.0	14.1	
			beta+		277.28	6.80	18.86	99.47	18.75	beta+		0.0	
			EC		510.61	21.60	110.29	98.29	108.40	IB	0.9	0.0	
			IT		583.02	86.00	501.40	97.58	489.29	Atomic e	37.9	1.0	
					763.06	1.64	12.51	95.21	11.91	Photon	3374.0	84.9	97.2
					860.30	12.00	103.24	93.58	96.61				
					2614.35	99.79	2608.86	77.62	2025.08				
Pb-209	644.4	3.253 d	beta-	100.00						beta-	198.0	99.9	
			beta+							beta+		0.0	
			EC							IB	0.1	0.1	
			IT							Atomic e		0.0	
										Photon		0.0	
Bi-210g	1161.5	5.013 d	beta-	100.00						beta-	389.0	99.9	
			beta+							beta+		0.0	
			EC							IB	0.5	0.1	
			IT							Atomic e		0.0	
										Photon	0.0	0.0	

Table 3.8.2 Determination of correction factors for beta-ray energy loss and energy cutoff. (1/2)

Sample	Nuclide	Energy Deposit				Fractional Energy Deposit			Cutoff Effect			
		In Sample [MeV]	In Tape [MeV]	In BGO [MeV]	Total [MeV]	In Sample [%]	In Tape [%]	In BGO [%]	in BGO [MeV]	<50keV [MeV]	Cutoff [%]	in BGO [%] Corrected
B4C	Be-11	0.052	0.078	4.337	4.468	1.17	1.75	**97.06**				
PTFE	O-19	0.092	0.000	1.641	1.733	5.31		**94.69**				
(CF2)	F-18	0.099	0.000	0.600	0.699	14.13		**85.87**				
Na2CO3	Ne-23	0.052	0.083	1.752	1.888	2.77	4.42	**92.78**				
	Na-24	0.056	0.082	0.416	0.554	10.09	14.82	**75.06**				
	Na-22	0.055	0.085	0.522	0.663	8.30	12.85	**78.85**				
Al	Mg-27	0.026		0.673	0.699	3.65		**96.32**				
	Na-24	0.027		0.526	0.553	4.94		**95.06**				
SiO2	Al-28	0.016	0.088	1.132	1.236	1.26	7.14	**91.54**				
	Al-29	0.016	0.091	0.866	0.972	1.61	9.33	**89.01**				
	Mg-27	0.016	0.091	0.593	0.700	2.34	13.00	**84.63**				
	Si-31	0.017	0.092	0.486	0.595	2.82	15.45	**81.74**				
S	P-34	0.037	0.082	2.170	2.289	1.60	3.56	**94.81**				
	Si-31	0.040	0.085	0.471	0.595	6.66	14.24	79.09	0.4707	0.0012	0.25	**78.89**
	P-32	0.039	0.084	0.570	0.693	5.62	12.15	82.20	0.5700	0.0009	0.16	**82.07**
	P-30	0.037	0.082	1.797	1.917	1.91	4.28	93.74				
K2CO3	K-38	0.157	0.074	1.465	1.696	9.27	4.35	**86.37**				
	Ar-41	0.142	0.057	0.260	0.459	30.92	12.51	**56.57**				
	K-42	0.156	0.071	1.193	1.420	10.99	4.99	**84.02**				
	Cl-38	0.152	0.069	1.381	1.601	9.47	4.29	**86.24**				
CaO	K-47	0.008	0.089	1.687	1.785	0.47	4.98	**94.53**				
	K-44	0.008	0.089	1.381	1.479	0.56	6.02	**93.37**				
	K-42	0.008	0.089	1.319	1.417	0.59	6.27	**93.13**				
	Ca-47	0.009	0.087	0.256	0.353	2.62	24.73	**72.65**				
	Sc-47	0.009	0.076	0.077	0.162	5.82	46.71	47.47	0.0768	0.0033	4.30	**45.43**
Ti	Sc-50	0.031		1.596	1.627	1.90		**98.10**				
	Sc-48	0.041		0.180	0.221	18.50		**81.50**				
	Sc-46g	0.040		0.071	0.111	35.97		**64.03**				
V	Ti-51	0.067		0.797	0.865	7.78		**92.19**				
	Sc-48	0.070		0.151	0.221	31.82		**68.18**				
Cr	V-52	0.060	0.081	0.930	1.071	5.61	7.51	**86.85**				
	Cr-49	0.062	0.082	0.972	1.117	5.53	7.38	**87.06**				
Mn	V-52	0.029	0.086	0.956	1.071	2.74	8.01	**89.20**				
	Mn-56	0.030	0.081	0.719	0.829	3.58	9.75	**86.68**				
	Cr-55	0.029	0.084	0.985	1.099	2.66	7.67	**89.65**				
Fe	Mn-57	0.028		1.074	1.102	2.55		**97.42**				
	Mn-56	0.030		0.797	0.827	3.66		**96.34**				
Co	Mn-56	0.036		0.791	0.827	4.40		**95.60**				
	Co-58g	0.037		0.605	0.642	5.74		**94.24**				
Ni	Co-62g	0.026		1.606	1.632	1.58		**98.42**				
	Ni-57	0.028		0.746	0.775	3.67		**96.30**				
	Co-58g	0.030		0.612	0.642	4.62		**95.35**				
	Co-62m	0.027		1.063	1.091	2.51		**97.49**				
	Co-60g	0.035		0.060	0.095	36.92		**63.08**				
Cu	Cu-62	0.025		1.761	1.786	1.38		**98.60**				
	Cu-64-	0.034		0.156	0.190	17.89		82.11	0.1558	0.0024	1.54	**80.84**
	Cu-64+	0.028		0.702	0.730	3.82		**96.16**				
	Co-60g	0.034		0.061	0.095	36.14		**63.86**				
SrCO3	Rb-88	0.014	0.084	2.010	2.109	0.67	3.98	**95.31**				
	Sr-83g	0.015	0.090	0.678	0.783	1.92	11.53	**86.55**				

Table 3.8.2 Determination of correction factors for beta-ray energy loss and energy cutoff. (2/2)

Sample	Nuclide	Energy Deposit				Fractional Energy Deposit			Cutoff Effect			
		In Sample [MeV]	In Tape [MeV]	In BGO [MeV]	Total [MeV]	In Sample [%]	In Tape [%]	In BGO [%]	in BGO [MeV]	<50keV [MeV]	Cutoff [%]	in BGO [%] Corrected
Y2O3	N-16	0.013	0.082	2.614	2.710	0.47	3.03	**96.45**				
Zr	Zr-89m	0.021		0.847	0.868	2.45		**97.55**				
	Y-94	0.020		1.830	1.850	1.06		**98.94**				
	Zr-89g	0.021		0.829	0.850	2.47		**97.50**				
	Zr-95	0.030		0.087	0.117	25.55		**74.45**				
	Nb-95g	0.025		0.018	0.043	58.62		**41.38**				
Nb												
Mo	Zr-89m	0.025		0.843	0.868	2.88		**97.12**				
	Mo-91g	0.022		1.993	2.016	1.12		**98.86**				
	Mo-99	0.029		0.360	0.389	7.52		**92.48**				
	Nb-95g	0.027		0.016	0.043	63.60		**36.40**				
	Zr-95	0.033		0.083	0.117	28.60		**71.40**				
SnO2	In-118m	0.009	0.091	0.444	0.544	1.74	16.67	**81.52**				
	Sn-123m	0.010	0.089	0.359	0.458	2.08	19.51	**78.42**				
	Sn-121g	0.011	0.063	0.041	0.115	9.20	55.07	35.73	0.0410	0.0032	7.73	**32.97**
	Sn-123g	0.010	0.088	0.419	0.517	1.88	17.08	81.04	0.4186	0.0014	0.34	**80.76**
BaCO3	Ba-139	0.006	0.091	0.797	0.895	0.71	10.17	**89.09**				
	Cs-136g	0.007	0.064	0.046	0.118	6.20	54.57	**39.24**				
Ta	Ta-180g	0.037		0.176	0.213	17.22		82.78	0.1763	0.0022	1.25	**81.74**
	Ta-182g	0.038		0.088	0.125	29.91		**70.09**				
	Hf-181	0.038		0.081	0.120	32.05		**67.95**				
W	Ta-185	0.043		0.600	0.643	6.64		**93.36**				
	Ta-186	0.041		0.860	0.901	4.55		**95.45**				
	Ta-184	0.046		0.352	0.398	11.58		**88.42**				
	W-185g	0.048		0.078	0.127	38.24		61.76	0.0783	0.0032	4.06	**59.25**
	W-187	0.047		0.228	0.275	17.23		82.77	0.2279	0.0020	0.88	**82.04**
Re	Re-188g	0.037	0.079	0.662	0.777	4.72	10.15	85.13	0.6616	0.0009	0.13	**85.02**
	Re-186g	0.038	0.072	0.239	0.349	10.94	20.70	68.35	0.2385	0.0020	0.84	**67.78**
Pb	Tl-208	0.026		0.539	0.565	4.62		**95.38**				
Bi	Tl-206	0.044	0.074	0.424	0.541	8.05	13.69	78.27	0.4238	0.0013	0.30	**78.03**
	Pb-209	0.045	0.057	0.096	0.197	22.64	28.89	48.47	0.0957	0.0029	3.05	**46.99**
	Bi-210g	0.045	0.070	0.275	0.390	11.49	18.04	70.46	0.2751	0.0019	0.69	**69.97**
Nichrome	V-52	0.022		1.047	1.070	2.10		**97.87**				
	Mn-56	0.025		0.801	0.826	3.00		**97.00**				
	Ni-57	0.024		0.752	0.775	3.04		**96.93**				
	Co-58g	0.024		0.618	0.642	3.79		**96.19**				
	Cr-49	0.023		1.091	1.114	2.02		**97.95**				
	Co-60g	0.031		0.064	0.095	32.26		**67.74**				
SS-304	V-52	0.032		1.037	1.069	2.97		**97.00**				
	Mn-56	0.034		0.793	0.827	4.14		**95.86**				
	Ni-57	0.033		0.742	0.776	4.31		**95.67**				
	Co-58g	0.034		0.608	0.643	5.35		**94.62**				
	Co-60g	0.039		0.056	0.095	41.55		**58.45**				
SS-316	V-52	0.032		1.037	1.069	2.97		**97.01**				
	Mn-56	0.034		0.793	0.827	4.06		**95.94**				
	Ni-57	0.034		0.742	0.776	4.33		**95.64**				
	Co-58g	0.034		0.609	0.643	5.26		**94.71**				
	Co-60g	0.038		0.057	0.095	40.49		**59.51**				
In600	V-52	0.095		0.977	1.072	8.82		**91.13**				
	Mn-56	0.096		0.733	0.829	11.53		**88.47**				
	Ni-57	0.100		0.677	0.777	12.87		**87.13**				
	Co-58g	0.099		0.544	0.644	15.40		**84.60**				
	Co-60g	0.068		0.027	0.095	71.28		**28.72**				

Table 3.8.3 Determination of correction factors for energy loss and energy cutoff of atomic electrons.

Sample	Nuclide	Energy Deposit				Energy Deposit			Cutoff Effect			
		In Sample [MeV]	In Tape [MeV]	In BGO [MeV]	Total [MeV]	In Sample [%]	In Tape [%]	In BGO [%]	in BGO [MeV]	<50keV [MeV]	Cutoff [%]	in BGO [%] Corrected
Zr	Zr-89m	0.0217		0.5484	0.5701	3.80		**96.19**				
Nb	Y-90m	0.0305		0.3612	0.3917	7.79		**92.21**				
Mo	Mo-99	0.0221		0.0364	0.0585	37.81		**62.19**				
	Zr-89m	0.0256		0.5447	0.5704	4.48		**95.51**				
	Nb-91m	0.0423		0.0488	0.0911	46.45		**53.55**				
SnO2	In-111g	0.0064	0.0142	0.0106	0.0312	20.56	45.48	**33.97**				
	Sn-117m	0.0074	0.0485	0.0226	0.0785	9.44	61.77	**28.78**				
	Sn-123m	0.0069	0.0490	0.0225	0.0784	8.85	62.49	**28.67**				
BaCO3	Ba-133m	0.0065	0.0309	0.0410	0.0785	8.25	39.41	52.27	0.0410	0.0012	3.02	**50.69**
	Ba-135m	0.0066	0.0601	0.0764	0.1432	4.59	41.98	53.39	0.0764	0.0026	3.45	**51.55**
	Ba-137m	0.0065	0.0570	0.3013	0.3658	1.78	15.57	**82.36**				
	Ba-131g	0.0063	0.0209	0.0045	0.0317	19.87	66.05	**14.06**				
Ta	Ta-180g	0.0217		0.0087	0.0305	71.29		28.71	0.0087	0.0021	24.00	**21.82**
	Hf-181	0.0398		0.0406	0.0804	49.50		**50.46**				
	Ta-182g	0.0304		0.0195	0.0499	60.92		**39.08**				
W	W-185m	0.0434		0.0243	0.0677	64.10		35.90	0.0243	0.0038	15.52	**30.32**
	Ta-185	0.0353		0.0160	0.0513	68.82		**31.16**				
	Ta-186	0.0408		0.0233	0.0607	67.19		**38.39**				
	Ta-184	0.0376		0.0282	0.0658	57.18		**42.78**				
	W-187	0.0163		0.0059	0.0222	73.60		**26.39**				
Re	Re-184m	0.0332	0.0138	0.0022	0.0492	67.54	28.04	**4.42**				
	W-185m	0.0363	0.0254	0.0061	0.0677	53.56	37.47	8.97	0.0061	0.0016	26.56	**6.59**
	Re-188g	0.0413	0.0371	0.0137	0.0921	44.84	40.30	**14.87**				
	Re-186g	0.0312	0.0254	0.0072	0.0639	48.90	39.76	**11.34**				
	Re-184g	0.0253	0.0136	0.0054	0.0444	57.02	30.70	**12.19**				
Pb	Pb-203g	0.0197		0.0512	0.0709	27.78		**72.20**				
	Pb-204m	0.0243		0.6331	0.6597	3.69		**95.97**				

Table 3.8.4 Correction factors for each nuclide finally adopted. (1/3)

		Fraction of Decay Energy [%]					Correction Factor				
Sample	Nuclide	Beta-	Beta+	IB *	Atom_Elec	Gamma	Beta-	Beta+	Atom_Elec	Gamma	Overall
B4C	Be-11	75.9		0.4		23.7	97.19			78.70	**92.79**
CF2	O-19	64.8		0.2		35.0	94.80			88.30	**92.52**
	F-18		19.6	0.0		80.3		85.58		98.50	**95.97**
Na2CO3	Ne-23	91.7		0.3		8.0	93.08			97.20	**93.41**
	Na-24	11.8				88.1	75.15			80.10	**79.52**
	Na-22		8.2			91.8		78.55		98.30	**96.68**
Al	Mg-27	43.4		0.1		56.5	96.49			92.90	**94.46**
	Na-24	11.8				88.1	95.30			80.10	**81.90**
SiO2	Al-28	41.1		0.1		58.8	91.73			81.20	**85.53**
	Al-29	41.5		0.1		58.4	89.26			85.50	**87.06**
	Mg-27	43.4		0.1		56.5	84.61			92.90	**89.30**
	Si-31	99.7		0.2		0.2	81.86			100.00	**81.90**
S	P-34	87.1		0.3		12.6	94.99			79.10	**92.98**
	Si-31	99.7		0.2		0.2	79.61			100.00	**79.65**
	P-32	99.8		0.2			82.52				**82.52**
	P-30	99.5		0.3		0.2	93.74				**93.55**
K2CO3	K-38		27.4	0.1		72.5		86.65		98.10	**94.96**
	Ar-41	26.5				73.4	57.22			86.40	**78.66**
	K-42	82.9		0.2		16.9	84.10			83.60	**84.02**
	Cl-38	52.1		0.2		47.7	86.24			80.20	**83.35**
CaO	K-47	41.0		0.1		58.9	94.77			83.70	**88.24**
	K-44	37.3		0.1		62.6	93.40			83.30	**87.07**
	K-42	82.9		0.2		16.9	93.19			83.60	**91.57**
	Ca-47	24.5				75.5	72.99			87.10	**83.64**
	Sc-47	60.0				40.0	47.47			99.40	**68.24**
Ti	Sc-50	33.7		0.1		66.2	98.24			87.40	**91.06**
	Sc-48	6.2				93.8	81.78			89.00	**88.55**
	Sc-46g	5.3				94.7	64.83			90.80	**89.42**
V	Ti-51	70.1		0.1		29.8	92.32			98.10	**94.04**
	Sc-48	6.2				93.8	68.65			89.00	**87.74**
Cr	V-52	42.5		0.1		57.4	87.15			84.60	**85.68**
	Cr-49		35.9	0.1		64.0		87.42		98.50	**94.52**
	Cr-51			0.3	8.6	91.1			0.00	99.40	**90.83**
Mn	V-52	42.5		0.1		57.4	89.47			84.60	**86.67**
	Mn-56	32.9				67.1	86.89			89.10	**88.37**
	Mn-54				0.4	99.6				94.00	**93.62**
	Cr-55	99.8		0.2			89.65				**89.65**
Fe	Mn-57	92.5		0.2	0.9	6.4	97.56			97.60	**96.68**
	Mn-56	32.9				67.1	96.43			89.10	**91.51**
	Mn-54				0.4	99.6				94.00	**93.62**
Co	Mn-56	32.9				67.1	95.73			89.10	**91.28**
	Co-58g		3.0	0.1	0.4	96.6		94.45		98.20	**97.69**

Table 3.8.4 Correction factors for each nuclide finally adopted. (2/3)

Sample	Nuclide	Fraction of Decay Energy [%]					Correction Factor				
		Beta-	Beta+	IB *	Atom_Elec	Gamma	Beta-	Beta+	Atom_Elec	Gamma	Overall
Ni	Co-62g	50.5		0.2		49.3	98.40			85.70	**92.13**
	Ni-57		6.9	0.0	0.2	92.8		96.43		98.00	**97.70**
	Co-58g		3.0	0.1	0.4	96.6		95.67		98.20	**97.73**
	Co-62m	28.2		0.1		71.7	97.49			85.70	**89.03**
	Co-60m	2.5			86.6	11.1	100.00		22.31	89.30	**31.67**
	Co-57				12.3	87.6				99.20	**86.99**
	Co-60g	3.7				96.3	63.08			88.50	**87.56**
Cu	Cu-62		56.1	0.2		43.7		98.68		98.50	**98.60**
	Cu-64	22.5	15.8	0.2	0.6	60.9	82.15	96.31		98.50	**93.87**
	Co-60g	3.7				96.3	63.28			88.50	**87.57**
SrCO3	Rb-88	76.5		0.3		23.3	95.52			83.20	**92.64**
	Sr-87m				17.4	82.6			68.79	99.10	**93.83**
	Sr-85g				1.6	98.4				98.30	**96.73**
	Sr-83g		13.1	0.1	2.8	83.9		86.55		98.30	**94.00**
Y2O3	N-16	95.3		0.4		4.2	96.66			78.10	**95.88**
	Y-88				0.2	99.8				85.70	**85.53**
	Y-89m				0.8	99.2				92.70	**91.96**
	Rb-86m				1.8	98.2				97.90	**96.14**
Zr	Zr-89m		1.0		3.6	95.3		97.66	96.42	98.00	**97.94**
	Y-94	70.0		0.2		29.8	98.98			91.80	**96.84**
	Zr-89g		7.1	0.1	0.9	91.9		97.60		98.30	**97.36**
	Zr-95	13.7		0.2	0.3	85.9	74.28			95.50	**92.30**
	Nb-95g	5.4				94.6	38.77			95.20	**92.15**
Nb	Y-89m				0.8	99.2				92.70	**91.96**
	Y-90m				7.0	93.0			92.49	98.80	**98.36**
	Nb-92m				0.6	99.4				92.70	**92.14**
Mo	Zr-89m		1.0		3.6	95.3		97.21	95.73	92.70	**92.85**
	Mo-91g		59.6	0.2		40.2		98.93		98.50	**98.76**
	Mo-99	57.3		0.1	2.6	40.0	92.66		61.68	97.50	**93.79**
	Nb-95g	5.4				94.6	34.49			95.20	**91.92**
	Nb-92m				0.6	99.4				92.70	**92.14**
	Nb-91m				63.8	36.2			53.55	89.50	**66.56**
	Zr-95	13.7			0.3	85.9	71.40			95.50	**91.91**
SnO2	In-118m	16.7			0.1	83.2	81.45			89.90	**88.40**
	Sn-123m	73.9		0.1	3.3	22.7	78.45		27.19	99.40	**81.52**
	Sn-121g	100.0					32.97				**32.97**
	Sn-117m				50.5	49.5			27.34	99.30	**62.96**
	Sn-123g	98.6		0.1		1.3	80.72			100.00	**80.97**
	In-111g				7.7	92.3			33.97	99.40	**94.36**
BaCO3	Ba-137m				9.8	90.2			82.85	96.70	**95.34**
	Ba-139	94.3		0.2	0.9	4.6	89.41			99.40	**89.06**
	Ba-133m				76.6	23.4			55.69	99.30	**65.89**
	Ba-135m				77.5	22.5			51.55	99.30	**62.29**
	Cs-136g	4.3			1.5	94.1	39.24			95.30	**91.46**
	Ba-131g			0.0	8.9	91.1			14.06	98.50	**90.98**
Ta	Ta-180g	27.2		0.3	25.5	47.0	81.65		21.82	98.90	**74.48**
	Ta-182g	8.4			5.4	86.3	68.58		35.31	89.10	**84.48**
	Hf-181	18.2		0.1	9.5	72.2	66.55		47.67	98.70	**87.99**

Table 3.8.4 Correction factors for each nuclide finally adopted. (3/3)

		Fraction of Decay Energy [%]					Correction Factor				
Sample	Nuclide	Beta-	Beta+	IB *	Atom_Elec	Gamma	Beta-	Beta+	Atom_Elec	Gamma	Overall
W	Ta-184	18.4			6.6	75.0	93.37		40.33	96.00	**91.84**
	W-185g	99.9					59.25				**59.25**
	Ta-185	72.4		0.1	11.1	16.3	88.35		28.09	99.30	**83.44**
	Ta-186	34.8		0.1	3.4	61.7	60.14		35.54	97.50	**82.38**
	W-185m				85.7	14.3			30.33	99.20	**40.18**
	W-187	37.0			5.0	58.0	82.77		26.39	97.40	**88.44**
Re	W-185m				85.7	14.3			7.50	99.20	**20.61**
	Re-188g	91.1		0.2	1.9	6.8	85.52		13.60	98.70	**85.05**
	Re-186g	90.6		0.1	3.9	5.4	68.65		9.91	99.20	**68.01**
	Re-184g				5.7	94.3			12.19	94.10	**89.43**
	Re-184m				26.4	73.6			4.42	95.80	**71.68**
Pb	Tl-208	14.1			1.0	84.9	95.20			97.20	**95.95**
	Pb-204m				4.9	95.1			96.00	93.80	**93.91**
	Pb-203g			0.2	13.6	86.3			71.24	99.30	**95.48**
Bi	Tl-206	99.7		0.1	0.1		78.17				**78.09**
	Pb-209	99.9		0.1			46.99				**46.99**
	Bi-210g	99.9		0.1			70.46				**70.46**
In-600	V-52	42.5		0.1		57.4	91.12			84.60	**87.37**
	Mn-56	32.9				67.1	88.51			89.10	**88.91**
	Ni-57		6.9	0.0	0.2	92.8		87.21		98.00	**97.06**
	Co-58g		3.0	0.1	0.4	96.6		84.30		98.20	**97.39**
	Co-57			0.1	12.3	87.6			0.00	99.20	**86.99**
	Co-60g	3.7				96.3	28.72			88.50	**86.29**
Nichrome	V-52	42.5		0.1		57.4	97.91			84.60	**90.26**
	Mn-56	32.9				67.1	97.05			89.10	**91.72**
	Ni-57		6.9	0.0	0.2	92.8		97.01		98.00	**97.74**
	Co-58g		3.0	0.1	0.4	96.6		96.29		98.20	**97.75**
	Cr-49		35.9	0.1		64.0		97.95		98.50	**98.30**
	Co-57			0.1	12.3	87.6			0.00	99.20	**86.99**
	Co-60g	3.7				96.3	67.74			88.50	**87.73**
SS-304	V-52	42.5		0.1		57.4	96.80			84.60	**89.79**
	Mn-56	32.9				67.1	95.23			89.10	**91.12**
	Ni-57		6.9	0.0	0.2	92.8		95.33		98.00	**97.62**
	Co-58g		3.0	0.1	0.4	96.6		94.04		98.20	**97.68**
	Mn-54				0.4	96.6				94.00	**93.61**
	Co-57			0.1	12.3	87.6			0.00	99.20	**86.99**
	Co-60g	3.7				96.3	58.45			88.50	**87.39**
SS-316	V-52	42.5		0.1		57.4	97.10			84.60	**89.92**
	Mn-56	32.9				67.1	95.95			89.10	**91.35**
	Ni-57		6.9	0.0	0.2	92.8		95.82		98.00	**97.65**
	Co-58g		3.0	0.1	0.4	96.6		94.78		98.20	**97.70**
	Mn-54				0.4	96.6				94.00	**93.61**
	Co-57			0.1	12.3	87.6			0.00	99.20	**86.99**
	Co-60g	3.7				96.3	59.51			88.50	**87.43**

* Internal bremsstrahlung

Table 3.9.1 Fluctuation ratios of neutron fluxes during irradiations.

Half-Life [Hours]	Fluctuation Ratio	
	Date of Irradiation	
	Aug. 2, 1996	Sep. 20, 1996
1	1.021	0.931
2	1.006	0.956
3	1.003	0.969
5	1.001	0.980
10	1.000	0.990
20	1.000	0.995
50	1.000	0.998

Table 3.9.2 Fluctuation ratios of neutron fluxes for the aluminum neutron fluence monitors and some short lived (< 10 hours) radioactive nuclides predominantly contributing to the measured decay heat.

Sample	Nuclide	Half-Life	Date of Irradiation	Fluctuation Ratio
Al-monitor	Na-24	14.9590 h	Aug. 2	1.000
Al-monitor	Na-24	14.9590 h	Sep. 20	0.993
CF_2	F-18	109.77 m	Sep. 20	0.953
K_2CO_3	Ar-41	109.34 m	Sep. 20	0.953
Fe	Mn-56	2.5785 h	Aug. 2	1.004
$SrCO_3$	Sr-87m	2.803 h	Sep. 20	0.967
W	Ta-184	8.7 h	Aug. 2	1.001
SS-304	Mn-56	2.5785 h	Aug. 2	1.004
SS-316	Mn-56	2.5785 h	Aug. 2	1.004

Table 3.11.1 Measured decay heat for the 5 minutes irradiations. (1/8)

B4C

Cooling Time [min]	Cooling Time [sec]	Decay Heat [microW/g]	Error [abs.]	Error [%]
1.22	73	4.982E-02	2.693E-03	5.41
1.48	89	2.718E-02	1.470E-03	5.41
1.75	105	1.629E-02	8.855E-04	5.44
2.20	132	1.061E-02	5.822E-04	5.49
2.82	169	8.204E-03	4.527E-04	5.52
3.43	206	7.062E-03	3.911E-04	5.54
4.32	259	6.199E-03	3.447E-04	5.56
5.43	326	5.289E-03	2.961E-04	5.60
6.55	393	4.528E-03	2.559E-04	5.65
8.18	491	3.971E-03	2.245E-04	5.65
10.30	618	3.324E-03	1.893E-04	5.70
12.42	745	2.880E-03	1.653E-04	5.74
14.55	873	2.611E-03	1.501E-04	5.75
17.68	1061	2.233E-03	1.301E-04	5.83
21.75	1305	1.860E-03	1.106E-04	5.94
25.87	1552	1.559E-03	9.549E-05	6.12
30.00	1800	1.277E-03	8.214E-05	6.43
37.08	2225	9.612E-04	6.794E-05	7.07
47.17	2830	5.912E-04	5.414E-05	9.16
57.23	3434	2.429E-04	4.596E-05	18.92

The slow decay component after 2 minutes is due to C-11 produced by the B-11(p,n) reactions.
Only the fast decay component (Be-11) should be compared with calculations.

CF2 (PTFE)

Cooling Time [min]	Cooling Time [sec]	Decay Heat [microW/g]	Error [abs.]	Error [%]
1.12	67	4.523E-01	2.426E-02	5.36
1.38	83	3.192E-01	1.710E-02	5.36
1.65	99	2.313E-01	1.239E-02	5.36
2.08	125	1.529E-01	8.185E-03	5.35
2.70	162	1.031E-01	5.518E-03	5.35
3.32	199	8.287E-02	4.359E-03	5.26
4.20	252	7.270E-02	3.760E-03	5.17
5.32	319	6.950E-02	3.595E-03	5.17
6.43	386	6.826E-02	3.531E-03	5.17
8.07	484	6.775E-02	3.504E-03	5.17
10.18	611	6.678E-02	3.454E-03	5.17
12.30	738	6.588E-02	3.408E-03	5.17
14.43	866	6.490E-02	3.357E-03	5.17
17.57	1054	6.340E-02	3.279E-03	5.17
21.63	1298	6.185E-02	3.199E-03	5.17
25.75	1545	6.011E-02	3.109E-03	5.17
29.87	1792	5.844E-02	3.022E-03	5.17
36.95	2217	5.574E-02	2.883E-03	5.17
47.03	2822	5.216E-02	2.698E-03	5.17
57.15	3429	4.886E-02	2.527E-03	5.17

Na2CO3

Cooling Time [min]	Cooling Time [sec]	Decay Heat [microW/g]	Error [abs.]	Error [%]
1.20	72	5.545E-01	3.060E-02	5.52
1.47	88	3.680E-01	1.997E-02	5.43
1.73	104	2.585E-01	1.392E-02	5.39
2.18	131	1.533E-01	8.214E-03	5.36
2.80	168	7.622E-02	4.075E-03	5.35
3.42	205	3.850E-02	2.058E-03	5.35
4.30	258	1.551E-02	8.321E-04	5.37
5.42	325	4.972E-03	2.759E-04	5.55
6.48	389	2.081E-03	1.713E-04	8.23
8.12	487	1.079E-03	1.437E-04	13.32
10.23	614	7.917E-04	1.435E-04	18.13
12.37	742	7.821E-04	1.755E-04	22.45
14.47	868	7.491E-04	1.667E-04	22.26
17.60	1056	6.821E-04	1.518E-04	22.26
21.68	1301	6.665E-04	1.473E-04	22.10
25.80	1548	5.934E-04	1.317E-04	22.20
29.87	1792	5.284E-04	1.182E-04	22.37
37.00	2220	5.276E-04	1.176E-04	22.28
47.13	2828	4.945E-04	1.107E-04	22.39
57.25	3435	3.416E-04	8.060E-05	23.59

Decay heat after 5 minutes is due to Na-24 produced by the Na-23(n,γ) reactions.

Al

Cooling Time [min]	Cooling Time [sec]	Decay Heat [microW/g]	Error [abs.]	Error [%]
1.35	81	1.201E+00	6.324E-02	5.26
1.60	96	1.180E+00	6.214E-02	5.26
1.87	112	1.152E+00	6.065E-02	5.26
2.32	139	1.116E+00	5.873E-02	5.26
2.93	176	1.066E+00	5.608E-02	5.26
3.55	213	1.022E+00	5.374E-02	5.26
4.42	265	9.602E-01	5.050E-02	5.26
5.53	332	8.853E-01	4.654E-02	5.26
6.65	399	8.160E-01	4.289E-02	5.26
8.28	497	7.315E-01	3.844E-02	5.26
10.40	624	6.350E-01	3.336E-02	5.25
12.52	751	5.506E-01	2.892E-02	5.25
14.63	878	4.802E-01	2.522E-02	5.25
17.72	1063	3.999E-01	2.110E-02	5.28
21.78	1307	3.178E-01	1.696E-02	5.34
25.90	1554	2.543E-01	1.375E-02	5.41
30.02	1801	2.096E-01	1.170E-02	5.58
37.10	2226	1.571E-01	9.116E-03	5.80
47.17	2830	1.145E-01	7.129E-03	6.22
57.30	3438	9.432E-02	6.372E-03	6.76

Table 3.11.1 Measured decay heat for the 5 minutes irradiations. (2/8)

Cooling Time [min]	Cooling Time [sec]	Decay Heat [microW/g]	Error [abs.]	Error [%]
SiO2				
1.15	69	7.549E+00	5.163E-01	6.84
1.42	85	6.941E+00	4.744E-01	6.83
1.68	101	6.369E+00	4.349E-01	6.83
2.12	127	5.591E+00	3.815E-01	6.82
2.73	164	4.633E+00	3.158E-01	6.82
3.37	202	3.832E+00	2.610E-01	6.81
4.23	254	2.946E+00	2.006E-01	6.81
5.35	321	2.110E+00	1.436E-01	6.81
6.43	386	1.531E+00	1.042E-01	6.80
8.07	484	9.587E-01	6.523E-02	6.80
10.13	608	5.238E-01	3.564E-02	6.80
12.25	735	2.893E-01	1.969E-02	6.81
14.37	862	1.630E-01	1.111E-02	6.82
17.45	1047	7.773E-02	5.287E-03	6.80
21.52	1291	3.283E-02	2.303E-03	7.01
25.63	1538	1.682E-02	1.315E-03	7.82
29.72	1783	1.085E-02	9.946E-04	9.17
36.85	2211	6.039E-03	7.941E-04	13.15
46.93	2816	3.527E-03	7.227E-04	20.49
57.00	3420	2.130E-03	6.959E-04	32.68
Contribution of impurities is included after 30 minutes.				
S				
1.10	66	1.361E-02	8.540E-04	6.27
1.35	81	9.540E-03	6.279E-04	6.58
1.62	97	7.283E-03	5.208E-04	7.15
2.07	124	6.600E-03	5.107E-04	7.74
2.68	161	6.425E-03	4.953E-04	7.71
3.30	198	6.415E-03	4.907E-04	7.65
4.13	248	6.138E-03	4.686E-04	7.63
5.25	315	5.699E-03	4.356E-04	7.64
6.37	382	5.430E-03	4.151E-04	7.65
8.00	480	5.147E-03	3.909E-04	7.60
10.12	607	5.076E-03	3.829E-04	7.54
12.23	734	4.892E-03	3.680E-04	7.52
14.35	861	4.852E-03	3.633E-04	7.49
17.43	1046	4.612E-03	3.452E-04	7.48
21.50	1290	4.491E-03	3.355E-04	7.47
25.62	1537	4.366E-03	3.261E-04	7.47
29.73	1784	4.256E-03	3.181E-04	7.47
36.83	2210	4.168E-03	3.114E-04	7.47
46.90	2814	3.985E-03	2.983E-04	7.49
57.03	3422	3.891E-03	2.918E-04	7.50

Cooling Time [min]	Cooling Time [sec]	Decay Heat [microW/g]	Error [abs.]	Error [%]
K2CO3				
1.10	66	1.247E-01	6.599E-03	5.29
1.37	82	1.109E-01	5.855E-03	5.28
1.63	98	1.061E-01	5.596E-03	5.27
2.08	125	1.018E-01	5.361E-03	5.27
2.70	162	9.641E-02	5.075E-03	5.26
3.30	198	9.185E-02	4.830E-03	5.26
4.13	248	8.552E-02	4.492E-03	5.25
5.25	315	7.786E-02	4.085E-03	5.25
6.37	382	7.099E-02	3.721E-03	5.24
8.00	480	6.224E-02	3.258E-03	5.23
10.12	607	5.252E-02	2.746E-03	5.23
12.18	731	4.464E-02	2.332E-03	5.22
14.32	859	3.775E-02	1.971E-03	5.22
17.45	1047	2.993E-02	1.562E-03	5.22
21.57	1294	2.278E-02	1.213E-03	5.32
25.68	1541	1.744E-02	9.408E-04	5.39
29.80	1788	1.396E-02	7.918E-04	5.67
36.95	2217	1.002E-02	6.070E-04	6.06
47.07	2824	6.727E-03	4.285E-04	6.37
57.18	3431	4.986E-03	3.233E-04	6.48
CaO				
1.10	66	2.420E-02	2.906E-03	12.01
1.37	82	1.785E-02	1.904E-03	10.67
1.63	98	1.582E-02	1.638E-03	10.35
2.08	125	1.502E-02	1.521E-03	10.13
2.70	162	1.486E-02	1.438E-03	9.68
3.32	199	1.474E-02	1.397E-03	9.48
4.15	249	1.400E-02	1.322E-03	9.44
5.22	313	1.288E-02	1.223E-03	9.49
6.33	380	1.173E-02	1.124E-03	9.58
7.97	478	1.145E-02	1.059E-03	9.25
10.05	603	1.049E-02	9.555E-04	9.11
12.18	731	9.681E-03	8.743E-04	9.03
14.25	855	9.087E-03	8.069E-04	8.88
17.38	1043	7.897E-03	7.024E-04	8.90
21.45	1287	7.006E-03	6.189E-04	8.83
25.57	1534	6.068E-03	5.395E-04	8.89
29.70	1782	5.164E-03	4.676E-04	9.05
36.78	2207	4.475E-03	4.093E-04	9.15
46.90	2814	3.472E-03	3.349E-04	9.65
56.98	3419	2.279E-03	2.596E-04	11.39

Table 3.11.1 Measured decay heat for the 5 minutes irradiations. (3/8)

Cooling Time [min]	Cooling Time [sec]	Decay Heat [microW/g]	Error [abs.]	Error [%]
Ti				
1.10	66	5.487E-02	3.003E-03	5.47
1.37	82	4.972E-02	2.721E-03	5.47
1.63	98	4.510E-02	2.469E-03	5.47
2.08	125	3.948E-02	2.161E-03	5.47
2.65	159	3.299E-02	1.806E-03	5.47
3.27	196	2.795E-02	1.530E-03	5.47
4.15	249	2.277E-02	1.246E-03	5.47
5.27	316	1.812E-02	1.010E-03	5.57
6.38	383	1.530E-02	8.685E-04	5.68
8.02	481	1.268E-02	7.265E-04	5.73
10.13	608	1.082E-02	6.205E-04	5.73
12.25	735	1.003E-02	5.753E-04	5.73
14.37	862	9.613E-03	5.512E-04	5.73
17.50	1050	9.192E-03	5.271E-04	5.73
21.57	1294	8.947E-03	5.132E-04	5.74
25.68	1541	8.740E-03	5.013E-04	5.74
29.80	1788	8.558E-03	4.909E-04	5.74
36.93	2216	8.252E-03	4.734E-04	5.74
47.02	2821	8.051E-03	4.620E-04	5.74
57.13	3428	7.785E-03	4.468E-04	5.74
V				
1.35	81	3.141E-01	1.655E-02	5.27
1.62	97	3.029E-01	1.596E-02	5.27
1.88	113	2.918E-01	1.538E-02	5.27
2.33	140	2.756E-01	1.452E-02	5.27
2.95	177	2.562E-01	1.349E-02	5.27
3.57	214	2.360E-01	1.242E-02	5.26
4.45	267	2.118E-01	1.115E-02	5.26
5.57	334	1.851E-01	9.741E-03	5.26
6.68	401	1.608E-01	8.461E-03	5.26
8.32	499	1.326E-01	6.973E-03	5.26
10.42	625	1.027E-01	5.402E-03	5.26
12.55	753	7.969E-02	4.191E-03	5.26
14.67	880	6.152E-02	3.236E-03	5.26
17.75	1065	4.351E-02	2.290E-03	5.26
21.87	1312	2.734E-02	1.442E-03	5.27
25.98	1559	1.751E-02	9.271E-04	5.29
30.10	1806	1.155E-02	6.173E-04	5.34
37.18	2231	6.276E-03	3.480E-04	5.54
47.25	2835	3.460E-03	2.246E-04	6.49
57.38	3443	2.675E-03	1.957E-04	7.32

Cooling Time [min]	Cooling Time [sec]	Decay Heat [microW/g]	Error [abs.]	Error [%]
Cr				
1.12	67	1.805E+00	1.169E-01	6.47
1.37	82	1.714E+00	1.104E-01	6.44
1.63	98	1.617E+00	1.035E-01	6.40
2.10	126	1.479E+00	9.405E-02	6.36
2.72	163	1.310E+00	8.264E-02	6.31
3.33	200	1.161E+00	7.280E-02	6.27
4.22	253	9.820E-01	6.117E-02	6.23
5.33	320	7.932E-01	4.912E-02	6.19
6.47	388	6.421E-01	3.961E-02	6.17
8.05	483	4.815E-01	2.961E-02	6.15
10.17	610	3.277E-01	2.011E-02	6.14
12.28	737	2.244E-01	1.375E-02	6.13
14.42	865	1.545E-01	9.462E-03	6.13
17.55	1053	9.110E-02	5.580E-03	6.12
21.68	1301	4.601E-02	2.733E-03	5.94
25.75	1545	2.478E-02	1.413E-03	5.70
29.87	1792	1.456E-02	8.041E-04	5.52
37.00	2220	7.871E-03	4.272E-04	5.43
47.13	2828	4.890E-03	2.673E-04	5.47
57.25	3435	3.891E-03	2.172E-04	5.58
Contribution of impurities (Na-24 from Al) is included after 30 minutes.				
Mn				
1.10	66	8.106E-01	4.961E-02	6.12
1.37	82	7.672E-01	4.689E-02	6.11
1.63	98	7.340E-01	4.481E-02	6.10
2.08	125	6.744E-01	4.110E-02	6.09
2.70	162	6.003E-01	3.650E-02	6.08
3.32	199	5.331E-01	3.236E-02	6.07
4.22	253	4.509E-01	2.732E-02	6.06
5.33	320	3.668E-01	2.219E-02	6.05
6.45	387	2.981E-01	1.801E-02	6.04
8.08	485	2.224E-01	1.343E-02	6.04
10.18	611	1.506E-01	9.084E-03	6.03
12.32	739	1.029E-01	6.207E-03	6.03
14.45	867	7.068E-02	4.263E-03	6.03
17.58	1055	4.204E-02	2.521E-03	6.00
21.70	1302	2.235E-02	1.740E-03	7.79
25.83	1550	1.298E-02	1.511E-03	11.64
29.90	1794	8.652E-03	1.397E-03	16.14
37.03	2222	5.965E-03	1.246E-03	20.89
47.17	2830	4.786E-03	1.001E-03	20.92
57.28	3437	4.158E-03	8.708E-04	20.94
Decay heat after 30 minutes is due to Mn-56 produced by the Mn-55(n,γ) reactions.				

Table 3.11.1 Measured decay heat for the 5 minutes irradiations. (4/8)

	Cooling Time [min]	Cooling Time [sec]	Decay Heat [microW/g]	Error [abs.]	Error [%]
Fe					
	1.10	66	1.282E-01	6.845E-03	5.34
	1.37	82	1.263E-01	6.831E-03	5.41
	1.63	98	1.263E-01	6.879E-03	5.45
	2.08	125	1.215E-01	6.616E-03	5.45
	2.68	161	1.166E-01	6.349E-03	5.44
	3.25	195	1.147E-01	6.242E-03	5.44
	4.13	248	1.114E-01	6.061E-03	5.44
	5.23	314	1.079E-01	5.875E-03	5.44
	6.35	381	1.050E-01	5.713E-03	5.44
	7.95	477	1.029E-01	5.597E-03	5.44
	10.07	604	9.977E-02	5.429E-03	5.44
	12.13	728	9.798E-02	5.332E-03	5.44
	14.25	855	9.584E-02	5.215E-03	5.44
	17.33	1040	9.379E-02	5.103E-03	5.44
	21.40	1284	9.058E-02	4.928E-03	5.44
	25.52	1531	8.799E-02	4.787E-03	5.44
	29.63	1778	8.580E-02	4.668E-03	5.44
	36.77	2206	8.264E-02	4.496E-03	5.44
	46.88	2813	7.843E-02	4.266E-03	5.44
	57.02	3421	7.507E-02	4.083E-03	5.44
Co					
	1.10	66	3.111E-02	1.696E-03	5.45
	1.35	81	3.202E-02	1.746E-03	5.45
	1.62	97	3.157E-02	1.721E-03	5.45
	2.07	124	3.152E-02	1.719E-03	5.45
	2.68	161	3.121E-02	1.702E-03	5.45
	3.30	198	3.090E-02	1.685E-03	5.45
	4.18	251	3.083E-02	1.681E-03	5.45
	5.28	317	3.080E-02	1.679E-03	5.45
	6.40	384	3.046E-02	1.661E-03	5.45
	7.98	479	3.043E-02	1.659E-03	5.45
	10.10	606	2.982E-02	1.626E-03	5.45
	12.22	733	2.954E-02	1.611E-03	5.45
	14.33	860	2.934E-02	1.600E-03	5.45
	17.42	1045	2.873E-02	1.566E-03	5.45
	21.48	1289	2.828E-02	1.542E-03	5.45
	25.62	1537	2.760E-02	1.505E-03	5.45
	29.73	1784	2.715E-02	1.480E-03	5.45
	36.87	2212	2.641E-02	1.440E-03	5.45
	46.93	2816	2.514E-02	1.371E-03	5.45
	57.00	3420	2.406E-02	1.312E-03	5.45

	Cooling Time [min]	Cooling Time [sec]	Decay Heat [microW/g]	Error [abs.]	Error [%]
Ni					
	1.10	66	4.366E-02	2.696E-03	6.17
	1.35	81	4.037E-02	2.518E-03	6.24
	1.62	97	3.606E-02	2.275E-03	6.31
	2.07	124	3.154E-02	2.029E-03	6.43
	2.68	161	2.681E-02	1.774E-03	6.62
	3.28	197	2.311E-02	1.573E-03	6.81
	4.17	250	1.950E-02	1.381E-03	7.08
	5.28	317	1.655E-02	1.228E-03	7.42
	6.40	384	1.454E-02	1.121E-03	7.71
	8.03	482	1.265E-02	1.016E-03	8.03
	10.15	609	1.120E-02	9.263E-04	8.27
	12.27	736	1.009E-02	8.446E-04	8.37
	14.40	864	9.258E-03	7.756E-04	8.38
	17.48	1049	8.020E-03	6.631E-04	8.27
	21.55	1293	6.920E-03	5.519E-04	7.98
	25.65	1539	5.994E-03	4.537E-04	7.57
	29.78	1787	5.157E-03	3.665E-04	7.11
	36.92	2215	4.101E-03	2.610E-04	6.36
	46.98	2819	3.152E-03	1.795E-04	5.70
	57.10	3426	2.590E-03	1.404E-04	5.42
Cu					
	1.10	66	4.156E+00	2.144E-01	5.16
	1.37	82	4.082E+00	2.105E-01	5.16
	1.63	98	3.994E+00	2.059E-01	5.16
	2.08	125	3.859E+00	1.989E-01	5.15
	2.70	162	3.687E+00	1.899E-01	5.15
	3.32	199	3.530E+00	1.817E-01	5.15
	4.20	252	3.295E+00	1.695E-01	5.14
	5.27	316	3.049E+00	1.567E-01	5.14
	6.37	382	2.820E+00	1.449E-01	5.14
	8.00	480	2.512E+00	1.290E-01	5.13
	10.12	607	2.154E+00	1.105E-01	5.13
	12.23	734	1.853E+00	9.500E-02	5.13
	14.35	861	1.594E+00	8.169E-02	5.12
	17.47	1048	1.280E+00	6.557E-02	5.12
	21.53	1292	9.616E-01	4.923E-02	5.12
	25.65	1539	7.222E-01	3.697E-02	5.12
	29.77	1786	5.378E-01	2.753E-02	5.12
	36.90	2214	3.328E-01	1.704E-02	5.12
	46.97	2818	1.660E-01	8.518E-03	5.13
	57.10	3426	8.437E-02	4.361E-03	5.17

Table 3.11.1 Measured decay heat for the 5 minutes irradiations. (5/8)

Cooling Time [min]	Cooling Time [sec]	Decay Heat [microW/g]	Error [abs.]	Error [%]
SrCO3				
1.10	66	7.481E-02	4.657E-03	6.22
1.37	82	7.140E-02	4.374E-03	6.13
1.63	98	6.921E-02	4.230E-03	6.11
2.07	124	6.747E-02	4.119E-03	6.10
2.63	158	6.611E-02	4.030E-03	6.10
3.25	195	6.319E-02	3.850E-03	6.09
4.08	245	6.076E-02	3.701E-03	6.09
5.15	309	5.788E-02	3.525E-03	6.09
6.27	376	5.445E-02	3.316E-03	6.09
7.90	474	5.204E-02	3.167E-03	6.09
10.03	602	4.804E-02	2.922E-03	6.08
12.15	729	4.481E-02	2.725E-03	6.08
14.22	853	4.229E-02	2.571E-03	6.08
17.35	1041	3.856E-02	2.343E-03	6.08
21.47	1288	3.447E-02	2.095E-03	6.08
25.60	1536	3.068E-02	1.858E-03	6.06
29.72	1783	2.756E-02	1.664E-03	6.04
36.82	2209	2.360E-02	1.422E-03	6.02
46.88	2813	1.913E-02	1.151E-03	6.02
56.97	3418	1.579E-02	9.511E-04	6.02
Y2O3				
1.10	66	2.284E-01	1.383E-02	6.05
1.37	82	1.170E-01	7.054E-03	6.03
1.63	98	6.078E-02	3.675E-03	6.05
2.08	125	2.319E-02	1.447E-03	6.24
2.70	162	8.304E-03	6.165E-04	7.42
3.27	196	4.895E-03	4.462E-04	9.12
4.15	249	3.357E-03	3.764E-04	11.21
5.27	316	2.422E-03	3.230E-04	13.33
6.38	383	1.854E-03	2.912E-04	15.70
8.03	482	1.650E-03	2.451E-04	14.85
10.15	609	1.456E-03	2.076E-04	14.26
12.27	736	1.165E-03	1.767E-04	15.17
14.33	860	1.211E-03	1.531E-04	12.64
17.47	1048	1.045E-03	1.309E-04	12.53
21.55	1293	9.761E-04	1.096E-04	11.23
25.67	1540	9.056E-04	9.713E-05	10.73
29.78	1787	7.807E-04	8.751E-05	11.21
36.87	2212	8.591E-04	8.289E-05	9.65
47.00	2820	8.390E-04	7.985E-05	9.52
57.12	3427	5.406E-04	6.997E-05	12.94

Cooling Time [min]	Cooling Time [sec]	Decay Heat [microW/g]	Error [abs.]	Error [%]
Zr				
1.37	82	2.670E-01	1.372E-02	5.14
1.63	98	2.588E-01	1.330E-02	5.14
1.88	113	2.448E-01	1.258E-02	5.14
2.33	140	2.266E-01	1.165E-02	5.14
2.95	177	2.058E-01	1.058E-02	5.14
3.57	214	1.844E-01	9.485E-03	5.14
4.45	267	1.623E-01	8.350E-03	5.15
5.57	334	1.375E-01	7.086E-03	5.15
6.68	401	1.151E-01	5.941E-03	5.16
8.32	499	9.111E-02	4.719E-03	5.18
10.43	626	6.819E-02	3.557E-03	5.22
12.50	750	5.054E-02	2.672E-03	5.29
14.57	874	3.916E-02	2.110E-03	5.39
17.70	1062	2.820E-02	1.583E-03	5.61
21.82	1309	1.961E-02	1.196E-03	6.10
25.95	1557	1.470E-02	9.955E-04	6.77
30.07	1804	1.169E-02	8.856E-04	7.58
37.20	2232	9.753E-03	8.211E-04	8.42
47.33	2840	8.170E-03	7.739E-04	9.47
57.40	3444	7.793E-03	7.635E-04	9.80
Nb				
1.02	61	3.727E-03	2.028E-04	5.44
1.28	77	3.065E-03	1.675E-04	5.46
1.55	93	2.634E-03	1.444E-04	5.48
2.00	120	2.379E-03	1.292E-04	5.43
2.62	157	2.285E-03	1.243E-04	5.44
3.23	194	2.258E-03	1.229E-04	5.44
4.07	244	2.230E-03	1.214E-04	5.44
5.18	311	2.206E-03	1.202E-04	5.45
6.30	378	2.131E-03	1.162E-04	5.46
7.93	476	2.099E-03	1.146E-04	5.46
10.05	603	2.031E-03	1.111E-04	5.47
12.17	730	1.991E-03	1.090E-04	5.47
14.23	854	1.975E-03	1.082E-04	5.48
17.37	1042	1.920E-03	1.053E-04	5.49
21.50	1290	1.883E-03	1.034E-04	5.49
25.57	1534	1.832E-03	1.008E-04	5.50
29.68	1781	1.806E-03	9.944E-05	5.51
36.82	2209	1.777E-03	9.797E-05	5.51
46.90	2814	1.743E-03	9.618E-05	5.52
57.02	3421	1.710E-03	9.451E-05	5.53

Table 3.11.1 Measured decay heat for the 5 minutes irradiations. (6/8)

Cooling Time [min]	Cooling Time [sec]	Decay Heat [microW/g]	Error [abs.]	Error [%]
Mo				
1.10	66	2.324E-01	1.210E-02	5.21
1.37	82	2.241E-01	1.165E-02	5.20
1.63	98	2.166E-01	1.125E-02	5.19
2.08	125	2.055E-01	1.065E-02	5.18
2.70	162	1.946E-01	1.007E-02	5.18
3.27	196	1.854E-01	9.584E-03	5.17
4.17	250	1.753E-01	9.054E-03	5.16
5.28	317	1.638E-01	8.450E-03	5.16
6.35	381	1.549E-01	7.981E-03	5.15
8.00	480	1.438E-01	7.402E-03	5.15
10.12	607	1.303E-01	6.700E-03	5.14
12.18	731	1.187E-01	6.095E-03	5.14
14.30	858	1.084E-01	5.562E-03	5.13
17.38	1043	9.465E-02	4.855E-03	5.13
21.45	1287	7.956E-02	4.077E-03	5.13
25.58	1535	6.673E-02	3.418E-03	5.12
29.65	1779	5.624E-02	2.880E-03	5.12
36.78	2207	4.200E-02	2.150E-03	5.12
46.87	2812	2.799E-02	1.432E-03	5.12
56.98	3419	1.894E-02	9.690E-04	5.12
SnO2				
1.10	66	7.069E-02	5.149E-03	7.28
1.37	82	6.611E-02	4.763E-03	7.20
1.63	98	6.306E-02	4.679E-03	7.42
2.08	125	5.783E-02	4.456E-03	7.71
2.70	162	5.321E-02	4.179E-03	7.85
3.32	199	4.880E-02	3.920E-03	8.03
4.22	253	4.445E-02	3.571E-03	8.03
5.33	320	3.923E-02	3.154E-03	8.04
6.45	387	3.547E-02	2.855E-03	8.05
8.08	485	3.214E-02	2.581E-03	8.03
10.22	613	2.801E-02	2.248E-03	8.03
12.33	740	2.517E-02	2.019E-03	8.02
14.45	867	2.314E-02	1.853E-03	8.01
17.58	1055	2.062E-02	1.650E-03	8.00
21.67	1300	1.815E-02	1.451E-03	7.99
25.78	1547	1.624E-02	1.298E-03	7.99
29.87	1792	1.468E-02	1.173E-03	7.99
36.95	2217	1.291E-02	1.031E-03	7.99
47.02	2821	1.066E-02	8.525E-04	7.99
57.15	3429	8.417E-03	6.751E-04	8.02

Cooling Time [min]	Cooling Time [sec]	Decay Heat [microW/g]	Error [abs.]	Error [%]
BaCO3				
1.10	66	1.312E+00	1.052E-01	8.02
1.37	82	1.223E+00	9.794E-02	8.01
1.63	98	1.144E+00	9.143E-02	7.99
2.10	126	1.014E+00	8.090E-02	7.98
2.67	160	8.762E-01	6.980E-02	7.97
3.28	197	7.480E-01	5.951E-02	7.96
4.18	251	5.917E-01	4.702E-02	7.95
5.30	318	4.443E-01	3.527E-02	7.94
6.42	385	3.349E-01	2.657E-02	7.94
8.05	483	2.279E-01	1.808E-02	7.93
10.18	611	1.399E-01	1.110E-02	7.93
12.25	735	9.092E-02	7.218E-03	7.94
14.38	863	6.254E-02	4.974E-03	7.95
17.53	1052	4.191E-02	3.353E-03	8.00
21.65	1299	3.101E-02	2.511E-03	8.10
25.72	1543	2.721E-02	2.238E-03	8.22
29.85	1791	2.489E-02	2.065E-03	8.30
36.93	2216	2.360E-02	1.958E-03	8.30
47.03	2822	2.146E-02	1.782E-03	8.31
57.15	3429	1.917E-02	1.596E-03	8.33
Contamination of F-18 is included. The contamination is significant after 10 minutes cooling.				
Ta				
1.08	65	4.481E-03	3.837E-04	8.56
1.35	81	4.412E-03	3.778E-04	8.56
1.62	97	4.482E-03	3.838E-04	8.56
2.07	124	4.412E-03	3.778E-04	8.56
2.68	161	4.414E-03	3.780E-04	8.56
3.28	197	4.339E-03	3.716E-04	8.56
4.17	250	4.355E-03	3.730E-04	8.56
5.28	317	4.259E-03	3.648E-04	8.56
6.40	384	4.217E-03	3.612E-04	8.56
8.03	482	4.167E-03	3.569E-04	8.57
10.13	608	4.133E-03	3.540E-04	8.57
12.20	732	3.999E-03	3.426E-04	8.57
14.32	859	3.942E-03	3.377E-04	8.57
17.40	1044	3.848E-03	3.297E-04	8.57
21.48	1289	3.830E-03	3.282E-04	8.57
25.60	1536	3.747E-03	3.211E-04	8.57
29.72	1783	3.666E-03	3.142E-04	8.57
36.85	2211	3.565E-03	3.056E-04	8.57
46.93	2816	3.429E-03	2.940E-04	8.57
57.05	3423	3.327E-03	2.854E-04	8.58

Table 3.11.1 Measured decay heat for the 5 minutes irradiations. (7/8)

	Cooling Time [min]	Cooling Time [sec]	Decay Heat [microW/g]	Error [abs.]	Error [%]
W					
	1.12	67	8.220E-02	2.387E-02	29.04
	1.52	91	6.941E-02	2.003E-02	28.86
	1.78	107	6.227E-02	1.789E-02	28.73
	2.23	134	5.211E-02	1.484E-02	28.48
	2.83	170	4.063E-02	1.141E-02	28.09
	3.40	204	3.243E-02	8.969E-03	27.66
	4.28	257	2.304E-02	6.184E-03	26.83
	5.38	323	1.518E-02	3.871E-03	25.50
	6.50	390	1.019E-02	2.421E-03	23.77
	8.13	488	6.048E-03	1.246E-03	20.59
	10.25	615	3.358E-03	5.347E-04	15.92
	12.37	742	2.094E-03	2.481E-04	11.85
	14.43	866	1.499E-03	1.387E-04	9.25
	17.52	1051	1.095E-03	8.238E-05	7.52
	21.57	1294	8.372E-04	5.859E-05	7.00
	25.68	1541	6.508E-04	5.017E-05	7.71
	29.80	1788	5.359E-04	5.089E-05	9.50
	36.93	2216	4.177E-04	5.003E-05	11.98
	47.02	2821	2.915E-04	4.426E-05	15.19
	57.08	3425	2.291E-04	4.230E-05	18.46
Re					
	1.10	66	3.724E-03	5.761E-04	15.47
	1.37	82	2.833E-03	4.027E-04	14.22
	1.63	98	2.523E-03	3.527E-04	13.98
	2.08	125	2.554E-03	3.454E-04	13.52
	2.63	158	2.202E-03	2.901E-04	13.17
	3.27	196	2.303E-03	2.870E-04	12.46
	4.15	249	2.294E-03	2.738E-04	11.93
	5.27	316	2.031E-03	2.394E-04	11.79
	6.40	384	2.020E-03	2.324E-04	11.50
	8.03	482	2.038E-03	2.264E-04	11.11
	10.10	606	1.998E-03	2.180E-04	10.91
	12.22	733	2.000E-03	2.157E-04	10.78
	14.30	858	2.103E-03	2.229E-04	10.60
	17.43	1046	2.001E-03	2.126E-04	10.63
	21.55	1293	1.928E-03	2.051E-04	10.64
	25.68	1541	1.931E-03	2.049E-04	10.61
	29.80	1788	1.878E-03	1.999E-04	10.65
	36.90	2214	1.936E-03	2.049E-04	10.58
	46.98	2819	1.894E-03	2.010E-04	10.61
	57.05	3423	1.838E-03	1.961E-04	10.67

	Cooling Time [min]	Cooling Time [sec]	Decay Heat [microW/g]	Error [abs.]	Error [%]
Pb					
	1.10	66	1.041E-02	5.390E-04	5.18
	1.35	81	1.008E-02	5.223E-04	5.18
	1.63	98	9.395E-03	4.867E-04	5.18
	2.08	125	8.453E-03	4.380E-04	5.18
	2.70	162	7.588E-03	3.932E-04	5.18
	3.32	199	6.766E-03	3.507E-04	5.18
	4.20	252	5.710E-03	2.962E-04	5.19
	5.27	316	4.741E-03	2.462E-04	5.19
	6.38	383	3.928E-03	2.042E-04	5.20
	8.02	481	3.054E-03	1.604E-04	5.25
	10.08	605	2.199E-03	1.168E-04	5.31
	12.20	732	1.733E-03	9.333E-05	5.38
	14.32	859	1.358E-03	7.421E-05	5.46
	17.45	1047	1.050E-03	5.873E-05	5.59
	21.52	1291	8.100E-04	4.700E-05	5.80
	25.63	1538	7.007E-04	4.184E-05	5.97
	29.77	1786	6.323E-04	3.870E-05	6.12
	36.85	2211	5.612E-04	3.553E-05	6.33
	46.98	2819	4.894E-04	3.244E-05	6.63
	57.07	3424	4.214E-04	2.968E-05	7.04
Bi					
	1.10	66	8.147E-04	2.460E-04	30.19
	1.37	82	7.232E-04	1.479E-04	20.45
	1.63	98	6.382E-04	1.229E-04	19.26
	2.08	125	6.921E-04	1.138E-04	16.45
	2.70	162	7.500E-04	1.032E-04	13.76
	3.32	199	6.692E-04	9.332E-05	13.94
	4.20	252	5.537E-04	8.349E-05	15.08
	5.32	319	4.040E-04	7.352E-05	18.19
	6.40	384	2.561E-04	6.602E-05	25.78
	8.03	482	2.480E-04	5.608E-05	22.62
	10.15	609	1.713E-04	4.660E-05	27.20
	12.22	733	9.243E-05	3.979E-05	43.05
	14.33	860	1.064E-04	3.382E-05	31.77
	17.42	1045	4.335E-05	3.229E-05	74.47
	21.53	1292	2.995E-05	3.146E-05	105.05
	25.67	1540	2.395E-05	3.400E-05	141.94
	29.78	1787	-3.098E-05	-3.470E-05	112.01
	36.88	2213	3.504E-05	3.181E-05	90.78
	46.97	2818	4.903E-05	3.198E-05	65.22
	57.05	3423	-4.270E-05	-3.232E-05	75.68

S/N ratios are not good over whole cooling time.

Table 3.11.1 Measured decay heat for the 5 minutes irradiations. (8/8)

Cooling Time [min]	Cooling Time [sec]	Decay Heat [microW/g]	Error [abs.]	Error [%]
Inconel-600				
1.10	66	4.066E-01	2.425E-02	5.96
1.35	81	3.812E-01	2.270E-02	5.95
1.62	97	3.618E-01	2.150E-02	5.94
2.05	123	3.287E-01	1.949E-02	5.93
2.67	160	2.887E-01	1.707E-02	5.91
3.28	197	2.557E-01	1.509E-02	5.90
4.17	250	2.149E-01	1.266E-02	5.89
5.28	317	1.744E-01	1.026E-02	5.88
6.40	384	1.432E-01	8.413E-03	5.88
8.03	482	1.090E-01	6.397E-03	5.87
10.13	608	7.816E-02	4.586E-03	5.87
12.27	736	5.756E-02	3.376E-03	5.87
14.38	863	4.350E-02	2.544E-03	5.85
17.47	1048	3.112E-02	1.808E-03	5.81
21.58	1295	2.157E-02	1.243E-03	5.76
25.70	1542	1.669E-02	9.559E-04	5.73
29.82	1789	1.377E-02	7.824E-04	5.68
36.95	2217	1.136E-02	6.457E-04	5.69
47.07	2824	9.580E-03	5.450E-04	5.69
57.18	3431	8.697E-03	4.950E-04	5.69
Nichrome				
1.10	66	4.224E-01	2.346E-02	5.56
1.37	82	3.964E-01	2.202E-02	5.56
1.63	98	3.749E-01	2.083E-02	5.55
2.08	125	3.350E-01	1.861E-02	5.55
2.72	163	2.962E-01	1.645E-02	5.55
3.33	200	2.567E-01	1.426E-02	5.55
4.22	253	2.180E-01	1.211E-02	5.55
5.28	317	1.775E-01	9.858E-03	5.55
6.40	384	1.436E-01	7.976E-03	5.55
7.98	479	1.069E-01	5.940E-03	5.56
10.10	606	7.320E-02	4.069E-03	5.56
12.22	733	5.151E-02	2.867E-03	5.57
14.35	861	3.648E-02	2.035E-03	5.58
17.48	1049	2.305E-02	1.296E-03	5.62
21.60	1296	1.345E-02	7.735E-04	5.75
25.72	1543	8.418E-03	4.962E-04	5.89
29.83	1790	5.891E-03	3.597E-04	6.11
36.97	2218	4.016E-03	2.845E-04	7.08
47.10	2826	2.933E-03	2.483E-04	8.47
57.22	3433	2.474E-03	2.366E-04	9.56

Cooling Time [min]	Cooling Time [sec]	Decay Heat [microW/g]	Error [abs.]	Error [%]
SS-304				
1.10	66	5.331E-01	3.066E-02	5.75
1.35	81	5.024E-01	2.880E-02	5.73
1.62	97	4.798E-01	2.745E-02	5.72
2.07	124	4.385E-01	2.499E-02	5.70
2.68	161	3.928E-01	2.230E-02	5.68
3.28	197	3.537E-01	2.002E-02	5.66
4.12	247	3.083E-01	1.740E-02	5.64
5.23	314	2.594E-01	1.460E-02	5.63
6.30	378	2.234E-01	1.255E-02	5.62
7.92	475	1.816E-01	1.015E-02	5.59
10.03	602	1.427E-01	7.832E-03	5.49
12.15	729	1.181E-01	6.468E-03	5.48
14.22	853	1.020E-01	5.583E-03	5.47
17.35	1041	8.704E-02	4.762E-03	5.47
21.47	1288	7.570E-02	4.141E-03	5.47
25.58	1535	6.945E-02	3.798E-03	5.47
29.70	1782	6.591E-02	3.605E-03	5.47
36.83	2210	6.213E-02	3.398E-03	5.47
46.97	2818	5.852E-02	3.201E-03	5.47
57.10	3426	5.569E-02	3.045E-03	5.47
SS-316				
1.13	68	5.651E-01	3.261E-02	5.77
1.40	84	5.334E-01	3.068E-02	5.75
1.67	100	5.053E-01	2.899E-02	5.74
2.12	127	4.624E-01	2.639E-02	5.71
2.75	165	4.115E-01	2.338E-02	5.68
3.37	202	3.669E-01	2.077E-02	5.66
4.27	256	3.151E-01	1.777E-02	5.64
5.38	323	2.647E-01	1.488E-02	5.62
6.50	390	2.243E-01	1.258E-02	5.61
8.13	488	1.801E-01	1.007E-02	5.59
10.25	615	1.399E-01	7.681E-03	5.49
12.37	742	1.143E-01	6.239E-03	5.46
14.43	866	9.803E-02	5.347E-03	5.45
17.57	1054	8.260E-02	4.503E-03	5.45
21.68	1301	7.119E-02	3.880E-03	5.45
25.82	1549	6.476E-02	3.530E-03	5.45
29.93	1796	6.091E-02	3.320E-03	5.45
37.07	2224	5.702E-02	3.108E-03	5.45
47.13	2828	5.313E-02	2.895E-03	5.45
57.22	3433	5.011E-02	2.731E-03	5.45

Table 3.11.2 Measured decay heat for the 7 hours irradiations. (1/3)

Cooling Time [days]	Decay Heat [microW/g]	Error [abs.]	Error [%]
B4C			
No detectable decay heat.			
CF2 (PTFE)			
0.66	4.932E-03	2.555E-04	5.18
1.72	1.591E-06	1.976E-06	124.21
Na2CO3			
0.67	3.726E-03	7.934E-04	21.29
1.72	1.291E-03	1.715E-04	13.28
3.87	4.550E-04	2.527E-05	5.55
6.74	3.820E-04	2.134E-05	5.59
12.19	3.731E-04	2.090E-05	5.60
24.20	3.768E-04	2.094E-05	5.56
49.95	3.819E-04	2.113E-05	5.53
100.08	3.486E-04	1.953E-05	5.60
197.95	3.358E-04	1.887E-05	5.62
402.16	2.829E-04	1.627E-05	5.75
Decay heat 2 days is due to Na-24 produced by the Na-23(n,γ) reactions.			
Al			
0.66	2.310E+00	3.347E-01	14.49
1.34	1.455E+00	1.736E-01	11.93
2.92	2.248E-01	1.542E-02	6.86
6.93	2.685E-03	1.819E-04	6.78
12.89	5.783E-05	1.286E-05	22.23
23.89	4.404E-05	1.273E-05	28.91
49.74	6.277E-05	1.279E-05	20.38
Contribution of impurities (Mn-54 from Fe) is dominant after 10 days.			
SiO2			
No detectable decay heat.			
S			
0.68	6.873E-02	4.677E-03	6.80
1.74	6.380E-02	4.333E-03	6.79
3.89	5.768E-02	3.910E-03	6.78
6.76	5.022E-02	3.397E-03	6.76
12.20	3.840E-02	2.590E-03	6.75
24.21	2.174E-02	1.462E-03	6.73
49.96	6.132E-03	4.121E-04	6.72
100.09	5.269E-04	3.730E-05	7.08
197.94	4.792E-06	1.158E-05	241.66
K2CO3			
0.65	4.208E-04	5.146E-05	12.23
1.71	6.617E-05	1.429E-05	21.60
Ca			
0.66	8.407E-03	7.020E-04	8.35
1.71	3.395E-03	2.979E-04	8.78
3.87	1.467E-03	1.538E-04	10.49
6.73	9.491E-04	1.105E-04	11.64
12.18	4.319E-04	7.894E-05	18.28
24.19	8.996E-05	7.144E-05	79.41
Ti			
0.65	3.384E-01	2.452E-02	7.24
1.32	2.540E-01	1.643E-02	6.47
2.90	1.412E-01	8.424E-03	5.97
6.87	3.445E-02	1.978E-03	5.74
12.87	6.159E-03	3.496E-04	5.68
23.86	2.434E-03	1.372E-04	5.64
49.71	1.849E-03	1.043E-04	5.64
99.90	1.248E-03	7.060E-05	5.66
200.12	5.510E-04	3.169E-05	5.75
402.96	1.235E-04	1.152E-05	9.33
V			
0.65	1.080E-01	6.939E-03	6.42
1.32	8.420E-02	5.209E-03	6.19
2.90	4.605E-02	2.729E-03	5.93
6.87	1.021E-02	5.946E-04	5.82
12.86	1.057E-03	6.155E-05	5.83
23.86	1.858E-05	3.407E-06	18.34
Cr			
0.69	1.397E-02	7.718E-04	5.53
1.74	5.392E-03	2.973E-04	5.51
3.89	1.825E-03	1.006E-04	5.51
6.75	1.366E-03	7.533E-05	5.51
12.20	1.142E-03	6.299E-05	5.51
24.21	8.312E-04	4.587E-05	5.52
49.96	4.035E-04	2.242E-05	5.56
100.09	1.147E-04	6.990E-06	6.10
197.96	1.180E-05	3.026E-06	25.64
402.14	-4.832E-07	-2.872E-06	594.32
Contribution of impurities (Na-24 from Al and Mn-56 from Fe) is dominant before 5 days.			
Mn			
0.68	8.582E-03	4.652E-04	5.42
1.73	7.638E-03	4.137E-04	5.42
3.89	7.522E-03	4.072E-04	5.41
6.75	7.429E-03	4.021E-04	5.41
12.20	7.254E-03	3.927E-04	5.41
24.21	7.187E-03	3.890E-04	5.41
49.96	6.743E-03	3.650E-04	5.41
100.10	5.930E-03	3.209E-04	5.41
197.97	4.879E-03	2.641E-04	5.41
402.18	3.067E-03	1.661E-04	5.41
Fe			
0.63	6.579E-02	3.616E-03	5.50
1.30	1.227E-03	6.710E-05	5.47
2.88	2.528E-04	1.525E-05	6.03
6.89	2.296E-04	1.425E-05	6.21
12.88	2.248E-04	1.399E-05	6.22
23.89	2.144E-04	1.348E-05	6.29
49.72	2.029E-04	1.301E-05	6.41
99.91	1.674E-04	1.140E-05	6.81
200.13	1.349E-04	9.681E-06	7.18
402.95	9.242E-05	1.047E-05	11.32

Table 3.11.2 Measured decay heat for the 7 hours irradiations. (2/3)

Cooling Time [days]	Decay Heat [microW/g]	Error [abs.]	Error [%]
Co			
0.63	5.903E-02	3.156E-03	5.35
1.31	4.280E-02	2.236E-03	5.22
2.89	4.333E-02	2.264E-03	5.23
6.86	4.188E-02	2.186E-03	5.22
12.85	3.939E-02	2.052E-03	5.21
23.84	3.516E-02	1.826E-03	5.19
49.70	2.693E-02	1.392E-03	5.17
99.89	1.629E-02	8.377E-04	5.14
200.11	5.948E-03	3.053E-04	5.13
402.95	8.207E-04	4.279E-05	5.21
Contribution of Co-58m is dropped in the experimental data.			
Ni			
0.60	9.170E-02	4.887E-03	5.33
1.31	7.005E-02	3.682E-03	5.26
2.89	3.962E-02	2.052E-03	5.18
6.86	1.593E-02	8.196E-04	5.14
12.85	1.126E-02	5.785E-04	5.14
23.85	9.924E-03	5.100E-04	5.14
49.70	7.871E-03	4.043E-04	5.14
99.89	4.925E-03	2.529E-04	5.13
200.11	2.375E-03	1.243E-04	5.23
402.94	7.269E-04	4.102E-05	5.64
Cu			
0.65	1.954E-01	1.301E-02	6.66
1.32	8.313E-02	4.629E-03	5.57
2.90	1.072E-02	5.660E-04	5.28
6.87	1.956E-04	1.400E-05	7.16
12.89	1.416E-04	1.217E-05	8.60
23.90	1.398E-04	1.202E-05	8.60
49.72	1.511E-04	1.255E-05	8.31
99.92	1.475E-04	1.224E-05	8.30
200.14	1.439E-04	1.155E-05	8.03
402.97	1.413E-04	1.392E-05	9.85

Cooling Time [days]	Decay Heat [microW/g]	Error [abs.]	Error [%]
SrCO3			
0.67	1.308E-02	7.673E-04	5.87
1.73	2.758E-03	1.643E-04	5.96
3.88	1.732E-03	1.030E-04	5.94
6.75	1.344E-03	8.049E-05	5.99
12.19	1.144E-03	6.941E-05	6.07
24.20	9.612E-04	5.912E-05	6.15
49.95	7.010E-04	4.527E-05	6.46
100.08	3.761E-04	3.002E-05	7.98
197.95	1.410E-04	2.208E-05	15.66
402.15	1.325E-05	1.998E-05	150.76
Y2O3			
0.68	5.346E-02	3.619E-03	6.77
1.73	5.270E-02	3.566E-03	6.77
3.89	5.140E-02	3.479E-03	6.77
6.76	4.996E-02	3.380E-03	6.77
12.20	4.759E-02	3.220E-03	6.77
24.21	4.451E-02	3.012E-03	6.77
49.96	3.813E-02	2.580E-03	6.77
100.09	2.679E-02	1.813E-03	6.77
197.96	1.420E-02	9.607E-04	6.77
402.17	3.674E-03	2.497E-04	6.80
Zr			
0.61	3.017E-01	2.179E-02	7.22
1.33	2.574E-01	1.733E-02	6.73
2.91	1.854E-01	1.117E-02	6.03
6.88	8.121E-02	4.330E-03	5.33
12.88	2.386E-02	1.231E-03	5.16
23.85	3.768E-03	1.969E-04	5.23
49.71	1.530E-03	8.287E-05	5.42
99.90	1.088E-03	5.923E-05	5.44
200.12	4.642E-04	2.617E-05	5.64
402.96	7.940E-05	1.173E-05	14.77
Nb			
0.62	1.094E-01	6.357E-03	5.81
1.32	1.031E-01	5.937E-03	5.76
2.90	9.076E-02	5.152E-03	5.68
6.86	6.807E-02	3.781E-03	5.55
12.86	4.482E-02	2.447E-03	5.46
23.85	2.103E-02	1.136E-03	5.40
49.70	3.622E-03	1.953E-04	5.39
99.89	1.254E-04	9.862E-06	7.87

Cooling Time [days]	Decay Heat [microW/g]	Error [abs.]	Error [%]
Mo			
0.64	8.873E-02	5.180E-03	5.84
1.31	7.228E-02	4.129E-03	5.71
2.90	4.540E-02	2.487E-03	5.48
6.86	1.705E-02	9.054E-04	5.31
12.86	4.707E-03	2.495E-04	5.30
23.86	9.947E-04	5.431E-05	5.46
49.71	3.144E-04	1.890E-05	6.01
99.90	1.072E-04	9.946E-06	9.28
200.14	4.637E-05	8.950E-06	19.30
SnO2			
0.68	1.492E-02	2.134E-03	14.31
1.73	1.191E-02	1.543E-03	12.96
3.88	8.884E-03	1.048E-03	11.79
6.75	6.930E-03	8.041E-04	11.60
12.20	4.935E-03	5.834E-04	11.82
24.20	2.828E-03	3.290E-04	11.63
49.95	9.568E-04	1.041E-04	10.88
100.08	3.197E-04	4.480E-05	14.01
197.93	1.849E-04	3.863E-05	20.89
402.13	5.179E-05	3.469E-05	66.98
BaCO3			
0.67	1.568E-02	2.294E-03	14.64
1.72	8.331E-03	1.205E-03	14.46
3.88	2.575E-03	3.774E-04	14.66
6.74	6.901E-04	1.258E-04	18.22
12.18	1.181E-04	6.113E-05	51.76
24.18	3.601E-05	5.137E-05	142.66
Ta			
0.60	6.789E-02	6.788E-03	10.00
1.33	1.616E-02	1.398E-03	8.65
2.91	8.641E-04	1.064E-04	12.31
6.88	2.735E-04	3.716E-05	13.59
12.88	2.626E-04	4.049E-05	15.42
23.88	2.361E-04	4.086E-05	17.31
49.72	2.039E-04	3.925E-05	19.25
99.91	1.377E-04	2.936E-05	21.32
200.13	7.574E-05	1.660E-05	21.92
402.97	3.424E-05	9.926E-06	28.99

Table 3.11.2 Measured decay heat for the 7 hours irradiations. (3/3)

Cooling Time [days]	Decay Heat [microW/g]	Error [abs.]	Error [%]
W			
0.61	3.174E-03	2.234E-04	7.04
1.33	2.021E-03	1.894E-04	9.37
2.91	1.411E-03	2.071E-04	14.68
6.88	1.082E-03	1.588E-04	14.68
12.87	9.859E-04	1.447E-04	14.68
23.87	8.585E-04	1.261E-04	14.68
49.71	6.865E-04	1.009E-04	14.69
99.90	3.476E-04	5.126E-05	14.74
200.12	2.033E-04	3.018E-05	14.85
402.95	4.257E-05	9.053E-06	21.27
Re			
0.69	1.141E-01	1.224E-02	10.73
1.74	9.317E-02	9.591E-03	10.30
3.90	6.707E-02	6.452E-03	9.62
6.76	4.605E-02	4.069E-03	8.84
12.21	2.609E-02	1.967E-03	7.54
24.22	1.366E-02	8.187E-04	5.99
49.97	7.881E-03	4.467E-04	5.67
100.10	3.387E-03	1.917E-04	5.66
197.96	1.011E-03	6.300E-05	6.23
402.17	2.783E-04	1.896E-05	6.81
Pb			
0.61	4.460E-03	2.320E-04	5.20
1.33	3.522E-03	1.831E-04	5.20
2.91	2.075E-03	1.080E-04	5.20
6.88	5.834E-04	3.087E-05	5.29
12.87	9.621E-05	7.686E-06	7.99
23.88	9.087E-06	5.790E-06	63.71
49.73	1.113E-05	5.860E-06	52.64
Bi			
0.66	1.388E-05	1.451E-05	104.53
1.70	-2.030E-06	-9.155E-06	451.00
3.85	1.999E-06	6.129E-06	306.62
6.73	2.283E-06	4.981E-06	218.15
12.17	-3.731E-06	-4.767E-06	127.77

S/N ratios are not good over whole cooling time.

Cooling Time [days]	Decay Heat [microW/g]	Error [abs.]	Error [%]
Inconel-600			
0.62	8.293E-02	6.117E-03	7.38
1.31	5.702E-02	3.583E-03	6.28
2.89	3.106E-02	1.732E-03	5.58
6.86	1.218E-02	6.396E-04	5.25
12.86	8.552E-03	4.453E-04	5.21
23.84	7.471E-03	3.879E-04	5.19
49.69	5.919E-03	3.061E-04	5.17
99.88	3.677E-03	1.892E-04	5.15
200.11	1.800E-03	9.435E-05	5.24
402.94	5.529E-04	3.066E-05	5.54
Nichrome			
0.64	7.397E-02	3.856E-03	5.21
1.30	5.754E-02	2.984E-03	5.19
2.88	3.260E-02	1.680E-03	5.16
6.85	1.305E-02	6.709E-04	5.14
12.85	9.182E-03	4.719E-04	5.14
23.85	8.068E-03	4.146E-04	5.14
49.70	6.365E-03	3.271E-04	5.14
99.89	3.957E-03	2.034E-04	5.14
200.12	1.877E-03	9.849E-05	5.25
402.94	5.920E-04	3.476E-05	5.87
SS304			
0.63	5.896E-02	3.266E-03	5.54
1.30	7.849E-03	4.029E-04	5.13
2.88	4.324E-03	2.219E-04	5.13
6.85	2.024E-03	1.040E-04	5.14
12.84	1.543E-03	7.938E-05	5.14
23.84	1.348E-03	6.938E-05	5.15
49.69	1.074E-03	5.538E-05	5.16
99.88	7.027E-04	3.650E-05	5.19
200.10	4.076E-04	2.210E-05	5.42
402.93	1.944E-04	1.305E-05	6.71
SS316			
0.62	6.243E-02	3.452E-03	5.53
1.30	1.304E-02	6.702E-04	5.14
2.88	7.242E-03	3.718E-04	5.13
6.85	3.167E-03	1.626E-04	5.13
12.84	2.191E-03	1.126E-04	5.14
23.83	1.835E-03	9.436E-05	5.14
49.69	1.454E-03	7.483E-05	5.15
99.88	9.305E-04	4.813E-05	5.17
200.10	5.227E-04	2.803E-05	5.36
402.93	2.218E-04	1.458E-05	6.58

Table 3.12.1 Number densities of isotopes contained in the sample materials. (1/4) Weight densities of all the materials are assumed to be 1.0 [g/cm^3] for easier comparison of experimental and calculated decay heat values in the unit of [W/g] instead of [W/cm^3].

Material	ID	Abundance of isotope	Weight % of Element	Atomic/Molecular Mass /mol	Number Density [atoms/cc]
B4C			100.00	55.25500	0.01089856
B		1.00000	78.26	10.81100	0.04359424
B-10	5010	0.19900			0.00867525
B-11	5011	0.80100			0.03491899
C-12	6012	1.00000	21.74	12.01100	0.01089856
CF2			100.00	50.00781	0.01204212
C-12	6012	1.00000	24.02	12.01100	0.01204212
F-19	9019	1.00000	75.98	18.99840	0.02408424
Na2CO3			100.00	105.98874	0.00568174
C-12	6012	1.00000	11.33	12.01100	0.00568200
O-16	8016	1.00000	45.29	15.99940	0.01704500
Na-23	11023	1.00000	43.38	22.98977	0.01136300
Al-27	13027	1.00000	100.00	26.98154	0.02231896
SiO2			100.00	60.08430	0.01002258
O-16	8016	1.00000	53.26	15.99940	0.02004517
Si		1.00000	46.74	28.08550	0.01002258
Si-28	14028	0.92230			0.00924383
Si-29	14029	0.04670			0.00046805
Si-30	14030	0.03100			0.00031070
S		1.00000	100.00	32.06600	0.01878002
S-32	16032	0.95020			0.01784477
S-33	16033	0.00750			0.00014085
S-34	16034	0.04210			0.00079064
S-36	16036	0.00020			0.00000376
K2CO3			100.00	138.20580	0.00435727
C-12	6012	1.00000	8.69	12.01100	0.00435727
O-16	8016	1.00000	34.73	15.99940	0.01307181
K		1.00000	56.58	39.09830	0.00871454
K-39	19039	0.93258			0.00812701
K-40	19040	0.00012			0.00000105
K-41	19041	0.06730			0.00058649
CaO			100.00	56.07740	0.01073873
O-16	8016	1.00000	28.53	15.99940	0.01073873
Ca		1.00000	71.47	40.07800	0.01073873
Ca-40	20040	0.96941			0.01041023
Ca-42	20042	0.00647			0.00006948
Ca-43	20043	0.00135			0.00001450
Ca-44	20044	0.02086			0.00022401
Ca-46	20046	0.00004			0.00000043
Ca-48	20048	0.00187			0.00002008
Ti		1.00000	100.00	47.86700	0.01258069
Ti-46	22046	0.08000			0.00100646
Ti-47	22047	0.07300			0.00091839
Ti-48	22048	0.73800			0.00928455
Ti-49	22049	0.05500			0.00069194
Ti-50	22050	0.05400			0.00067936
V		1.00000	100.00	50.94150	0.01182140
V-50	23050	0.00250			0.00002955
V-51	23051	0.99750			0.01179185

Table 3.12.1 Continued. (2/4)

Material	ID	Abundance of isotope	Weight % of Element	Atomic/Molecular Mass /mol	Number Density [atoms/cc]
Cr		1.00000	100.00	51.99610	0.01158164
Cr-50	24050	0.04345			0.00050322
Cr-52	24052	0.83789			0.00970414
Cr-53	24053	0.09501			0.00110037
Cr-54	24054	0.02365			0.00027391
Mn-55	25055	1.00000	100.00	54.93805	0.01096144
Fe		1.00000	100.00	55.84500	0.01078342
Fe-54	26054	0.05800			0.00062544
Fe-56	26056	0.91720			0.00989055
Fe-57	26057	0.02200			0.00023724
Fe-58	26058	0.00280			0.00003019
Co-59	27059	1.00000	100.00	58.93320	0.01021835
Ni		1.00000	100.00	58.69340	0.01026010
Ni-58	28058	0.68077			0.00698477
Ni-60	28060	0.26223			0.00269051
Ni-61	28061	0.01140			0.00011697
Ni-62	28062	0.03634			0.00037285
Ni-64	28064	0.00926			0.00009501
Cu		1.00000	100.00	63.54600	0.00947660
Cu-63	29063	0.69170			0.00655496
Cu-65	29065	0.30830			0.00292164
SrCO3			100.00	147.62920	0.00407914
C-12	6012	1.00000	8.14	12.01100	0.00407914
O-16	8016	1.00000	32.51	15.99940	0.01223742
Sr		1.00000	59.35	87.62000	0.00407914
Sr-84	38084	0.00560			0.00002284
Sr-86	38086	0.09860			0.00040220
Sr-87	38087	0.07000			0.00028554
Sr-88	38088	0.82580			0.00336855
Y2O3			100.00	225.80990	0.00266684
O-16	8016	1.00000	21.26	15.99940	0.00800053
Y-89	39089	1.00000	78.74	88.90585	0.00533369
Zr		1.00000	100.00	91.22400	0.00660133
Zr-90	40090	0.51450			0.00339639
Zr-91	40091	0.11220			0.00074067
Zr-92	40092	0.17150			0.00113213
Zr-94	40094	0.17380			0.00114731
Zr-96	40096	0.02800			0.00018484
Nb-93	41093	1.00000	100.00	92.90638	0.00648179
Mo		1.00000	100.00	95.94000	0.00627684
Mo-92	42092	0.14840			0.00093148
Mo-94	42094	0.09250			0.00058061
Mo-95	42095	0.15920			0.00099927
Mo-96	42096	0.16680			0.00104698
Mo-97	42097	0.09550			0.00059944
Mo-98	42098	0.24130			0.00151460
Mo-100	42000	0.09630			0.00060446

Table 3.12.1 Continued. (3/4)

Material	ID	Abundance of isotope	Weight % of Element	Atomic/Molecular Mass /mol	Number Density [atoms/cc]
SnO2			100.00	150.69800	0.00399607
O-16	8016	1.00000	21.23	15.99940	0.00799214
Sn		1.00000	78.77	118.71000	0.00399607
Sn-112	50012	0.00970			0.00003876
Sn-114	50014	0.00650			0.00002597
Sn-115	50015	0.00340			0.00001359
Sn-116	50016	0.14530			0.00058063
Sn-117	50017	0.07680			0.00030690
Sn-118	50018	0.24230			0.00096825
Sn-119	50019	0.08590			0.00034326
Sn-120	50020	0.32590			0.00130232
Sn-122	50022	0.04630			0.00018502
Sn-124	50024	0.05790			0.00023137
BaCO3			100.00	197.33620	0.00305164
C-12	6012		6.09	12.01100	0.00305164
O-16	8016		24.32	15.99940	0.00915493
Ba		1.00000	69.59	137.32700	0.00305164
Ba-130	56030	0.00106			0.00000323
Ba-132	56032	0.00101			0.00000308
Ba-134	56034	0.02417			0.00007376
Ba-135	56035	0.06592			0.00020116
Ba-136	56036	0.07854			0.00023968
Ba-137	56037	0.11230			0.00034270
Ba-138	56038	0.71700			0.00218803
Ta		1.00000	100.00	180.94790	0.00332803
Ta-180	73080	0.00012			0.00000040
Ta-181	73081	0.99988			0.00332763
W		1.00000	100.00	183.84000	0.00327567
W-180	74080	0.00130			0.00000426
W-182	74082	0.26300			0.00086150
W-183	74083	0.14300			0.00046842
W-184	74084	0.30670			0.00100465
W-186	74086	0.28600			0.00093684
Re		1.00000	100.00	186.20700	0.00323404
Re-185	75085	0.37400			0.00120953
Re-187	75087	0.62600			0.00202451
Pb		1.00000	100.00	207.20000	0.00290637
Pb-204	82004	0.01400			0.00004069
Pb-206	82006	0.24100			0.00070044
Pb-207	82007	0.22100			0.00064231
Pb-208	82008	0.52400			0.00152294
Bi-209	83009	1.00000	100.00	208.98037	0.00288161
Inconel-600			100.00	57.27162	0.01051481
Cr		1.00000	15.97	51.99610	0.00184959
Cr-50	24050	0.04345			0.00008036
Cr-52	24052	0.83789			0.00154975
Cr-53	24053	0.09501			0.00017573
Cr-54	24054	0.02365			0.00004374
Fe		1.00000	7.82	55.84500	0.00084326
Fe-54	26054	0.05800			0.00004891
Fe-56	26056	0.91720			0.00077344
Fe-57	26057	0.02200			0.00001855
Fe-58	26058	0.00280			0.00000236
Mn	25055		0.39	54.93805	0.00004275
Ni		1.00000	75.82	58.69340	0.00777921
Ni-58	28058	0.68077			0.00529585
Ni-60	28060	0.26223			0.00203994
Ni-61	28061	0.01140			0.00008868
Ni-62	28062	0.03634			0.00028270
Ni-64	28064	0.00926			0.00007204

Table 3.12.1 Continued. (4/4)

Material	ID	Abundance of isotope	Weight % of Element	Atomic/Molecular Mass /mol	Number Density [atoms/cc]
Nichrome			100.00	57.24355	0.01051996
Cr		1.00000	19.64	51.99610	0.00227463
Cr-50	24050	0.04345			0.00009883
Cr-52	24052	0.83789			0.00190589
Cr-53	24053	0.09501			0.00021611
Cr-54	24054	0.02365			0.00005380
Fe		1.00000	0.06	55.84500	0.00000647
Fe-54	26054	0.05800			0.00000038
Fe-56	26056	0.91720			0.00000593
Fe-57	26057	0.02200			0.00000014
Fe-58	26058	0.00280			0.00000002
Ni		1.00000	80.30	58.69340	0.00823886
Ni-58	28058	0.68077			0.00560877
Ni-60	28060	0.26223			0.00216048
Ni-61	28061	0.01140			0.00009392
Ni-62	28062	0.03634			0.00029940
Ni-64	28064	0.00926			0.00007629
SS304			100.00	55.03421	0.01094228
Cr		1.00000	18.02	51.99610	0.00208701
Cr-50	24050	0.04345			0.00009068
Cr-52	24052	0.83789			0.00174869
Cr-53	24053	0.09501			0.00019829
Cr-54	24054	0.02365			0.00004936
Mn	25055	1.00000	1.44	54.93805	0.00015784
Ni		1.00000	8.82	58.69340	0.00090494
Ni-58	28058	0.68077			0.00061606
Ni-60	28060	0.26223			0.00023730
Ni-61	28061	0.01140			0.00001032
Ni-62	28062	0.03634			0.00003289
Ni-64	28064	0.00926			0.00000838
Si		1.00000	0.55	28.08550	0.00011793
Si-28	14028	0.92230			0.00010877
Si-29	14029	0.04670			0.00000551
Si-30	14030	0.03100			0.00000366
Fe		1.00000	71.17	55.84500	0.00767456
Fe-54	26054	0.05800			0.00044512
Fe-56	26056	0.91720			0.00703911
Fe-57	26057	0.02200			0.00016884
Fe-58	26058	0.00280			0.00002149
SS316			100.00	55.40409	0.01086923
Cr		1.00000	18.28	51.99610	0.00211726
Cr-50	24050	0.04345			0.00009199
Cr-52	24052	0.83789			0.00177403
Cr-53	24053	0.09501			0.00020116
Cr-54	24054	0.02365			0.00005007
Mn	25055	1.00000	1.44	54.93805	0.00015785
Ni		1.00000	13.49	58.69340	0.00138418
Ni-58	28058	0.68077			0.00094231
Ni-60	28060	0.26223			0.00036297
Ni-61	28061	0.01140			0.00001578
Ni-62	28062	0.03634			0.00005030
Ni-64	28064	0.00926			0.00001282
Mo		1.00000	2.11	95.94000	0.00013245
Mo-92	42092	0.14840			0.00001966
Mo-94	42094	0.09250			0.00001225
Mo-95	42095	0.15920			0.00002109
Mo-96	42096	0.16680			0.00002209
Mo-97	42097	0.09550			0.00001265
Mo-98	42098	0.24130			0.00003196
Mo-100	42000	0.09630			0.00001275
Si		1.00000	0.96	28.08550	0.00020447
Si-28	14028	0.92230			0.00195275
Si-29	14029	0.04670			0.00009888
Si-30	14030	0.03100			0.00006564
Fe		1.00000	63.72	55.84500	0.00687164
Fe-54	26054	0.05800			0.00039856
Fe-56	26056	0.91720			0.00630267
Fe-57	26057	0.02200			0.00015118
Fe-58	26058	0.00280			0.00001924

Table 3.12.2 Source conditions for the Vitamin-J 175-energy group structure. (1/2)

Energy Group Boundaries in eV

1.96403E+7	1.73325E+7	1.69046E+7	1.64872E+7	1.56831E+7	1.49183E+7
1.45499E+7	1.41907E+7	1.38403E+7	1.34986E+7	1.28400E+7	1.25232E+7
1.22140E+7	1.16183E+7	1.10517E+7	1.05127E+7	1.00000E+7	9.51229E+6
9.04837E+6	8.60708E+6	8.18731E+6	7.78801E+6	7.40818E+6	7.04688E+6
6.70320E+6	6.59238E+6	6.37628E+6	6.06531E+6	5.76950E+6	5.48812E+6
5.22046E+6	4.96585E+6	4.72367E+6	4.49329E+6	4.06570E+6	3.67879E+6
3.32871E+6	3.16637E+6	3.01194E+6	2.86505E+6	2.72532E+6	2.59240E+6
2.46597E+6	2.38521E+6	2.36525E+6	2.34570E+6	2.30686E+6	2.23130E+6
2.12248E+6	2.01897E+6	1.92050E+6	1.82684E+6	1.73774E+6	1.65299E+6
1.57237E+6	1.49569E+6	1.42274E+6	1.35335E+6	1.28735E+6	1.22456E+6
1.16484E+6	1.10803E+6	1.00259E+6	9.61640E+5	9.07180E+5	8.62936E+5
8.20850E+5	7.80817E+5	7.42736E+5	7.06512E+5	6.72055E+5	6.39279E+5
6.08101E+5	5.78444E+5	5.50232E+5	5.23397E+5	4.97871E+5	4.50492E+5
4.07622E+5	3.87742E+5	3.68832E+5	3.33733E+5	3.01974E+5	2.98491E+5
2.97211E+5	2.94518E+5	2.87247E+5	2.73237E+5	2.47235E+5	2.35177E+5
2.23708E+5	2.12797E+5	2.02419E+5	1.92547E+5	1.83156E+5	1.74224E+5
1.65727E+5	1.57644E+5	1.49956E+5	1.42642E+5	1.35686E+5	1.29068E+5
1.22773E+5	1.16786E+5	1.11090E+5	9.80366E+4	8.65169E+4	8.25034E+4
7.94987E+4	7.19981E+4	6.73794E+4	5.65622E+4	5.24752E+4	4.63092E+4
4.08677E+4	3.43067E+4	3.18278E+4	2.85011E+4	2.70001E+4	2.60584E+4
2.47875E+4	2.41755E+4	2.35786E+4	2.18749E+4	1.93045E+4	1.50344E+4
1.17088E+4	1.05946E+4	9.11882E+3	7.10174E+3	5.53084E+3	4.30742E+3
3.70744E+3	3.35463E+3	3.03539E+3	2.74654E+3	2.61259E+3	2.48517E+3
2.24867E+3	2.03468E+3	1.58461E+3	1.23410E+3	9.61116E+2	7.48518E+2
5.82947E+2	4.53999E+2	3.53575E+2	2.75364E+2	2.14454E+2	1.67017E+2
1.30073E+2	1.01301E+2	7.88932E+1	6.14421E+1	4.78512E+1	3.72665E+1
2.90232E+1	2.26033E+1	1.76035E+1	1.37096E+1	1.06770E+1	8.31529E+0
6.47595E+0	5.04348E+0	3.92786E+0	3.05902E+0	2.38237E+0	1.85539E+0
1.44498E+0	1.12535E+0	8.76425E-1	6.82560E-1	5.31578E-1	4.13994E-1
1.00001E-1	1.00001E-5				

Source Neutron Spectrum for Position #1 [n/Group/cm^2/Sec]
Normalization Factor 2.950e+12

.00000E+0	.00000E+0	.00000E+0	.00000E+0	1.53144E-3	1.63121E-3
1.30724E-4	1.22077E-5	1.35464E-5	1.65288E-5	7.74344E-6	6.10261E-6
1.01475E-5	1.02720E-5	1.04328E-5	9.54947E-6	1.03850E-5	8.24373E-6
8.41811E-6	7.70782E-6	7.52319E-6	7.45561E-6	8.26328E-6	8.14740E-6
2.43247E-6	4.70429E-6	7.05315E-6	7.15116E-6	6.80481E-6	6.92390E-6
6.93735E-6	6.82097E-6	7.45818E-6	1.39811E-5	1.34438E-5	1.37968E-5
6.62898E-6	6.53793E-6	6.41896E-6	6.48403E-6	6.56981E-6	6.40774E-6
4.35006E-6	1.01328E-6	9.05651E-7	2.10484E-6	4.32033E-6	6.50079E-6
6.18417E-6	6.20704E-6	6.49262E-6	6.47644E-6	6.23852E-6	6.20158E-6
6.37230E-6	6.42171E-6	6.18297E-6	6.13037E-6	5.71892E-6	5.27039E-6
5.40396E-6	1.07953E-5	4.54586E-6	6.28249E-6	4.93256E-6	4.50637E-6
4.70980E-6	4.82106E-6	4.28096E-6	4.61289E-6	4.09480E-6	4.22633E-6
3.89221E-6	3.33932E-6	3.86511E-6	3.42077E-6	6.89275E-6	6.23523E-6
2.76939E-6	3.07958E-6	5.32794E-6	4.79035E-6	5.41039E-7	1.29460E-7
3.89339E-7	8.68000E-7	1.94047E-6	4.08217E-6	1.82848E-6	1.46283E-6
1.67413E-6	1.51122E-6	1.24839E-6	1.36665E-6	1.32352E-6	1.15565E-6
1.15891E-6	9.69880E-7	9.98081E-7	1.28309E-6	9.55581E-7	1.00994E-6
8.18683E-7	9.21757E-7	2.03269E-6	1.48598E-6	5.78828E-7	4.73071E-7
1.32502E-6	7.43130E-7	1.77678E-6	6.59398E-7	1.08408E-6	1.07276E-6
1.14773E-6	5.50681E-7	8.91160E-7	2.70690E-7	2.29833E-7	2.88417E-7
1.39498E-7	1.42190E-7	4.72699E-7	5.89589E-7	1.30019E-6	1.03184E-6
3.60985E-7	5.38806E-7	8.50897E-7	8.52545E-7	6.76271E-7	4.33943E-7
3.37312E-7	2.67811E-7	1.88490E-7	1.16319E-7	9.71637E-8	3.22823E-7
2.70823E-7	6.06863E-7	5.36032E-7	3.49940E-7	3.93648E-7	3.52166E-7
2.71850E-7	2.14632E-7	2.54564E-7	2.77724E-7	2.17188E-7	2.14586E-7
1.00137E-7	1.77674E-7	1.31727E-7	1.30138E-7	1.10719E-7	9.21939E-8
1.34634E-7	1.09177E-7	1.07016E-7	1.08217E-7	8.23902E-8	2.98245E-8
6.17108E-8	9.87746E-9	3.69939E-8	3.65945E-8	2.93287E-8	3.36730E-8
6.58011E-8	4.83481E-8	7.12476E-9	3.99966E-8	1.08719E-8	1.22634E-7
2.09076E-7					

Source Neutron Spectrum for Position #2 [n/Group/cm^2/Sec]
Normalization Factor 5.634e+11

.00000E+0	.00000E+0	.00000E+0	.00000E+0	6.43027E-3	9.75030E-3
1.23844E-3	6.09828E-5	4.92822E-5	6.46589E-5	2.91193E-5	2.35518E-5
3.68894E-5	3.35444E-5	3.34111E-5	2.33337E-5	2.38331E-5	2.55598E-5
2.81972E-5	2.72467E-5	2.79092E-5	2.87732E-5	2.97333E-5	3.05626E-5
9.44982E-6	1.71068E-5	2.73607E-5	2.86235E-5	2.95206E-5	2.80941E-5
2.87404E-5	3.05165E-5	3.16474E-5	6.17805E-5	6.36025E-5	6.34363E-5
3.13136E-5	3.09405E-5	3.20495E-5	3.16240E-5	3.19517E-5	3.09608E-5
2.06005E-5	4.95449E-6	5.25216E-6	1.05581E-5	2.03497E-5	3.09214E-5
3.12000E-5	2.99707E-5	2.96463E-5	2.99971E-5	2.86510E-5	2.89171E-5
2.98685E-5	2.83607E-5	2.90368E-5	2.88329E-5	2.74463E-5	2.71762E-5
2.63012E-5	5.12257E-5	2.11220E-5	2.69125E-5	2.30236E-5	2.23742E-5
2.13306E-5	2.13494E-5	2.02618E-5	2.09093E-5	1.89171E-5	1.85684E-5
1.77088E-5	1.63521E-5	1.58633E-5	1.57674E-5	2.97206E-5	2.61825E-5
1.34547E-5	1.22989E-5	2.40094E-5	2.13070E-5	2.55056E-6	7.09785E-7
1.73693E-6	4.74559E-6	9.56437E-6	1.85409E-5	8.01017E-6	7.83443E-6

Table 3.12.2 Source conditions for the Vitamin-J 175-energy group structure. (2/2)

```
 6.84674E-6 6.88058E-6 7.12356E-6 6.66614E-6 6.03310E-6 5.85951E-6
 5.20123E-6 4.77672E-6 4.77366E-6 5.10735E-6 5.41072E-6 4.82041E-6
 3.97046E-6 4.50143E-6 9.64730E-6 7.90902E-6 3.15053E-6 2.80883E-6
 6.96123E-6 3.96456E-6 9.04310E-6 3.83440E-6 5.65050E-6 5.15421E-6
 6.10706E-6 3.12127E-6 4.81925E-6 1.71283E-6 1.25748E-6 1.51516E-6
 9.66782E-7 9.12271E-7 2.29717E-6 3.89359E-6 6.64091E-6 6.32866E-6
 2.10768E-6 2.81784E-6 4.83856E-6 4.72670E-6 4.02094E-6 2.34407E-6
 1.51705E-6 1.52125E-6 1.28136E-6 6.92067E-7 6.21636E-7 1.10139E-6
 1.05204E-6 2.60939E-6 2.54641E-6 2.23727E-6 1.87300E-6 1.88845E-6
 1.71239E-6 1.45360E-6 1.51785E-6 1.30427E-6 1.21629E-6 1.14463E-6
 9.68726E-7 8.57410E-7 8.72794E-7 7.52335E-7 6.53859E-7 6.50928E-7
 5.61006E-7 5.90746E-7 3.78450E-7 4.16924E-7 3.98772E-7 3.71935E-7
 4.50932E-7 2.15036E-7 3.19135E-7 2.28931E-7 2.62151E-7 1.85134E-7
 1.60751E-7 2.23317E-7 1.80806E-7 9.08540E-8 1.12441E-7 5.70380E-7
 9.01011E-7

Source Neutron Spectrum for Position #3  [n/Group/cm^2/Sec]
     Normalization Factor 3.042e+11

  .00000E+0  .00000E+0  .00000E+0  .00000E+0 9.22168E-3 1.89034E-2
 3.75614E-3 1.87158E-4 1.21773E-4 1.70275E-4 7.19471E-5 5.83186E-5
 1.03884E-4 9.74356E-5 9.37323E-5 8.43975E-5 8.00553E-5 7.27707E-5
 6.90263E-5 6.66849E-5 6.63458E-5 6.76845E-5 6.95085E-5 6.80549E-5
 2.12845E-5 4.01181E-5 6.00707E-5 6.12797E-5 5.89932E-5 5.85238E-5
 5.75498E-5 6.14351E-5 6.22742E-5 1.18864E-4 1.16898E-4 1.14572E-4
 5.53231E-5 5.68070E-5 5.59637E-5 5.64856E-5 5.71855E-5 5.63844E-5
 3.63639E-5 9.63942E-6 9.29112E-6 1.88843E-5 3.69615E-5 5.48531E-5
 5.45515E-5 5.37525E-5 5.37249E-5 5.27956E-5 5.15189E-5 5.24511E-5
 5.12457E-5 4.99851E-5 5.01997E-5 4.94688E-5 4.69074E-5 4.65089E-5
 4.55357E-5 9.00409E-5 3.57282E-5 4.83215E-5 4.00760E-5 3.88128E-5
 3.74567E-5 3.71154E-5 3.49684E-5 3.46894E-5 3.27471E-5 3.13254E-5
 3.04877E-5 2.82772E-5 2.80317E-5 2.68286E-5 5.10971E-5 4.54924E-5
 2.21575E-5 2.11669E-5 4.08660E-5 3.56658E-5 4.11545E-6 1.32446E-6
 2.98782E-6 8.47863E-6 1.62684E-5 3.13724E-5 1.36224E-5 1.28701E-5
 1.27796E-5 1.16470E-5 1.20933E-5 1.19775E-5 1.07320E-5 9.89323E-6
 8.24947E-6 8.64409E-6 8.28130E-6 9.32089E-6 9.10753E-6 8.44599E-6
 6.93911E-6 7.08898E-6 1.65405E-5 1.34325E-5 5.62235E-6 4.43248E-6
 1.14387E-5 6.72457E-6 1.54173E-5 6.14257E-6 9.20559E-6 8.88981E-6
 1.00304E-5 5.51337E-6 7.47848E-6 3.32140E-6 1.99429E-6 2.85658E-6
 1.33704E-6 1.55614E-6 3.91193E-6 6.18528E-6 1.17385E-5 1.00038E-5
 3.93465E-6 5.46117E-6 8.45762E-6 7.20850E-6 6.91376E-6 4.18530E-6
 2.73138E-6 2.15927E-6 2.39941E-6 1.13668E-6 1.19213E-6 2.27016E-6
 2.16590E-6 4.88210E-6 4.18627E-6 3.78042E-6 3.43237E-6 3.08205E-6
 2.90162E-6 2.91888E-6 2.42176E-6 2.41879E-6 2.30244E-6 2.04062E-6
 1.81126E-6 1.45723E-6 1.69379E-6 1.32988E-6 1.09720E-6 9.39865E-7
 1.13930E-6 9.68038E-7 9.25022E-7 8.53797E-7 7.42514E-7 6.66160E-7
 6.99580E-7 7.68421E-7 4.27899E-7 5.00135E-7 3.88651E-7 4.29901E-7
 3.37608E-7 2.90690E-7 2.78412E-7 2.41690E-7 2.59388E-7 1.42315E-6
 1.95964E-6

Source Neutron Spectrum for Position #7  [n/Group/cm^2/Sec]
     Normalization Factor 9.653e+10

  .00000E+0  .00000E+0  .00000E+0  .00000E+0 9.14548E-3 3.78176E-2
 5.47378E-2 1.13509E-3 1.57677E-4 2.07896E-4 7.46900E-5 4.77809E-5
 7.44187E-5 7.84172E-5 6.62109E-5 5.76040E-5 5.49062E-5 5.21111E-5
 5.16973E-5 5.52736E-5 6.14919E-5 6.01367E-5 6.21665E-5 6.01998E-5
 1.98978E-5 3.90887E-5 6.07050E-5 5.94459E-5 6.17950E-5 6.33007E-5
 6.65773E-5 6.81581E-5 6.73333E-5 1.43343E-4 1.52515E-4 1.53292E-4
 7.77094E-5 7.95262E-5 8.22658E-5 8.75919E-5 8.94898E-5 8.92740E-5
 6.00680E-5 1.65435E-5 1.50084E-5 3.10124E-5 6.17298E-5 9.64032E-5
 9.35522E-5 9.35349E-5 9.82910E-5 9.41851E-5 9.83041E-5 9.64690E-5
 9.38253E-5 9.21795E-5 9.26899E-5 9.14957E-5 8.83669E-5 9.26079E-5
 8.94928E-5 1.62111E-4 6.78499E-5 8.90736E-5 7.67973E-5 7.52537E-5
 7.10078E-5 6.88056E-5 6.58229E-5 6.37980E-5 6.07558E-5 5.78139E-5
 5.42333E-5 5.20447E-5 4.73396E-5 4.68779E-5 8.85052E-5 7.74978E-5
 3.83798E-5 3.64000E-5 7.05413E-5 6.29789E-5 6.74477E-6 2.28854E-6
 4.83562E-6 1.41522E-5 2.54132E-5 4.76441E-5 2.18693E-5 1.93063E-5
 1.78869E-5 1.65744E-5 1.65652E-5 1.47507E-5 1.57750E-5 1.25070E-5
 1.23537E-5 1.11183E-5 8.98182E-6 9.80459E-6 8.49062E-6 8.18293E-6
 7.27833E-6 6.73192E-6 1.56192E-5 1.30280E-5 4.41585E-6 3.54188E-6
 8.13658E-6 4.78975E-6 1.05375E-5 3.79190E-6 6.14403E-6 4.86097E-6
 5.24644E-6 1.84928E-6 2.41565E-6 1.16255E-6 7.42051E-7 1.18666E-6
 4.73462E-7 5.37341E-7 1.24944E-6 1.96679E-6 3.48689E-6 2.98664E-6
 8.73435E-7 9.55665E-7 1.68952E-6 1.26558E-6 9.44125E-7 4.48933E-7
 3.82678E-7 2.32160E-7 2.44597E-7 6.83717E-8 5.81228E-8 1.84523E-7
 1.56874E-7 4.32855E-7 4.39060E-7 3.19253E-7 3.12357E-7 9.08416E-8
 1.55260E-7 2.60281E-7 1.44746E-7 1.47498E-7 1.11591E-7 5.63518E-8
 9.99882E-9 5.76604E-8 1.27731E-7 1.01771E-8 4.31713E-8 2.17870E-8
 5.68747E-9 1.28708E-8 3.94321E-8  .00000E+0  .00000E+0 1.41124E-8
 9.57135E-9 1.34319E-8 6.01118E-8  .00000E+0 1.01181E-8 8.87569E-9
  .00000E+0 5.17524E-8  .00000E+0  .00000E+0  .00000E+0  .00000E+0
 2.17946E-8
```

Table 3.12.3 Source conditions for the 125-energy group structure. (1/2)

Energy Group Boundaries in eV

1.64870E+7	1.62310E+7	1.59800E+7	1.57320E+7	1.54880E+7	1.52480E+7
1.50120E+7	1.47790E+7	1.45500E+7	1.43240E+7	1.41020E+7	1.38830E+7
1.36680E+7	1.34560E+7	1.32480E+7	1.30420E+7	1.28400E+7	1.26410E+7
1.24450E+7	1.22520E+7	1.20620E+7	1.18750E+7	1.16910E+7	1.15100E+7
1.13310E+7	1.11560E+7	1.09830E+7	1.08120E+7	1.06450E+7	1.04800E+7
1.03170E+7	1.01570E+7	9.99990E+6	9.39400E+6	8.82490E+6	8.29020E+6
7.78790E+6	7.31610E+6	6.87280E+6	6.45640E+6	6.06520E+6	5.69780E+6
5.35250E+6	5.02820E+6	4.72360E+6	4.43740E+6	4.16860E+6	3.91600E+6
3.67870E+6	3.45590E+6	3.24650E+6	3.04980E+6	2.86500E+6	2.69140E+6
2.52840E+6	2.37520E+6	2.23130E+6	2.09610E+6	1.96910E+6	1.84980E+6
1.73770E+6	1.53350E+6	1.35330E+6	1.19430E+6	1.05400E+6	9.30130E+5
8.20840E+5	7.24380E+5	6.39270E+5	5.64150E+5	4.97860E+5	4.39360E+5
3.87740E+5	3.42170E+5	3.01970E+5	2.66490E+5	2.35170E+5	2.07540E+5
1.83150E+5	1.61630E+5	1.42640E+5	1.25880E+5	1.11090E+5	9.80350E+4
8.65150E+4	7.63490E+4	6.73780E+4	5.94610E+4	5.24740E+4	4.63080E+4
4.08670E+4	3.60650E+4	3.18270E+4	2.80870E+4	2.47870E+4	2.18740E+4
1.93040E+4	1.50340E+4	1.17090E+4	9.11860E+3	7.10160E+3	5.53070E+3
4.30730E+3	3.35460E+3	2.61250E+3	2.03460E+3	1.58460E+3	1.23410E+3
9.61100E+2	5.82930E+2	3.53570E+2	2.14450E+2	1.30070E+2	7.88910E+1
4.78500E+1	2.90230E+1	1.76030E+1	1.06770E+1	6.47580E+0	3.92780E+0
2.38230E+0	1.44490E+0	8.76400E-1	5.31560E-1	3.22410E-1	1.00100E-5

Source Neutron Spectrum for Position #1 [n/Group/cm^2/Sec]
Normalization Factor 2.950e+12

.00000E+0	.00000E+0	.00000E+0	.00000E+0	3.55067E-4	7.51123E-4
1.19097E-3	8.65317E-4	1.22440E-4	1.17373E-5	7.44865E-6	9.06544E-6
7.18241E-6	5.48053E-6	4.64298E-6	5.18322E-6	4.91059E-6	4.33858E-6
3.84473E-6	3.35023E-6	3.18513E-6	3.06315E-6	3.41144E-6	3.08130E-6
3.20469E-6	3.23647E-6	3.27524E-6	3.28621E-6	3.12937E-6	3.04094E-6
2.61385E-6	3.28959E-6	1.22793E-5	1.05593E-5	1.00756E-5	9.35989E-6
9.60690E-6	1.03696E-5	9.24493E-6	8.83474E-6	8.99878E-6	8.39239E-6
8.71039E-6	8.53663E-6	9.28917E-6	8.65822E-6	8.58666E-6	8.36319E-6
8.32671E-6	8.71807E-6	8.22520E-6	8.09848E-6	8.04888E-6	8.27315E-6
8.08339E-6	7.75032E-6	7.93363E-6	7.82164E-6	7.84394E-6	8.26184E-6
1.57683E-5	1.56579E-5	1.45252E-5	1.34394E-5	1.37034E-5	1.19114E-5
1.16509E-5	1.08664E-5	9.96516E-6	8.77859E-6	8.54180E-6	7.35557E-6
7.02705E-6	6.17081E-6	4.94908E-6	4.82989E-6	3.90891E-6	3.35432E-6
3.09186E-6	2.51418E-6	2.84489E-6	2.14417E-6	2.03269E-6	1.48598E-6
1.60620E-6	1.51385E-6	1.32960E-6	1.10658E-6	1.08408E-6	1.07276E-6
8.69324E-7	8.29087E-7	9.77228E-7	7.02872E-7	7.54387E-7	5.89589E-7
1.30019E-6	1.03184E-6	8.99791E-7	8.50897E-7	8.52545E-7	6.76271E-7
7.71254E-7	5.72621E-7	6.90810E-7	6.06863E-7	5.36032E-7	3.49940E-7
7.45814E-7	4.86482E-7	5.32288E-7	4.31774E-7	2.77812E-7	2.61865E-7
2.02913E-7	2.43810E-7	2.15233E-7	1.12215E-7	7.15883E-8	7.35884E-8
6.30017E-8	1.14149E-7	4.71213E-8	2.39519E-8	3.18629E-7	

Source Neutron Spectrum for Position #2 [n/Group/cm^2/Sec]
Normalization Factor 5.634e+11

.00000E+0	.00000E+0	.00000E+0	.00000E+0	9.74737E-4	3.37950E-3
6.01890E-3	5.80615E-3	1.19424E-3	6.18188E-5	3.75713E-5	3.53414E-5
2.53093E-5	2.16951E-5	1.95574E-5	1.91174E-5	1.89979E-5	1.65869E-5
1.43984E-5	1.26737E-5	1.12327E-5	1.13687E-5	1.05252E-5	1.05184E-5
1.07456E-5	1.02566E-5	1.04205E-5	1.08905E-5	9.45644E-6	7.07446E-6
7.58317E-6	7.12786E-6	3.04811E-5	3.32071E-5	3.42508E-5	3.48089E-5
3.59499E-5	3.78058E-5	3.53280E-5	3.39480E-5	3.57466E-5	3.64582E-5
3.54441E-5	3.78112E-5	3.89723E-5	3.83901E-5	3.99996E-5	3.96730E-5
3.93764E-5	4.01221E-5	3.85782E-5	3.96573E-5	3.99840E-5	3.93376E-5
3.83720E-5	3.85395E-5	3.85866E-5	3.86546E-5	3.65899E-5	3.78153E-5
7.25269E-5	7.23097E-5	7.02661E-5	6.56051E-5	6.16569E-5	5.68757E-5
5.31442E-5	4.96293E-5	4.43549E-5	3.99064E-5	3.64530E-5	3.28957E-5
3.02212E-5	2.73941E-5	2.42713E-5	2.15909E-5	1.81971E-5	1.71505E-5
1.46618E-5	1.19825E-5	1.29585E-5	1.08519E-5	9.64730E-6	7.90902E-6
8.93364E-6	7.95152E-6	6.51978E-6	6.35771E-6	5.65050E-6	5.15421E-6
4.68296E-6	4.54980E-6	5.32531E-6	3.97499E-6	4.18717E-6	3.88869E-6
6.63486E-6	6.32866E-6	4.92552E-6	4.83856E-6	4.72670E-6	4.02094E-6
3.86112E-6	3.49468E-6	2.77506E-6	2.60939E-6	2.54641E-6	2.23727E-6
3.76146E-6	3.16599E-6	2.82212E-6	2.36092E-6	1.82614E-6	1.62513E-6
1.30479E-6	1.15175E-6	7.95374E-7	7.70706E-7	6.65969E-7	5.48066E-7
4.47285E-7	3.84068E-7	2.71660E-7	1.76231E-7	1.40760E-6	

Table 3.12.3 Source conditions for the 125-energy group structure. (2/2)

```
Source Neutron Spectrum for Position #3   [n/Group/cm^2/Sec]
     Normalization Factor 3.042e+11

  .00000E+0  .00000E+0  .00000E+0  .00000E+0 9.54386E-4 4.87004E-3
 1.01443E-2 1.21528E-2 3.59062E-3 2.27889E-4 1.10159E-4 8.62564E-5
 6.60345E-5 5.77917E-5 5.17779E-5 4.83975E-5 4.69562E-5 4.04804E-5
 3.63472E-5 3.36165E-5 3.26453E-5 3.16210E-5 3.13753E-5 3.10707E-5
 3.02209E-5 2.94763E-5 3.00628E-5 2.91378E-5 2.73977E-5 2.62917E-5
 2.61244E-5 2.69447E-5 9.92189E-5 8.88292E-5 8.36092E-5 8.31893E-5
 8.49174E-5 8.70378E-5 7.97524E-5 7.50341E-5 7.62472E-5 7.30041E-5
 7.23010E-5 7.61977E-5 7.74349E-5 7.43997E-5 7.27104E-5 7.35271E-5
 7.17592E-5 7.07517E-5 7.04015E-5 6.97226E-5 7.09032E-5 7.07198E-5
 6.97812E-5 6.97792E-5 6.82371E-5 6.78471E-5 6.72963E-5 6.63159E-5
 1.29928E-4 1.25499E-4 1.20122E-4 1.14671E-4 1.07246E-4 9.93149E-5
 9.26634E-5 8.43249E-5 7.61403E-5 6.88213E-5 6.22664E-5 5.64582E-5
 5.18839E-5 4.58148E-5 4.12300E-5 3.69472E-5 3.13340E-5 3.00424E-5
 2.50319E-5 2.07578E-5 2.26977E-5 1.81989E-5 1.65405E-5 1.34375E-5
 1.46504E-5 1.35627E-5 1.08715E-5 1.06884E-5 9.20559E-6 8.89165E-6
 7.62386E-6 7.92960E-6 8.46961E-6 7.16959E-6 6.80510E-6 6.18979E-6
 1.17340E-5 1.00038E-5 9.39582E-6 8.45762E-6 7.20850E-6 6.91376E-6
 6.91668E-6 5.70242E-6 5.62115E-6 4.88210E-6 4.18627E-6 3.78042E-6
 6.51442E-6 5.82049E-6 4.84056E-6 4.34306E-6 3.26849E-6 3.02368E-6
 2.03707E-6 2.10734E-6 1.77882E-6 1.40867E-6 1.46800E-6 9.28034E-7
 8.18552E-7 6.28299E-7 5.20102E-7 4.89986E-7 3.15219E-6


Source Neutron Spectrum for Position #7   [n/Group/cm^2/Sec]
     Normalization Factor 9.653e+10

  .00000E+0  .00000E+0  .00000E+0  .00000E+0 7.83809E-4 4.52515E-3
 1.31649E-2 2.84732E-2 4.08963E-2 1.47777E-2 1.93582E-4 1.08653E-4
 8.69338E-5 7.89020E-5 5.91716E-5 5.33166E-5 5.05674E-5 3.82635E-5
 2.86383E-5 2.38839E-5 2.28360E-5 2.33864E-5 2.28337E-5 2.47094E-5
 2.47897E-5 2.42138E-5 2.17281E-5 1.99284E-5 1.98644E-5 1.88568E-5
 1.74378E-5 1.71840E-5 6.83628E-5 6.57928E-5 6.53778E-5 7.59644E-5
 7.53652E-5 7.76181E-5 7.34516E-5 7.57420E-5 7.48714E-5 7.69912E-5
 8.22981E-5 8.51429E-5 8.48575E-5 8.88223E-5 9.43695E-5 9.51671E-5
 9.62320E-5 9.56572E-5 9.89122E-5 1.01994E-4 1.10078E-4 1.12230E-4
 1.12837E-4 1.15520E-4 1.19539E-4 1.17250E-4 1.20893E-4 1.18309E-4
 2.42962E-4 2.30564E-4 2.26116E-4 2.18985E-4 1.97311E-4 1.90581E-4
 1.73139E-4 1.57056E-4 1.38185E-4 1.20092E-4 1.08200E-4 9.61832E-5
 8.99204E-5 7.99998E-5 6.64881E-5 5.64847E-5 4.58488E-5 3.92095E-5
 3.45698E-5 2.61661E-5 2.25691E-5 1.79193E-5 1.56192E-5 1.30280E-5
 1.14603E-5 9.42380E-6 7.36983E-6 6.95957E-6 6.14403E-6 4.86097E-6
 3.64272E-6 3.45299E-6 2.73798E-6 2.76894E-6 2.26024E-6 1.96679E-6
 3.48689E-6 2.98664E-6 1.82910E-6 1.68952E-6 1.26558E-6 9.44125E-7
 8.31611E-7 5.45129E-7 3.99520E-7 4.32855E-7 4.39060E-7 3.19253E-7
 4.02198E-7 4.15541E-7 2.92244E-7 1.67942E-7 6.76593E-8 1.37908E-7
 6.49584E-8 1.85583E-8 3.94321E-8 1.41124E-8 2.30032E-8 6.01118E-8
 1.89938E-8 5.17524E-8  .00000E+0  .00000E+0  .00000E+0
```

Table 3.12.4 Source conditions for the GAM-II 100-energy group structure. (1/2)

Energy Group Boundaries in eV

1.9640E+7	1.3499E+7	1.2214E+7	1.1052E+7	1.0000E+7	9.0484E+6
8.1873E+6	7.4082E+6	6.7032E+6	6.0653E+6	5.4881E+6	4.9659E+6
4.4933E+6	4.0657E+6	3.6788E+6	3.3287E+6	3.0119E+6	2.7253E+6
2.4660E+6	2.2313E+6	2.0190E+6	1.8268E+6	1.6530E+6	1.4957E+6
1.3534E+6	1.2246E+6	1.1080E+6	1.0026E+6	9.0718E+5	8.2085E+5
7.4274E+5	6.7206E+5	6.0810E+5	5.5023E+5	4.9787E+5	4.5049E+5
4.0762E+5	3.6883E+5	3.3373E+5	3.0197E+5	2.7324E+5	2.4724E+5
2.2371E+5	2.0242E+5	1.8316E+5	1.6573E+5	1.4996E+5	1.3569E+5
1.2277E+5	1.1109E+5	8.6517E+4	6.7379E+4	5.2475E+4	4.0868E+4
3.1828E+4	2.4788E+4	1.9305E+4	1.5034E+4	1.1709E+4	9.1188E+3
7.1017E+3	5.5308E+3	4.3074E+3	3.3546E+3	2.6126E+3	2.0347E+3
1.5846E+3	1.2341E+3	9.6112E+2	7.4852E+2	5.8295E+2	4.5400E+2
3.5358E+2	2.7536E+2	2.1445E+2	1.6702E+2	1.3007E+2	1.0130E+2
7.8893E+1	6.1442E+1	4.7851E+1	3.7267E+1	2.9023E+1	2.2603E+1
1.7603E+1	1.3710E+1	1.0677E+1	8.3153E+0	6.4760E+0	5.0435E+0
3.9279E+0	3.0590E+0	2.3824E+0	1.8554E+0	1.4450E+0	1.1254E+0
8.7642E-1	6.8256E-1	5.3158E-1	4.1399E-1	1.0000E-5	

Source Neutron Spectrum for Position #1 [n/Group/cm^2/Sec]
Normalization Factor 2.950e+12

3.3189E-3	3.0444E-5	2.0645E-5	1.9761E-5	1.8095E-5	1.6008E-5
1.5458E-5	1.5765E-5	1.3919E-5	1.3796E-5	1.3431E-5	1.3926E-5
1.4258E-5	1.3737E-5	1.3549E-5	1.2907E-5	1.3295E-5	1.3155E-5
1.2730E-5	1.2546E-5	1.2828E-5	1.2665E-5	1.2654E-5	1.2344E-5
1.1720E-5	1.1220E-5	1.0613E-5	1.0557E-5	9.4635E-6	9.3908E-6
8.9255E-6	8.0059E-6	7.2561E-6	6.9881E-6	6.6906E-6	5.9355E-6
5.6302E-6	5.1968E-6	4.8083E-6	4.0977E-6	3.9163E-6	3.4037E-6
2.9633E-6	2.8550E-6	2.6056E-6	2.3129E-6	2.2906E-6	2.1986E-6
1.8109E-6	3.6595E-6	3.3485E-6	2.5289E-6	2.1359E-6	1.7095E-6
1.7181E-6	1.4086E-6	1.1909E-6	1.0403E-6	1.0411E-6	8.4767E-7
8.2493E-7	7.9980E-7	8.4493E-7	5.6653E-7	5.6360E-7	5.0523E-7
4.8164E-7	3.7221E-7	3.6215E-7	3.6544E-7	2.5270E-7	2.1971E-7
2.6566E-7	2.4302E-7	2.2290E-7	1.7616E-7	1.5135E-7	1.7101E-7
1.5677E-7	1.4416E-7	1.2588E-7	8.4504E-8	1.0757E-7	9.4429E-8
1.0916E-7	9.4663E-8	6.5741E-8	5.0527E-8	5.5720E-8	4.1558E-8
3.1967E-8	2.7266E-8	2.6483E-8	2.3777E-8	6.1192E-8	2.6435E-8
1.4512E-8	2.5938E-8	2.5062E-8	2.7922E-7		

Source Neutron Spectrum for Position #2 [n/Group/cm^2/Sec]
Normalization Factor 5.634e+11

1.7528E-2	1.1638E-4	7.0738E-5	5.5472E-5	4.9477E-5	5.4304E-5
5.6611E-5	6.1307E-5	5.5078E-5	5.7551E-5	5.6886E-5	6.0528E-5
6.1956E-5	6.3339E-5	6.3339E-5	6.2750E-5	6.3111E-5	6.2719E-5
6.2205E-5	6.1560E-5	6.0818E-5	5.9956E-5	5.8863E-5	5.7496E-5
5.5614E-5	5.3451E-5	5.2011E-5	4.8256E-5	4.5431E-5	4.3128E-5
4.0867E-5	3.6934E-5	3.4573E-5	3.1568E-5	2.9291E-5	2.6576E-5
2.5371E-5	2.3816E-5	2.1043E-5	1.9420E-5	1.8471E-5	1.5641E-5
1.4131E-5	1.3506E-5	1.2138E-5	9.9069E-6	1.0033E-5	1.0732E-5
8.5546E-6	1.7587E-5	1.6414E-5	1.2989E-5	1.0901E-5	8.9724E-6
9.1192E-6	7.6694E-6	6.4580E-6	6.1422E-6	5.1755E-6	4.7385E-6
4.3261E-6	3.9290E-6	3.7663E-6	3.3028E-6	2.9885E-6	2.7150E-6
2.4038E-6	2.1902E-6	1.9875E-6	1.7806E-6	1.7092E-6	1.5302E-6
1.5337E-6	1.2250E-6	1.1408E-6	9.9978E-7	9.7080E-7	8.5074E-7
8.8009E-7	7.4103E-7	6.3597E-7	6.2282E-7	5.5588E-7	5.1773E-7
4.8002E-7	3.9808E-7	3.9288E-7	3.6289E-7	3.8818E-7	3.0821E-7
2.9329E-7	2.3438E-7	2.2322E-7	1.8799E-7	2.2198E-7	1.7964E-7
1.4592E-7	1.6927E-7	1.4140E-7	1.6653E-6		

Table 3.12.4 Source conditions for the GAM-II 100-energy group structure. (2/2)

Source Neutron Spectrum for Position #3 [n/Group/cm^2/Sec]
Normalization Factor 3.042e+11

3.2194E-2	3.0052E-4	2.0159E-4	1.7658E-4	1.5196E-4	1.3706E-4
1.3412E-4	1.3682E-4	1.2093E-4	1.1961E-4	1.1678E-4	1.2163E-4
1.2010E-4	1.1722E-4	1.1520E-4	1.1279E-4	1.1249E-4	1.1311E-4
1.1107E-4	1.0918E-4	1.0720E-4	1.0504E-4	1.0311E-4	1.0109E-4
9.7046E-5	9.3555E-5	8.9872E-5	8.4537E-5	7.8949E-5	7.4540E-5
6.9099E-5	6.3624E-5	5.9000E-5	5.4819E-5	5.0205E-5	4.5579E-5
4.3963E-5	4.0323E-5	3.6127E-5	3.2983E-5	3.0644E-5	2.6793E-5
2.4024E-5	2.3816E-5	2.0501E-5	1.7277E-5	1.8059E-5	1.8067E-5
1.4187E-5	3.0003E-5	2.8357E-5	2.1693E-5	1.8600E-5	1.5564E-5
1.5737E-5	1.2800E-5	1.1415E-5	1.0239E-5	9.3117E-6	8.2842E-6
7.3253E-6	7.0568E-6	6.5774E-6	5.5598E-6	5.3084E-6	4.7577E-6
4.3870E-6	3.7599E-6	3.5991E-6	3.2022E-6	3.0990E-6	2.8019E-6
2.6021E-6	2.3674E-6	2.2450E-6	1.9417E-6	1.7954E-6	1.5210E-6
1.5011E-6	1.3000E-6	1.1999E-6	1.0897E-6	1.0587E-6	1.0711E-6
9.3633E-7	8.6767E-7	7.6828E-7	6.5594E-7	6.8949E-7	6.4919E-7
4.7526E-7	5.1042E-7	4.3620E-7	3.5958E-7	3.2356E-7	3.4545E-7
3.8371E-7	2.8620E-7	2.8004E-7	3.1081E-6		

Source Neutron Spectrum for Position #7 [n/Group/cm^2/Sec]
Normalization Factor 9.653e+10

5.8553E-2	1.8916E-4	8.5705E-5	7.1008E-5	6.0277E-5	6.1118E-5
6.8887E-5	6.9189E-5	6.7117E-5	6.9197E-5	7.3949E-5	7.6819E-5
8.1892E-5	8.4678E-5	8.6762E-5	9.0008E-5	9.6579E-5	1.0297E-4
1.0520E-4	1.0675E-4	1.0813E-4	1.0928E-4	1.0877E-4	1.0733E-4
1.0404E-4	1.0196E-4	9.4257E-5	9.1065E-5	8.6547E-5	7.9165E-5
7.3832E-5	6.7173E-5	6.0023E-5	5.4869E-5	5.0693E-5	4.4825E-5
4.3159E-5	3.9742E-5	3.5516E-5	3.1064E-5	2.6928E-5	2.3489E-5
2.0135E-5	1.7486E-5	1.5341E-5	1.3068E-5	1.1273E-5	1.0038E-5
8.3553E-6	1.6671E-5	1.1745E-5	8.2302E-6	6.0304E-6	4.4225E-6
3.1842E-6	2.6201E-6	1.9772E-6	1.6461E-6	1.1429E-6	9.6532E-7
8.1380E-7	6.3268E-7	5.6088E-7	3.7355E-7	3.4847E-7	2.8023E-7
2.1617E-7	1.9590E-7	1.5748E-7	9.7407E-8	1.1042E-7	9.8820E-8
8.8370E-8	8.2647E-8	4.0862E-8	4.6031E-8	3.1485E-8	1.8562E-8
2.8776E-8	1.1883E-8	1.4284E-8	1.0228E-8	4.4034E-9	8.3000E-9
1.3076E-8	1.0643E-9	3.5543E-9	2.6992E-9	5.7858E-9	1.3110E-9
1.2962E-8	0.0000E+0	9.8753e-10	2.1520E-9	0.0000E+0	6.0904E-9
0.0000E+0	0.0000E+0	0.0000E+0	8.0173E-9		

Table 3.12.5 Source conditions for the 42-energy group structure.

```
Energy Group Boundaries in eV

  1.5000E+7  1.3720E+7  1.2549E+7  1.1478E+7  1.0500E+7  9.3140E+6
  8.2610E+6  7.3280E+6  6.5000E+6  5.7570E+6  5.0990E+6  4.5160E+6
  4.0000E+6  3.1620E+6  2.5000E+6  1.8710E+6  1.4000E+6  1.0580E+6
  8.0000E+5  5.6600E+5  4.0000E+5  2.8300E+5  2.0000E+5  1.4100E+5
  1.0000E+5  4.6500E+4  2.1500E+4  1.0000E+4  4.6500E+3  2.1500E+3
  1.0000E+3  4.6500E+2  2.1500E+2  1.0000E+2  4.6500E+1  2.1500E+1
  1.0000E+1  4.6500E+0  2.1500E+0  1.0000E+0  4.6500E-1  2.1500E-1
  1.0000E-3


Source Neutron Spectrum for Position #1  [n/Group/cm^2/Sec]
     Normalization Factor 2.950e+12

 3.31057E-3 3.25940E-5 1.96755E-5 1.80737E-5 2.28089E-5 1.96607E-5
 1.82059E-5 1.90017E-5 1.68476E-5 1.63969E-5 1.68226E-5 1.69609E-5
 3.18447E-5 3.10059E-5 3.63662E-5 3.68384E-5 3.21411E-5 2.78145E-5
 2.93090E-5 2.28018E-5 1.71143E-5 1.21454E-5 8.40166E-6 6.65878E-6
 8.64024E-6 5.32845E-6 3.40480E-6 2.69348E-6 2.05608E-6 1.49718E-6
 9.18416E-7 8.26664E-7 5.28776E-7 4.71889E-7 3.29515E-7 3.04631E-7
 1.59680E-7 1.01377E-7 1.30600E-7 7.82683E-8 7.12012E-8 2.31836E-7


Source Neutron Spectrum for Position #2  [n/Group/cm^2/Sec]
     Normalization Factor 5.634e+11

 1.74975E-2 1.21427E-4 7.11220E-5 5.90394E-5 5.71081E-5 6.47127E-5
 6.79389E-5 7.08315E-5 6.82298E-5 6.95119E-5 7.25638E-5 7.57976E-5
 1.48850E-4 1.49046E-4 1.77104E-4 1.70686E-4 1.53217E-4 1.32467E-4
 1.34778E-4 1.01519E-4 7.83531E-5 5.62555E-5 4.00766E-5 3.12619E-5
 4.44570E-5 2.85722E-5 1.92199E-5 1.38615E-5 1.04883E-5 7.72867E-6
 5.46896E-6 4.45202E-6 3.30429E-6 2.47715E-6 1.88919E-6 1.37473E-6
 1.22980E-6 7.51948E-7 5.99910E-7 4.62933E-7 3.25494E-7 1.42963E-6


Source Neutron Spectrum for Position #3  [n/Group/cm^2/Sec]
     Normalization Factor 3.042e+11

 3.21151E-2 3.10371E-4 1.91463E-4 1.68217E-4 1.93839E-4 1.64512E-4
 1.61036E-4 1.61393E-4 1.46255E-4 1.41777E-4 1.46807E-4 1.45386E-4
 2.69871E-4 2.65753E-4 3.17095E-4 3.00862E-4 2.67120E-4 2.29866E-4
 2.31758E-4 1.75395E-4 1.32821E-4 9.67998E-5 6.93145E-5 5.32431E-5
 7.46973E-5 4.81368E-5 3.31985E-5 2.37681E-5 1.84008E-5 1.32865E-5
 1.00722E-5 8.12730E-6 6.12317E-6 4.47152E-6 3.24023E-6 2.79961E-6
 2.34590E-6 1.55999E-6 1.07001E-6 9.19044E-7 6.67616E-7 2.54307E-6


Source Neutron Spectrum for Position #7  [n/Group/cm^2/Sec]
     Normalization Factor 9.653e+10

 5.84844E-2 2.13833E-4 8.24868E-5 7.18279E-5 7.63678E-5 7.16921E-5
 8.22620E-5 8.26232E-5 8.23187E-5 8.62534E-5 9.30136E-5 9.97520E-5
 2.02595E-4 2.28601E-4 3.07167E-4 3.13009E-4 2.84686E-4 2.46104E-4
 2.44147E-4 1.72685E-4 1.29535E-4 8.27473E-5 5.18250E-5 2.96340E-5
 3.22188E-5 1.17440E-5 5.32651E-6 2.48288E-6 1.23927E-6 7.20569E-7
 3.57484E-7 3.10886E-7 1.15743E-7 9.86148E-8 2.88595E-8 2.07846E-8
 1.42998E-8 2.92255E-8 1.22303E-8 1.58835E-8  .00000E+0 8.66092E-9
```

Table 4.1.1 Calculation codes and nuclear data bases.

No.	Code	Cross Section Library	Decay Data Library
1	ACT4	FENDL/A-2.0	ENSDF & Table of Radioactive Isotopes
2	ACT4	JENDL Activation File	
3	CINAC-V4	FENDL/A-2.0	
4	CINAC-V4	1990's Library (Lib90)	

Table 4.5.1 List of institutes participated to the workshop with calculation codes and nuclear data bases used by the participants.

Institute (Country)	Code	Activation Cross Section	Decay Data
ENEA with Bologna University (Italy)	ANITA-4	FENDL/A-2.0	JEF-2
TSI Research (US)	REAC-3	FENDL/A-2.0	FENDL/D-2.0
University of Wisconsin-Madison (US)	DKR	FENDL/A-2.0	FENDL/D-2.0
UCLA (US)	DKRICF	FENDL/A-1.0	ENDF/B-V
UKAEA Fusion (UK)	FISPACT97	FENDL/A-2.0	FENDL/D-2.0
JAERI (Japan)	ACT4	FENDL/A-2.0	ENSDF

The workshop on "Decay Heat Validation for Fusion Reactors" held at ITER Joint Work Site at San Diego, U.S.A, on October 2-3, 1997.

Table 5.2.1 List of standard reactions and decay properties of the products used for the justification of the measurement and calculation.

Sample	Reaction	Half-Life	E_γ (I_γ) *	E_β-max (I_β) **	Correction Factor for the Product
Al	$^{27}Al(n,\alpha)^{24}Na$	14.96 hr	1369 (100.0) 2754 (99.9)	1393 (99.9)	0.8190
Al	$^{27}Al(n,p)^{27}Mg$	9.458 m	844 (71.8) 1014 (28.0)	1596 (29.0) 1767 (71.0)	0.9446
S	$^{32}S(n,p)^{32}P$	14.26 d	no-γ	1711 (100.0)	0.8252
Fe	$^{56}Fe(n,p)^{56}Mn$	2.579 hr	847 (98.9) 1811 (27.2) 2113 (14.3)	735 (14.6) 1038 (27.9) 2849 (56.3)	0.9151
Zr	$^{90}Zr(n,2n)^{89m+g}Zr$	78.41 hr	511 (46.0) 909 (99.9)	1923 (98.9)	0.9736
Nb	$^{93}Nb(n,2n)^{92m}Nb$	10.15 d	934 (99.1)	no-β	0.9214

* The E_γ and I_γ stand for gamma-ray energy in keV and its intensity in percentages.
** The E_β-max and I_β stand for maximum beta-ray energy in keV and its intensity in percentages.

Table 5.2.2 Ratios of activation cross sections in JENDL Activation File to the measured values, and C/E ratios of decay heat for the ACT4 calculations.

Sample	Reaction	Sample Position	D-T Peak Energy [MeV]	JENDL/Expt. of Cross Section	C/E of Decay Heat
Al	$^{27}Al(n,\alpha)^{24}Na$	7	14.3	1.02	1.01
Al	$^{27}Al(n,p)^{27}Mg$	1	14.9	1.08	1.04
S	$^{32}S(n,p)^{32}P$	7	14.3	0.96	1.04
Fe	$^{56}Fe(n,p)^{56}Mn$	2	14.8	0.98	0.99
Zr	$^{90}Zr(n,2n)^{89m+g}Zr$	7	14.3	1.00	1.03
Nb	$^{93}Nb(n,2n)^{92m}Nb$	7	14.3	1.03	0.94

Table 5.3.1 List of dominant nuclides with their half-lives, production cross sections and decay data for the measured decay heat. (1/5) The activation cross sections based on FENDL/A-2.0 and JENDL Activation File for the ninth group (14.324 ~ 14.550 MeV) of the 125 energy bins are compared with the cross sections measured [10, 22 ~ 26] at FNS and the OKTAVIAN facility at Osaka University. Beta- and gamma-ray energy per decay used in the calculations and taken from Ref. 13) are compared. Ratios of total decay energy due to both beta- and gamma-rays used in the calculations to those taken from Ref. 13) are also shown.

Reaction# & Produced Nuclide	Half-Life	Activation Cross Section [mb]					Decay Energy [keV] *				
		FENDL	JENDL@	Experimental	E_n [MeV]	Ref.	Used in Calc. (A) β	(B) γ	Ref. 13) (C) β	(D) γ	Ratio (A+B) / (C+D)
$^{11}B(n,p)^{11}Be$	13.81 s	5.8	4.4				4659	1446	4652	1455	1.000
$^{19}F(n,p)^{19}O$	26.91 s	17.9	14.1	18.97	(14.44)	25)	1819	957	1742	939	1.035
$^{19}F(n,2n)^{18}F$	109.77 m	45.1	49.3	45.3	(14.45)	10)	240	1022	242	990	1.024
$^{23}Na(n,p)^{23}Ne$	37.24 s	39.0	44.4				1915	164	1902	165	1.006
$^{23}Na(n,2n)^{22}Na$	2.602 y	30.0	26.7	31.3	(14.43)	10)	184	2193	195	2187	0.998
$^{27}Al(n,p)^{27}Mg$	9.458 m	69.6	73.7	67.5	(14.42)	22)	719	891	702	913	0.997
$^{27}Al(n,\alpha)^{24m+g}Na$	14.959 h	116.6	117.1	114.5	(14.42)	22)	570	4123	554	4123	1.003
$^{28}Si(n,p)^{28}Al$	2.2414 m	247.3	247.3	248.	(14.41)	10)	1261	1779	1242	1779	1.006
$^{29}Si(n,p)^{29}Al$	6.56 m	138.1	138.1	139.	(14.44)	10)	994	1379	977	1376	1.008
$^{30}Si(n,\alpha)^{27}Mg$	9.458 m	66.5	66.5	65.6	(14.44)	26)	719	891	702	913	0.997
$^{32}S(n,p)^{32}P$	14.262 d	229.0	232.7	241.3	(14.41)	23)	716	0	695	0	1.030
$^{32}S(n,t)^{30}P$	2.498 m	0.016	0.006				1422	1022	1435	1022	0.995
$^{34}S(n,p)^{34}P$	12.43 s	82.1	75.6				2329	334	2306	334	1.009
$^{34}S(n,\alpha)^{31}Si$	157.3 m	135.4	48.3				615	1	595	1	1.034
$^{39}K(n,2n)^{38m+g}K$	7.636 m	3.2	3.4	3.21	(14.46)	10)	1186	3187	1204	3187	0.996
$^{41}K(n,p)^{41}Ar$	109.34 m	49.5	49.5	51.5	(14.42)	10)	488	1284	464	1284	1.014
$^{41}K(n,\alpha)^{38m+g}Cl$	37.24 m	33.4	31.8	36.7	(14.42)	10)	1571	1421	1553	1421	1.006
$^{40}Ca(n,t)^{38m+g}K$	7.636 m	8.0	.00015				1186	3187	1204	3187	0.996
$^{42}Ca(n,p)^{42}K$	12.360 h	183.4	183.4	175.	(14.42)	10)	1441	290	1425	290	1.009
$^{44}Ca(n,p)^{44}K$	22.13 m	39.2	39.7	38.1	(14.43)	10)	1485	2377	1414	2377	1.019
$^{48}Ca(n,2n)^{47}Ca$	4.536 d	776.7	776.7	764.	(14.43)	10)	375	1047	345	1063	1.010

Table 5.3.1 Continued. (2/5)

Reaction# & Produced Nuclide	Half-Life	Activation Cross Section [mb]					Decay Energy [keV] *				
		FENDL	JENDL@	Experimental	E_n [MeV]	Ref.	Used in Calc. (A) β	(B) γ	Ref. 13) (C) β	(D) γ	Ratio (A+B) / (C+D)
$^{46}Ti(n,p)^{46m+g}Sc$	83.79 d	232.8	246.1	240.	(14.42)	10)	129	2009	112	2010	1.008
$^{47}Ti(n,d)^{46m+g}Sc$	83.79 d	76.6	61.3	130.5	(14.42)	10)	129	2009	112	2010	1.008
$Ti(n,x)^{46m+g}Sc$	83.79 d	24.2	24.2	28.7	(14.42)	10)	129	2009	112	2010	1.008
$^{48}Ti(n,p)^{48}Sc$	43.67 h	61.5	61.7	59.5	(14.44)	10)	256	3349	221	3349	1.010
$^{49}Ti(n,d)^{48}Sc$	43.67 h	2.6	11.7	5.5	(14.44)	10)	256	3349	221	3349	1.010
$Ti(n,x)^{48}Sc$	43.67 h	45.7	46.3	44.3	(14.44)	10)	256	3349	221	3349	1.010
$^{50}Ti(n,p)^{50m+g}Sc$	102.5 s	17.3	11.9	11.6	(14.43)	10)	1695	3193	1626	3192	1.015
$^{51}V(n,p)^{51}Ti$	5.76 m	30.4	30.4	26.8	(14.43)	10)	900	369	868	369	1.026
$^{51}V(n,\alpha)^{48}Sc$	43.67 h	16.0	16.4	16.47	(14.44)	10)	256	3349	221	3349	1.010
$^{50}Cr(n,2n)^{49}Cr$	42.3 m	15.6	15.6	22.8	(14.47)	10)	595	1053	595	1059	0.996
$^{52}Cr(n,2n)^{51}Cr$	27.702 d	340.6	312.1	310.	(14.45)	10)	0	32	0	33	0.970
$^{52}Cr(n,p)^{52}V$	3.75 m	75.4	78.8	78.5	(14.43)	10)	1102	1445	1068	1445	1.014
$^{55}Mn(n,2n)^{54}Mn$	312.12 d	785.8	759.9	781.	(14.44)	10)	0	835	3	836	0.995
$^{55}Mn(n,p)^{55}Cr$	3.497 m	36.1	31.4				1084	1	1101	0	0.985
$^{55}Mn(n,\alpha)^{52}V$	3.75 m	28.8	28.8				1102	1445	1068	1445	1.014
$^{54}Fe(n,p)^{54}Mn$	312.12 d	325.7	325.7	300.	(14.41)	10)	0	835	3	836	0.995
$^{56}Fe(n,p)^{56}Mn$	2.5785 h	111.1	109.7	111.1	(14.42)	22)	864	1692	830	1692	1.013
$^{57}Fe(n,d)^{56}Mn$	2.5785 h	19.6	16.9	15.0	(14.46)	10)	864	1692	830	1692	1.013
$Fe(n,x)^{56}Mn$	2.5785 h	102.3	100.9	102.2	(14.42)	10+22)	864	1692	830	1692	1.013
$^{59}Co(n,2n)^{58m}Co$	9.15 h	384.2	483.4				21	0	21	2	0.913
$^{59}Co(n,2n)^{58g}Co$	70.82 d	323.6	239.3				26	974	34	976	0.990
$^{59}Co(n,2n)^{58m+g}Co$	70.82 d	707.8	722.7	729.	(14.44)	10)	26	974	34	976	0.990
$^{59}Co(n,\alpha)^{56}Mn$	2.5785 h	30.1	32.4	32.7	(14.43)	10)	864	1692	830	1692	1.013
$^{58}Ni(n,2n)^{57}Ni$	35.60 h	32.4	31.7	32.3	(14.44)	10)	136	1941	147	1918	1.006
$^{58}Ni(n,p)^{58m+g}Co$	70.82 d	315.9	317.0	320.	(14.41)	10)	26	974	34	976	0.990
$^{58}Ni(n,d)^{57}Co$	271.79 d	578.0	617.8	609.	(14.44)	10)	0	121	18	125	0.846

Table 5.3.1 Continued. (3/5)

Reaction# & Produced Nuclide	Half-Life	Activation Cross Section [mb]					Decay Energy [keV] *				
		FENDL	JENDL@	Experimental	E_n [MeV]	Ref.	Used in Calc. (A) β	(B) γ	Ref. 13) (C) β	(D) γ	Ratio (A+B) / (C+D)
^{60}Ni(n,p)$^{60m+g}$Co	5.2714 y	145.4	145.1	143.2	(14.42)	24)	115	2504	96	2504	1.007
^{61}Ni(n,d)$^{60m+g}$Co	5.2714 y	117.9	23.9				115	2504	96	2504	1.007
Ni(n,x)$^{60m+g}$Co	5.2714 y	39.6	38.3				115	2504	96	2504	1.007
^{62}Ni(n,p)^{62m}Co	13.91 m	12.1	13.0	17.2	(14.44)	25)	1055	2698	1058	2690	1.001
^{62}Ni(n,p)^{62g}Co	1.50 m	21.8	17.3	27.5	(14.44)	25)	1645	1602	1639	1599	1.003
^{63}Cu(n,2n)^{62}Cu	9.74 m	504.7	532.7				1256	1007	1280	998	0.993
^{63}Cu(n,α)$^{60m+g}$Co	5.2714 y	36.6	36.6	41.8	(14.42)	24)	115	2504	96	2504	1.007
^{65}Cu(n,2n)^{64}Cu	12.700 h	927.3	927.3	885.	(14.43)	10)	125	190	123	192	1.000
^{84}Sr(n,2n)$^{83m+g}$Sr	32.41 h	652.5	x	549.	(14.44)	24)	104	788	149	785	0.955
^{86}Sr(n,2n)$^{85m+g}$Sr	64.84 d	988.4	946.3	852.	(14.44)	24)	0	505	8	518	0.960
^{87}Sr(n,n')^{87m}Sr	2.803 h	86.0	x				67	320	67	321	0.997
^{88}Sr(n,2n)^{87m}Sr	2.803 h	226.5	+	249.	(14.44)	24)	67	320	67	321	0.997
^{88}Sr(n,p)^{88}Rb	17.78 m	13.3	14.4	21.4	(14.44)	25)	2147	637	2068	629	1.032
^{89}Y(n,2n)^{88}Y	106.65 d	962.6	962.6	968.	(14.44)	24)	1	2686	6	2686	0.998
^{89}Y(n,n')^{89m}Y	16.06 s	462.0	x				8	901	8	901	1.000
^{89}Y(n,α)^{86m}Rb	1.017 m	0.8	+	1.8	(14.8)	26)	10	546	10	546	1.000
^{90}Zr(n,2n)^{89m}Zr	4.18 m	120.1	x	109.4	(14.45)	10)	27	633	32	649	0.969
^{90}Zr(n,2n)^{89g}Zr	78.41 h	571.0	744.1				81	1159	102	1161	0.982
^{90}Zr(n,2n)$^{89m+g}$Zr	78.41 h	691.1	x	732.7	(14.44)	22)	81	1159	102	1161	0.982
^{94}Zr(n,p)^{94}Y	18.7 m	10.9	7.2	7.5	(14.44)	10)	1889	772	1813	772	1.029
^{96}Zr(n,2n)^{95}Zr	64.02 d	1517.1	1517.1	1550.	(14.43)	10)	141	732	120	733	1.023
^{93}Nb(n,2n)^{92m}Nb	10.15 d	473.3	473.3	457.	(14.42)	22)	0	958	6	968	0.984
^{93}Nb(n,α)^{90m}Y	3.19 h	4.5	4.6	5.09	(14.43)	10)	48	633	48	634	0.999
^{93}Nb(n,nα)^{89m}Y	16.06 s	1.4	x				8	901	8	901	1.000
^{92}Mo(n,2n)^{91m}Mo	65.0 s	18.7	14.7	14.2	(14.47)	10)	404	1389	553	1393	0.921
^{92}Mo(n,2n)^{91g}Mo	15.49 m	241.5	197.2	184.4	(14.44)	27)	1428	977	1453	980	0.988

Table 5.3.1 Continued. (4/5)

Reaction# & Produced Nuclide	Half-Life	Activation Cross Section [mb]					Decay Energy [keV] *				
		FENDL	JENDL@	Experimental	E_n [MeV]	Ref.	Used in Calc. (A) β	(B) γ	Ref. 13) (C) β	(D) γ	Ratio (A+B) / (C+D)
^{92}Mo(n,p)^{92m}Nb	10.15 d	63.8	69.1	67.3	(14.41)	10)	0	958	6	968	0.984
^{92}Mo(n,d)^{91m}Nb	60.86 d	199.3	192.9	166.	(14.43)	24)	90	43	90	51	0.943
(^{95}Mo(n,p)$^{95m+g}$Nb	34.975 d	42.7	42.6	41.6	(14.43)	10)	56	764	44	764	1.015
(^{96}Mo(n,d)$^{95m+g}$Nb	34.975 d	6.2	6.2	5.46	(14.45)	10)	56	764	44	764	1.015
^{100}Mo(n,2n)^{99}Mo	65.94 h	1400.2	1400.2	1540.	(14.43)	10)	437	149	408	145	1.060
^{112}Sn(n,2n)^{111}Sn	35.3 m	1192	1265.	1480	(14.44)	10)	182	489	199	503	0.956
^{112}Sn(n,d)$^{111m+g}$In	2.8049 d	121.5	34.4				0	385	34	405	0.877
^{118}Sn(n,2n)^{117m}Sn	13.60 d	758.4	=	787.	(14.43)	10)	161	140	161	158	0.944
^{119}Sn(n,n')^{119m}Sn	293.1 d	143.8	=				78	4	78	11	0.921
^{120}Sn(n,2n)^{119m}Sn	293.1 d	820.8	=				78	4	78	11	0.921
^{122}Sn(n,2n)^{121g}Sn	27.06 d	676.4	495.3				141	0	115	0	1.226
^{124}Sn(n,2n)^{123m}Sn	40.06 m	552.0	552.0	544.	(14.42)	10)	501	138	479	141	1.031
^{124}Sn(n,2n)^{123g}Sn	129.2 d	1082.2	1082.2				1140	14	523	7	2.177
^{132}Ba(n,2n)$^{131m+g}$Ba	11.50 d	1450.3	1592.8	1703.	(14.44)	24)	0	428	45	458	0.851
^{134}Ba(n,2n)^{133m}Ba	38.9 h	795.5	774.5	834.	(14.43)	10)	219	49	219	67	0.937
(^{135}Ba(n,n')^{135m}Ba	28.7 h	185.2	=				207	42	207	60	0.933
(^{136}Ba(n,2n)^{135m}Ba	28.7 h	1016.2	+	912.	(14.43)	10)	207	42	207	60	0.933
^{136}Ba(n,p)$^{136m+g}$Cs	13.16 d	5.99	5.87	5.81	(14.44)	10)	145	2125	135	2171	0.984
(^{137}Ba(n,d)$^{136m+g}$Cs	13.16 d	1.00	1.25	0.86	(14.48)	10)	145	2125	135	2171	0.984
(^{138}Ba(n,t)$^{136m+g}$Cs	13.16 d	0.01	0.00				145	2125	135	2171	0.984
(Ba(n,x)$^{136m+g}$Cs	13.16 d	0.59	0.60				145	2125	135	2171	0.984
^{138}Ba(n,2n)^{137m}Ba	2.552 m	994.6	=	885.	(14.44)	10)	65	596	65	599	0.995
^{138}Ba(n,p)$^{138m+g}$Cs	33.41 m	1.9	2.7	2.76	(14.44)	10)	1334	2361	1243	2361	1.025
^{181}Ta(n,2n)^{180g}Ta	8.152 h	1783.1	1163.2	1311.	(14.42)	10)	54	0	54	48	0.529
^{181}Ta(n,p)^{181}Hf	42.39 d	4.5	4.1	3.6	(14.44)	25)	158	502	199	518	0.921
^{181}Ta(n,α)^{178m}Lu	23.1 m	0.05	0.75				322	1015	568	1056	0.823
^{181}Ta(n,α)^{178g}Lu	28.4 m	0.90	0.33				787	140	754	151	1.024

Table 5.3.1 Continued. (5/5)

Reaction# & Produced Nuclide	Half-Life	Activation Cross Section [mb]					Decay Energy [keV] *				
		FENDL	JENDL@	Experimental	E_n [MeV]	Ref.	Used in Calc. (A) β	(B) γ	Ref. 13) (C) β	(D) γ	Ratio (A+B) / (C+D)
$^{184}W(n,p)^{184}Ta$	8.7 h	3.5	2.6	2.52	(14.45)	10)	484	1547	536	1610	0.946
$^{186}W(n,2n)^{185m}W$	1.67 m	781.6	781.6				165	18	165	28	0.948
$^{186}W(n,2n)^{185g}W$	75.1 d	1047.8	1047.8				159	0	127	0	1.252
$^{186}W(n,2n)^{185m+g}W$	75.1 d	1829.4	1829.4				159	0	127	0	1.252
$^{186}W(n,p)^{186}Ta$	10.5 m	2.1	2.7				918	1371	967	1563	0.905
$^{185}Re(n,2n)^{184m}Re$	169 d	435.1	695.8	335.	(14.43)	24)	140	330	140	390	0.887
$^{185}Re(n,2n)^{184g}Re$	38.0 d	1779.2	1338.8	1370.	(14.43)	24)	0	835	54	893	0.882
$^{185}Re(n,p)^{185m}W$	1.67 m	2.3	2.0				165	18	165	28	0.948
$^{187}Re(n,2n)^{186g}Re$	90.64 h	1587.2	1388.5				415	12	337	20	1.196
$^{204}Pb(n,2n)^{203m+g}Pb$	51.873 h	2140.7	1994.4	2210.	(14.43)	10)	0	244	49	310	0.680
$^{204}Pb(n,n')^{204m}Pb$	67.2 m	95.5	x				109	2102	109	2102	1.000
$^{206}Pb(n,p)^{206m+g}Tl$	4.199 m	1.8	3.0				626	0	537	1	1.164
$^{208}Pb(n,p)^{208}Tl$	3.053 m	0.70	0.43				651	3354	598	3374	1.008
$^{208}Pb(n,\alpha)^{205m+g}Hg$	5.2 m	1.48	0.18				634	5	-	5	-
$^{209}Bi(n,p)^{209}Pb$	3.253 h	0.63	3.89				245	0	198	0	1.237
$^{209}Bi(n,\alpha)^{206m+g}Tl$	4.199 m	0.58	0.66				626	0	537	0	1.166

The (n,d) reactions includes both (n,d) and (n,np) reactions.
* Decay energy due to β-rays includes conversion electron energy.
@ x: Cross section is not given in JENDL Activation File.
+: Cross section is given in JENDL, but the excitation level of the product is assigned as the ground state.
=: The isomeric state production cross section is given properly in JENDL, but treated for the ground state production in the processed decay data library.

Table 5.4.1 Comparison of decay data in Lib90 and the processed library from ENSDF used in the CINAC calculations for S, Cu and SS-304. (1/2) Nuclides with mass numbers > 100 stand for meta-stable nuclides, e.g., 13-AL-126 is ^{26m}Al.

Nuclide	Lib90 Half-Life	Lib90 E-Beta [MeV]	Lib90 E-Gamma [MeV]	Library from ENSDF+α Half-Life	Library from ENSDF+α E-Beta [MeV]	Library from ENSDF+α E-Gamma [MeV]	Ratio (Lib90/ENSDF+α) E-Beta [MeV]	Ratio (Lib90/ENSDF+α) E-Gamma [MeV]
12-MG 27	9.46 MIN	5.83000E-01	9.14102E-01	9.46 MIN	7.18980E-01	8.91217E-01	0.811	1.026
12-MG 28	21.0 HR	4.59000E-01	1.54374E+00	20.9 HR	1.67460E-01	1.37050E+00	2.741	1.126
13-AL 26	7.160E+5 YR	2.33700E-01	2.70856E+00					
13-AL 28	2.24 MIN	8.60000E-01	1.77870E+00	2.24 MIN	1.26060E+00	1.77880E+00	0.682	1.000
13-AL 29	6.56 MIN	7.17000E-01	1.38390E+00	6.56 MIN	9.94020E-01	1.37934E+00	0.721	1.003
13-AL 30	3.68 SEC	1.14000E+00	3.45606E+00	3.60 SEC	2.32080E+00	3.36527E+00	0.491	1.027
13-AL126	6.35 SEC	9.63000E-01	1.02200E+00					
14-SI 31	2.62 HR	4.11000E-01	8.86340E-04	2.62 HR	6.15250E-01	8.86270E-04	0.668	1.000
14-SI 32	650. YR	2.13700E-01	.00000E+00	330. YR	7.49700E-02	.00000E+00	2.850	
14-SI 33	6.20 SEC	1.31000E+00	2.29908E+00	6.11 SEC	.00000E+00	2.31415E+00		0.993
15-P 30	2.49 MIN	1.08000E+00	1.02338E+00	2.50 MIN	1.42150E+00	1.02206E+00	0.760	1.001
15-P 32	14.3 DAY	5.70000E-01	.00000E+00	14.3 DAY	7.16320E-01	.00000E+00	0.796	
15-P 33	25.2 DAY	8.30000E-02	.00000E+00	25.3 DAY	8.81510E-02	.00000E+00	0.942	
15-P 34	12.5 SEC	1.70000E+00	3.34319E-01	12.4 SEC	2.32870E+00	3.34170E-01	0.730	1.000
15-P 35	47.0 SEC	3.91700E+00	1.56748E+00	47.3 SEC	1.00980E+00	1.57220E+00	3.879	0.997
15-P 36	1.00 SEC	.00000E+00	.00000E+00	5.90 SEC	.00000E+00	4.60772E+00		0.000
16-S 31				2.58 SEC	1.98280E+00	1.03808E+00		
16-S 35	2.89 MON	5.57000E-01	.00000E+00	2.88 MON	5.81000E-02	.00000E+00	9.587	
16-S 37	5.07 MIN	6.37000E-01	2.93149E+00	5.05 MIN	8.23260E-01	2.93166E+00	0.774	1.000
22-TI 51	5.80 MIN	6.24000E-01	3.84075E-01	5.76 MIN	8.99530E-01	3.69253E-01	0.694	1.040
22-TI 52				1.70 MIN	7.73350E-01	1.27510E-01		
23-V 48				16.0 DAY	1.33650E-01	2.91230E+00		
23-V 49	10.7 MON	.00000E+00	.00000E+00	11.1 MON	.00000E+00	.00000E+00		
23-V 52	3.76 MIN	7.35000E-01	1.44370E+00	3.75 MIN	1.10200E+00	1.44493E+00	0.667	0.999
23-V 53	1.60 MIN	7.41000E-01	5.25548E-01	1.61 MIN	1.08710E+00	1.04280E+00	0.682	0.504
23-V 54	43.0 SEC	9.30000E-01	3.96316E+00	49.8 SEC	1.59800E+00	4.84290E+00	0.582	0.818
24-CR 49	41.9 MIN	4.29000E-01	1.12289E+00	42.3 MIN	5.95000E-01	1.05281E+00	0.721	1.067
24-CR 51	27.7 DAY	.00000E+00	3.26400E-02	27.7 DAY	.00000E+00	3.22641E-02		1.012
24-CR 55	3.52 MIN	7.44000E-01	5.69944E-04	3.50 MIN	1.08360E+00	6.73087E-04	0.687	0.847
24-CR 56				5.94 MIN	6.22780E-01	9.18211E-02		

Table 5.4.1 Continued. (2/2)

Nuclide	Lib90 Half-Life	Lib90 E-Beta [MeV]	Lib90 E-Gamma [MeV]	Library from ENSDF+α Half-Life	Library from ENSDF+α E-Beta [MeV]	Library from ENSDF+α E-Gamma [MeV]	Ratio (Lib90/ENSDF+α) E-Beta [MeV]	Ratio (Lib90/ENSDF+α) E-Gamma [MeV]
25-MN 52	5.59 DAY	1.33920E-02	3.49646E+00	5.59 DAY	6.40300E-02	3.46503E+00	0.209	1.009
25-MN 53	3.740E+6 YR	.00000E+00	.00000E+00	3.700E+6 YR	.00000E+00	.00000E+00		
25-MN 54	10.3 MON	.00000E+00	8.34830E-01	10.3 MON	.00000E+00	8.34630E-01		1.000
25-MN 56	2.58 HR	5.97000E-01	1.69317E+00	2.58 HR	8.64060E-01	1.69156E+00	0.691	1.001
25-MN 57	1.54 MIN	7.38000E-01	7.04005E-02	1.45 MIN	1.06390E+00	1.01373E-01	0.694	0.694
25-MN 58	1.09 MIN	1.13000E+00	2.19040E+00	1.09 MIN	1.62710E+00	2.39084E+00	0.694	0.916
25-MN152	21.1 MIN	7.44251E-01	2.42452E+00	21.1 MIN	9.37521E-01	2.41027E+00	0.794	1.006
~~25-MN158~~				~~3.00 SEC~~	~~2.84100E+00~~	~~.00000E+00~~		
26-FE 53	8.51 MIN	7.77000E-01	2.44300E+00	8.51 MIN	1.13200E+00	1.16540E+00	0.686	2.096
26-FE 55	2.68 YR	.00000E+00	.00000E+00	2.73 YR	.00000E+00	.00000E+00		
26-FE 59	1.46 MON	1.13000E-01	1.19015E+00	1.46 MON	1.35530E-01	1.18833E+00	0.834	1.002
26-FE 60	3.000E+5 YR	.00000E+00	.00000E+00	7.500E+6 YR	6.33880E-02	.00000E+00	0.000	
26-FE 61	5.98 MIN	7.20000E-01	1.39663E+00	5.98 MIN	1.28360E+00	1.39100E+00	0.561	1.004
26-FE 62				1.13 MIN	8.80810E-01	5.06100E-01		
26-FE153	2.51 MIN	.00000E+00	3.03507E+00					
27-CO 56	2.59 MON	1.57890E-02	3.59063E+00	2.53 MON	1.10230E-01	3.63798E+00	0.143	0.987
27-CO 57	8.92 MON	.00000E+00	1.22217E-01	8.93 MON	.00000E+00	1.21650E-01		1.005
27-CO 58	2.33 MON	3.19500E-03	9.74971E-01	2.33 MON	2.63170E-02	9.74052E-01	0.121	1.001
27-CO 60	5.27 YR	9.00000E-02	2.50568E+00	5.27 YR	1.14660E-01	2.50440E+00	0.785	1.001
27-CO 61	1.65 HR	3.57000E-01	9.02301E-02	1.65 HR	4.78420E-01	9.66415E-02	0.746	0.934
27-CO 62	1.50 MIN	1.06000E+00	1.62084E+00	1.50 MIN	1.64450E+00	1.60168E+00	0.645	1.012
27-CO 63	27.5 SEC	1.03000E+00	1.21201E-01	27.4 SEC	1.58780E+00	1.17608E-01	0.649	1.031
27-CO 64	.300 SEC	2.05000E+00	1.81169E-01	.300 SEC	3.34840E+00	1.92550E-01	0.612	0.941
27-CO158	9.15 HR	.00000E+00	8.75000E-06	9.15 HR	2.08000E-02	9.18404E-06	0.000	0.953
27-CO160	10.5 MIN	2.80000E-06	4.37200E-03	10.5 MIN	5.35800E-02	3.27700E-03	0.000	1.334
27-CO161	1.65 HR	3.57000E-01	.00000E+00					
27-CO162	13.9 MIN	7.23000E-01	2.71332E+00	13.9 MIN	1.05450E+00	2.69823E+00	0.686	1.006
28-NI 57	1.50 DAY	3.90000E-02	1.90153E+00	1.49 DAY	1.35680E-01	1.94077E+00	0.287	0.980
28-NI 59	7.500E+4 YR	.00000E+00	.00000E+00	7.500E+4 YR	2.60020E-09	1.53300E-07	0.000	0.000
28-NI 63	100. YR	1.98000E-02	.00000E+00	100. YR	2.23570E-02	.00000E+00	0.886	
28-NI 65	2.52 HR	4.74000E-01	5.52476E-01	2.52 HR	6.71050E-01	5.48571E-01	0.706	1.007
29-CU 62	9.73 MIN	8.42058E-01	1.00859E+00	9.74 MIN	1.25590E+00	1.00684E+00	0.670	1.002
29-CU 64	12.7 HR	3.12902E-02	2.02256E-01	12.7 HR	1.25175E-01	1.89512E-01	0.250	1.067
29-CU 66	5.10 MIN	7.65000E-01	8.43113E-02	5.10 MIN	1.11180E+00	7.83541E-02	0.688	1.076

Table 5.5.1 Recommendation for modification of activation cross sections in FENDL/A-2.0 and JENDL Activation File. These factors should be multiplied to the present cross sections.

Reaction	Half-Life	FENDL	JENDL
$^{11}B(n,p)^{11}Be$	13.81 s		1.3
$^{19}F(n,p)^{19}O$	26.91 s		1.2
$^{19}F(n,2n)^{18}F$	109.77 m		0.9
$^{23}Na(n,p)^{23}Ne$	37.24 s	1.15	
$^{23}Na(n,2n)^{22}Na$	2.602 y	1.1	1.2
$^{32}S(n,t)^{30}P$	2.498 m	0.5	
$^{40}Ca(n,t)^{38m+g}K$	7.636 m	0.001	
$^{50}Ti(n,p)^{50m+g}Sc$	102.5 s	0.8	
$^{52}Cr(n,p)^{52}V$	3.75 m	1.05	
$^{62}Ni(n,p)^{62m}Co$	13.91 m	1.3	1.3
$^{62}Ni(n,p)^{62g}Co$	1.50 m		1.2
$^{63}Cu(n,\alpha)^{60m+g}Co$	5.2714 y	1.2	1.2
$^{88}Sr(n,2n)^{87m}Sr$	2.803 h	1.1	
$^{88}Sr(n,p)^{88}Rb$	17.78 m	1.3	1.3
$^{89}Y(n,\alpha)^{86m}Rb$	1.017 m	2	
$^{92}Mo(n,2n)^{91m}Mo$	65.0 s	0.8	
$^{112}Sn(n,2n)^{111}Sn$	35.3 m	1.2	1.2
$^{181}Ta(n,2n)^{180g}Ta$	8.152 h	0.65	1.1
$^{185}Re(n,2n)^{184m}Re$	169 d		0.6
$^{187}Re(n,2n)^{186g}Re$	90.64 h	0.85	

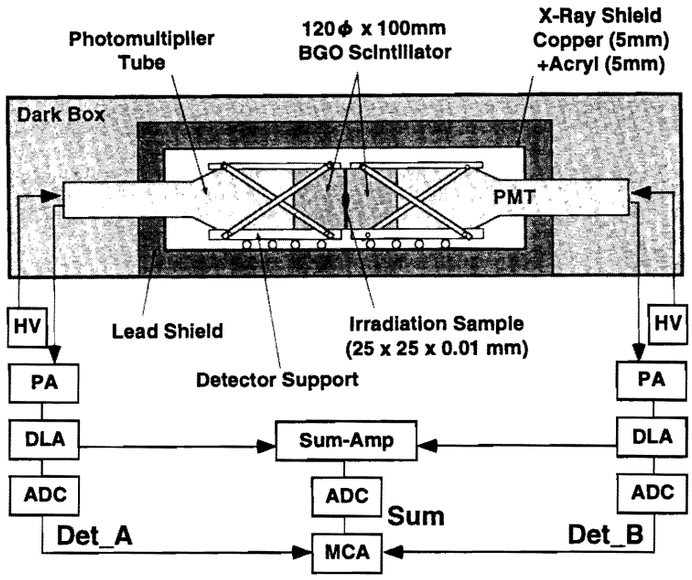

Fig. 2.1.1 Schematic diagram of the Whole Energy Absorption Spectrometer (WEAS) with an associated electronic circuit.

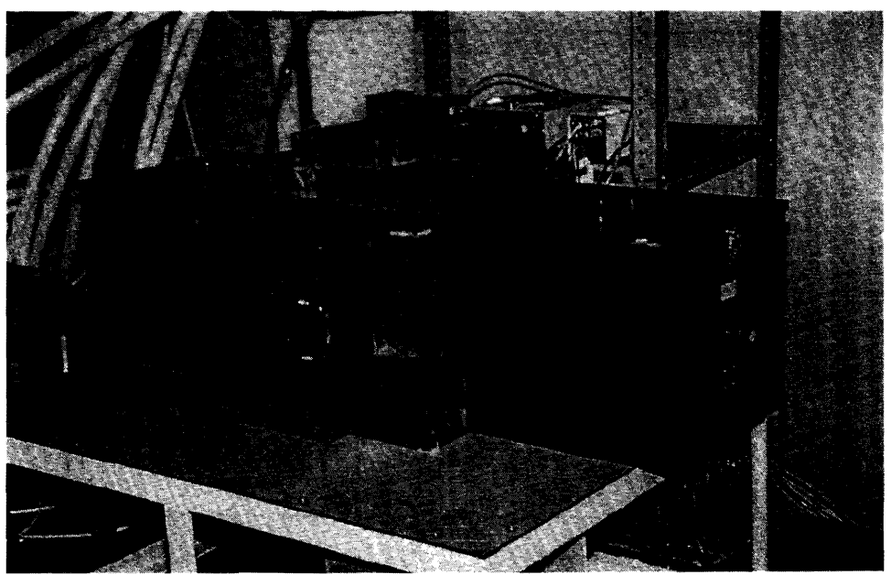

Fig. 2.1.2 Outside view of WEAS. The dark box, additional lead shield blocks and the opening in the lead shield for sample insertion are seen.

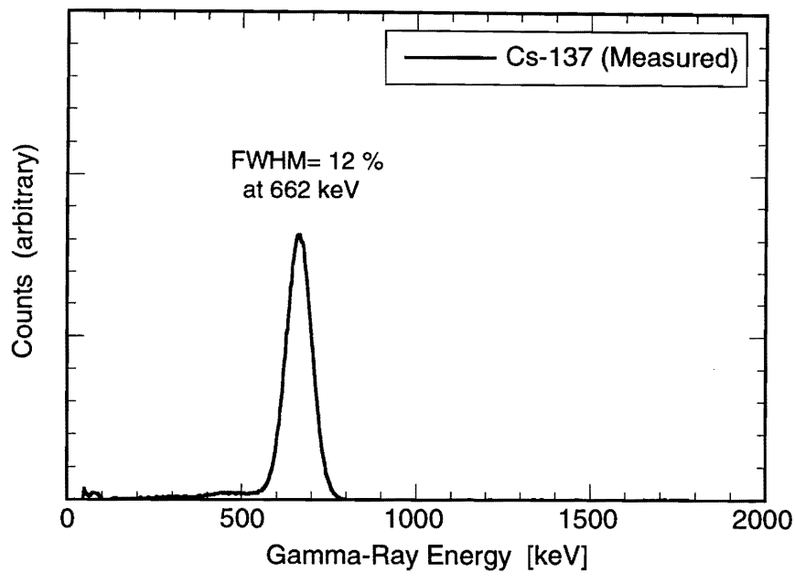

Fig. 2.2.1 Gamma-ray pulse height spectrum from a Cs-137 source measured with the BGO scintillator.

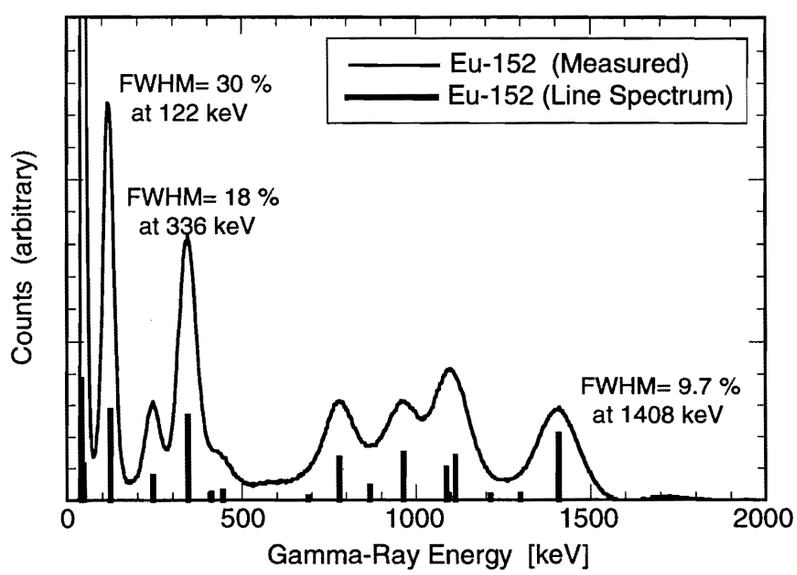

Fig. 2.2.2 Gamma-ray pulse height spectrum from a Eu-152 source measured with the BGO scintillator and an expected line spectrum.

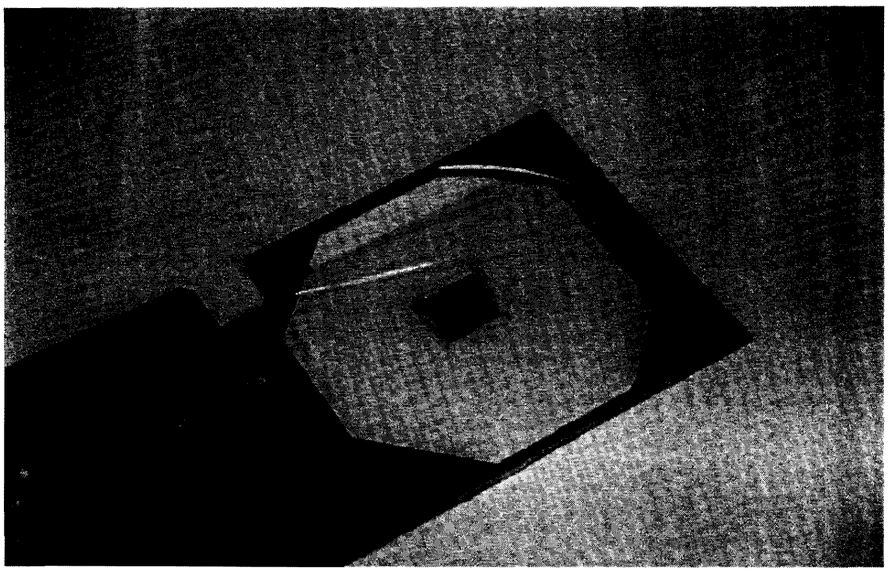

Fig. 2.2.3 The sample cassette. A copper sample is mounted on a thin plastic film.

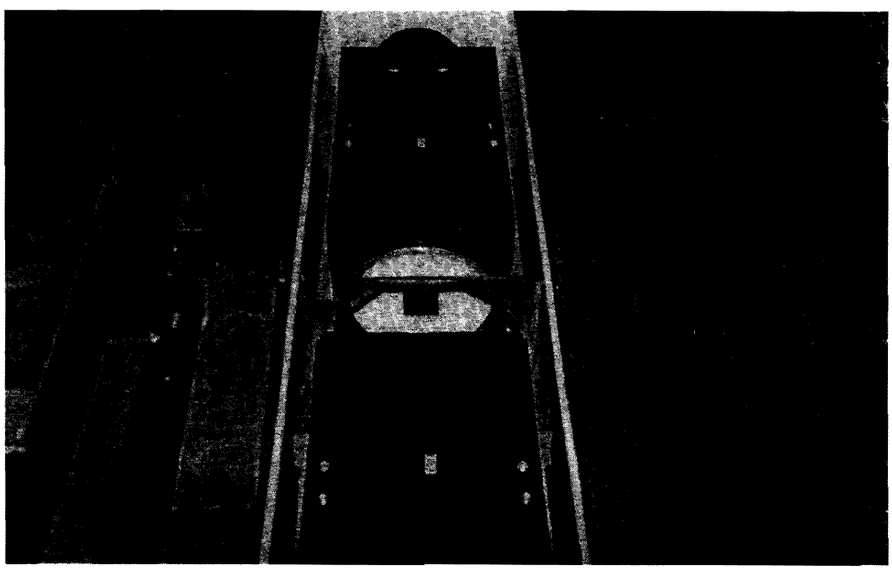

Fig. 2.2.4 Inside of WEAS. The BGO scintillators with the square window and the sample cassette are installed in the radiation shield.

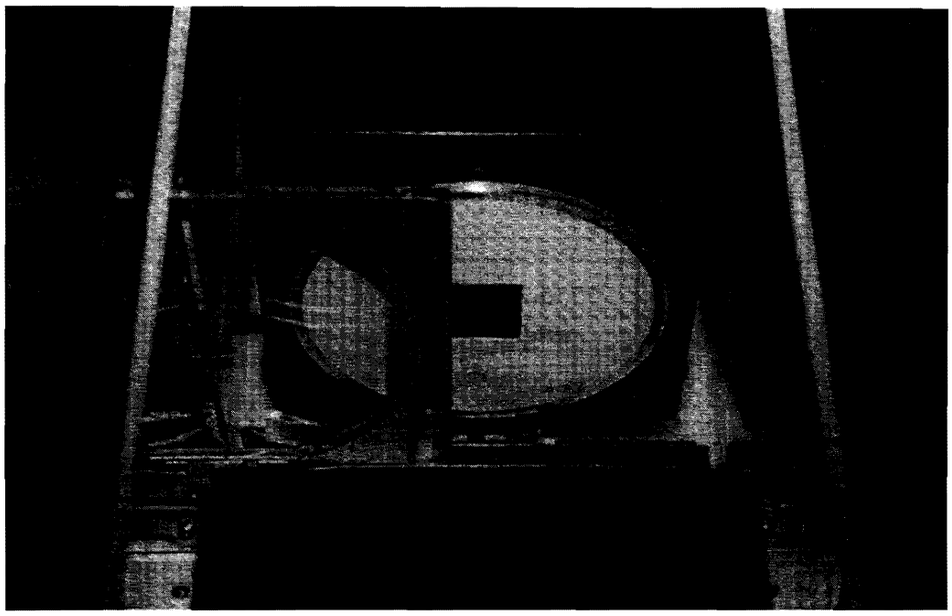

Fig. 2.2.5 A picture when the sample cassette is about to be inserted in WEAS.

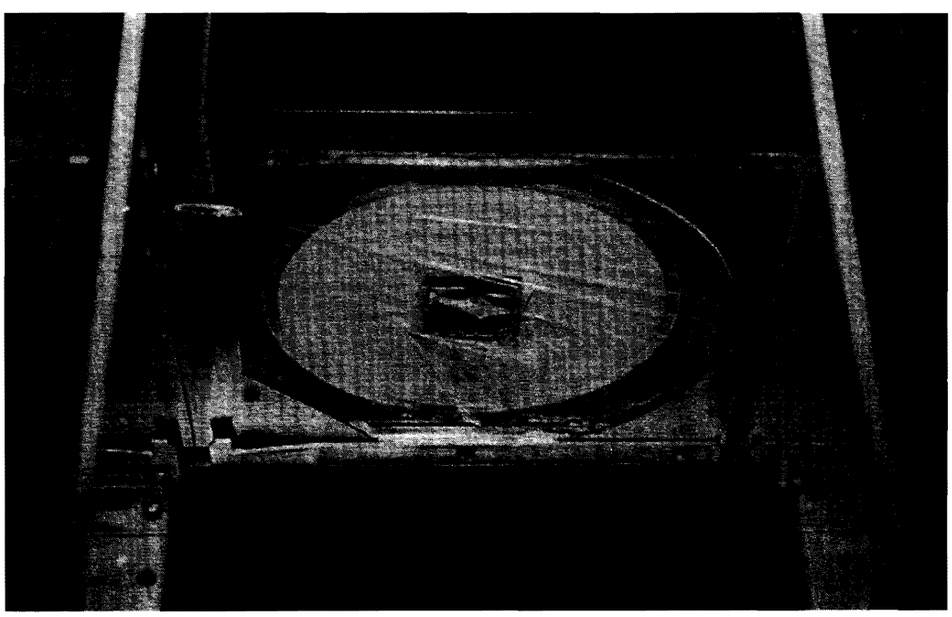

Fig. 2.2.6 A picture when the sample cassette is inserted completely at the right position in WEAS.

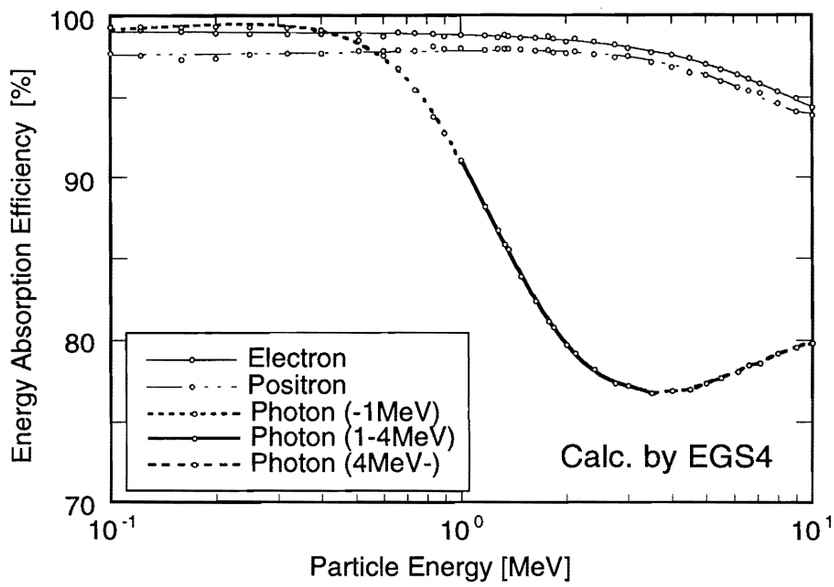

Fig. 2.4.1 Energy absorption efficiencies for electron, positron and photons calculated by EGS4 (open circles) and fitted (lines).

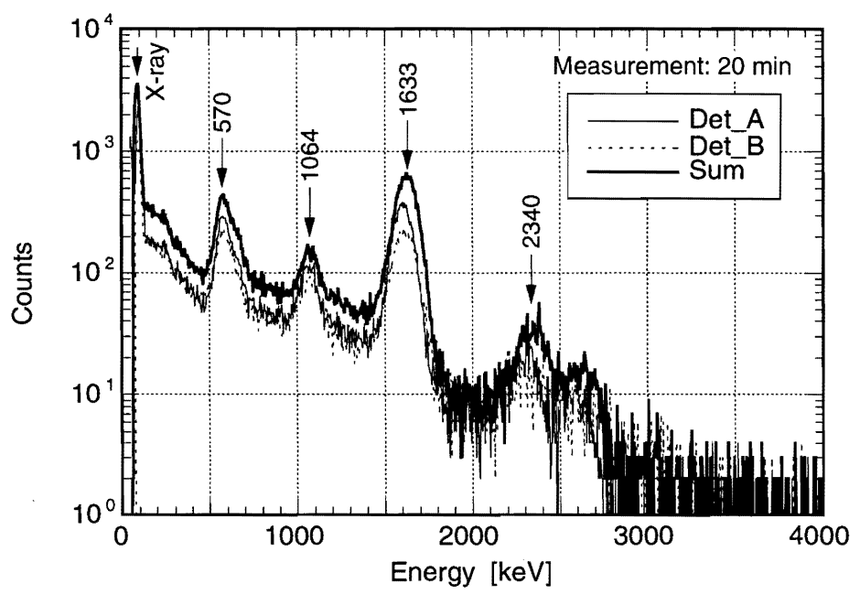

Fig. 2.5.1 Background spectrum of WEAS measured for 20 minutes.

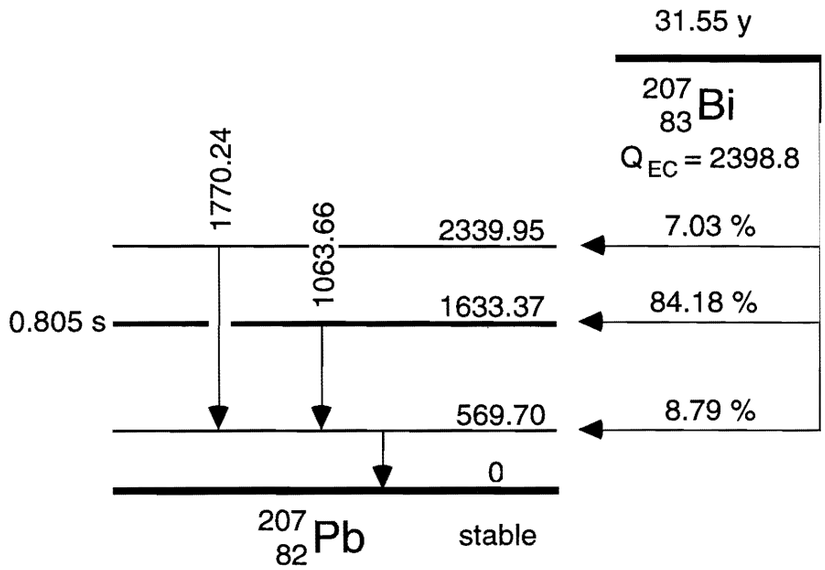

Fig. 2.5.2 Simplified decay scheme of bismuth-207.

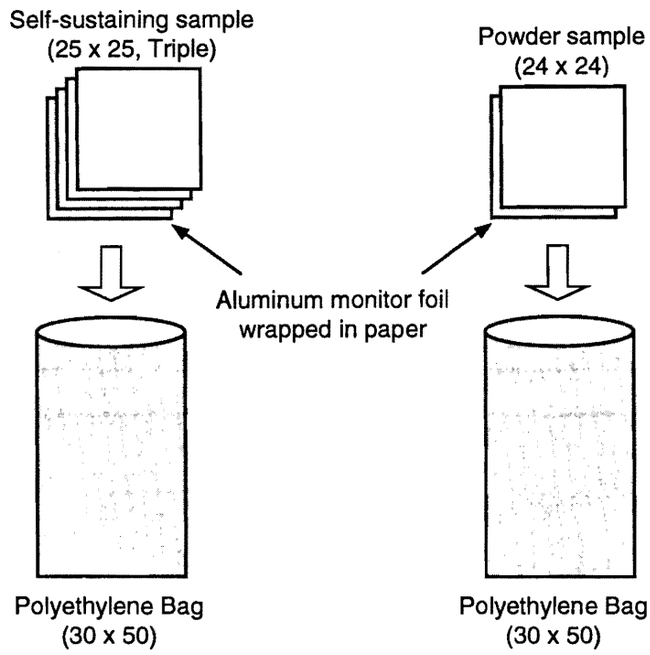

Fig. 3.1.1 Preparation of irradiation samples.

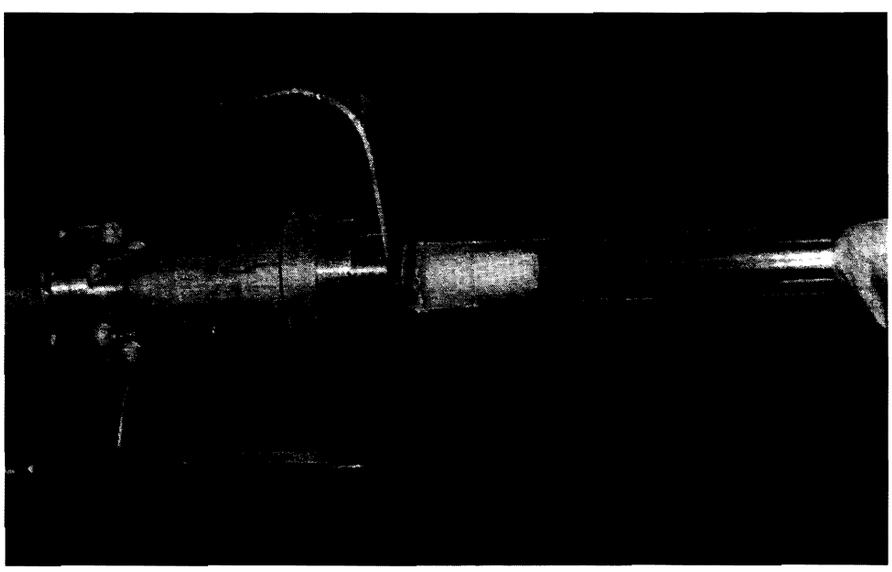

Fig. 3.2.1 The D-T neutron source for the 80 degree beam line of FNS (left-hand side) and the rabbit in the pneumatic tube (right-hand side).

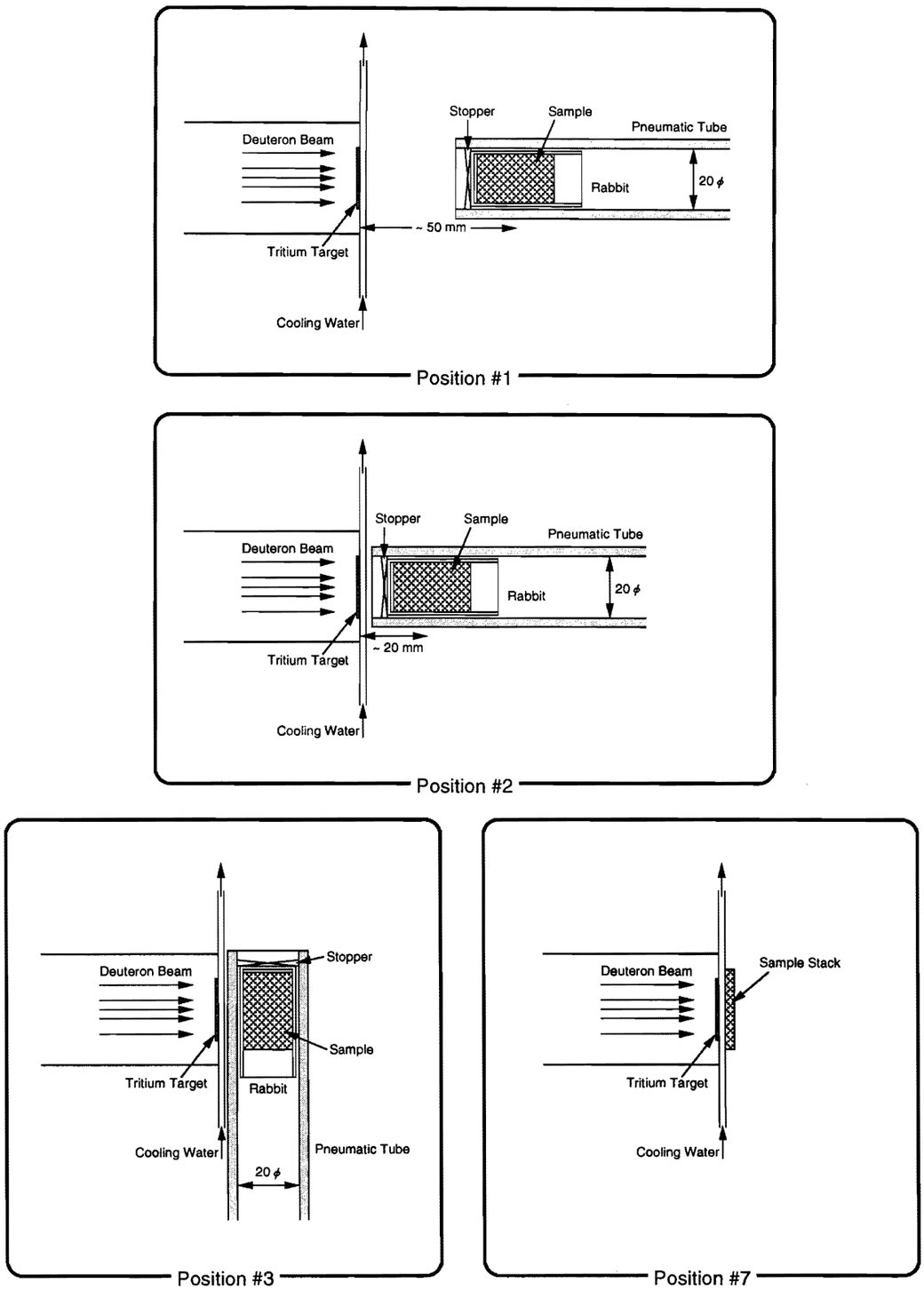

Fig. 3.2.2 The three sample positions #1, #2 and #3 for the 5 minutes irradiations, and the sample position #7 for the 7 hours irradiations.

```
$inq name "file name"
$number=0
$
$kaisu=3
$lt   =10
$pars/command fm1 preal='lt'
$pars/command fm2 preal='lt'
$pars/command fm3 preal='lt'
$turn=0
$
$l1:
$turn=turn+1
$number=number+1
$mca on fm1
$mca on fm2
$mca on fm3
$mca wait fm1
$mca wait fm2
$mca wait fm3
$move fm1 'name'_a_'number'
$move fm2 'name'_b_'number'
$move fm3 'name'_s_'number'
$dir 'name'*
$mca er fm1
$mca er fm2
$mca er fm3
$if turn.ne.'kaisu' then goto l1
$
$kaisu=3
$lt   =30
$pars/command fm1 preal='lt'
$pars/command fm2 preal='lt'
$pars/command fm3 preal='lt'
$turn=0
$
$l2:
$turn=turn+1
$number=number+1
$mca on fm1
$mca on fm2
$mca on fm3
$mca wait fm1
$mca wait fm2
$mca wait fm3
$move fm1 'name'_a_'number'
$move fm2 'name'_b_'number'
$move fm3 'name'_s_'number'
$dir 'name'*
$mca er fm1
$mca er fm2
$mca er fm3
$if turn.ne.'kaisu' then goto l2
$
$kaisu=3
$lt   =60
$pars/command fm1 preal='lt'
$pars/command fm2 preal='lt'
$pars/command fm3 preal='lt'
$turn=0
$
$l3:
$turn=turn+1
$number=number+1
$mca on fm1
$mca on fm2
$mca on fm3
$mca wait fm1
$mca wait fm2
$mca wait fm3
$move fm1 'name'_a_'number'
$move fm2 'name'_b_'number'
$move fm3 'name'_s_'number'
$dir 'name'*
$mca er fm1
$mca er fm2
$mca er fm3
$if turn.ne.'kaisu' then goto l3
$
$kaisu=4
$lt   =120
$pars/command fm1 preal='lt'
$pars/command fm2 preal='lt'
$pars/command fm3 preal='lt'
$turn=0
$
$l4:
$turn=turn+1
$number=number+1
$mca on fm1
$mca on fm2
$mca on fm3
$mca wait fm1
$mca wait fm2
$mca wait fm3
$move fm1 'name'_a_'number'
$move fm2 'name'_b_'number'
$move fm3 'name'_s_'number'
$dir 'name'*
$mca er fm1
$mca er fm2
$mca er fm3
$if turn.ne.'kaisu' then goto l4
$
$kaisu=4
$lt   =240
$pars/command fm1 preal='lt'
$pars/command fm2 preal='lt'
$pars/command fm3 preal='lt'
$turn=0
$
$l5:
$turn=turn+1
$number=number+1
$mca on fm1
$mca on fm2
$mca on fm3
$mca wait fm1
$mca wait fm2
$mca wait fm3
$move fm1 'name'_a_'number'
$move fm2 'name'_b_'number'
$move fm3 'name'_s_'number'
$dir 'name'*
$mca er fm1
$mca er fm2
$mca er fm3
$if turn.ne.'kaisu' then goto l5
$
$kaisu=3
$lt   =600
$pars/command fm1 preal='lt'
$pars/command fm2 preal='lt'
$pars/command fm3 preal='lt'
$turn=0
$
$l6:
$turn=turn+1
$number=number+1
$mca on fm1
$mca on fm2
$mca on fm3
$mca wait fm1
$mca wait fm2
$mca wait fm3
$move fm1 'name'_a_'number'
$move fm2 'name'_b_'number'
$move fm3 'name'_s_'number'
$dir 'name'*
$mca er fm1
$mca er fm2
$mca er fm3
$if turn.ne.'kaisu' then goto l6
$
$pars/command fm1 preal=0
$pars/command fm2 preal=0
$pars/command fm3 preal=0
```

Fig. 3.2.3 A command procedure for measurements of 5 minutes irradiations for the CANBERRA Genie System on a VAX computer.

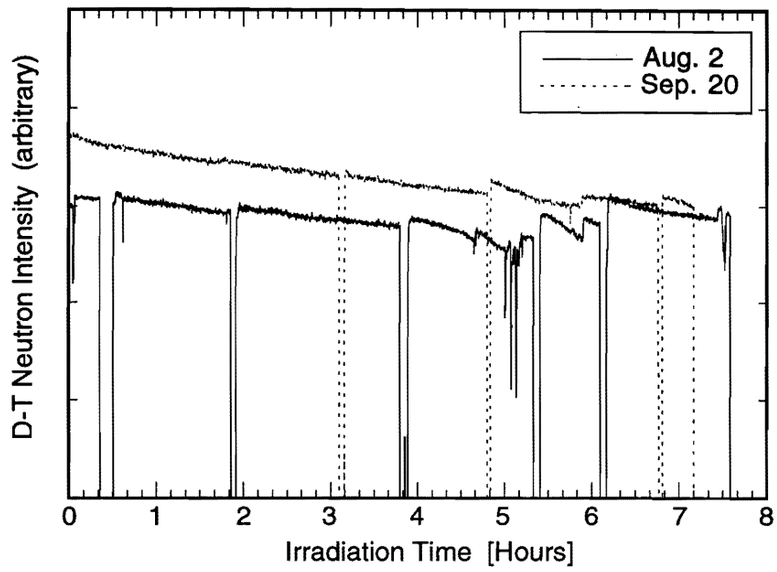

Fig. 3.2.4 Fluctuation of D-T neutron intensity during the 7 hours irradiations monitored by the associated alpha-particle counter.

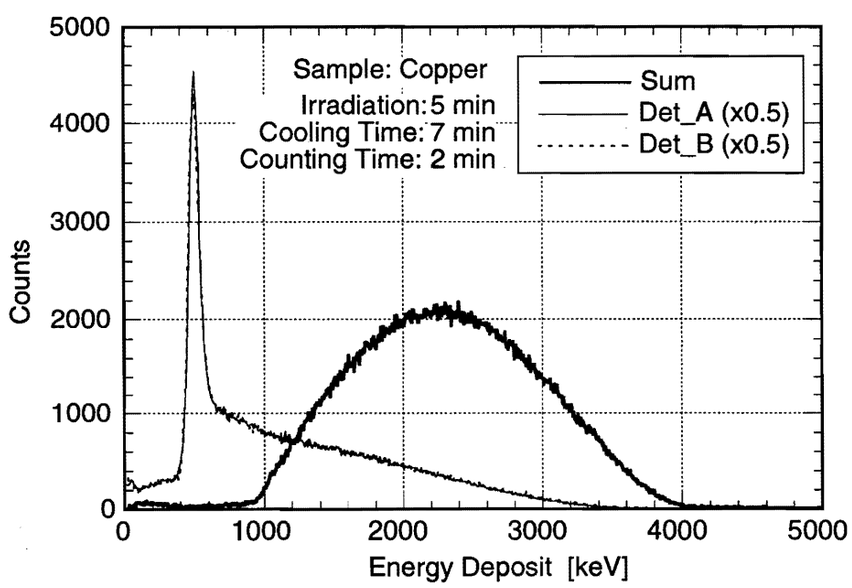

Fig. 3.3.1 Measured pulse height spectra for a copper sample irradiated for 5 minutes. Copper-62 produced by the ^{63}Cu(n,2n) reactions are predominantly observed.

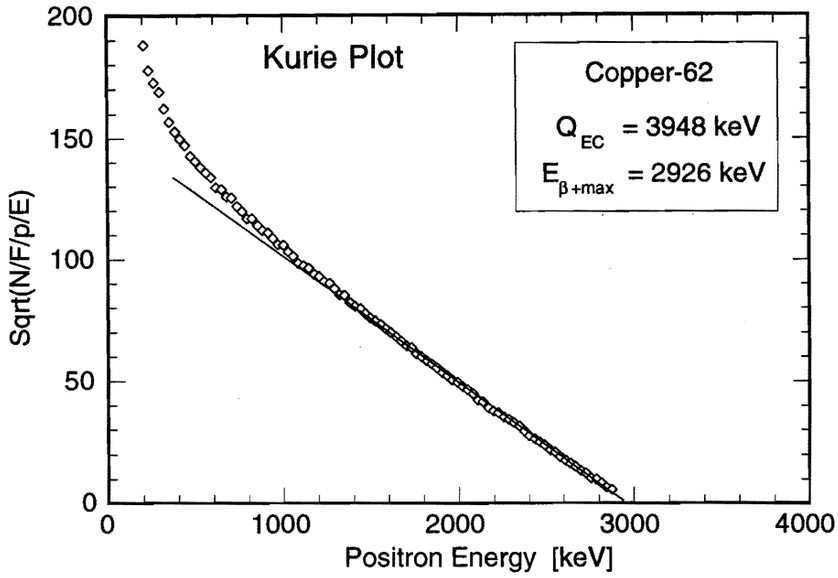

Fig. 3.3.2 Kurie plot for copper-62.

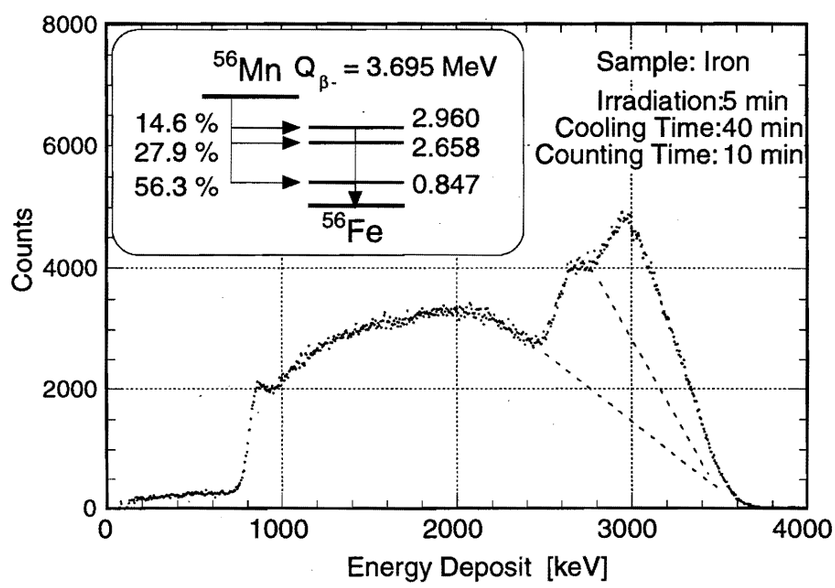

Fig. 3.3.3 Measured pulse height spectra for an iron sample irradiated for 5 minutes. Manganese-56 produced by the ^{56}Fe(n,p) reactions are predominantly observed.

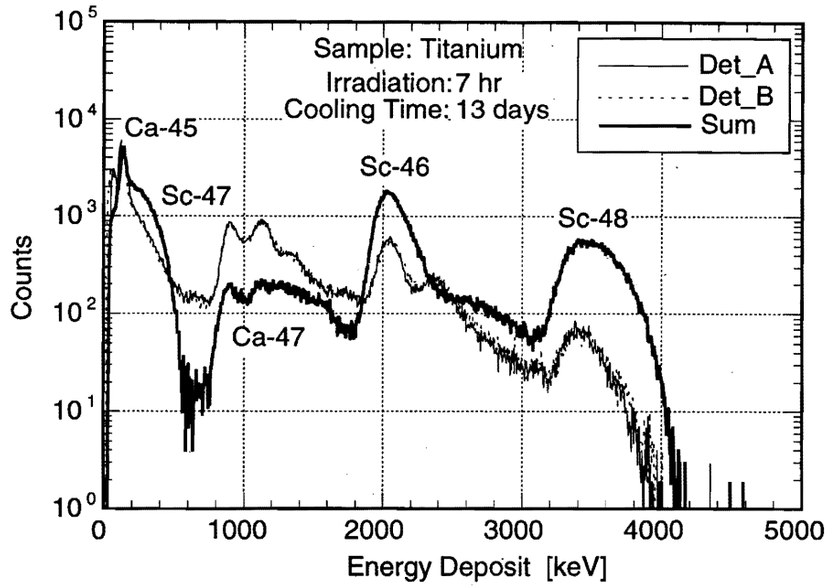

Fig. 3.3.4 Measured pulse height spectra for a titanium sample irradiated for 7 hours. The spectra are composed with various radioactivities produced in the sample.

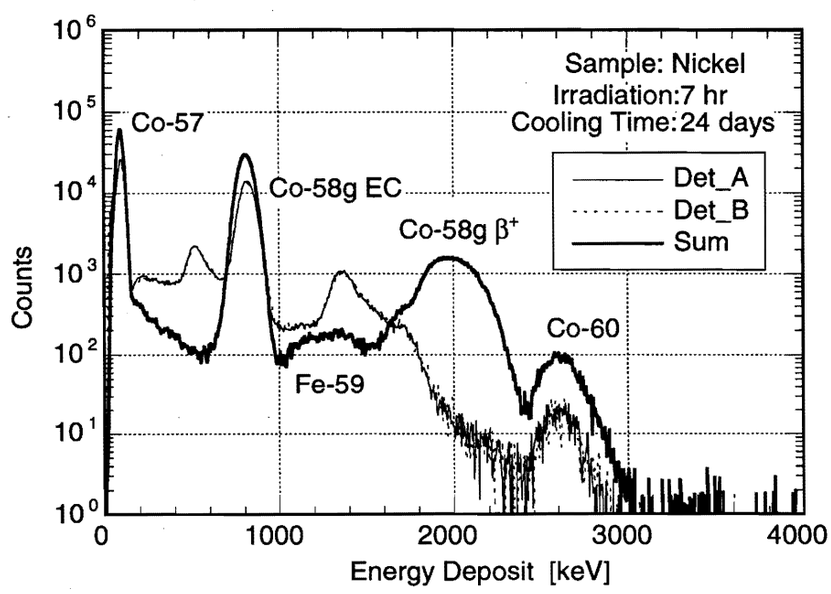

Fig. 3.3.5 Measured pulse height spectra for a nickel sample irradiated for 7 hours. The spectra are composed with various radioactivities produced in the sample.

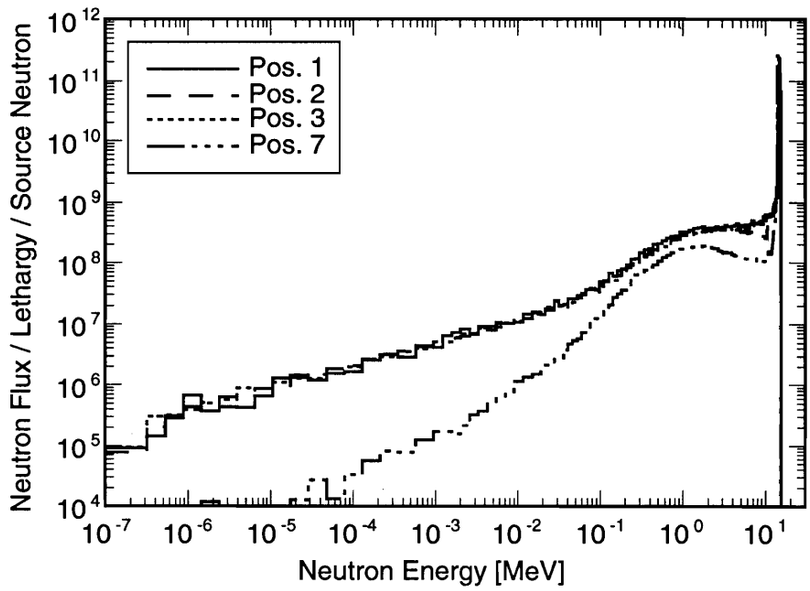

Fig. 3.4.1 Source neutron spectra at the four sample positions plotted with a logarithmic vertical scale.

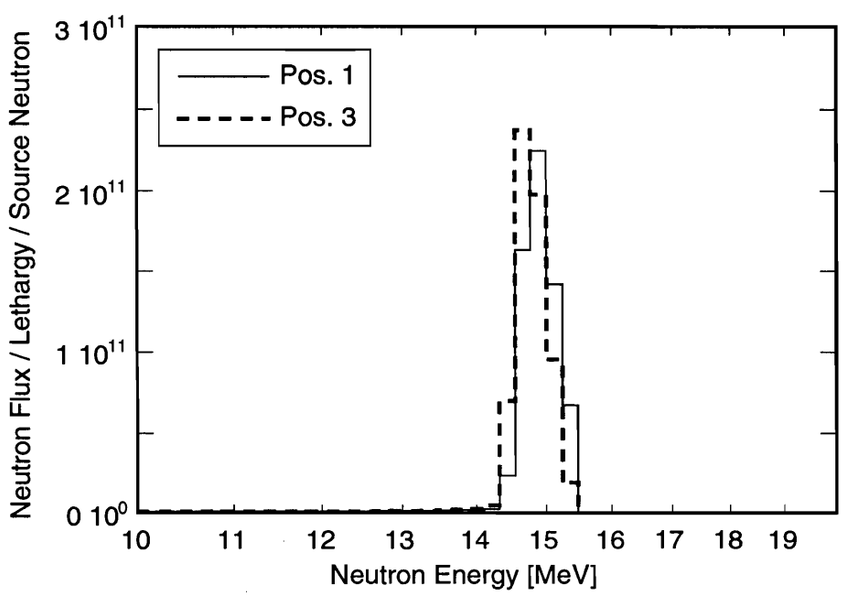

Fig. 3.4.2 Source neutron spectra at the sample positions #1 and #3 plotted with a linear vertical scale.

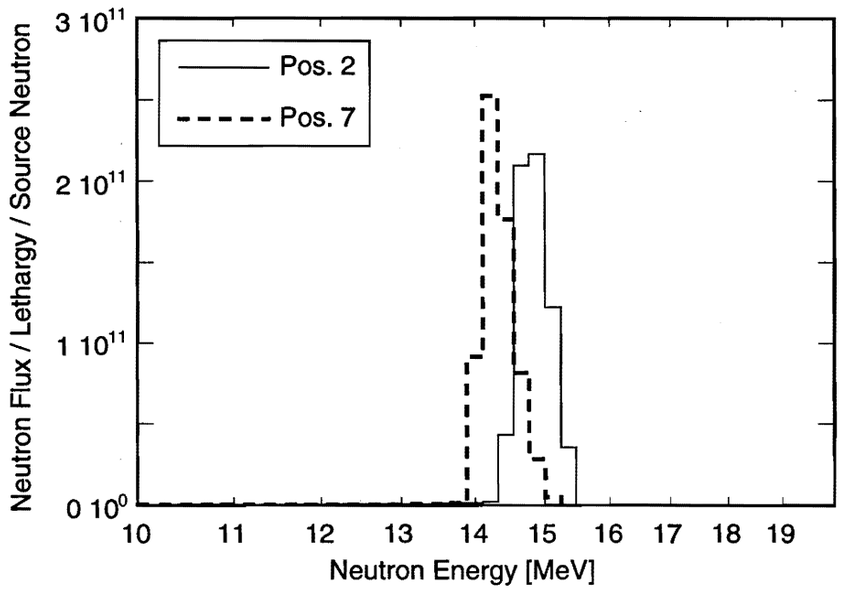

Fig. 3.4.3 Source neutron spectra at the sample positions #2 and #7 plotted with a linear vertical scale.

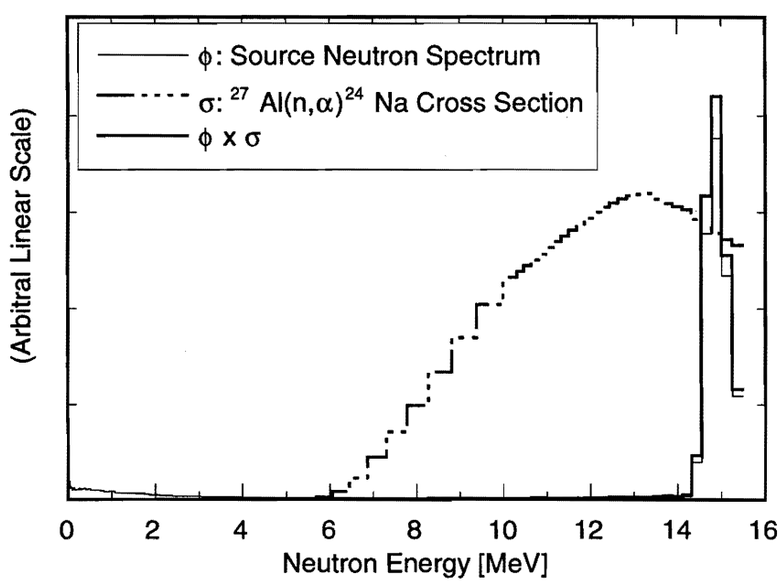

Fig. 3.4.4 Source neutron spectrum at the position #1 (ϕ), the $^{27}Al(n,\alpha)^{24}Na$ reaction cross section (σ) and products of both (ϕ x σ).

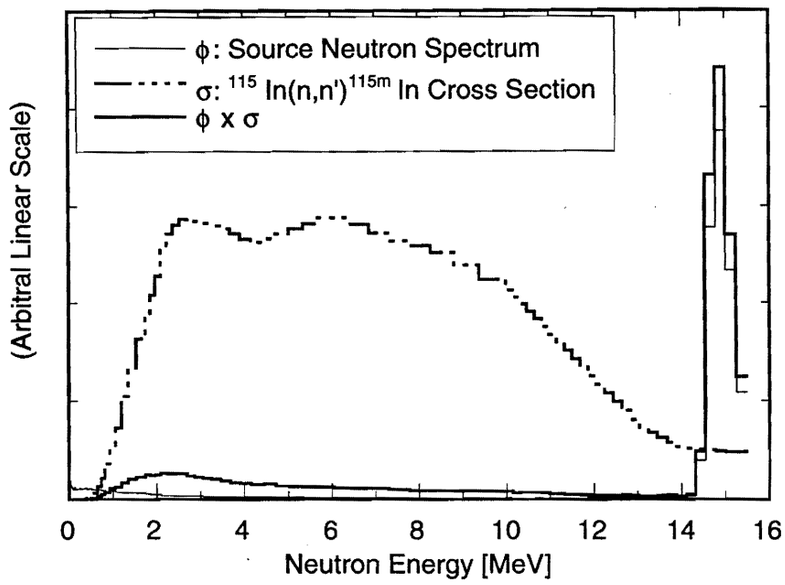

Fig. 3.4.5 Source neutron spectrum at the position #1 (ϕ), the $^{115}In(n,n')^{115m}In$ reaction cross section (σ) and products of both (ϕ x σ).

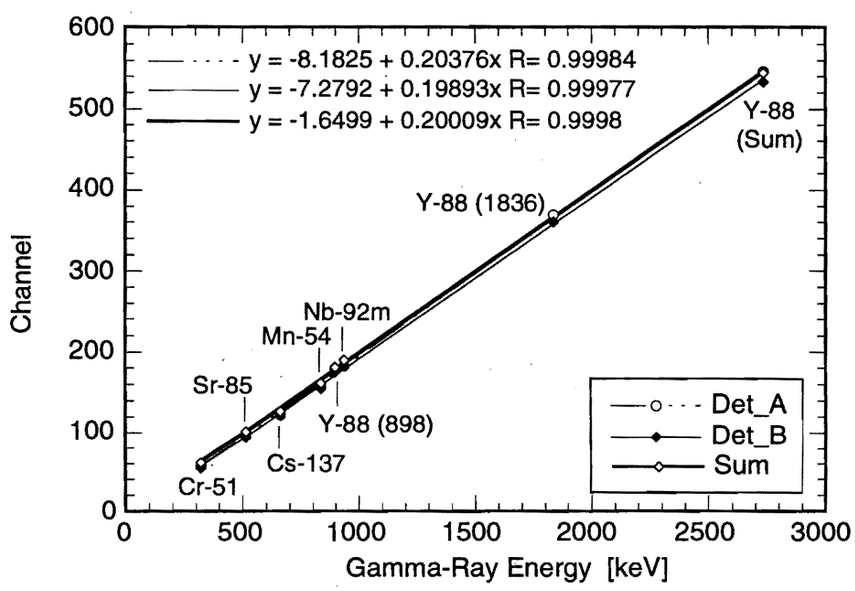

Fig. 3.6.1 Energy calibration of WEAS with pure gamma-ray emitters and fitted lines.

```
      program Beta
C
      parameter (ix=2000)
      COMPLEX  CA  ,TCGAM
      dimension Eb(ix), Bb(ix), s(0:ix), spec(0:ix)
C
C
      open (1,file='beta.inp')
        read (1,*) IZ, IM, Q, IB
c
        sum=0.0
        do 10 i=1,ib
          read (1,*) Eb(i), Bb(i)
          sum=sum+Bb(i)
   10   continue
      close (1)
c
        Q=Q/1000.0
        do 11 i=1,ib
          Eb(i)=Eb(i)/1000.0
          Bb(i)=Bb(i)/sum
   11   continue
c
      if (IM.eq.+1) then
        z       = -real(IZ-1)
      else if (IM.eq.-1) then
        z       = +real(IZ+1)
      else
        stop ' IM .ne. -1 nor +1'
      endif
c
      do 12 i=1,ix
        spec(i)=0.0
   12 continue
c
c
c
      imax    = 0
      do 20 m=1,ib
      sum     = 0.0
      btmx    = Q-Eb(m)+0.511062
      iii     = int((btmx-0.005-0.511062)/0.01)
c         write (*,*) btmx, iii
      do 1 i=0,iii
        EM      = 0.511062
        TB      = 0.005+0.01*real(i)+EM
        EMM     = EM*EM
        ALP     = 0.0072972
        CP      = TB*TB-EMM
        SCP     = SQRT(CP)
        ALPZ    = ALP*Z
        V       = ALPZ*TB/SCP
        ALPZ2   = ALPZ*ALPZ
C       R0      = SQRT(1.0-(ALP*Z)**2.0)
        R0      = SQRT(1.0-ALPZ2)
        CA      = CMPLX(R0,V)
        CA      = TCGAM(CA)
        GM      = CABS(CA)**2.0
        FZ      = CP**(R0-1.0) * EXP(3.14159*V)*GM
        BTSP    = FZ*(BTMX-TB)**2.0 * SCP*TB
        factor  = sqrt(1.0/(fz)/tb/scp)
c        write (*,'(1p10e12.3)') tb-em, scp, fz*cp, factor,  btsp
        s(i)=btsp
        sum=sum+btsp
    1 continue
        do 21 i=0,iii
          spec(i)=spec(i)+s(i)/sum*Bb(m)
   21 continue
        imax = max(iii,imax)
   20 continue
c
        open (2,file='beta.out')
          write (2,'(i5,f7.3,''  :Number_of_Data  Delta_E''i)')
     &          iii+1, 0.01
          do 22 i=0,iii
            write (2,'(1pe12.5)') spec(i)
   22     continue
        close (2)
c
        open (3,file='mcnp.out')
          write (3,'(a9,i6,a1,f8.3)') 'si1   0.0',iii,'i',real(iii+1)*0.01
          write (3,'(a9)') 'sp1   0.0'
          write (3,'(tr5,1p6e11.4)') (spec(i),i=0,iii)
          write (3,'(a9,i6,a1,f8.3)')
     &                'e0    0.0',iii+10,'i',real(iii+11)*0.01
        close (3)
c
c
        END
C-----------------------------------------------------------------------
        COMPLEX FUNCTION   TCGAM(ZZ)
C
C
        COMPLEX  Z,ZM,T,TT,SUM,TERM,DEN,CGAMMA,PI,A,ZZ
        DIMENSION C(12)
        LOGICAL  REFLEK
C
C
        PI      = (3.1415927   ,0.0)
        Z       = ZZ
        X       = REAL(Z)
        Y       = AIMAG(Z)
C TOL = LIMIT OF PRECISION COMPUTER SYSTEM IN SINGLE PRECISION
        TOL     = 1.0E-8
        REFLEK  = .TRUE.
C DETERMINE WHETHER Z IS TOO CLOSE TO A POLE
C CHECK WHETHER TOO CLOSE TO ORIGIN
        IF(X.GE.TOL)  GO TO 20
C FIND THE NEAREST POLE AND COMPUTE DISTANCE TO IT
        XDIST   = X-AINT(X-.5)
        ZM      = CMPLX(XDIST,Y)
        IF(CABS(ZM).GE.TOL)  GO TO 10
C IF Z IS TOO CLOSE TO A POLE, PRINT ERROR MESSAGE AND RETURN
C WITH CGAMMA = (1.E8  ,0.E0)
        WRITE(6,900)  Z
        CGAMMA  = (1.E8  ,0.E0)
        GO TO 130
C FOR REAL(Z) NEGATIVE EMPLOY THE REFLECTION FORMULA
C               GAMMA(Z) = PI/(SIN(PI*Z)*GAMMA(1-Z))
C AND COMPUTE GAMMA(1-Z).  NOTE REFLEK IS A TAG TO INDICATE THAT
C THIS RELATION MUST BE USED LATER.
   10 IF(X.GE.0.0)  GO TO 20
```

Fig. 3.8.1 Program list of beta.f for calculation of beta-ray spectra. (1/2)

```
      REFLEK   = .FALSE.
      Z        = (1.0,0.0)-Z
      X        = 1.0-X
      Y        = -Y
C IF Z NOT TOO CLOSE TO A POLE, MAKE REAL(Z)>10
   20 M        = 0
   40 IF(X.GE.10.)  GO TO 60
      X        = X+1.0
      M        = M+1
      GO TO 40
   60 T        = CMPLX(X,Y)
      TT       = T*T
      DEN      = T
C COEFFICIENTS IN STIRLING'S APPROXIMATION FOR LN(GAMMA(T))
      C(1)     = 0.83333333E-01
      C(2)     = -.27777778E-02
      C(3)     = 0.79365079E-03
      C(4)     = -.59523810E-03
      C(5)     = 0.84175084E-03
      C(6)     = -.19175269E-02
      C(7)     = 0.64102564E-02
      C(8)     = -.29550654E-01
      C(9)     = 0.17964437E+00
      C(10)    = -.13924322E+01
      C(11)    = 0.13402864E+02
      SUM      = (T-(.5,0.0))*CLOG(T)-T+CMPLX(.91893853    ,0.0)
C     0.91893 85332 ..... = LOG(SQRT(2*PI))/2
      J        = 1
 70    TERM    = CMPLX(C(J),0.0)/DEN
C TEST REAL AND IMAGINARY PARTS OF LN(GAMMA(Z)) SEPARATELY FOR
C CONVERGENCE.  IF Z IS REAL SKIP IMAGINARY PART OF CHECK.
      IF(ABS(REAL(TERM)/REAL(SUM)).GE.TOL)  GO TO 80
      IF(Y.EQ.0.0)  GO TO 100
      IF(ABS(AIMAG(TERM)/AIMAG(SUM)).LT.TOL)  GO TO 100
   80 SUM      = SUM+TERM
      J        = J + 1
      DEN      = DEN*TT
C TEST FOR NONCONVERGENCE
      IF(J.EQ.12)  GO TO 90
      GO TO 70
C STIRLING'S SERIES DID NOT CONVERGENCE.  PRINT ERROR MESSAGE AND
C PROCEDURE.
   90 WRITE(   6,910)  Z
C RECURSION RELATION USED TO OBTAIN GAMMA(Z) = GAMMA(Z+M)/(Z*(Z+1)*...
C                                            *(Z+M-1))
  100 CGAMMA   = CEXP(SUM)
      IF(M.EQ.0)  GO TO 120
      DO 110 I=1,M
      A        = CMPLX(FLOAT(I)    -1.,0.0)
  110 CGAMMA   = CGAMMA/(Z+A)
C CHECK TO SEE IF REFLECTION FORMULA SHOULD BE USED
  120 IF(REFLEK)  GO TO 130
      CGAMMA   = PI/(CSIN(PI*Z)*CGAMMA)
  130 TCGAM    = CGAMMA
      RETURN
  900 FORMAT(1X,2E14.7,10X,49HARGUMENT OF GAMMA FUNCTION IS TOO CLOSE TO
     & A POLE)
  910 FORMAT(44H ERROR - STIRLING'S SERIES HAS NOT CONVERGED/14X,4HZ =,
     &2E14.7)
      END
```

Fig. 3.8.1 Continued. (2/2)

Explanation of the input cards for beta.f

Card 1 IZ, IM, Q, IB

- IZ: Atomic number of the parent nuclide
- IM: Decay mode -1 for beta-minus decay, +1 for beta-plus decay
- Q: Q-value of the decay in keV
- IB: Number of excitation levels

Card 2 ~ Card IB+1

Eb, Bb

- Eb: Excitation energy in keV
- Bb: Branching ratio

An example of input cards for magnesium-27

```
12  -1  2610.32  2
1014.45 29.0
 843.76 71.0
```

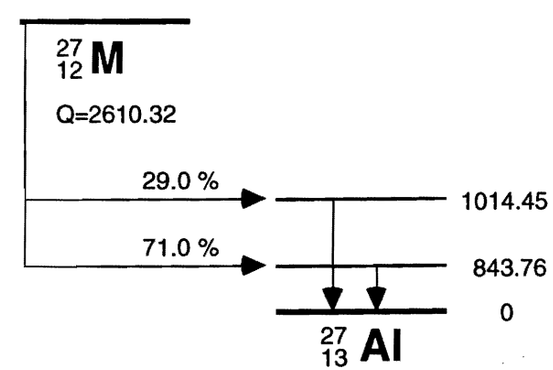

Fig. 3.8.2 Explanation of the input cards and an example of input data for magnesium-27 with its decay scheme.

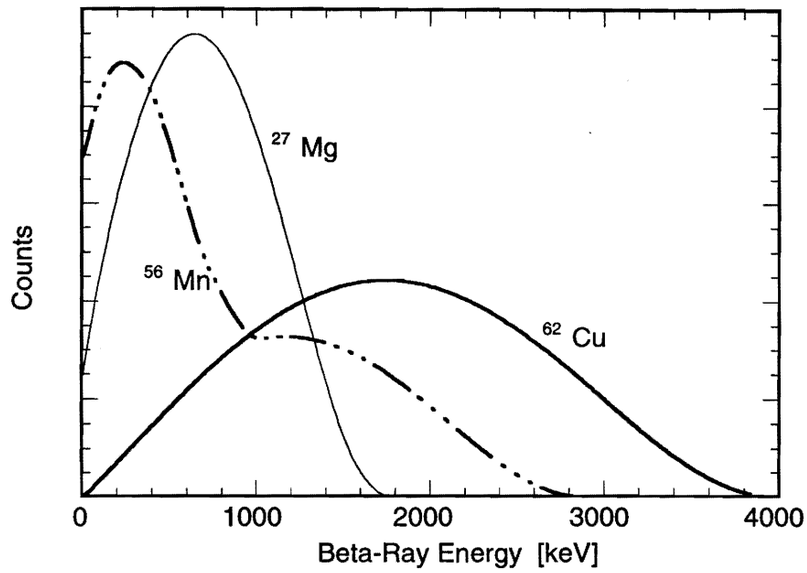

Fig. 3.8.3 Several examples of calculated beta-ray spectra which are used to calculate the correction factors of beta-ray energy loss in the samples with MCNP-4B.

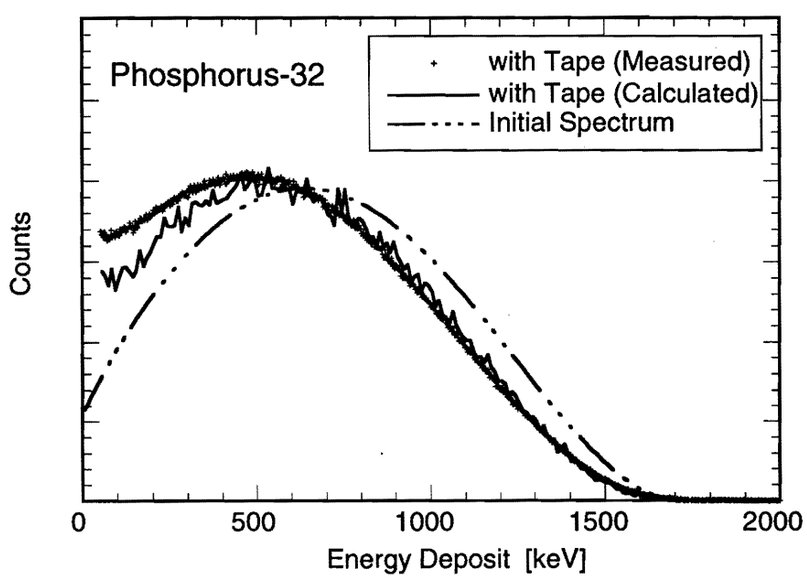

Fig. 3.8.4 Spectra of beta-rays emitted from phosphorous-32 nuclei produced in the sulfur sample. The sample is sandwiched by plastic tapes, and the energy loss of beta-rays in the plastic tapes is calculated adequately to reproduce the measured spectrum.

```
Subroutine ACTCHN

  110 CONTINUE
      TIME    = TIMECV(TIME,UNIT)
      IF(TIME.EQ.0.0)                    GO TO  120
      IF(TIME.LT.1.0)     TIME = 1.0
      TIME    = 0.69315 / TIME
  120 DCY(KACP) = TIME
      KCS     = KCSLOK(ACTAB,ACTYP,1)
      KCSN(KACP) = KCS
      IF(ZAP.EQ.ZA0)                     GO TO  380
      IF(IERR.EQ.0 )                     GO TO  290
      ENRG    = 0.0
      KCC     = KACP - IZNC
      DO  285  KC=KCC,KACP-1
cfm      ENRG    = ENRG+EMEAN(KC)*BETA(KC)                          for Item (2)
      ENRG    = ENRG+EMEAN(KC)*1.0                                   for Item (2)
      IF(KC.GT.KCC)       EMEAN(KC) = 0.0                            for Item (1)
  285 CONTINUE
```

Fig. 4.2.1 Correction of the ACT4 code. Three lines indicated in bold letters are corrected for the items (1) and (2) explained in the main text.

```
Subroutine CHAIN

C
C  2.3  UNIFY THE SAME DECAY BRUNCHES
C
      DO 23 L = 1, LMAX
        IF ( NACT(L).GT. 0)  GO TO 23
        DO 24 LL = L+1, LMAX
          IF( NP(L).NE. NP(LL).OR. ND(L).NE. ND(LL))  GO TO 24
cfm         EBETA(L)  = RATIO(L)*EBETA(L) + RATIO(LL)*EBETA(LL)      for Item (3)
            EBETA(L)  = 1.0      *EBETA(L) + 1.0       *EBETA(LL)    for Item (3)
            RATIO(L)  = RATIO(L) + RATIO(LL)
            RATIO(LL) = -1.
   24   CONTINUE
   23 CONTINUE
C


C
C  SECTION 08 --- SET GLOBAL TABLE
C
C                                          "LOCAL NUCLIDE TABLE SET"
      DO 1300 L = 1, N2
        N       = LTAB(L)
        PTAB(L) = PROB(N)
cfm     ETAB(L) = RATIO(N)*EBETA(N)                                  for Item (3)
        ETAB(L) = 1.0      *EBETA(N)                                 for Item (3)
        NN      = LCTAB(N)
 1305   IF( NN.LE. 0)  GO TO 1300
cfm       ETAB(L) = ETAB(L) + RATIO(NN)*EBETA(NN)                    for Item (3)
          ETAB(L) = ETAB(L) + 1.0      *EBETA(NN)                    for Item (3)
          NN      = LCTAB(NN)
          GO TO 1305
 1300 CONTINUE


Subroutine CHAIN

C                                            "READ CROSSLIB HEADERS
  145 READ(IN2,550,END=165) NCS, IX
cfm  550 FORMAT(A8,4X,I12)                                           for Item (4)
  550 FORMAT(A12,I12)                                                for Item (4)
      CALL  DECOMP(NCS,IFLG)
      KASW=0
      IF( NCS(1:6).EQ. ACTCS(1:6))  GO TO 150
CRC   IF( NCS(1:NL).EQ. ACTCS(1:NL))  GO TO 150
```

Fig. 4.2.2 Correction of the CINAC code. Lines indicated in bold letters are corrected for the items (3) and (4) explained in the main text.

```
Decay Heat Calculation for S6n5m
          1M          5M          5M          1Y          2Y          3Y
          5M
   125     1     1     1    30    54    20     1     0     0     0
     0     0     0     0     0     0     0     0     0
     1    -2     0     0     0    -1    -1    -1     0     0
     1     1     1     1     1
    -1
 0.00000E+00 5.63400E+17    1.0       0.0         0.0         0.0
         68S         84S        100S        127S        165S        202S
        256S        323S        390S        488S        615S        742S
        866S       1054S       1301S       1549S       1796S       2224S
       2828S       3433S
    T
9$$   101
10$$  3R14  4R24   1R25   4R26   5R28  7R42  6R101
11$$  14028  14029  14030
        24050  24052  24053  24054
        25055
        26054  26056  26057  26058
        28058  28060  28061  28062  28064
        42092  42094  42095  42096  42097  42098  42000
        14     24     25     26     28     42
12**  0.92230  0.04670  0.031
      0.04345  0.83789  0.09501  0.02365
      1.0
      0.058    0.9172   0.022    0.0028
      0.68077  0.26223  0.0114   0.03634  0.00926
      0.1484   0.0925   0.1592   0.1668   0.0955   0.2413   0.0963
      0.000206 0.002117 0.000172 0.006857 0.001384 0.000132
  T
  .00000E+00  .00000E+00  .00000E+00  .00000E+00 9.74737E-04 3.37950E-03
 6.01890E-03 5.80615E-03 1.19424E-03 6.18188E-05 3.75713E-05 3.53414E-05
 2.53093E-05 2.16951E-05 1.95574E-05 1.91174E-05 1.89979E-05 1.65869E-05
 1.43984E-05 1.26737E-05 1.12327E-05 1.13687E-05 1.05252E-05 1.05184E-05
 1.07456E-05 1.02566E-05 1.04205E-05 1.08905E-05 9.45644E-06 7.07446E-06
 7.58317E-06 7.12786E-06 3.04811E-05 3.32071E-05 3.42508E-05 3.48089E-05
 3.59499E-05 3.78058E-05 3.53280E-05 3.39480E-05 3.57466E-05 3.64582E-05
 3.54441E-05 3.78112E-05 3.89723E-05 3.83901E-05 3.99996E-05 3.96730E-05
 3.93764E-05 4.01221E-05 3.85782E-05 3.96573E-05 3.99840E-05 3.93376E-05
 3.83720E-05 3.85395E-05 3.85866E-05 3.86546E-05 3.65899E-05 3.78153E-05
 7.25269E-05 7.23097E-05 7.02661E-05 6.56051E-05 6.16569E-05 5.68757E-05
 5.31442E-05 4.96293E-05 4.43549E-05 3.99064E-05 3.64530E-05 3.28957E-05
 3.02212E-05 2.73941E-05 2.42713E-05 2.15909E-05 1.81971E-05 1.71505E-05
 1.46618E-05 1.19825E-05 1.29585E-05 1.08519E-05 9.64730E-06 7.90902E-06
 8.93364E-06 7.95152E-06 6.51978E-06 6.35771E-06 5.65050E-06 5.15421E-06
 4.68296E-06 4.54980E-06 5.32531E-06 3.97499E-06 4.18717E-06 3.88869E-06
 6.63486E-06 6.32866E-06 4.92552E-06 4.83856E-06 4.72670E-06 4.02094E-06
 3.86112E-06 3.49468E-06 2.77506E-06 2.60939E-06 2.54641E-06 2.23727E-06
 3.76146E-06 3.16599E-06 2.82212E-06 2.36092E-06 1.82614E-06 1.62513E-06
 1.30479E-06 1.15175E-06 7.95374E-07 7.70706E-07 6.65969E-07 5.48066E-07
 4.47285E-07 3.84068E-07 2.71660E-07 1.76231E-07 1.40760E-06
GAMMA
     1     2     0
END
```

Fig. 4.4.1 Input data of the ACT4 code for the calculation of SS-316 samples irradiated for 5 minutes.

```
CINAC-V4 Decay Heat CALC. S6n5m
     2     0     1     1     1     1    30   125   -54    20
     1     1     0     0     0     0
      0.056606   1.0E+00     0
9$$   101
10$$  3R14  4R24   1R25   4R26   5R28  7R42  6R101
11$$  14028  14029  14030
        24050  24052  24053  24054
        25055
        26054  26056  26057  26058
        28058  28060  28061  28062  28064
        42092  42094  42095  42096  42097  42098  42000
        14     24     25     26     28     42
12**  0.92230  0.04670  0.031
      0.04345  0.83789  0.09501  0.02365
      1.0
      0.058    0.9172   0.022    0.0028
      0.68077  0.26223  0.0114   0.03634  0.00926
      0.1484   0.0925   0.1592   0.1668   0.0955   0.2413   0.0963
      0.000206 0.002117 0.000172 0.006857 0.001384 0.000132
  T
     1     1     1     1     1
     0
    -1     0     0     0     0
     1     1     1
 P1  STEP  300   1    5.63400E+17
 LAST P1
    END
68
84
100
127
165
202
256
323
390
488
615
742
866
1054
1301
1549
1796
2224
2828
3433
```

Fig. 4.4.2 Input data of the CINAC code for the calculation of SS-316 samples irradiated for 5 minutes.

BORON CARBIDE (B4C)

5 Minutes Irradiation

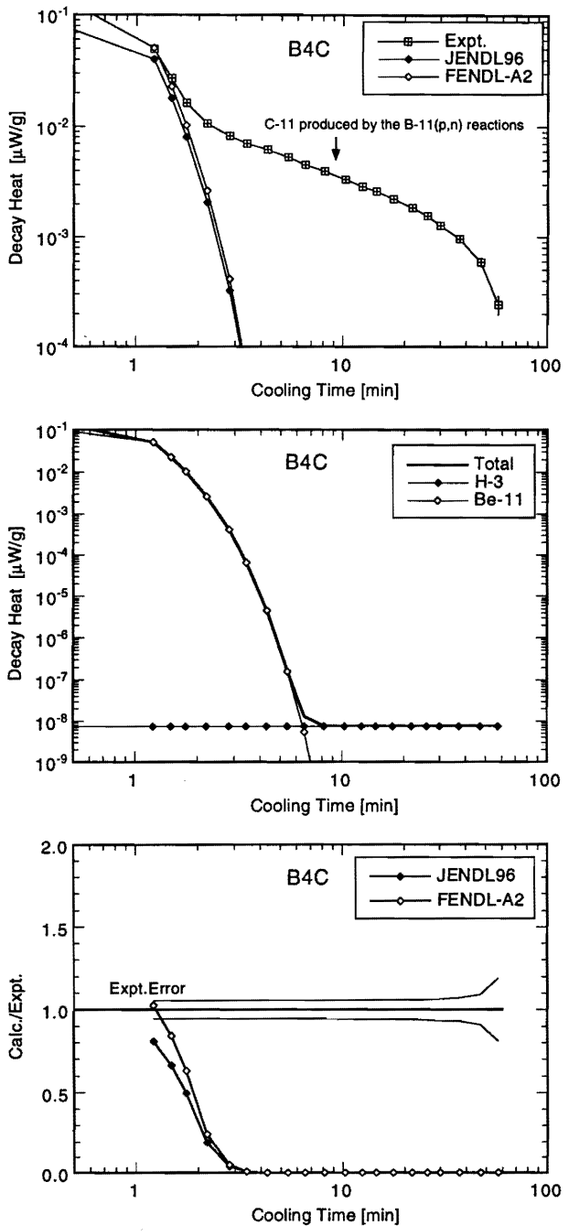

7 Hours Irradiation

No experimentally observed decay heat.

Fig. 5.1.1 Results for the B4C sample with the ACT4 code for the 5 minutes irradiation.

Polytetrafluoroethylene (PTFE, CF2)

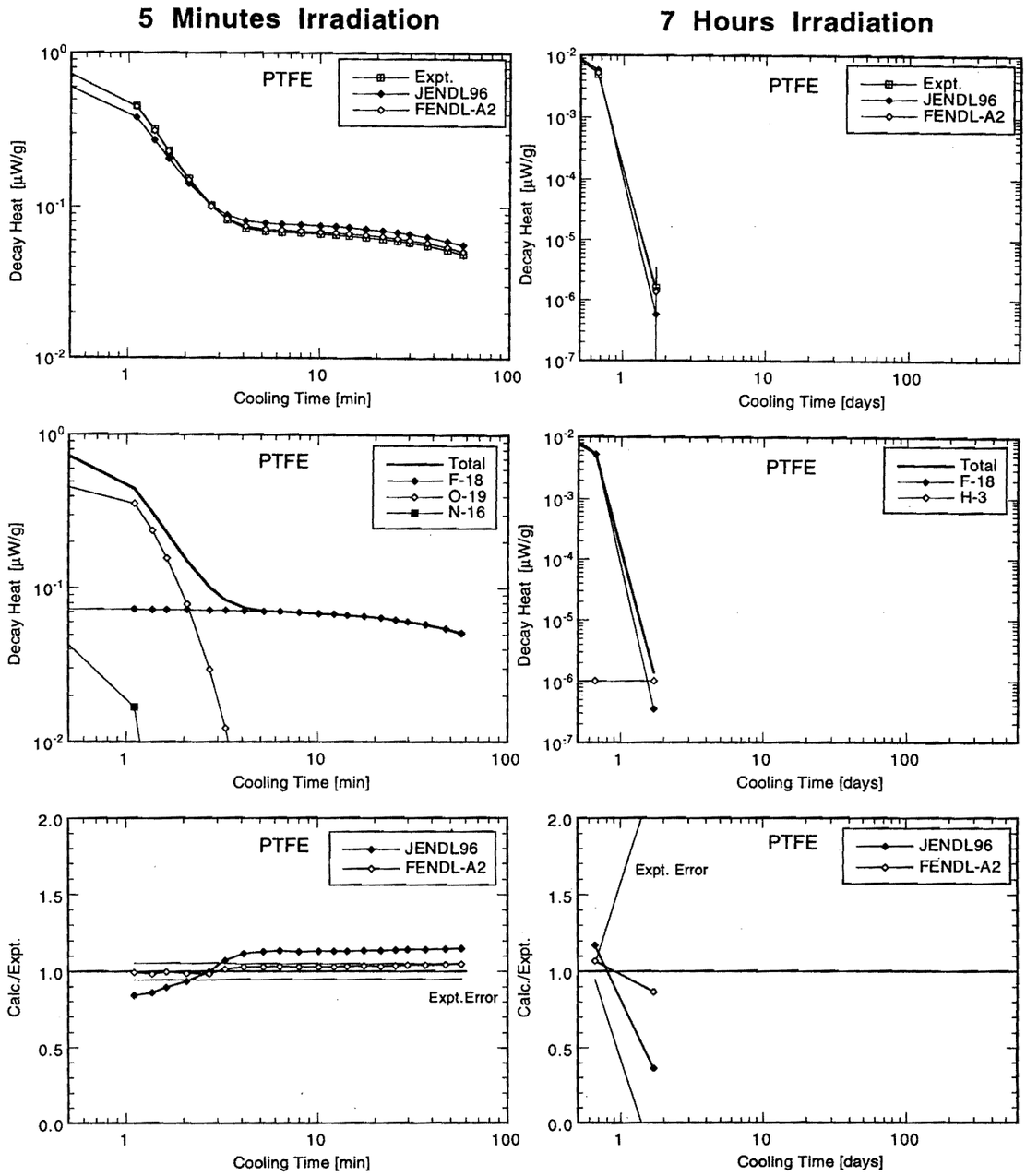

Fig. 5.1.2 Results for the PTFE (CF2) sample with the ACT4 code.

SODIUM CARBONATE (Na2CO3)

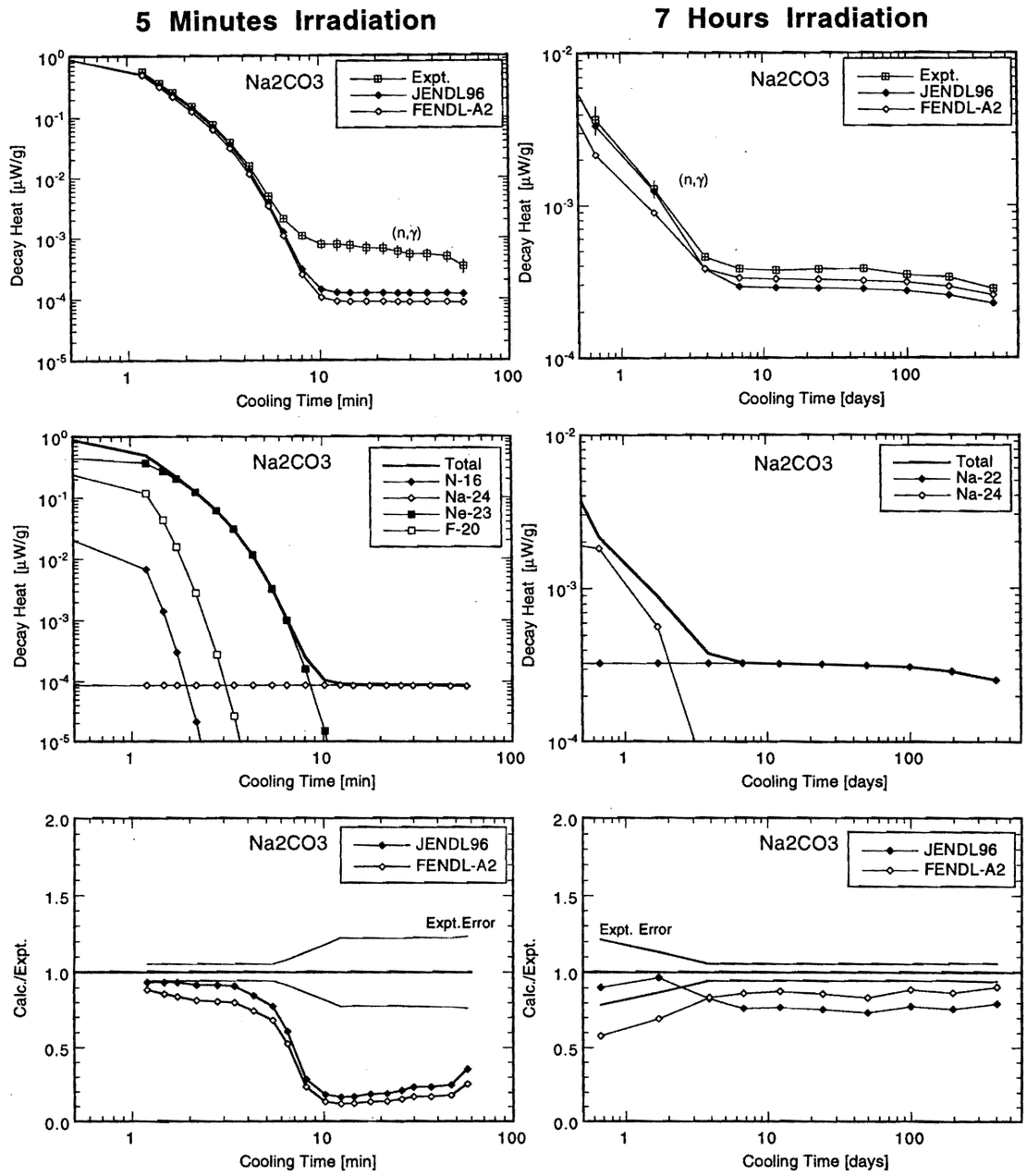

Fig. 5.1.3 Results for the Na2CO3 sample with the ACT4 code.

ALUMINUM

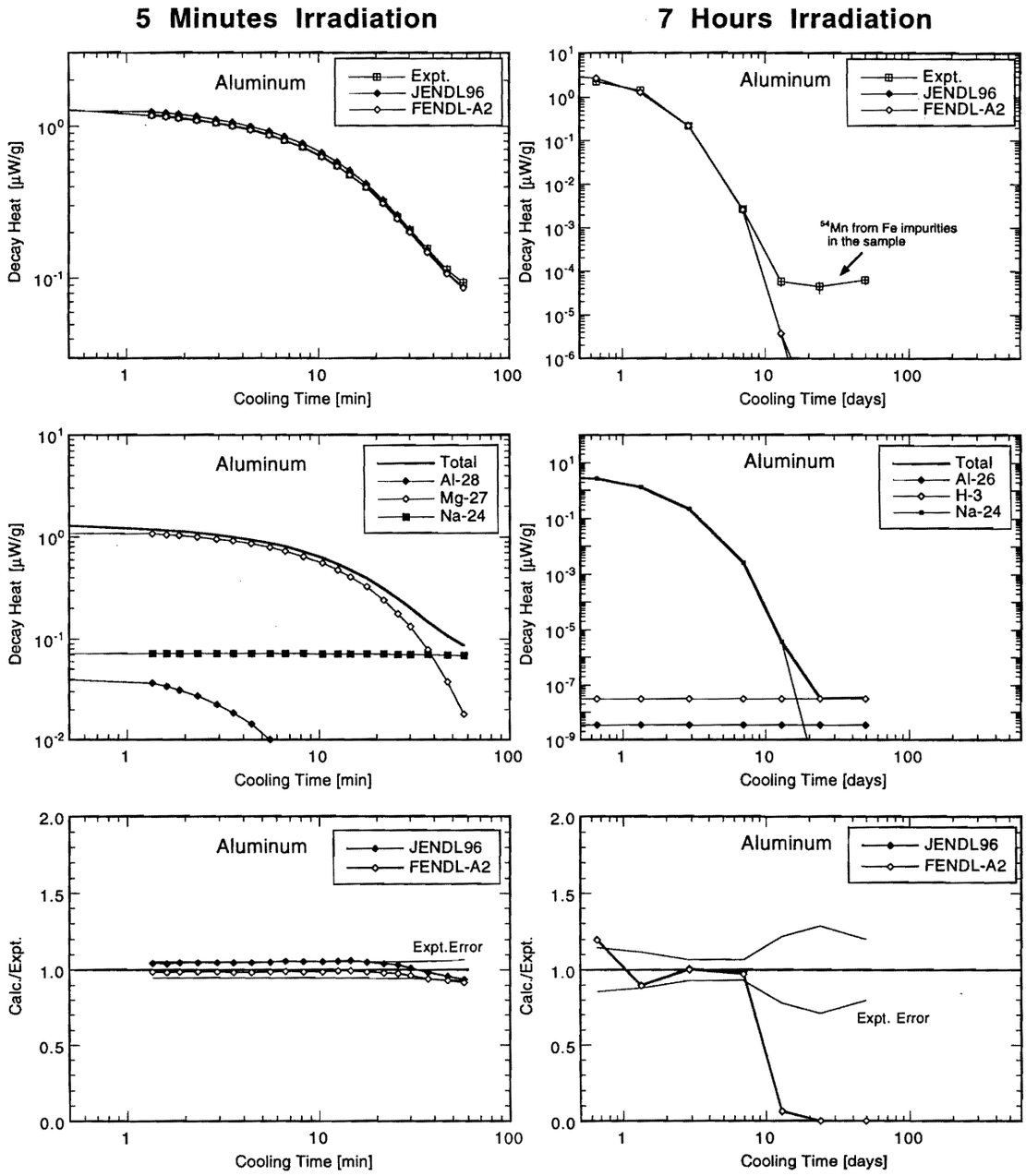

Fig. 5.1.4 Results for the aluminum sample with the ACT4 code.

SILICON DIOXIDE (SiO2)

5 Minutes Irradiation

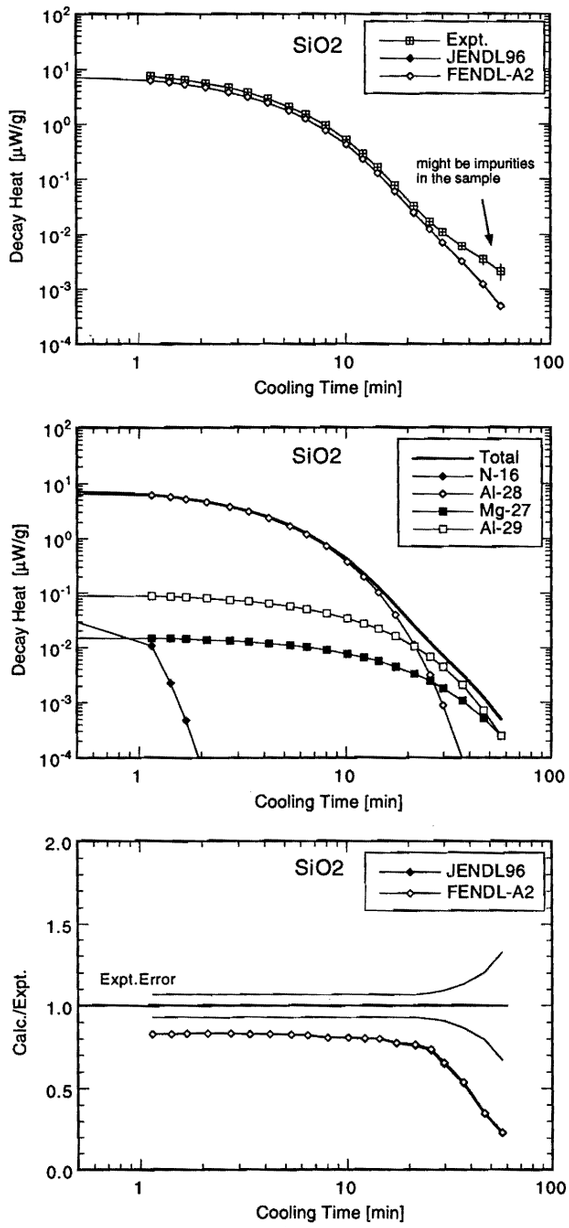

7 Hours Irradiation

No experimentally observed decay heat.

Fig. 5.1.5 Results for the SiO2 sample with the ACT4 code for the 5 minutes irradiation.

SULFUR

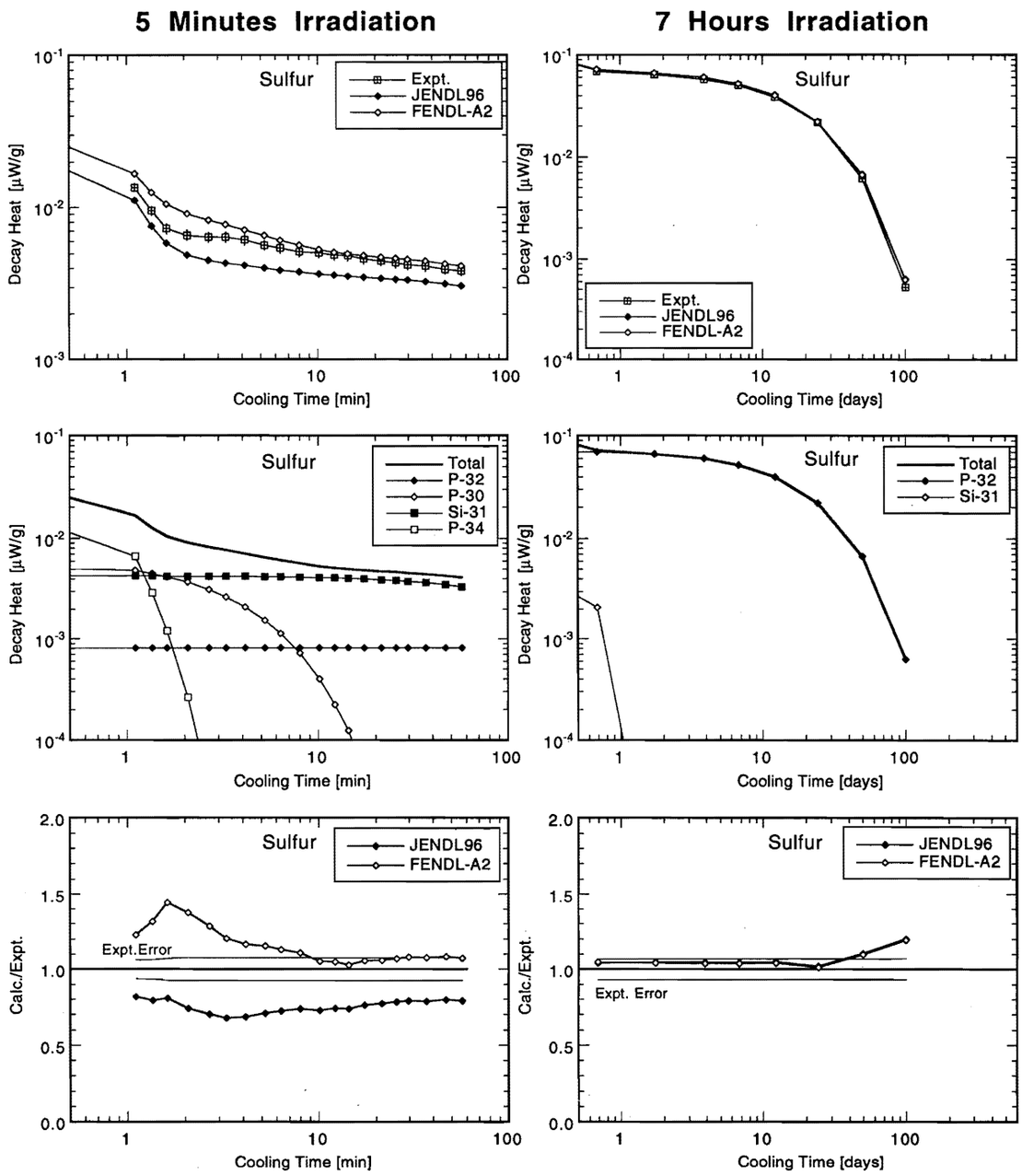

Fig. 5.1.6 Results for the sulfur sample with the ACT4 code.

POTASSIUM CARBONATE (K2CO3)

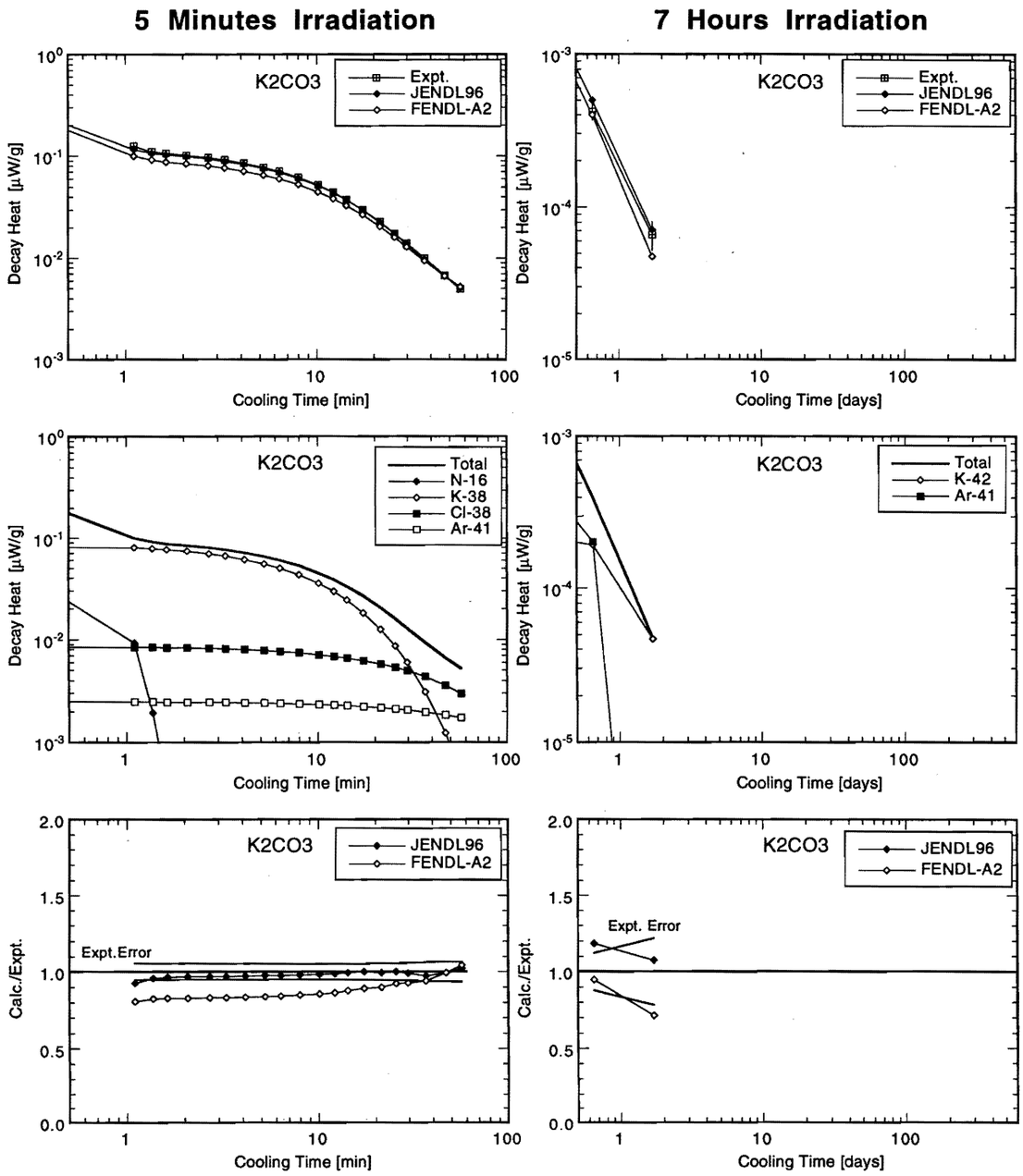

Fig. 5.1.7 Results for the K2CO3 sample with the ACT4 code.

CALCIUM OXIDE (CaO)

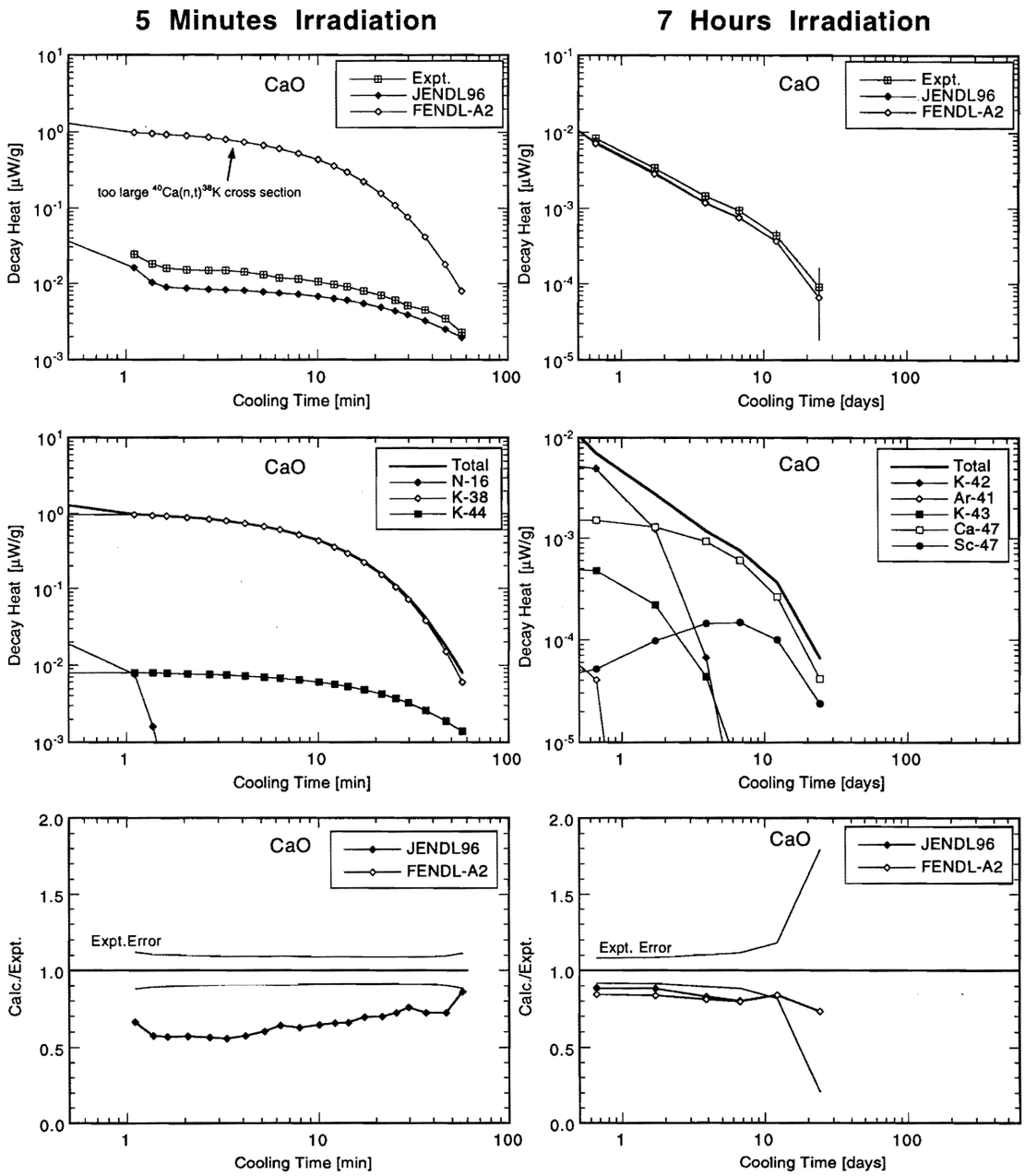

Fig. 5.1.8 Results for the CaO sample with the ACT4 code.

TITANIUM

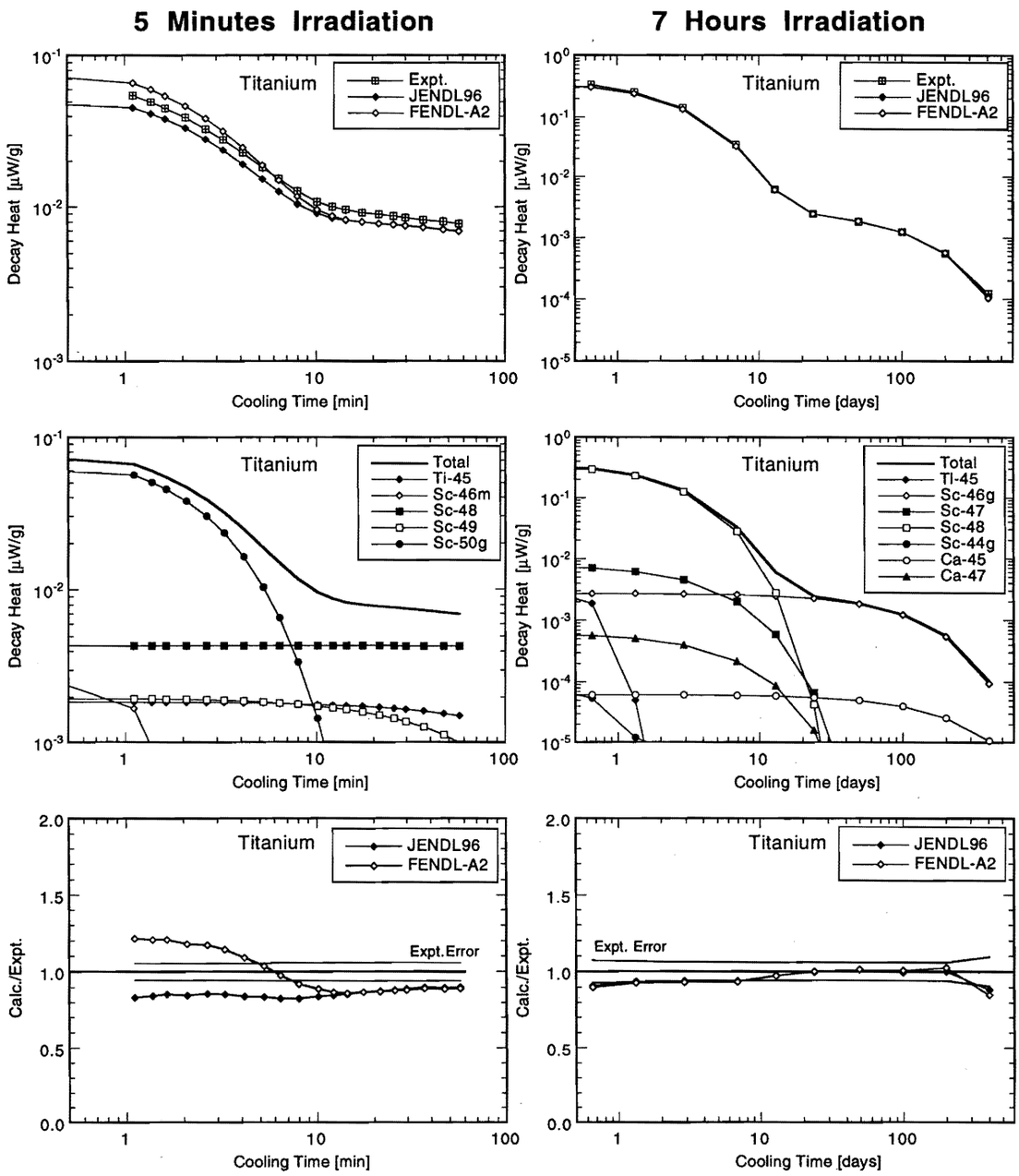

Fig. 5.1.9 Results for the titanium sample with the ACT4 code.

VANADIUM

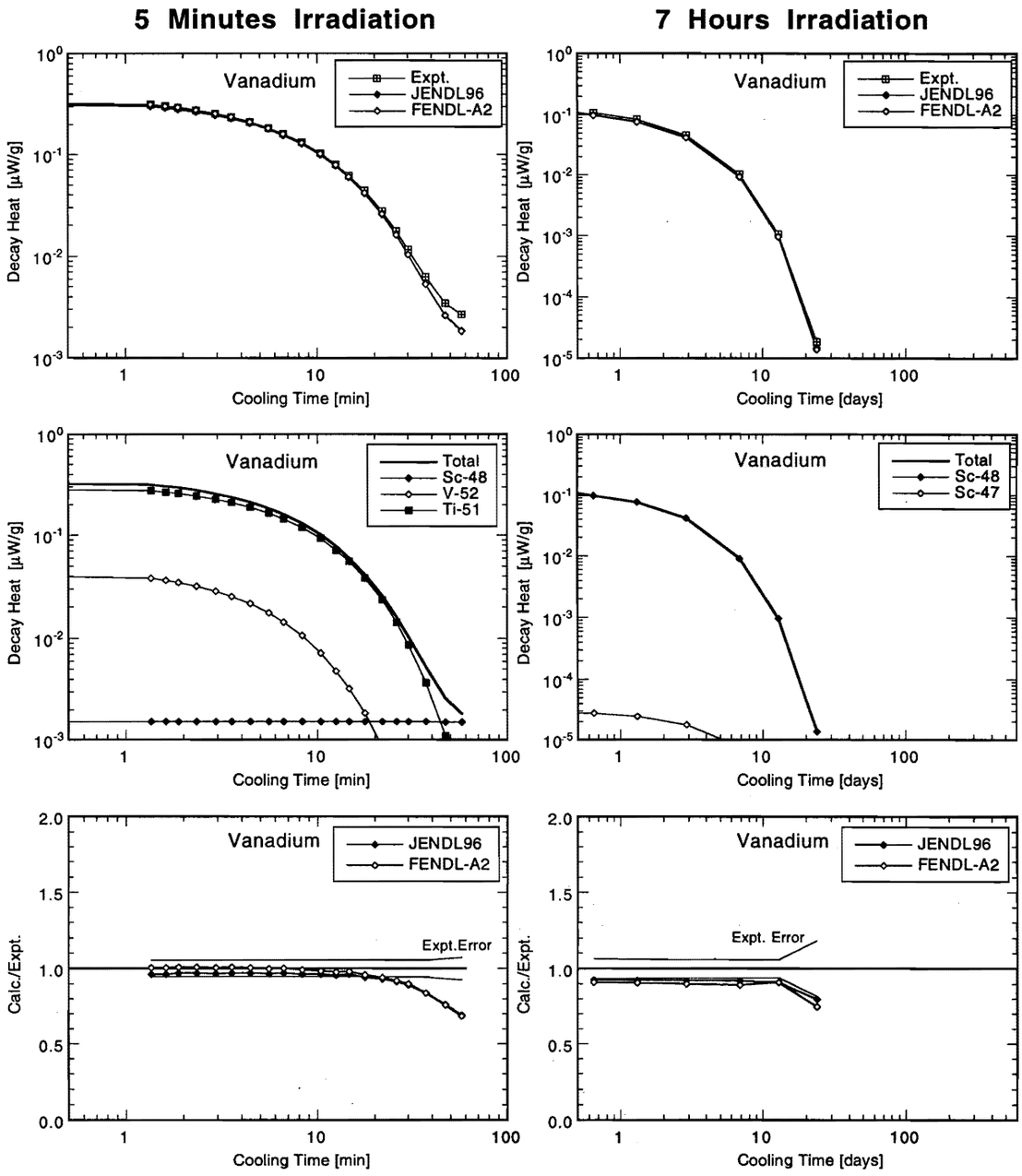

Fig. 5.1.10 Results for the vanadium sample with the ACT4 code.

CHROMIUM

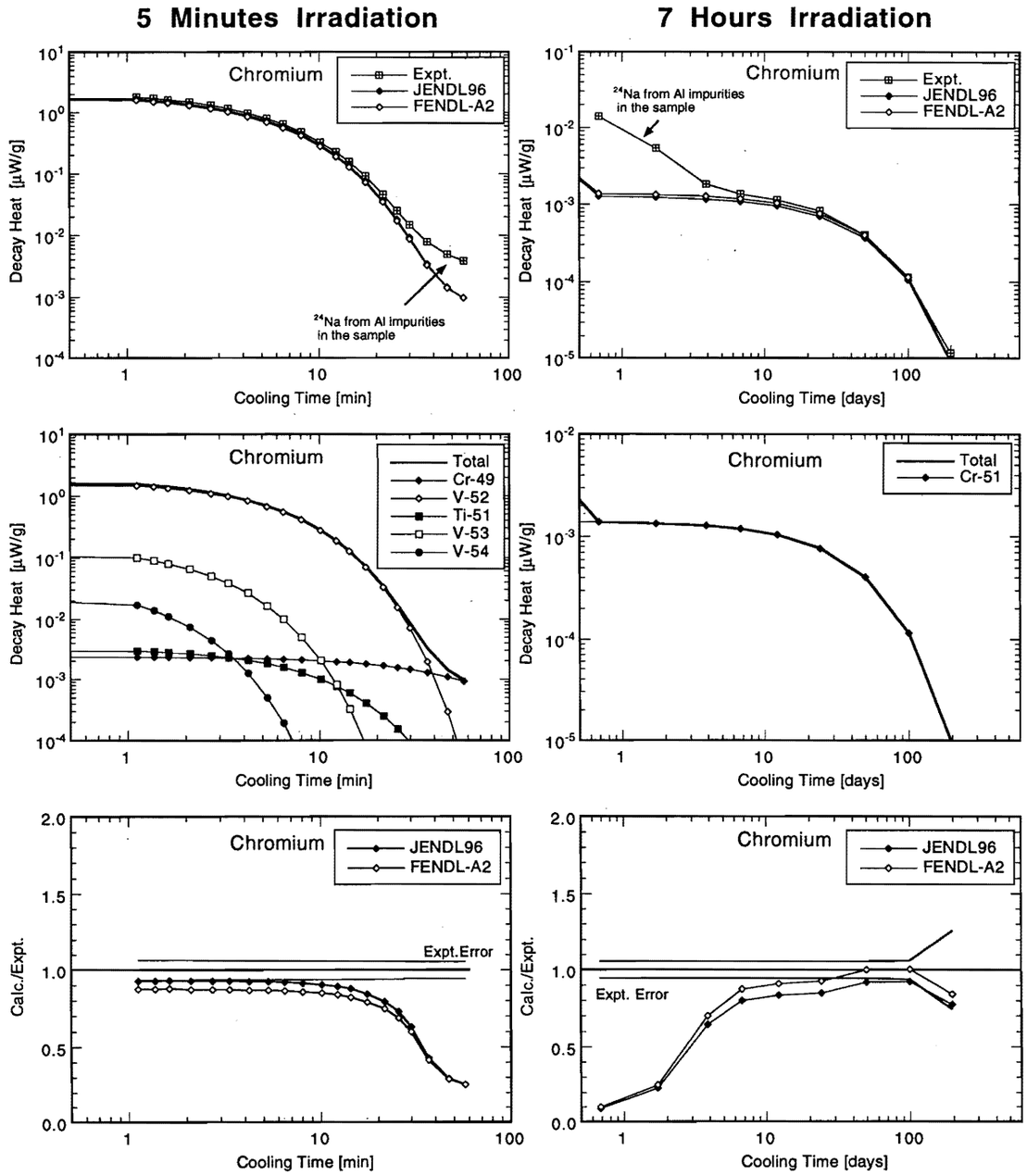

Fig. 5.1.11 Results for the chromium sample with the ACT4 code.

MANGANESE

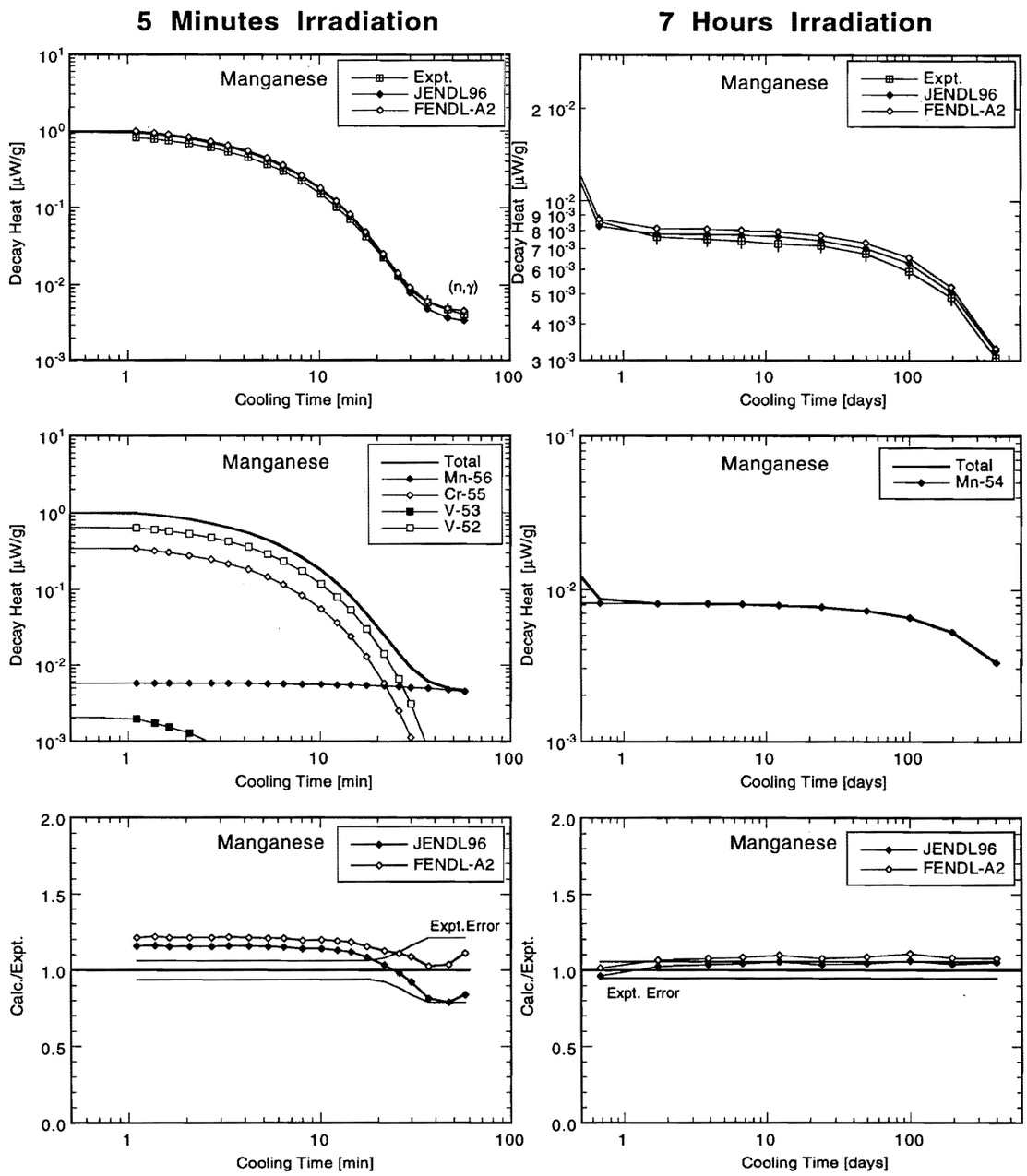

Fig. 5.1.12 Results for the manganese sample with the ACT4 code.

IRON

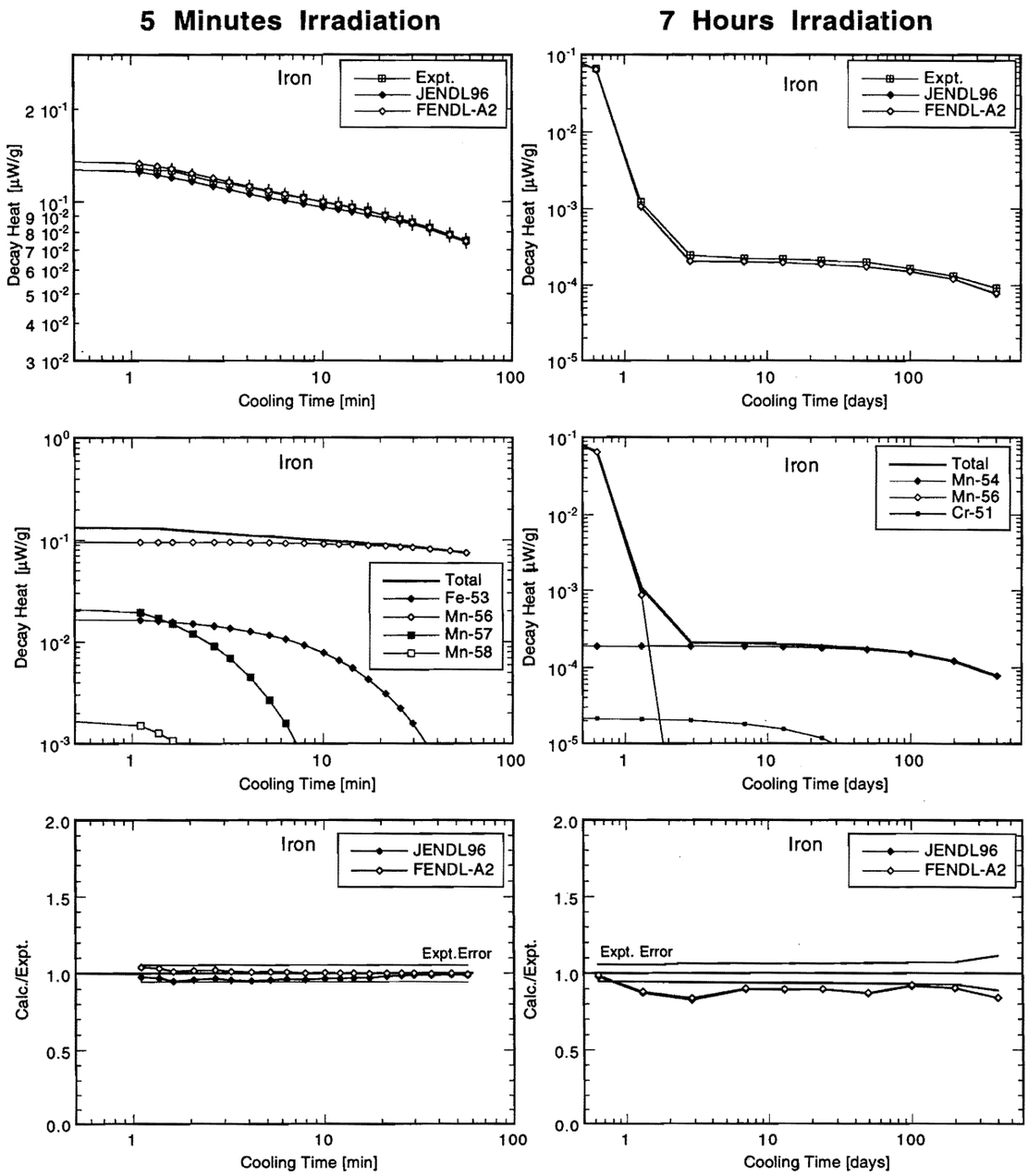

Fig. 5.1.13 Results for the iron sample with the ACT4 code.

COBALT

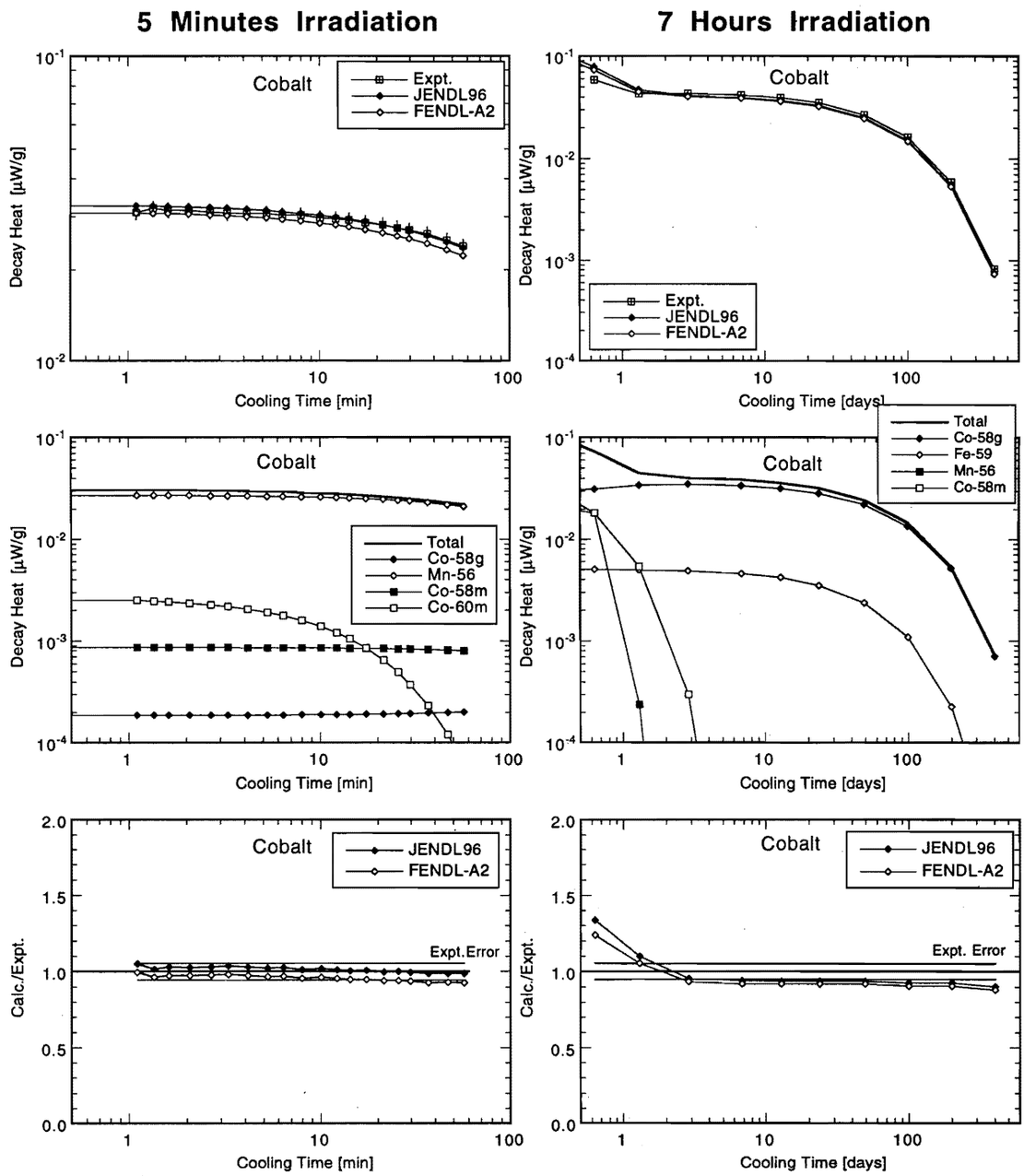

Fig. 5.1.14 Results for the cobalt sample with the ACT4 code.

NICKEL

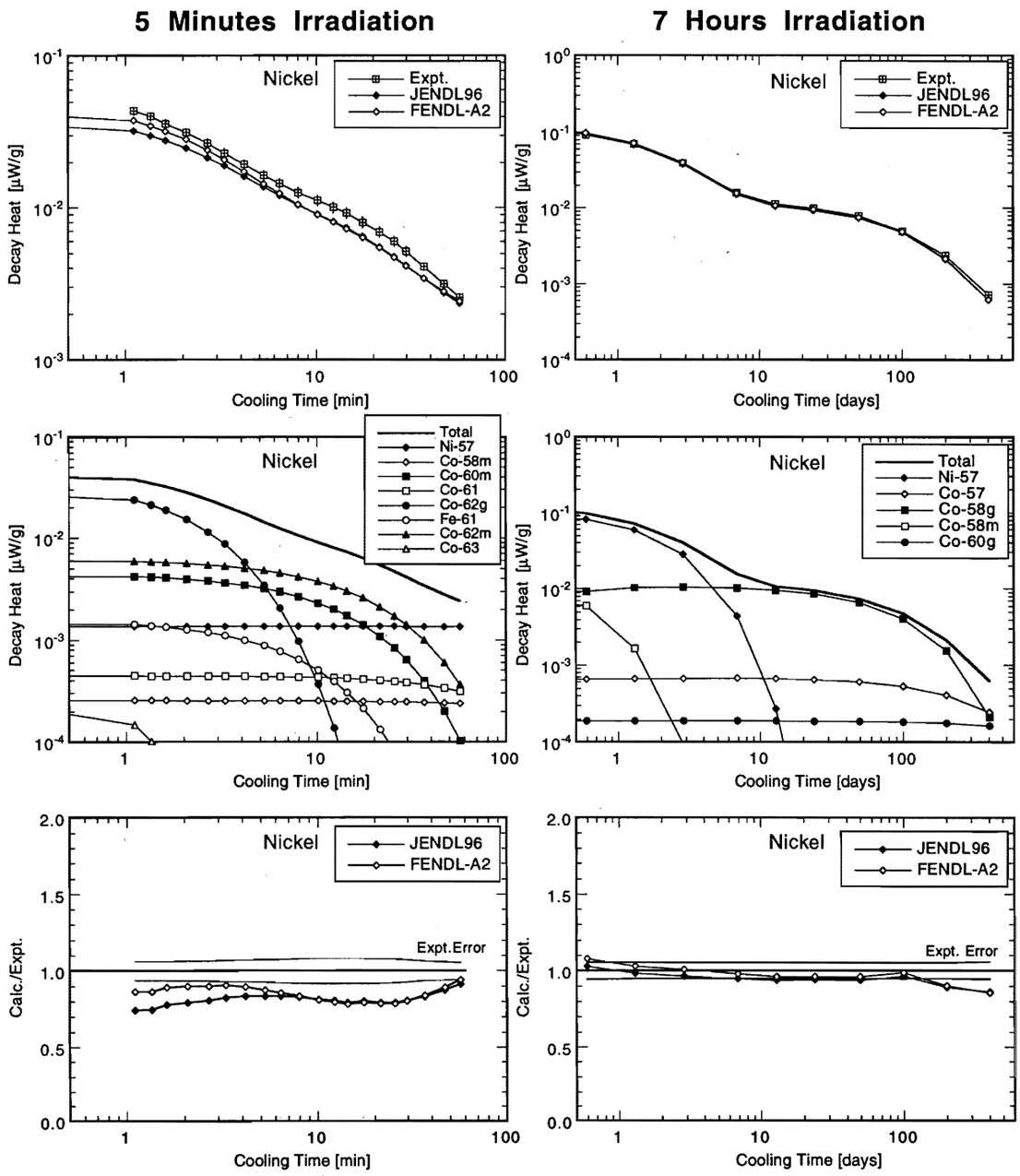

Fig. 5.1.15 Results for the nickel sample with the ACT4 code.

COPPER

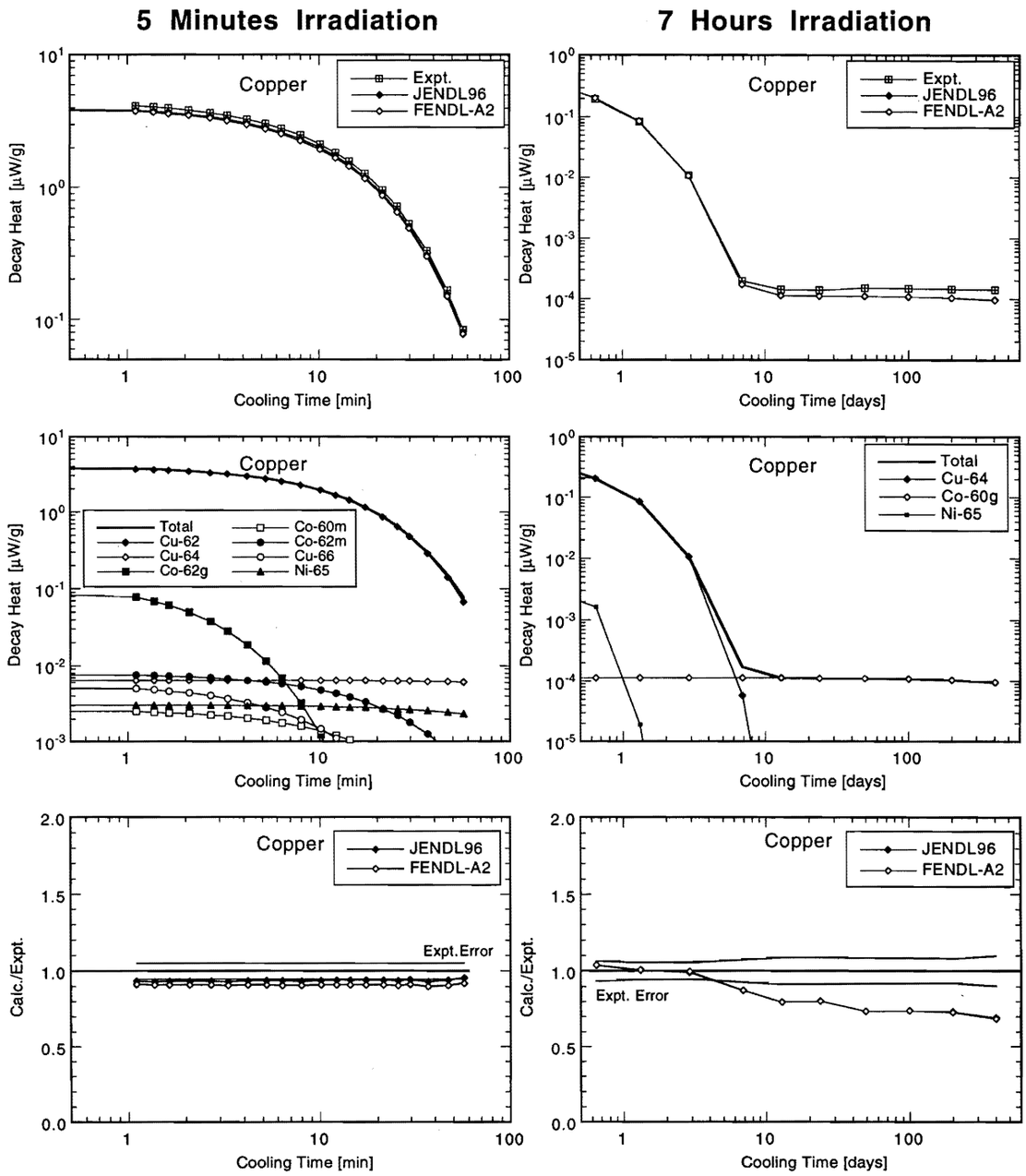

Fig. 5.1.16 Results for the copper sample with the ACT4 code.

STRONTIUM CARBONATE (SrCO3)

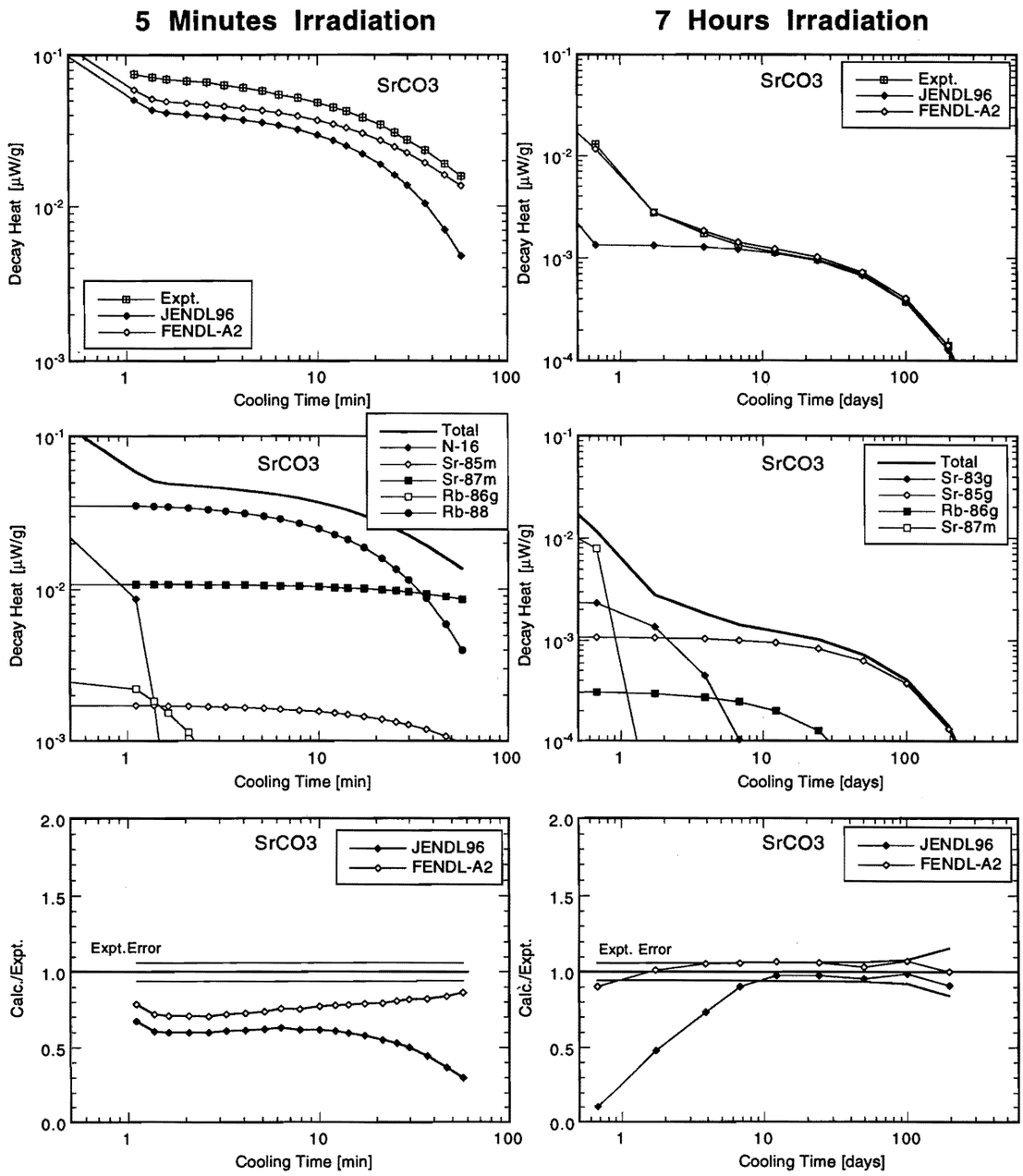

Fig. 5.1.17 Results for the SrCO3 sample with the ACT4 code.

YTTRIUM OXIDE (Y2O3)

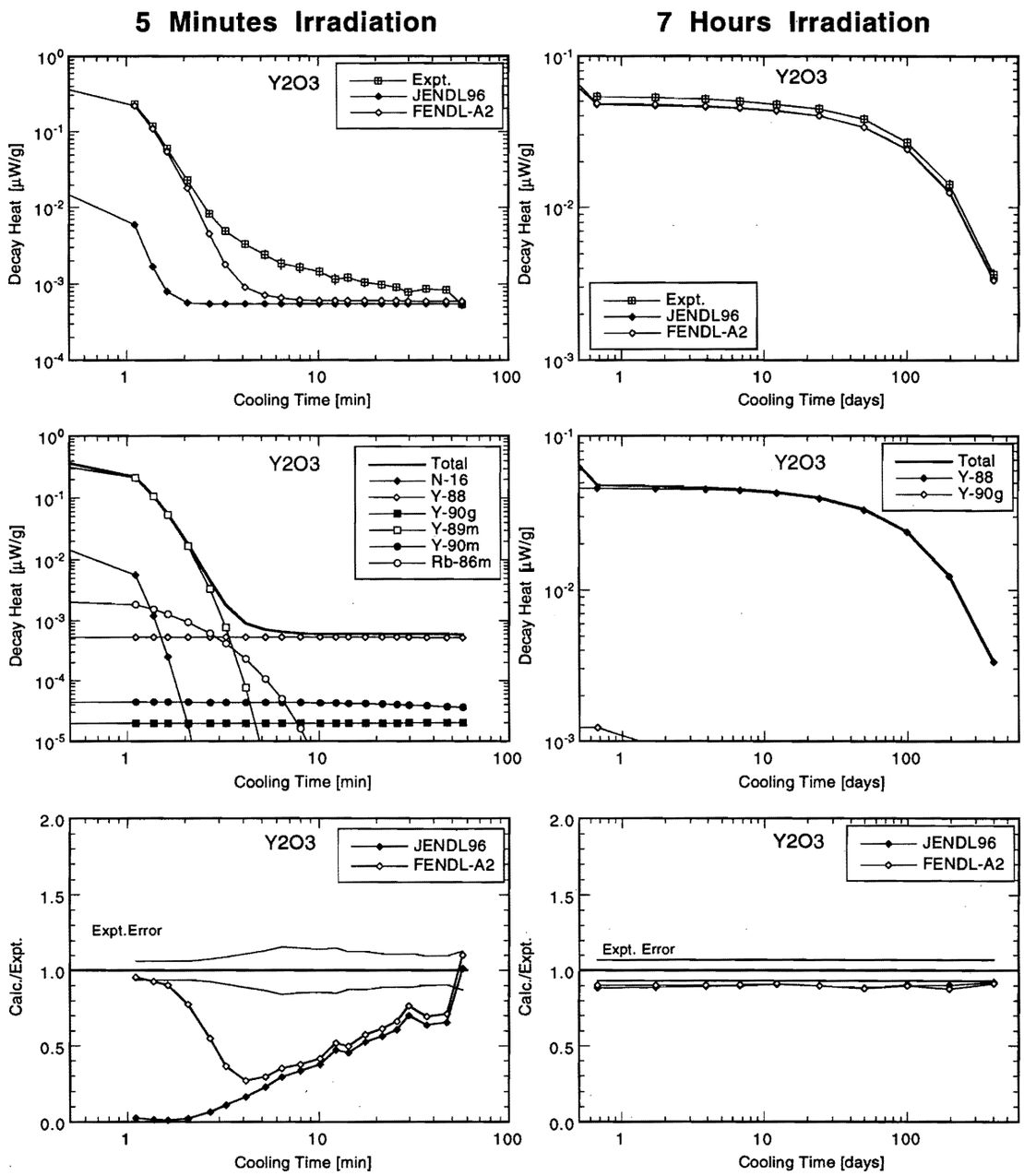

Fig. 5.1.18 Results for the Y2O3 sample with the ACT4 code.

ZIRCONIUM

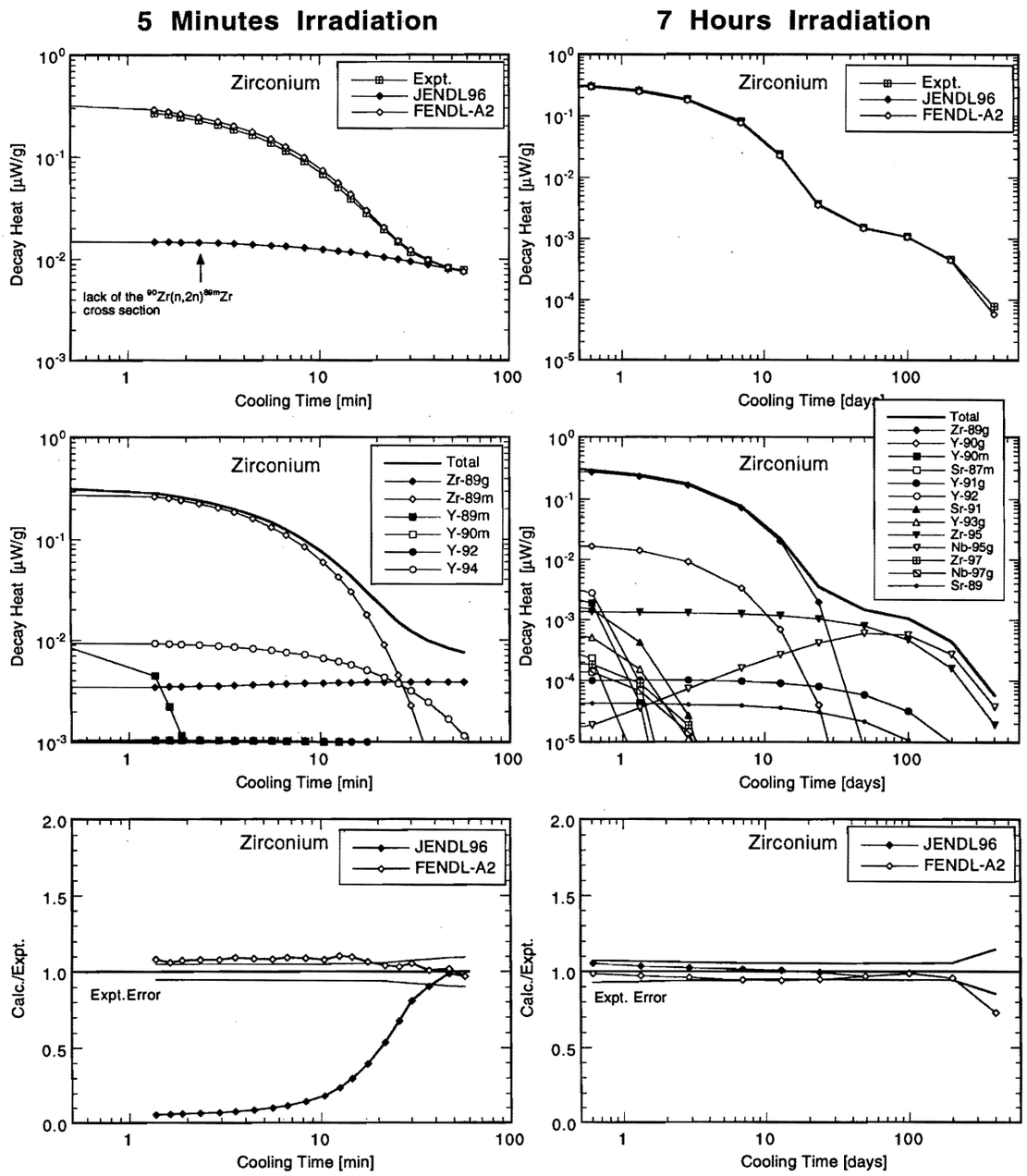

Fig. 5.1.19 Results for the zirconium sample with the ACT4 code.

NIOBIUM

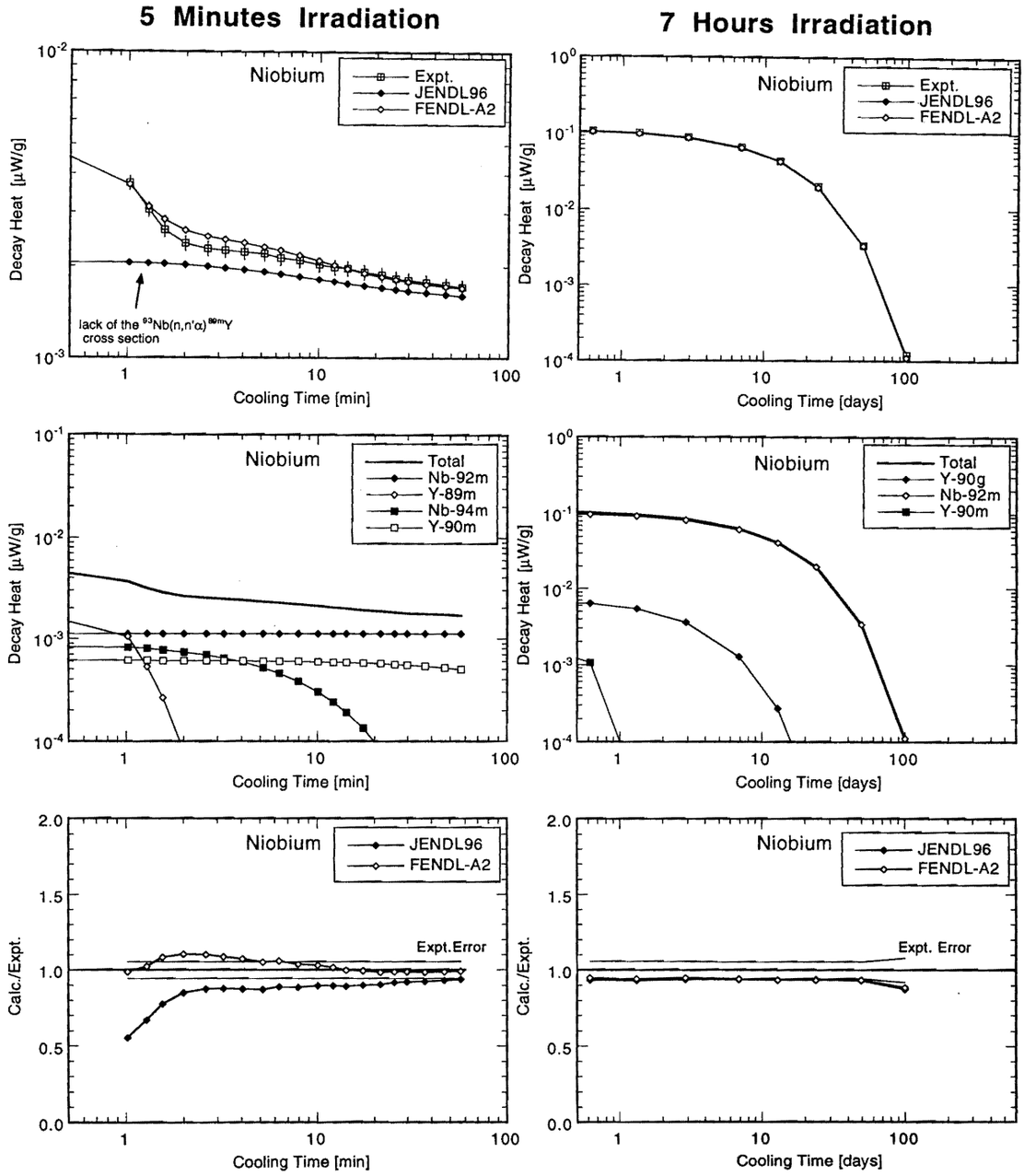

Fig. 5.1.20 Results for the niobium sample with the ACT4 code.

MOLYBDENUM

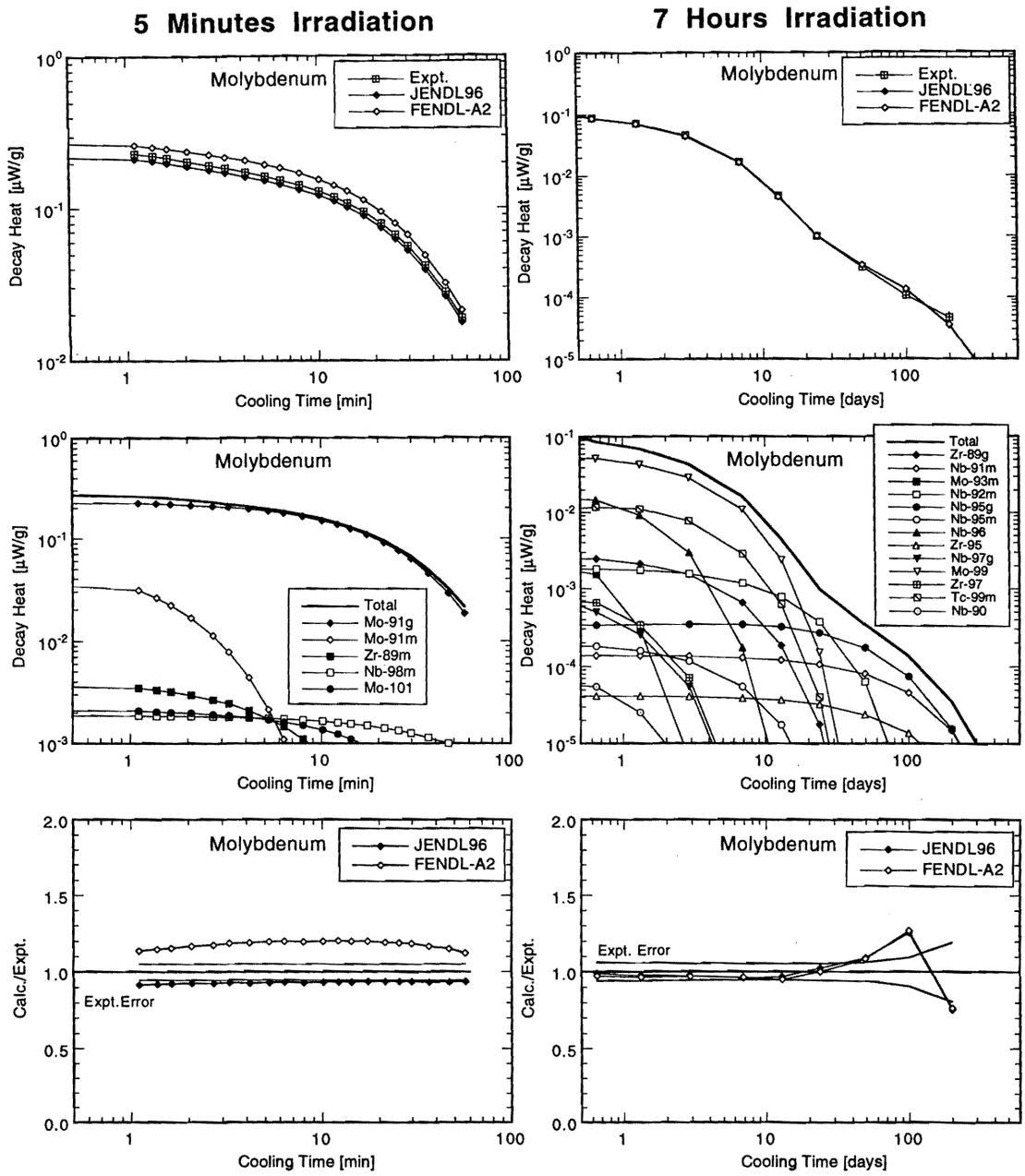

Fig. 5.1.21 Results for the molybdenum sample with the ACT4 code.

TIN DIOXIDE (SnO2)

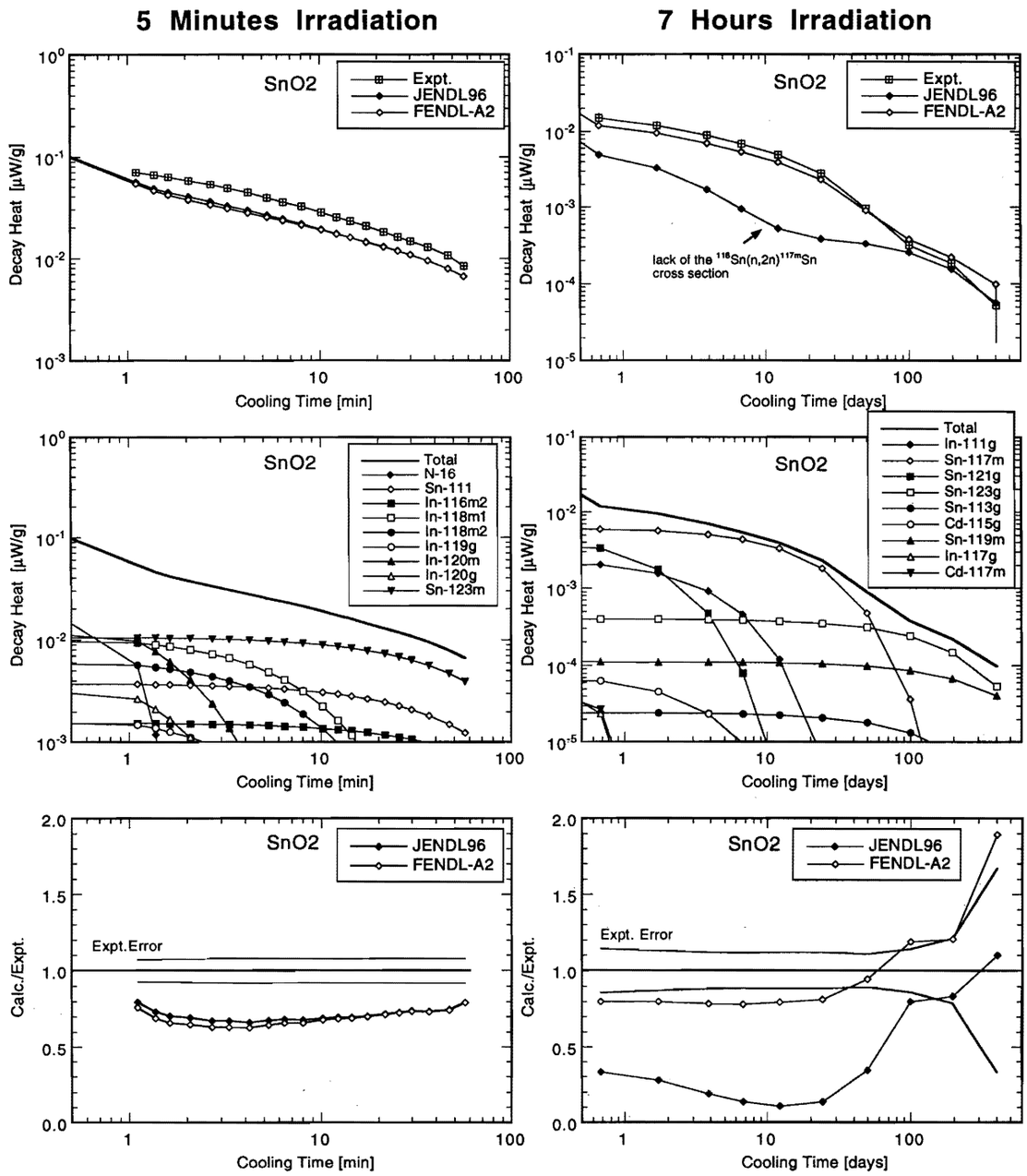

Fig. 5.1.22 Results for the SnO2 sample with the ACT4 code.

BARIUM CARBONATE (BaCO3)

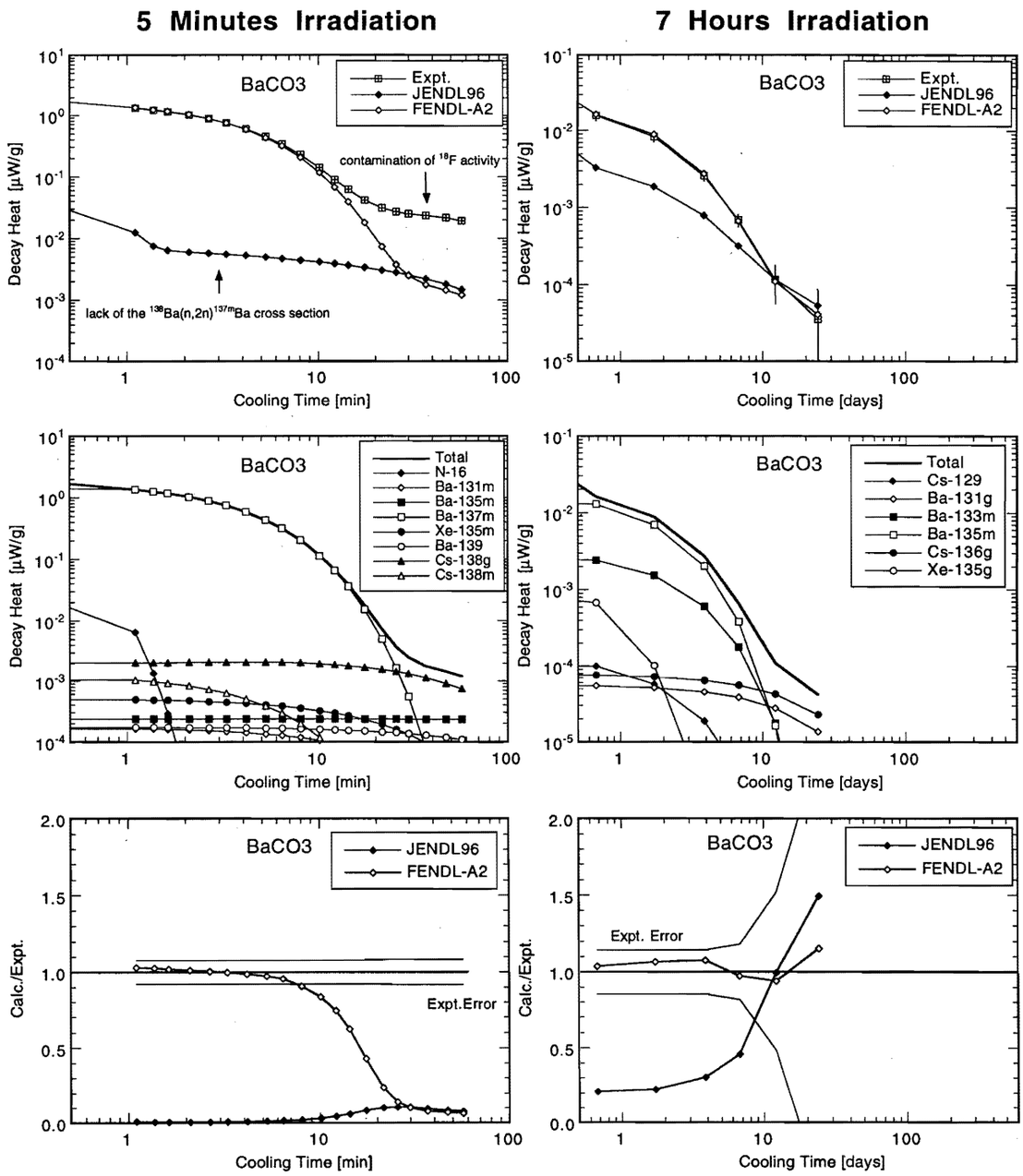

Fig. 5.1.23 Results for the BaCO3 sample with the ACT4 code.

TANTALUM

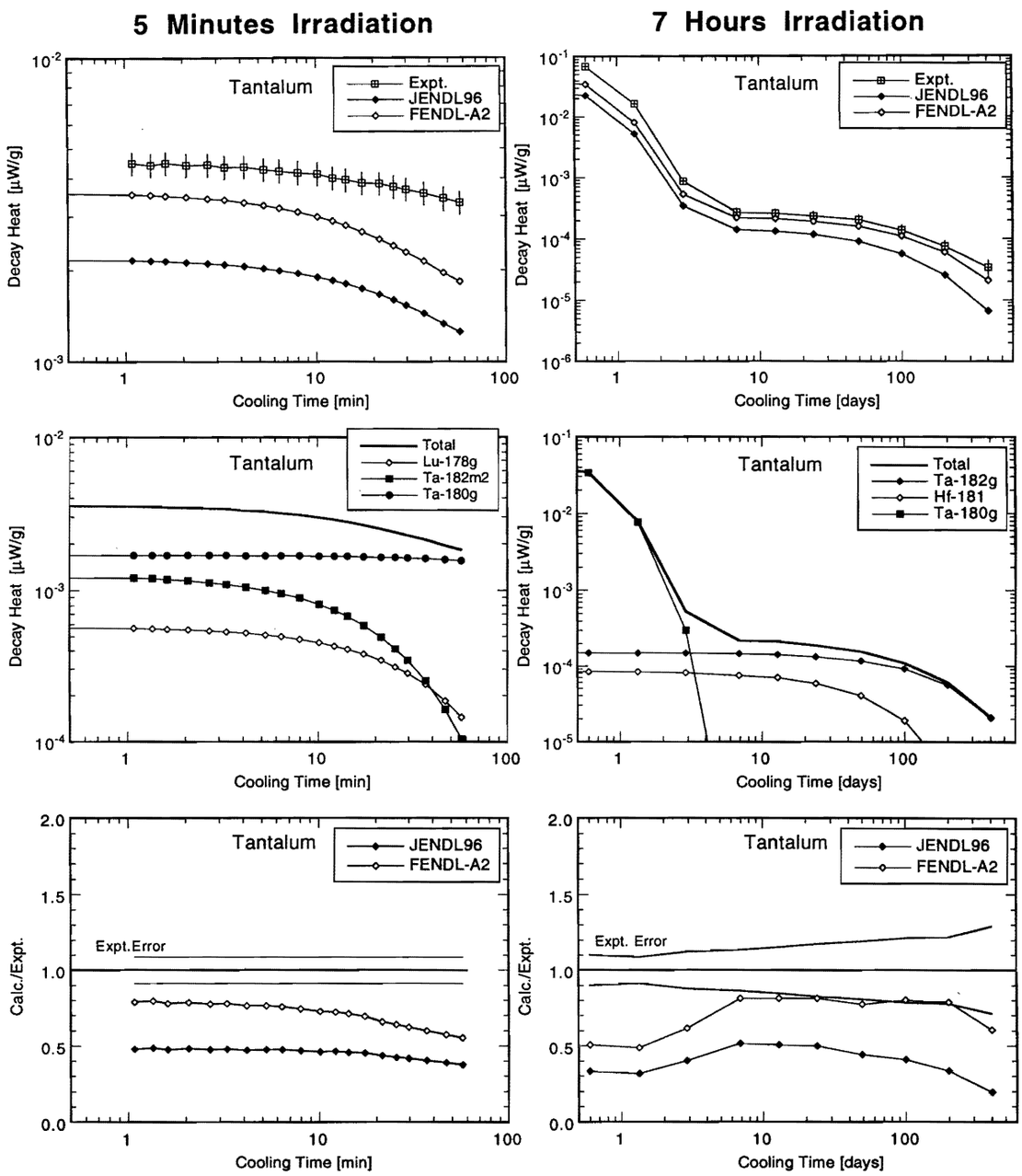

Fig. 5.1.24 Results for the tantalum sample with the ACT4 code.

TUNGSTEN

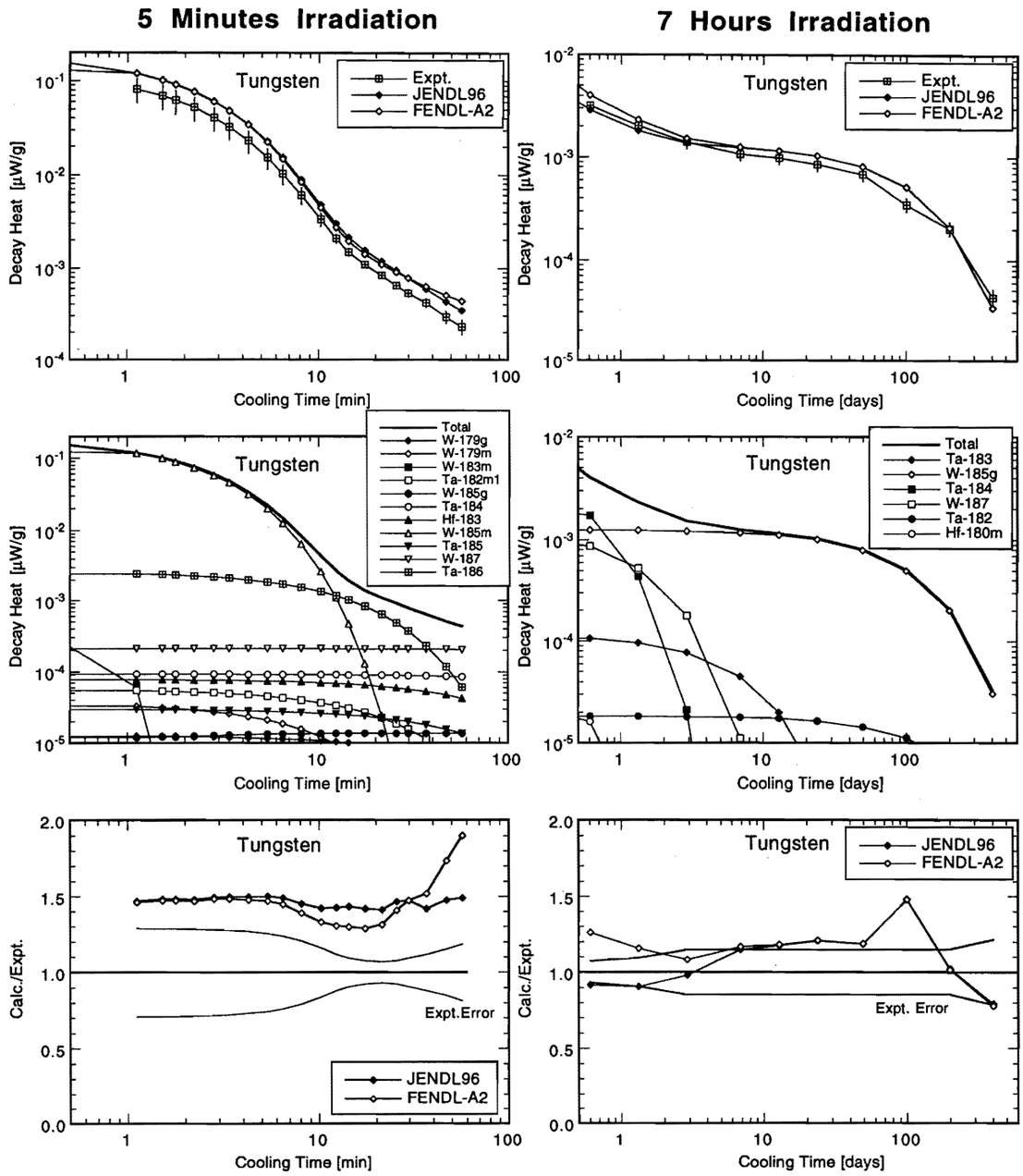

Fig. 5.1.25 Results for the tungsten sample with the ACT4 code.

RHENIUM

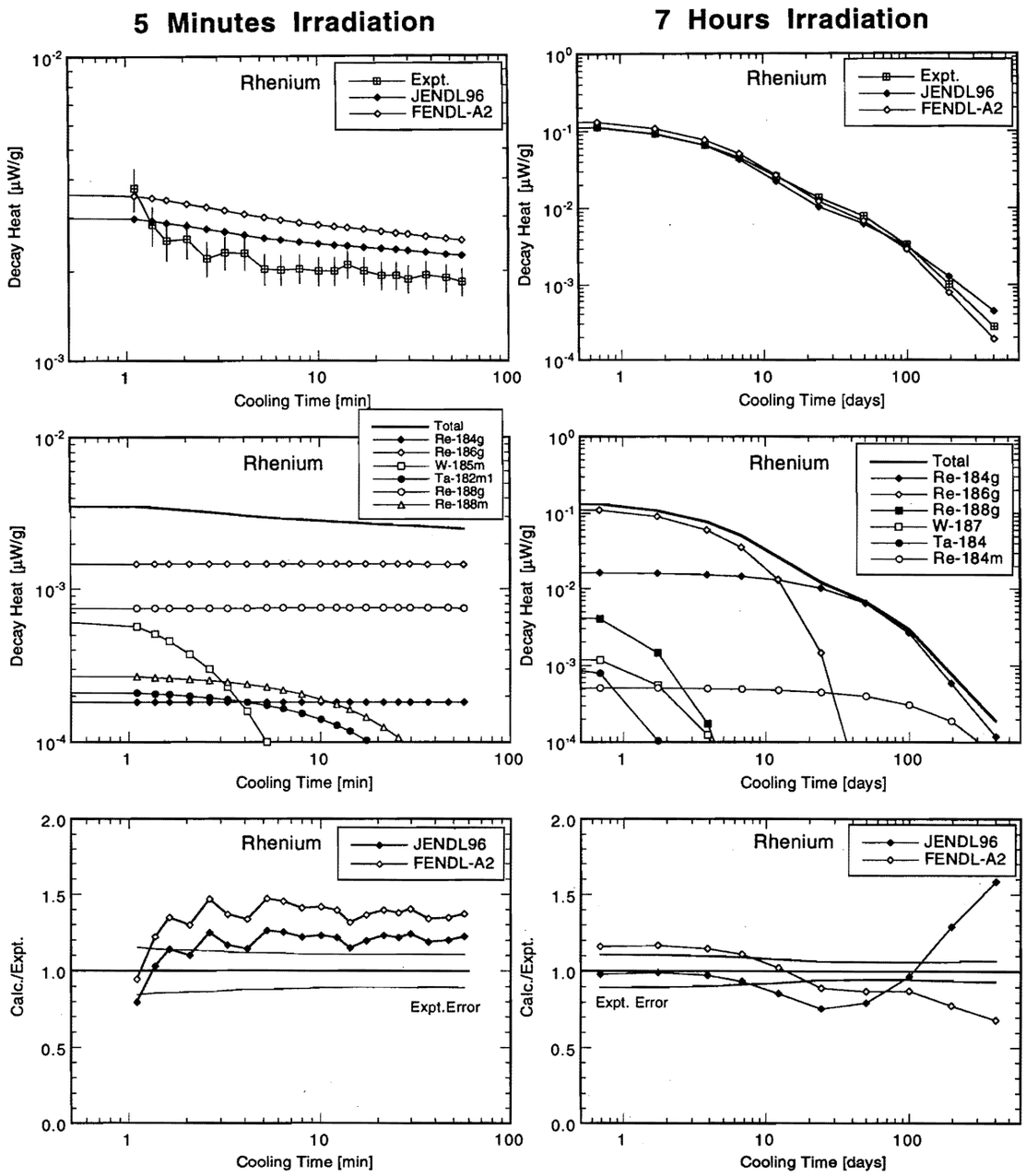

Fig. 5.1.26 Results for the rhenium sample with the ACT4 code.

LEAD

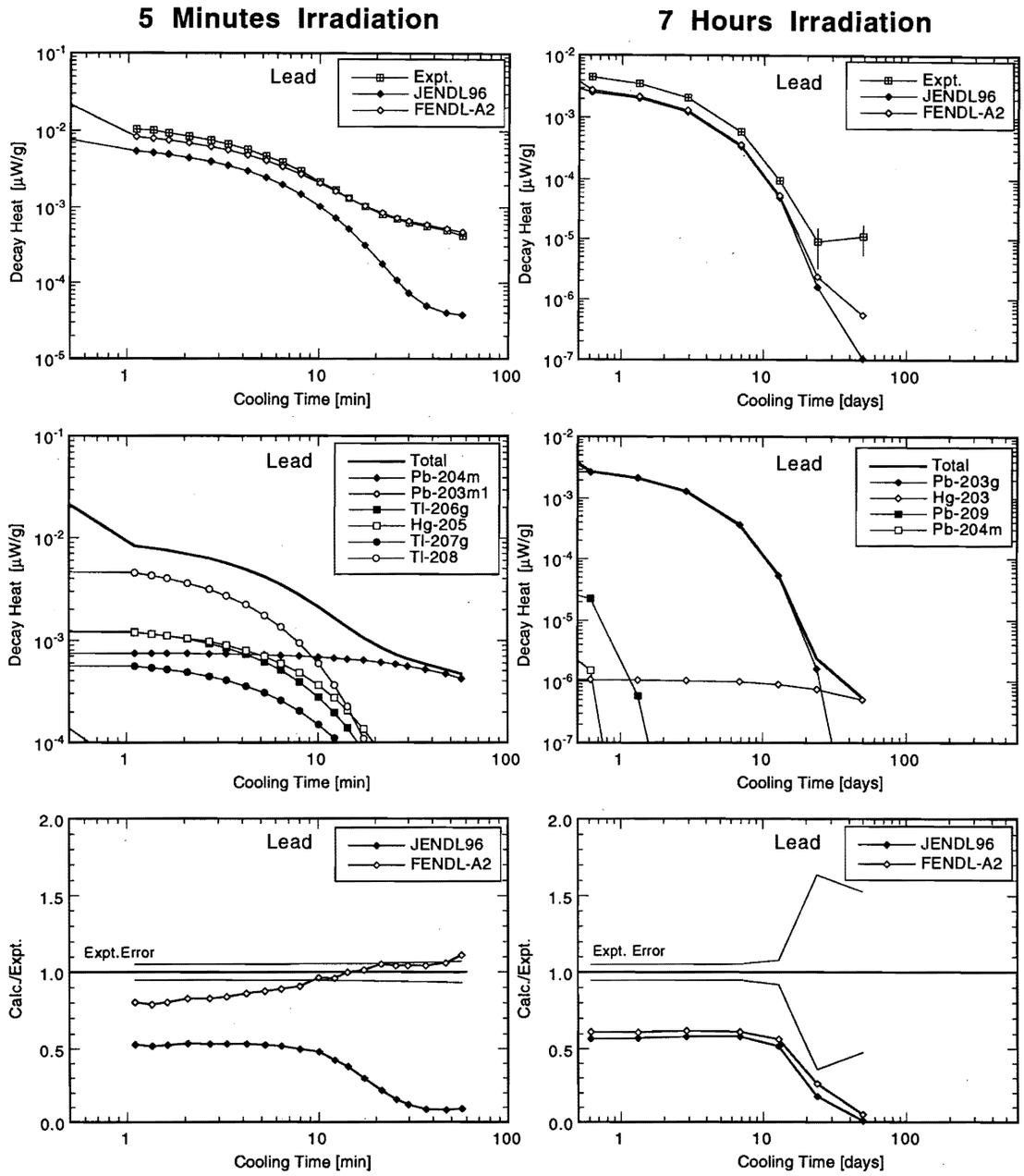

Fig. 5.1.27 Results for the lead sample with the ACT4 code.

BISMUTH

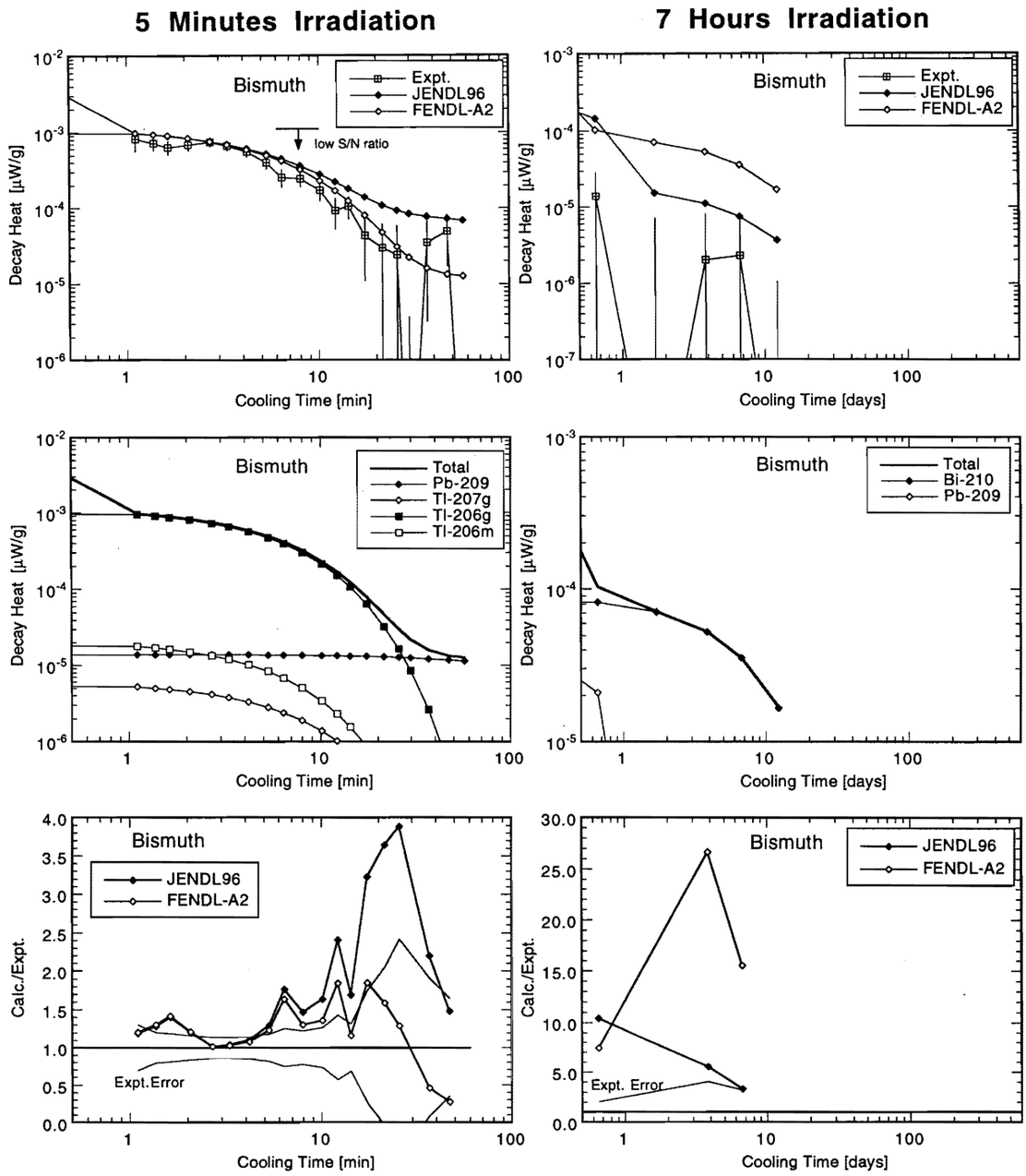

Fig. 5.1.28 Results for the bismuth sample with the ACT4 code.

INCONEL-600

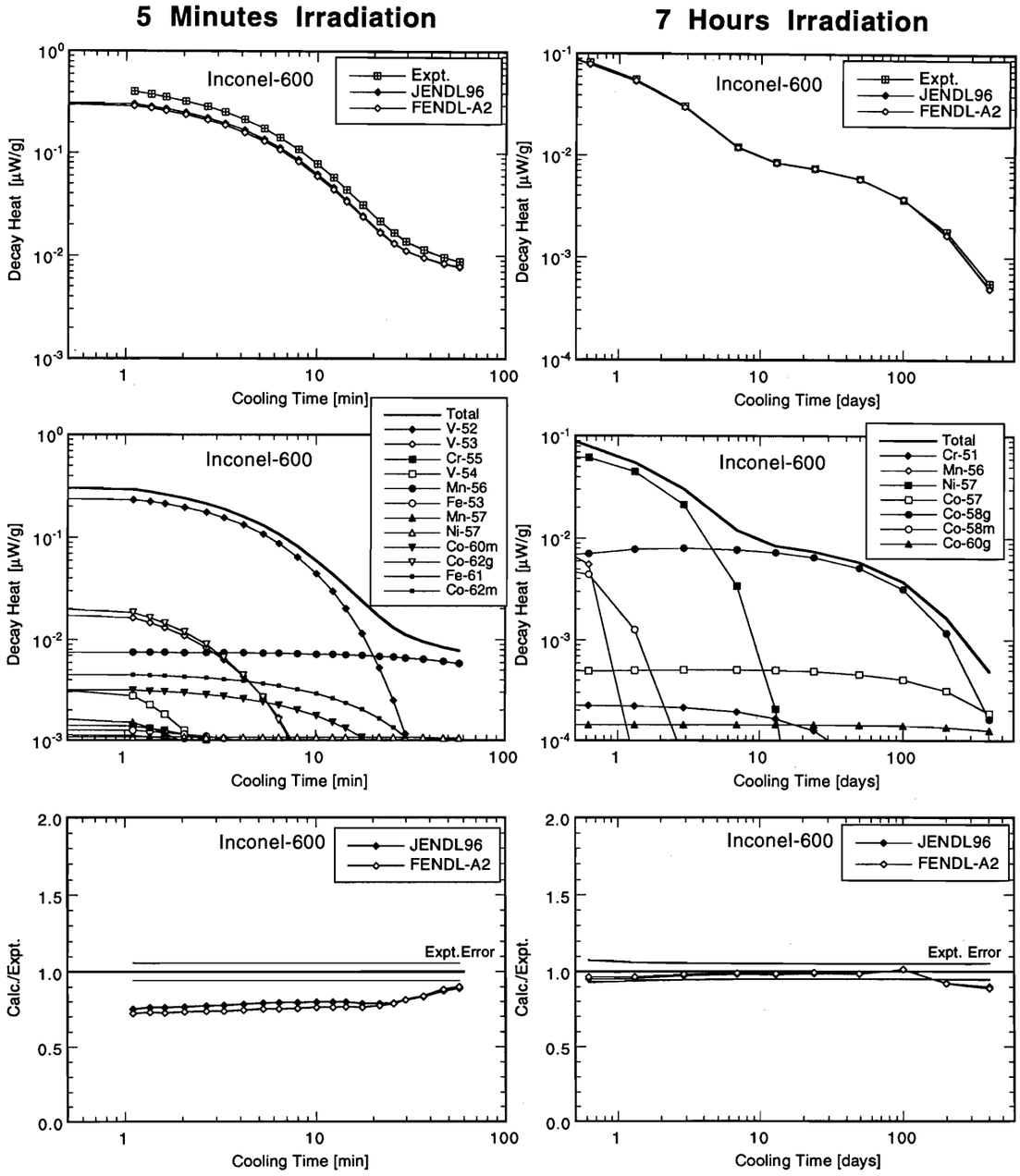

Fig. 5.1.29 Results for the Inconel-600 sample with the ACT4 code.

NICHROME

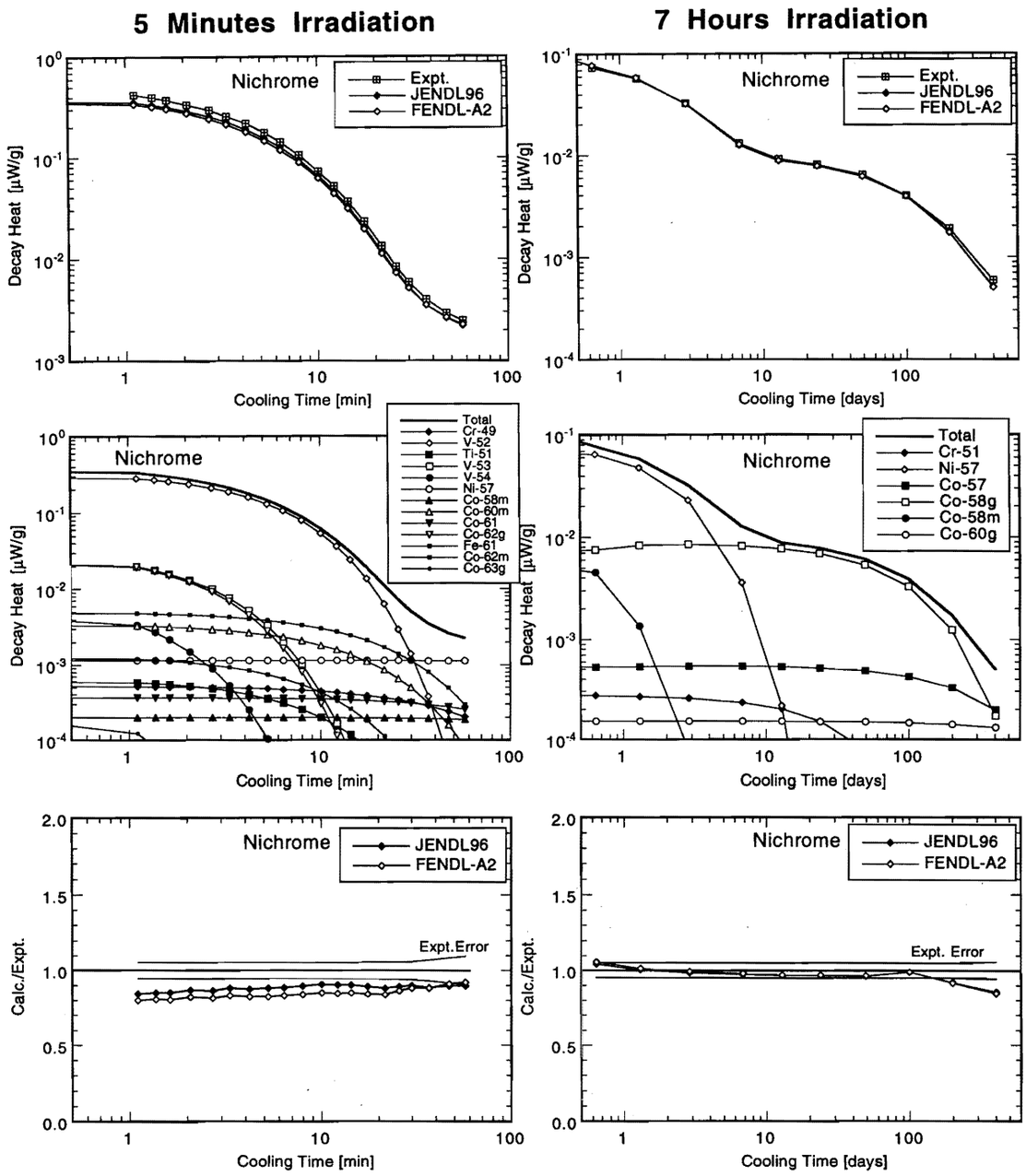

Fig. 5.1.30 Results for the Nichrome sample with the ACT4 code.

SS-304

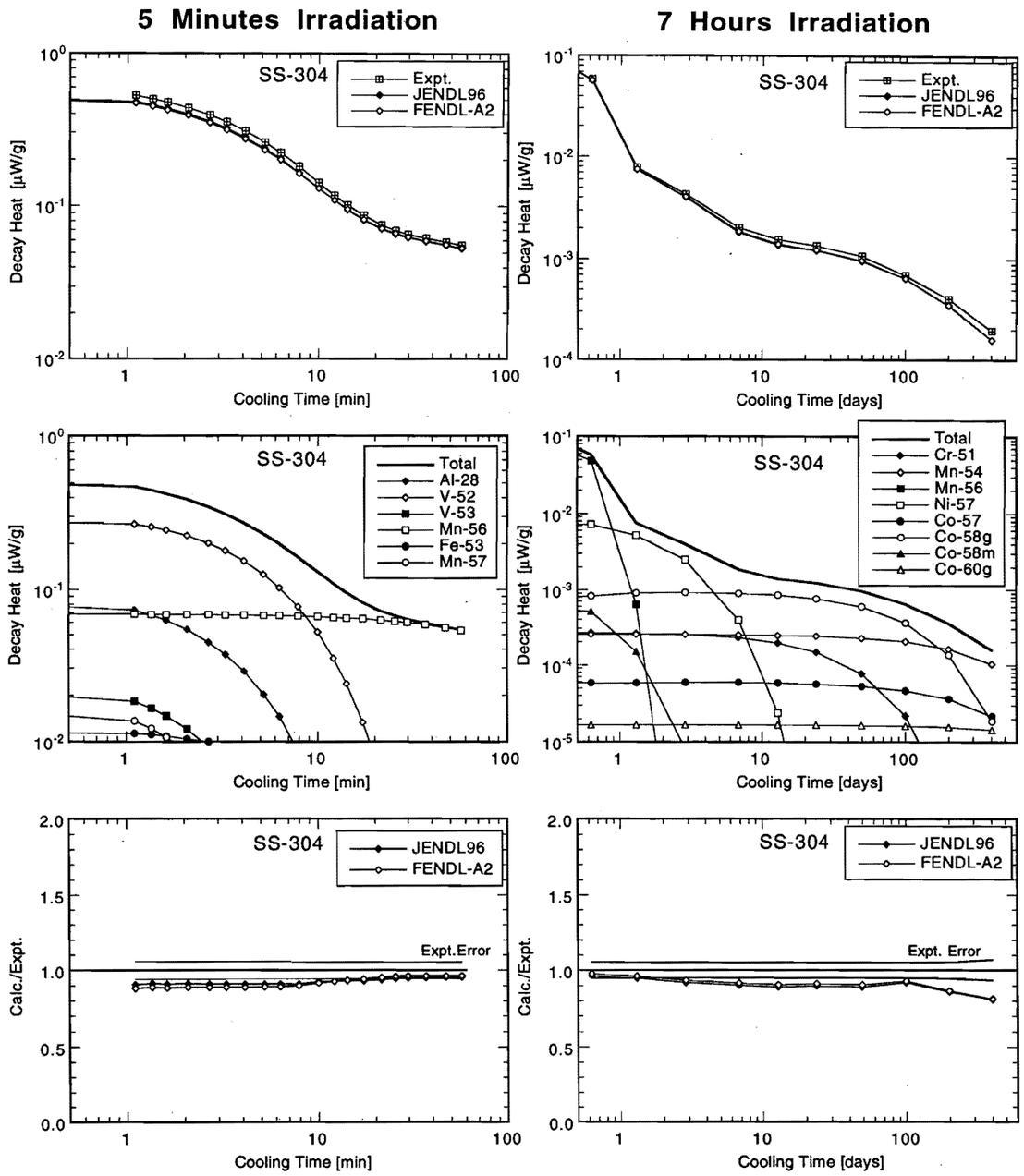

Fig. 5.1.31 Results for the SS-304 sample with the ACT4 code.

SS-316

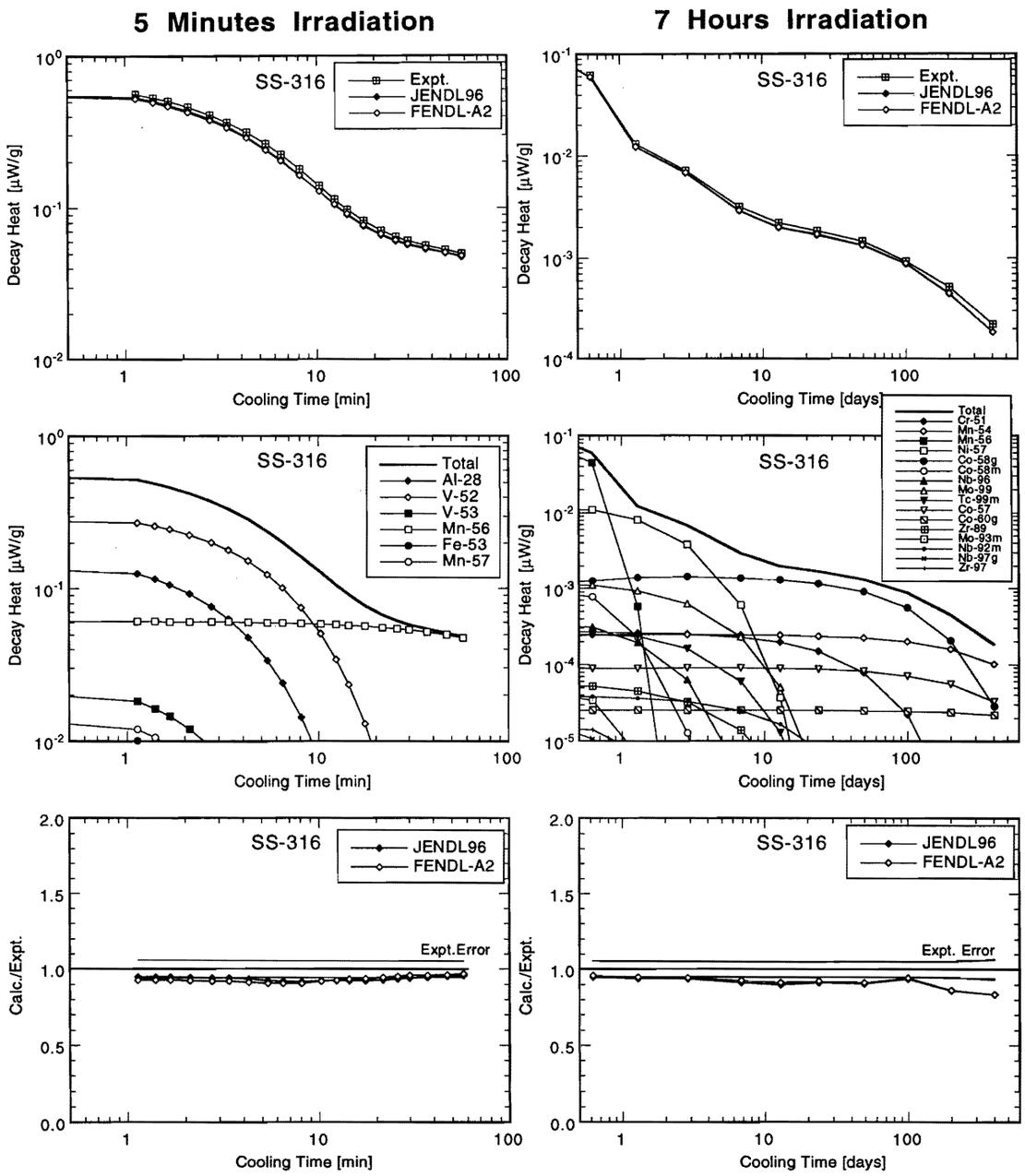

Fig. 5.1.32 Results for the SS-316 sample with the ACT4 code.

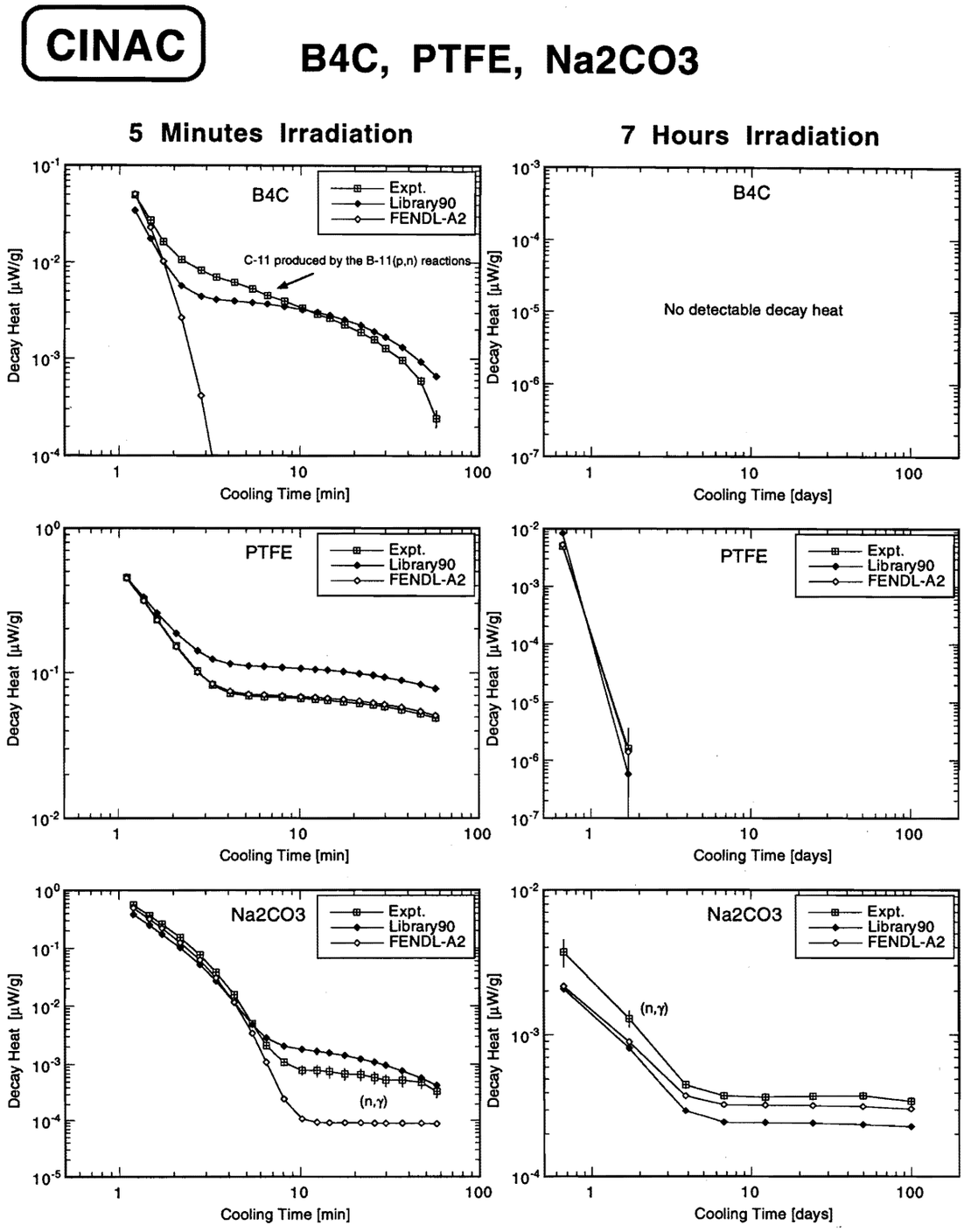

Fig. 5.1.33 Results of the CINAC calculations for the B4C, PTFE (CF2) and Na2CO3 samples. The left and right hand side figures correspond to the 5 minutes and 7 hours irradiations, respectively.

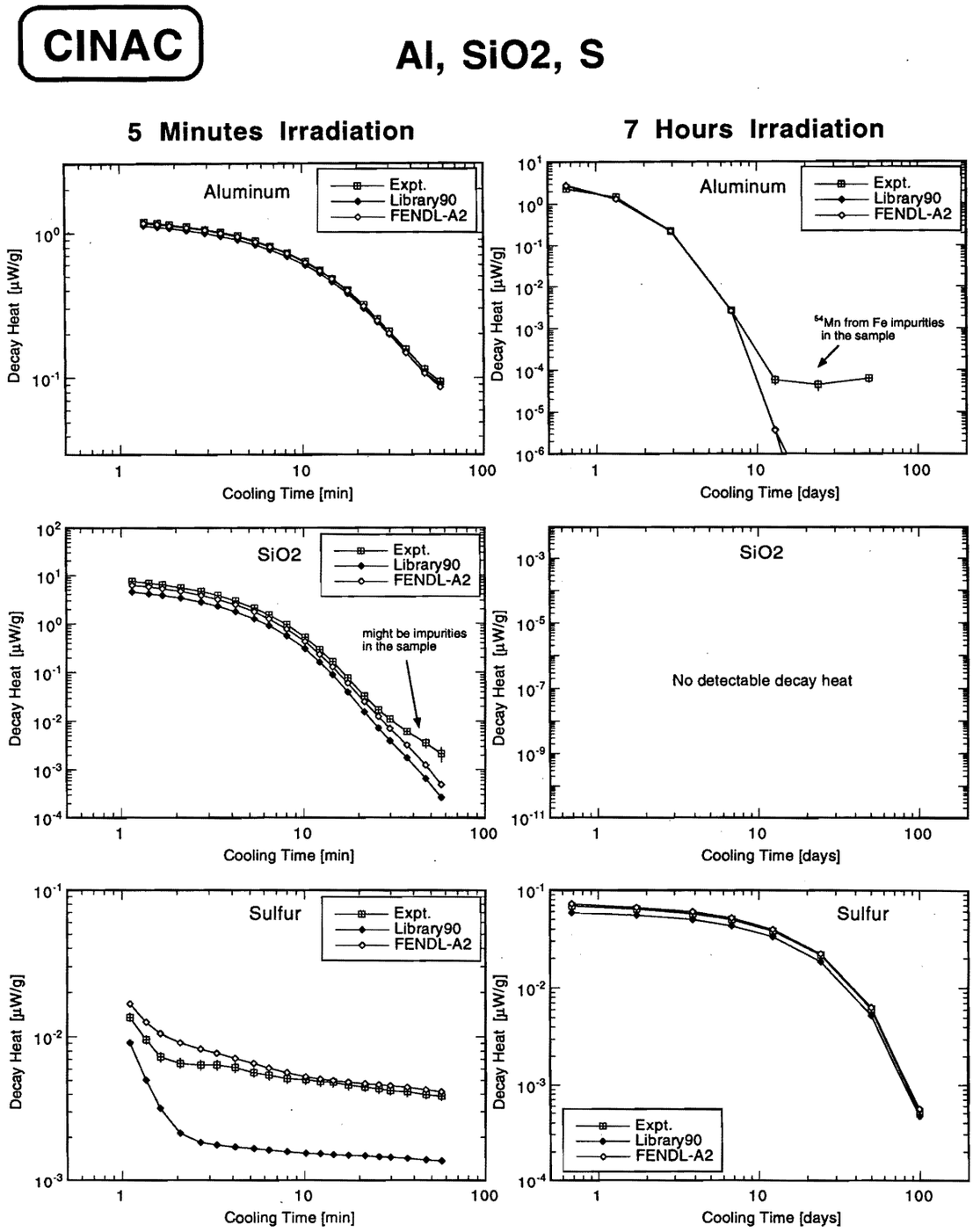

Fig. 5.1.34 Results of the CINAC calculations for the Al, SiO2 and S samples. The left and right hand side figures correspond to the 5 minutes and 7 hours irradiations, respectively.

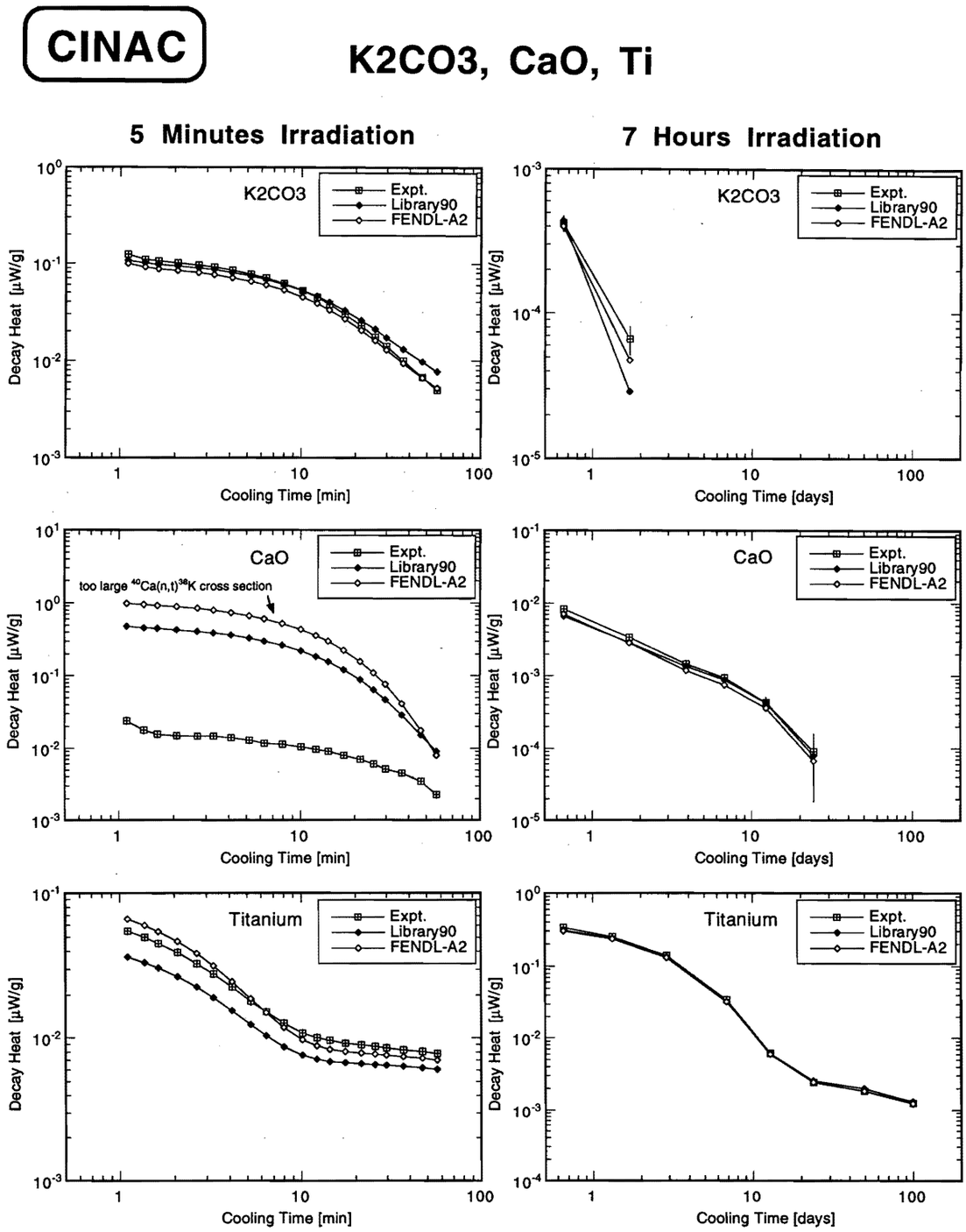

Fig. 5.1.35 Results of the CINAC calculations for the K2CO3, CaO and Ti samples. The left and right hand side figures correspond to the 5 minutes and 7 hours irradiations, respectively.

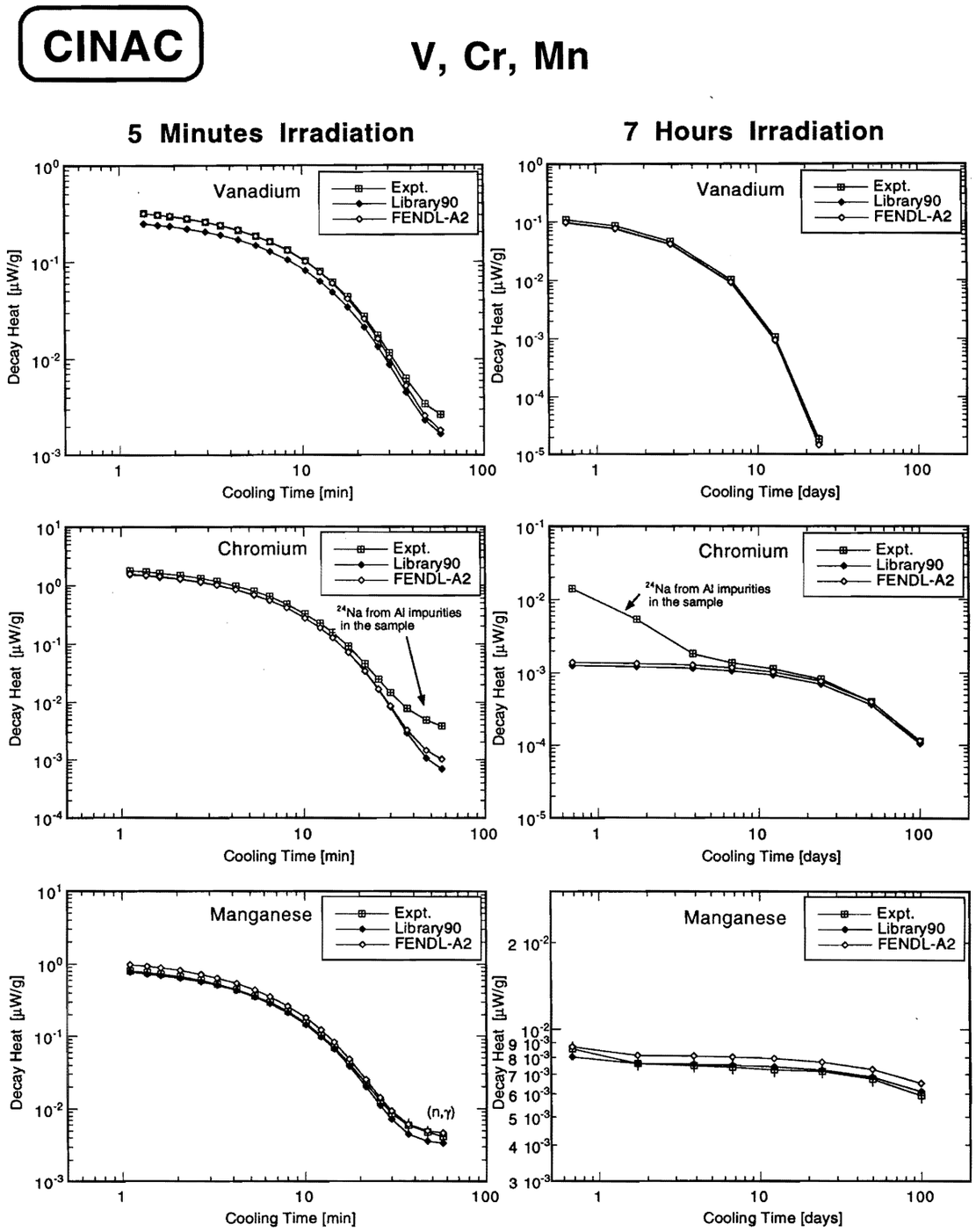

Fig. 5.1.36 Results of the CINAC calculations for the V, Cr and Mn samples. The left and right hand side figures correspond to the 5 minutes and 7 hours irradiations, respectively.

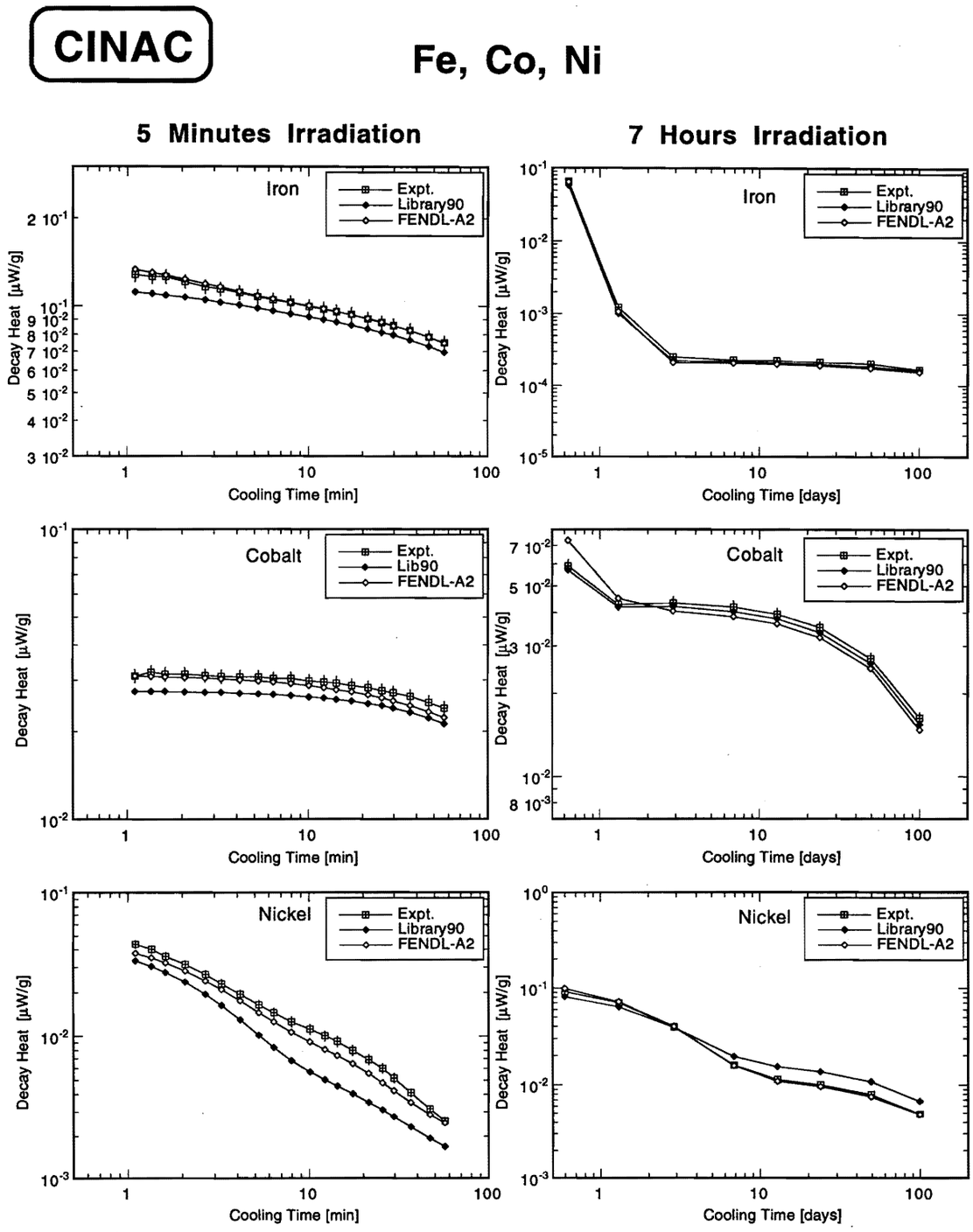

Fig. 5.1.37 Results of the CINAC calculations for the Fe, Co and Ni samples. The left and right hand side figures correspond to the 5 minutes and 7 hours irradiations, respectively.

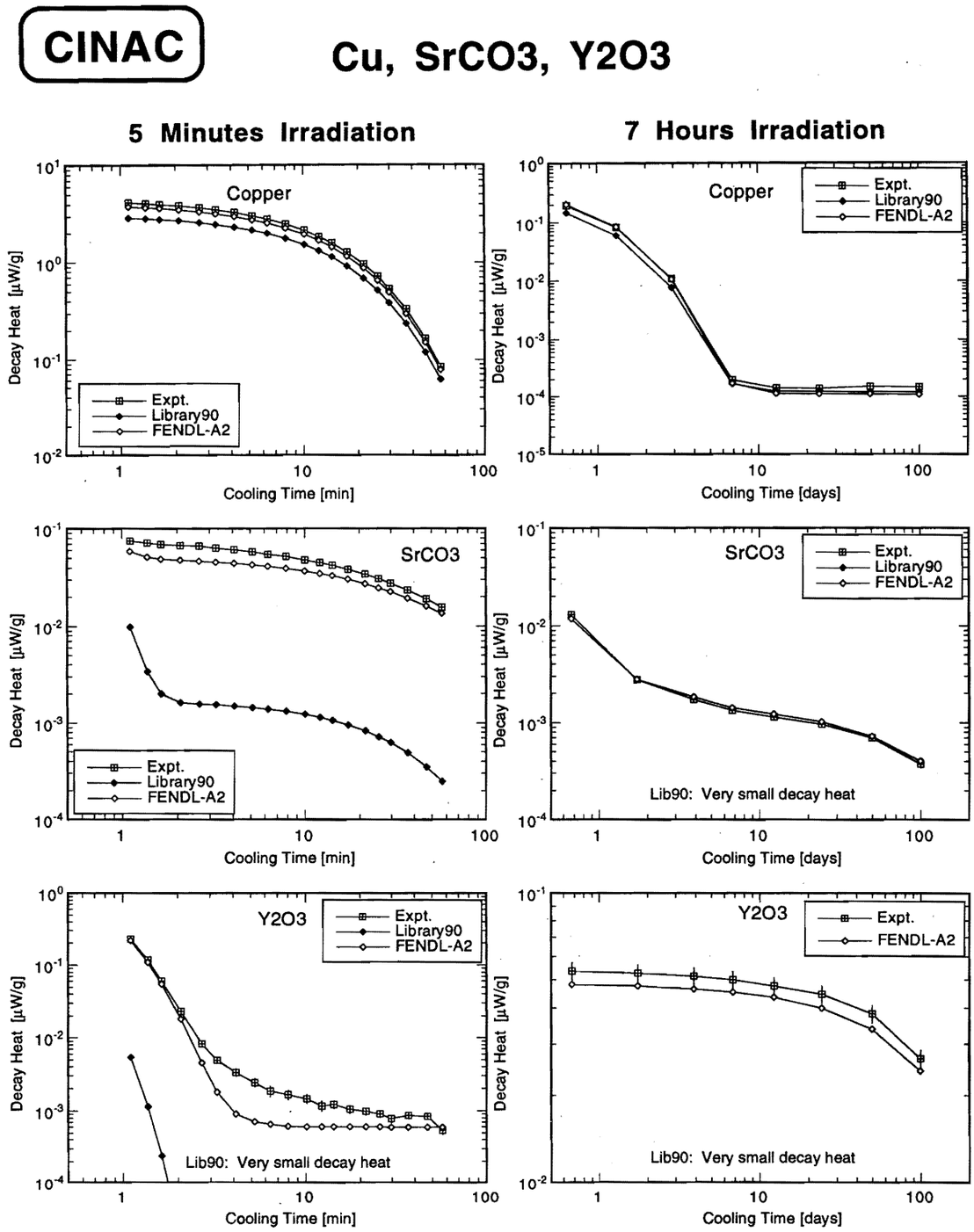

Fig. 5.1.38 Results of the CINAC calculations for the Cu, SrCO3 and Y2O3 samples. The left and right hand side figures correspond to the 5 minutes and 7 hours irradiations, respectively.

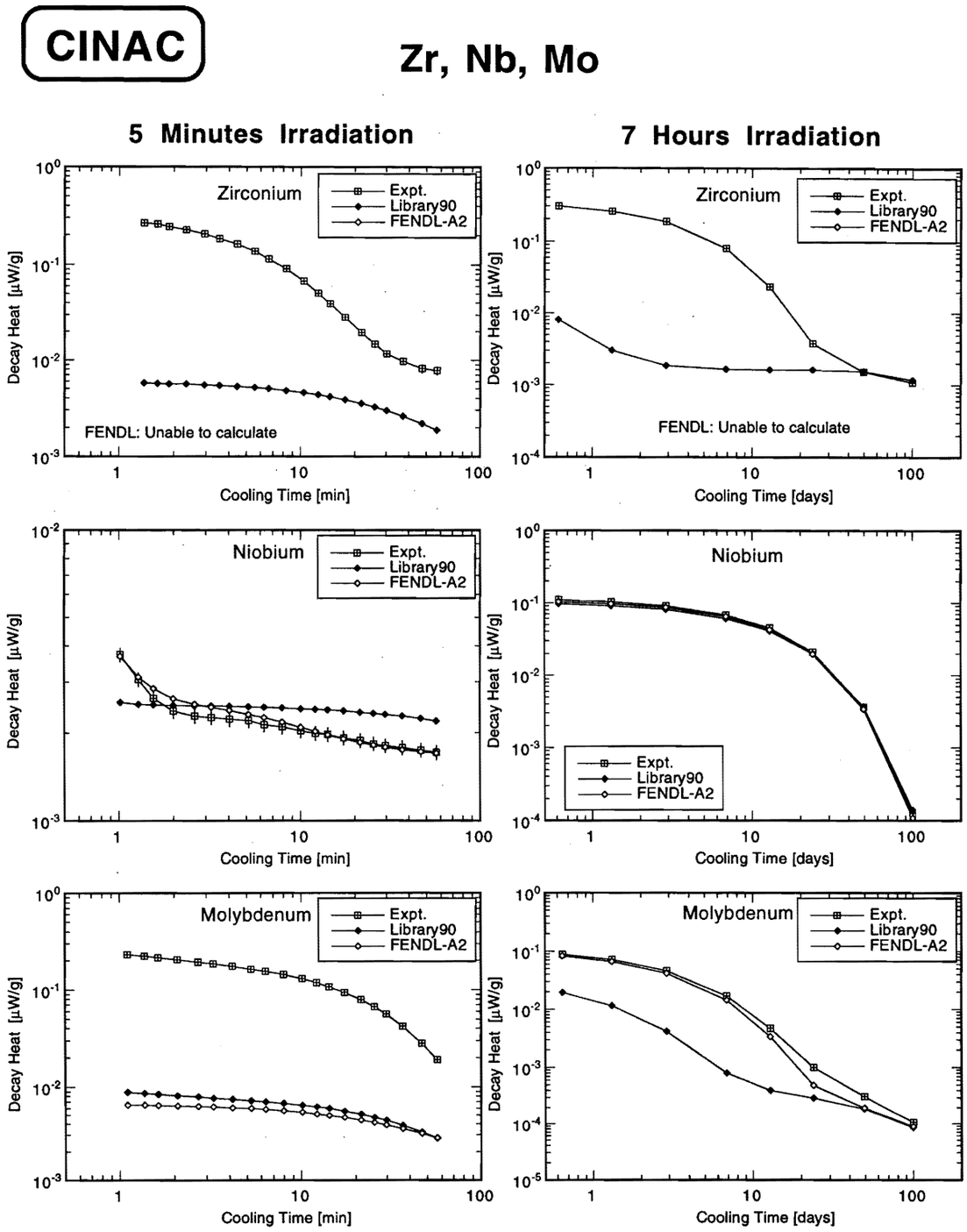

Fig. 5.1.39 Results of the CINAC calculations for the Zr, Nb and Mo samples. The left and right hand side figures correspond to the 5 minutes and 7 hours irradiations, respectively.

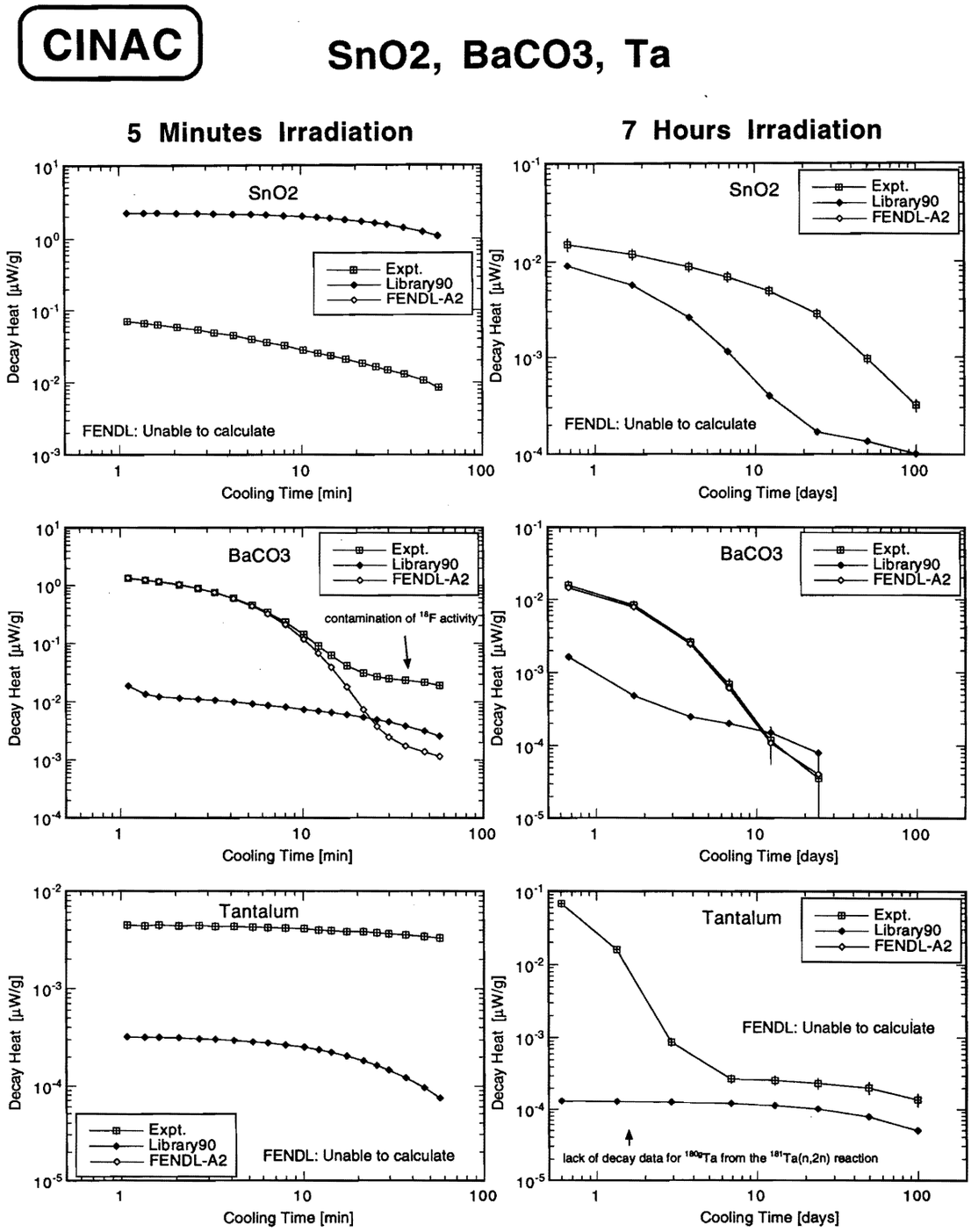

Fig. 5.1.40 Results of the CINAC calculations for the SnO2, BaCO3 and Ta samples. The left and right hand side figures correspond to the 5 minutes and 7 hours irradiations, respectively.

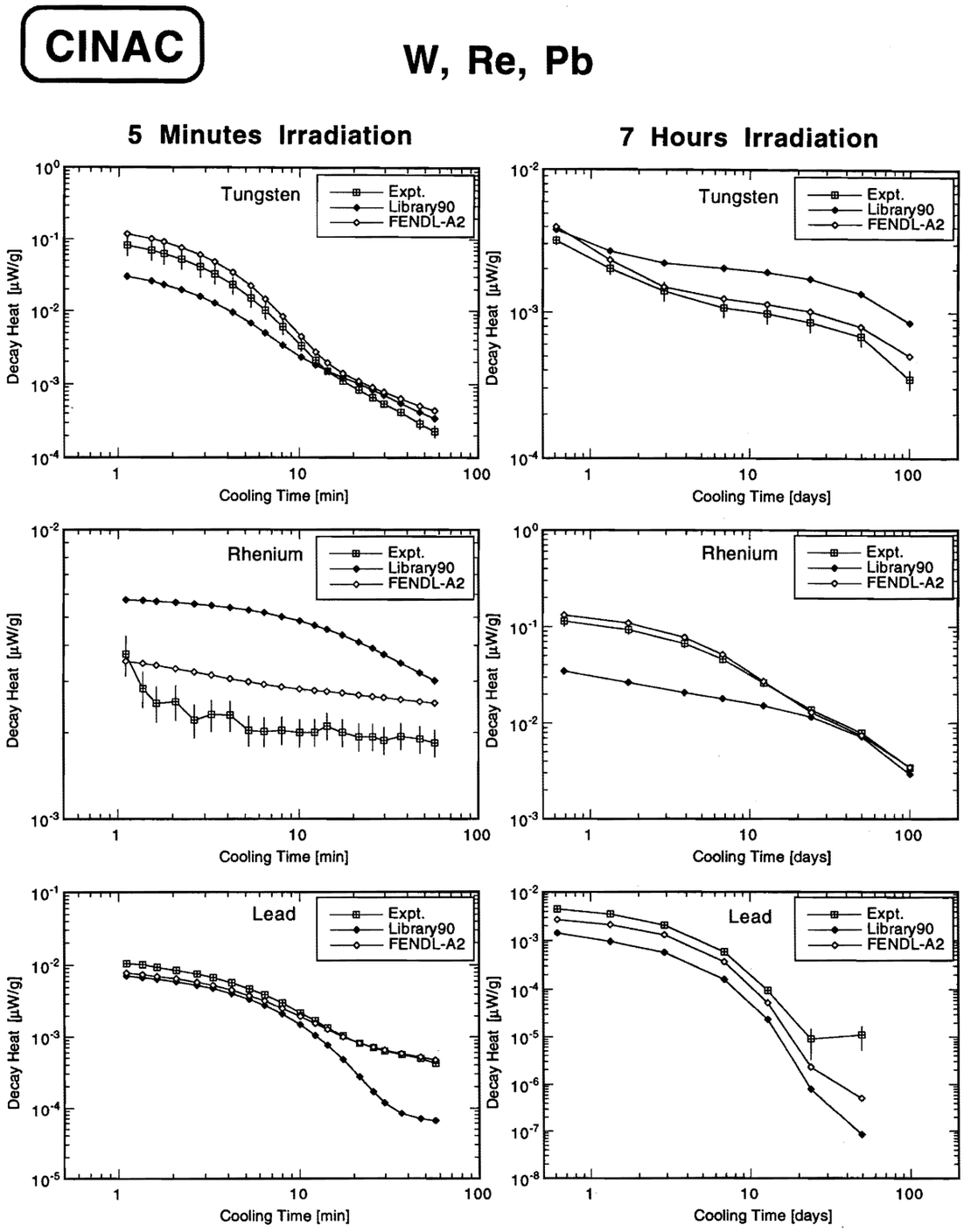

Fig. 5.1.41 Results of the CINAC calculations for the W, Re and Pb samples. The left and right hand side figures correspond to the 5 minutes and 7 hours irradiations, respectively.

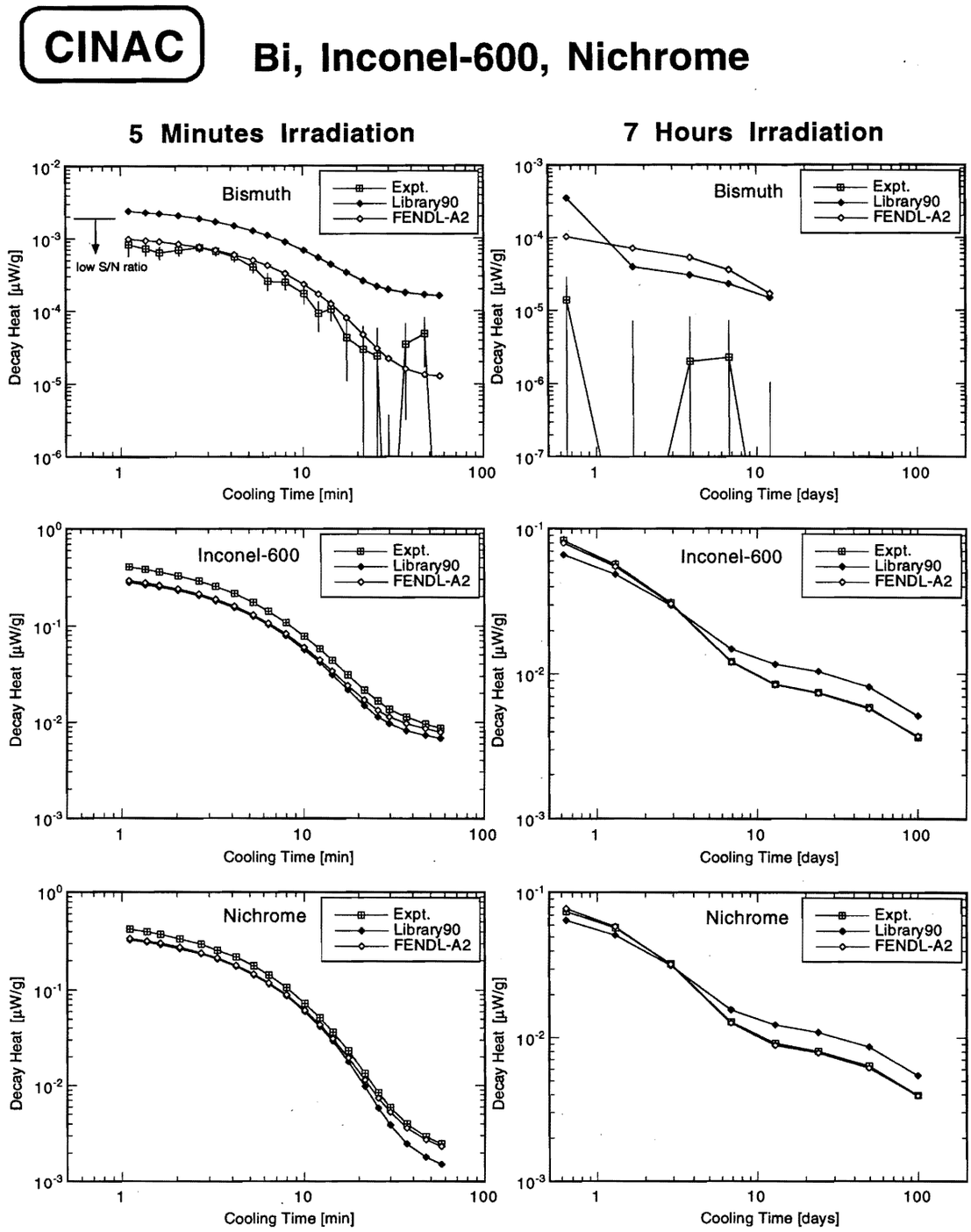

Fig. 5.1.42 Results of the CINAC calculations for the Bi, Inconel-600 and Nichrome samples. The left and right hand side figures correspond to the 5 minutes and 7 hours irradiations, respectively.

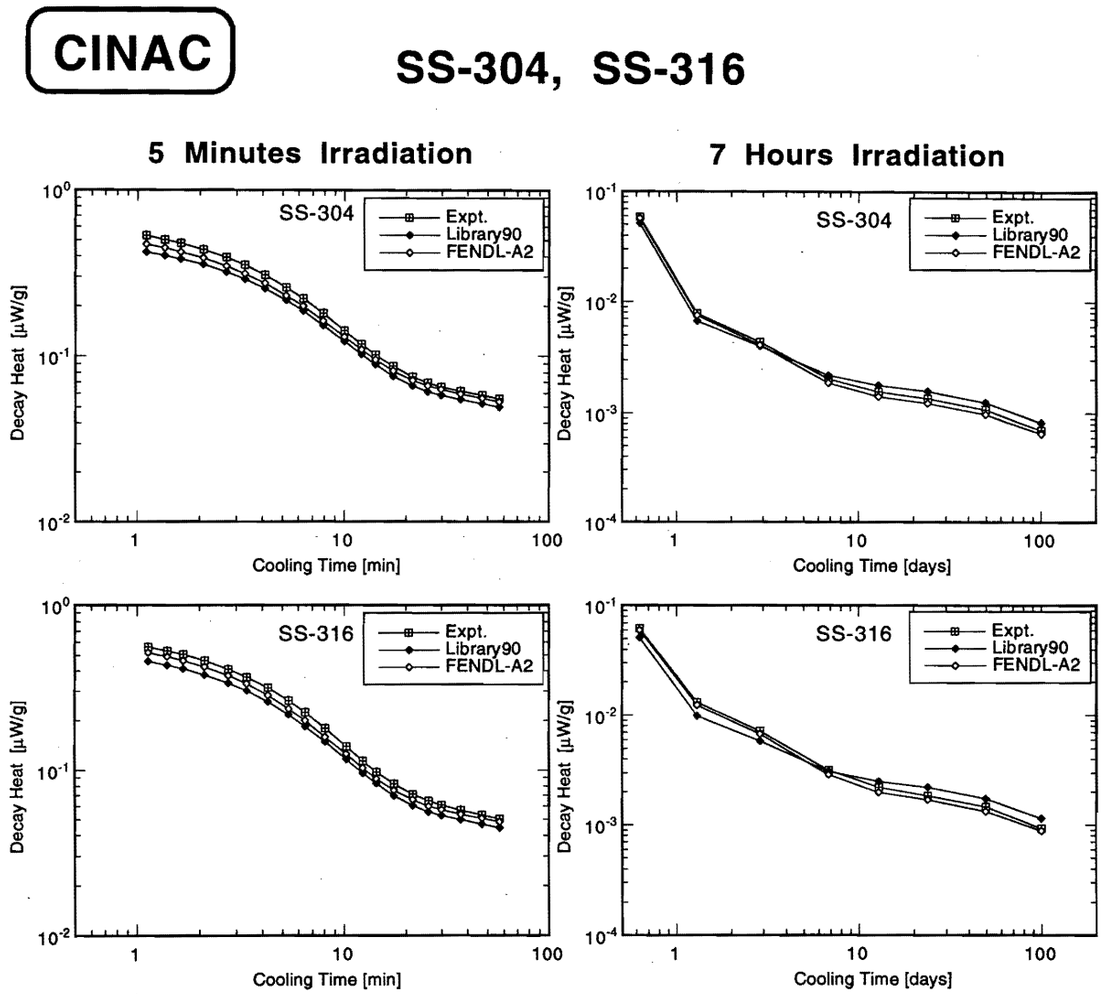

Fig. 5.1.43 Results of the CINAC calculations for the SS-304 and SS-316 samples. The left and right hand side figures correspond to the 5 minutes and 7 hours irradiations, respectively.

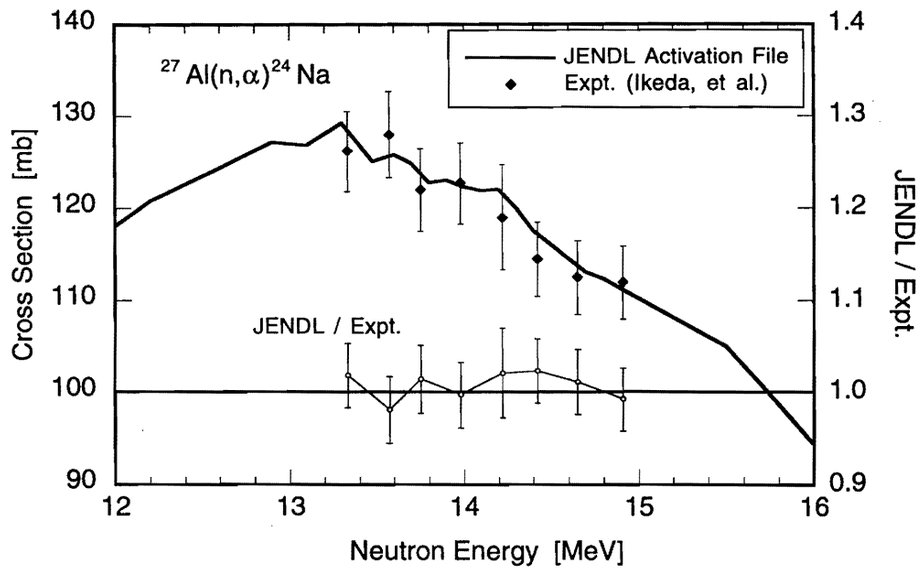

Fig. 5.2.1 Comparison of activation cross sections measured at FNS and taken from JENDL Activation File for the $^{27}Al(n,\alpha)^{24}Na$ reaction.

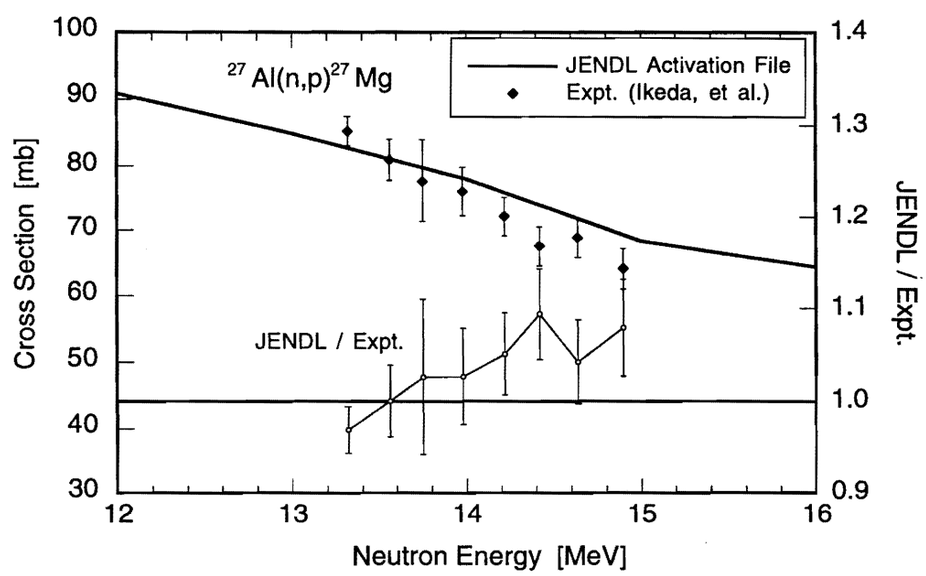

Fig. 5.2.2 Comparison of activation cross sections measured at FNS and taken from JENDL Activation File for the $^{27}Al(n,p)^{27}Mg$ reaction.

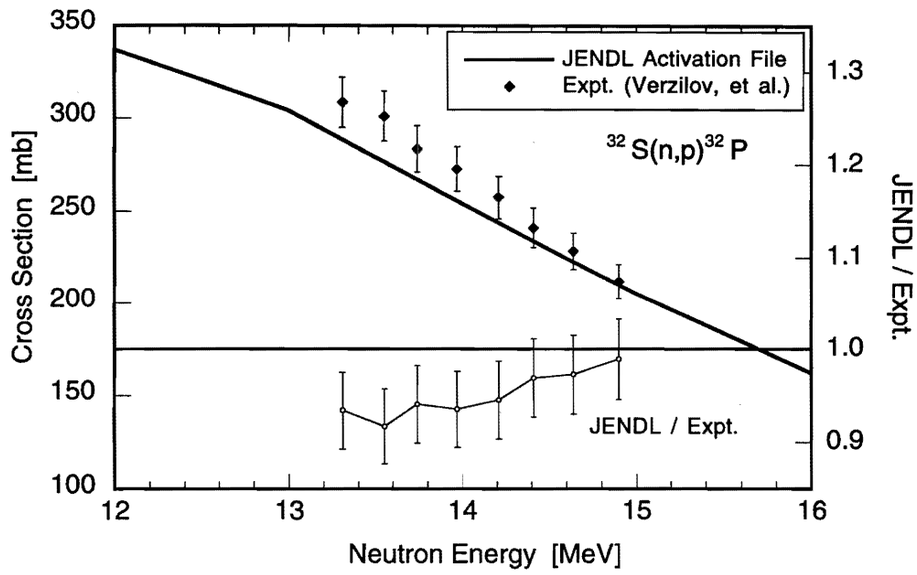

Fig. 5.2.3 Comparison of activation cross sections measured at FNS and taken from JENDL Activation File for the $^{32}S(n,p)^{32}P$ reaction.

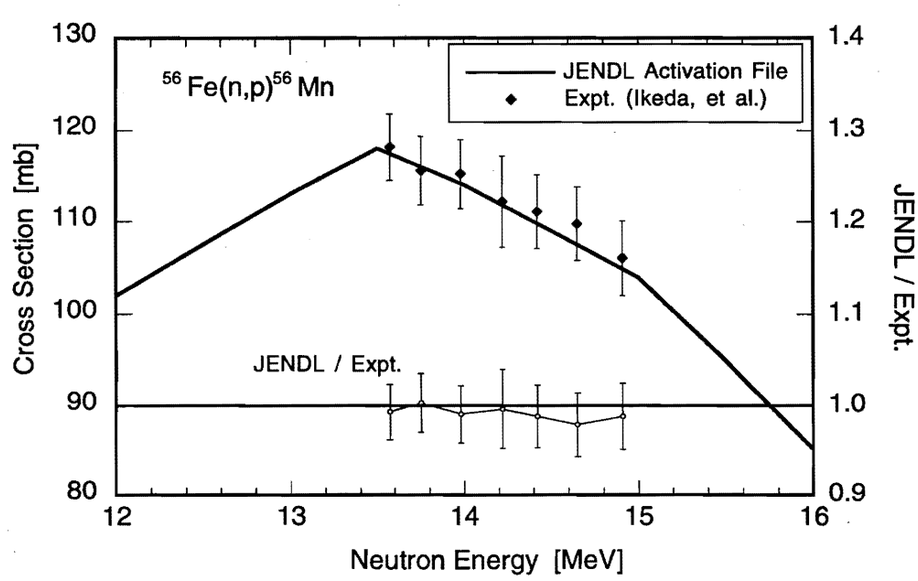

Fig. 5.2.4 Comparison of activation cross sections measured at FNS and taken from JENDL Activation File for the $^{56}Fe(n,p)^{56}Mn$ reaction.

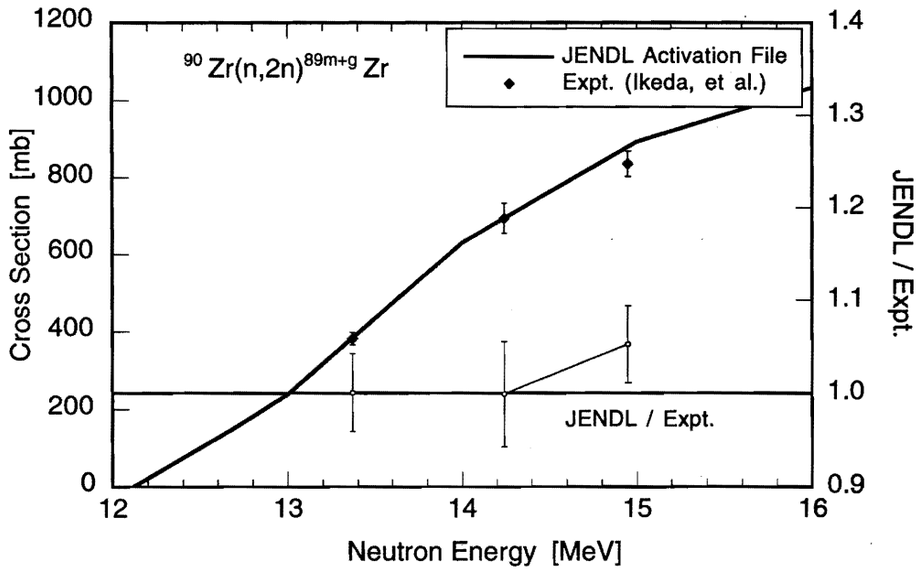

Fig. 5.2.5 Comparison of activation cross sections measured at FNS and taken from JENDL Activation File for the ^{90}Zr(n,2n)$^{89m+g}$Zr reaction.

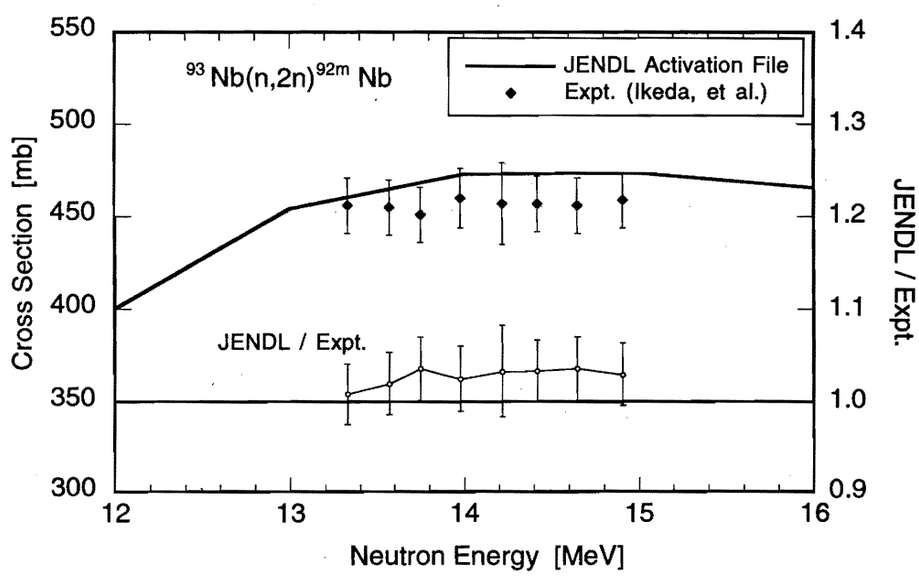

Fig. 5.2.6 Comparison of activation cross sections measured at FNS and taken from JENDL Activation File for the ^{93}Nb(n,2n)^{92m}Nb reaction.

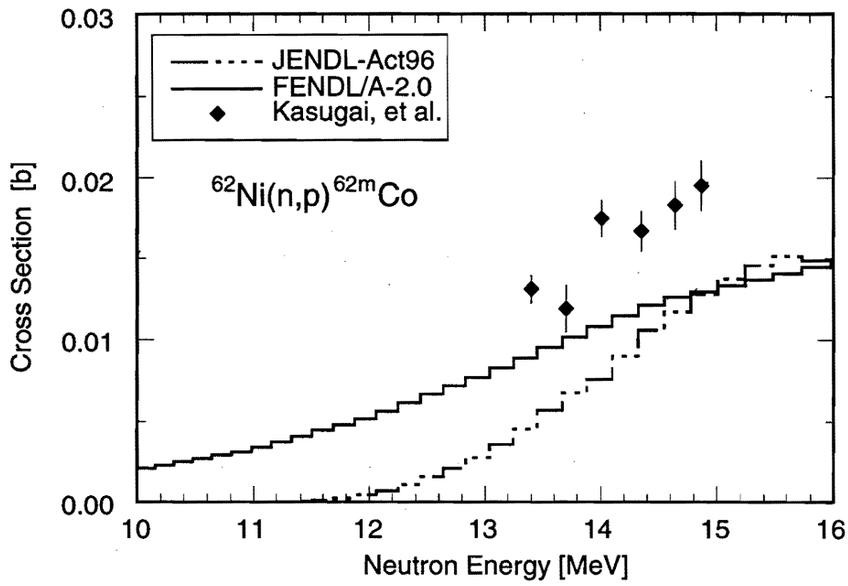

Fig. 5.3.1 The $^{62}Ni(n,p)^{62m}Co$ cross section in FENDL/A-2.0 and JENDL Activation File compared with the experimental data[25].

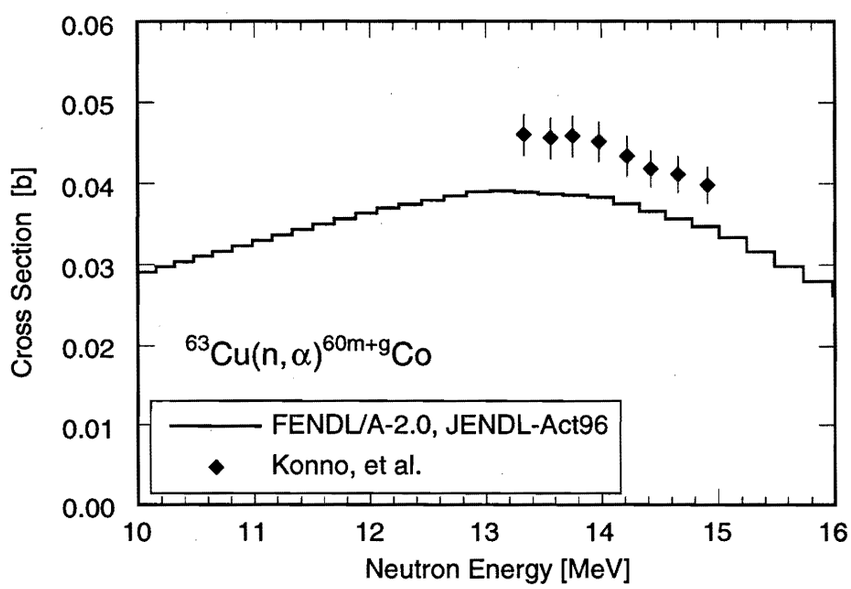

Fig. 5.3.2 The $^{63}Cu(n,\alpha)^{60m+g}Co$ cross section in FENDL/A-2.0 and JENDL Activation File compared with the experimental data[24].